EPA
United States
Environmental
Protection Agency

EPA 600/R-23/346 | Febuary 2024 | www.epa.gov/research

Technical Support Document for the All Ages Lead Model (AALM) version 3.0 – Parameters, Equations, and Evaluations

Office of Research and Development
Center for Public Health and Environmental Assessment

United States Environmental Protection Agency

EPA/600/R-23/346
February 2024

Technical Support Document for the All Ages Lead Model (AALM) version 3.0 – Parameters, Equations, and Evaluations

Office of Research and Development

U.S. Environmental Protection Agency

Washington, DC 20460

DISCLAIMER

This document has been reviewed in accordance with U.S. Environmental Protection Agency policy and approved for publication. Any mention of trade names, manufacturers or products does not imply an endorsement by the United States Government or the U.S. Environmental Protection Agency. EPA and its employees do not endorse any commercial products, services, or enterprises. This document was developed, and the work described in it was conducted, under contracts EP-W-17-008, EP-W-09-031, EP-BPA-11-C-018, EP-13-H-000037, EP-08-H-000055, EP-C-14-001, and 68HERC22D0004.

DISCLAIMER OF SOFTWARE INSTALLATION/APPLICATION

Execution of any installation program, and modification to system configuration files must be made at the user's own risk. Neither the U.S. EPA nor the program author(s) can assume responsibility for program modification, content, output, interpretation, or usage. AALM 3.0 has been extensively tested and verified. However, as for all complex software, these programs may not be completely free of errors and may not be applicable for all cases. In no event will the U.S. EPA be liable for direct, indirect, special, incidental, or consequential damages arising out of the use of the programs and/or associated documentation.

ACKNOWLEDGMENTS

Cover photograph of Coeur d'Alene River shows Black Bridge and the Trail of the Coeur d'Alene's bike path in Enaville. Photograph from Coeur d'Alene River Road on July 1, 2014 provided courtesy of Jill Dorsey of Alta Science & Engineering, Inc.

AUTHORS AND CONTRIBUTERS

Dr. James S. Brown — Center for Public Health and Environmental Assessment, Office of Research and Development, U.S. EPA, Research Triangle Park, NC

Dr. Gary L. Diamond — SRC, Inc., North Syracuse, NY

Dr. Mark H. Follansbee — SRC, Inc., Scarborough, ME

Dr. Graham Glen — ICF, Durham, NC

Dr. Cara Henning — ICF, Durham, NC

Ms. Delaney Reilly — ICF, Durham, NC

PEER REVIEWERS

U.S. Environmental Protection Agency Science Advisory Board (SAB)

All Ages Lead Model External Review Draft 2.0 Peer Review Panel

CHAIR

Dr. Hugh A. Barton, Independent Consultant, Mystic, CT

MEMBERS

Dr. Harvey Clewell, Principal Consultant, Ramboll Environment and Health Consulting, Raleigh, NC

Dr. Joel M. Cohen, Senior Toxicologist, Gradient, Cambridge, MA

Dr. Deborah Cory-Slechta, Professor of Environmental Medicine, Pediatrics, and Public Health Sciences, Department of Environmental Medicine, University of Rochester Medical Center, Rochester, NY

Dr. Philip Goodrum, Principal Toxicologist, GSI Environmental Inc., Fayetteville, NY

Dr. Michael Kosnett, Department of Medicine, Division of Clinical Pharmacology & Toxicology University of Colorado School of Medicine, Aurora, CO

Dr. Anne Loccisano, Senior Toxicologist, Exponent Inc., Alexandria, VA

Dr. Steven Marcus, Professor Emeritus, Departments of Emergency Medicine, Pediatrics, Preventive Medicine and Community Health, NJ Medical School, Rutgers University, Newark, NJ

Dr. Clyde Martin, Horn Professor of Mathematics Emeritus, Department of Mathematics and Statistics, Texas Tech University, Crofton, MD

Dr. Isaac Pessah, Distinguished Professor and Associate Dean of Research and Graduate Education UC Davis School of Veterinary Medicine, Davis, CA

Dr. Robert Phalen, Professor, Air Pollution Health Effects Laboratory, Medicine, Department of Medicine, University of California-Irvine, Irvine, CA

Dr. Ian von Lindern, Co-founder and Senior Scientist, TerraGraphics International Foundation (TIFO), Moscow, ID

Dr. Kathleen Vork, Staff Toxicologist, Air Toxicology and Risk Assessment Section, Air and Site Assessment and Climate Indicator Branch, Office of Environmental Health Hazard Assessment, California Environmental Protection Agency, Oakland, CA

Dr. Michael Weitzman, Professor, Department of Pediatrics, New York University School of Medicine, New York, NY

TABLE OF CONTENTS

LIST OF TABLES

LIST OF FIGURES

ACRONYMS AND ABBREVIATIONS (A COMPLETE LIST OF MODEL PARAMETERS APPEARS IN APPENDICES C AND D)

AALM	All Ages Lead Model
AALM-LG	ACSL implementation of Leggett model
AALM-OF	ACSL implementation of O'Flaherty model
ABLOOD	amount of Pb in blood
ABONE	amount of Pb in bone
ACSL	Advanced Continuous Simulation Language
AF	absorption fraction
AKIDNEY	amount of Pb in kidney
ALIVER	amount of Pb in liver
ALM	Adult Lead Methodology
ASOFT	amount of Pb in soft tissue
ATSDR	Agency for Toxic Substances and Disease Registry
AMTBLD	Leggett model blood volume
BLDHCT	age-dependent hematocrit
BLL	blood lead level
CB	O'Flaherty model blood Pb concentration
CF	AALM adjustment factor for Pb deposition into RBCs
CSFII	continuing survey of food intakes
CSV	comma-delimited text file
DF	deposition fractions
EFH	Exposure Factors Handbook
EPA	Environmental Protection Agency
EVF	extravascular fluid
FRX	O'Flaherty model Pb excretory clearance
GI	gastrointestinal
GIT	gastrointestinal tract
GFR	glomerular filtration rate
GM	geometric mean

GSD	geometric standard deviation
HCTA	adult hematocrit
HRTM	Human Respiratory Tract Model
ICR	Information Collection Request
ICRP	International Commission on Radiological Protection
IEUBK	Integrated Exposure Uptake Biokinetics
IVBA	validated in vitro bioaccessibility
LALV	Lung-Alveolar
LET	Lung-Extrathoracic
LINT	Lung-Interstitial
LTB	Lung-Tracheobronchial
LFM	Leggett Fortran Model
LLIC	lower large intestine contents
NCEA	National Center for Environmental Assessment
NHANES	National Health and Nutrition Examination Survey
NHEXAS	National Human Exposure Assessment Survey
NSLAH	National Survey of Lead and Allergens
NTIS	National Technical Information Service
OCSPP	Office of Chemical Safety and Pollution Prevention
OEHHA	Office of Environmental Health Hazard Assessment
OLEM	Office of Land and Emergency Management
OPPT	Office of Pollution Prevention and Toxics
ORD	Office of Research and Development
OSWER	Office of Solid Waste and Emergency Response
Pb	lead
PK	O'Flaherty model plasma-kidney partition coefficient
PL	O'Flaherty model plasma-liver partition coefficient
PP	O'Flaherty model plasma-poorly perfused tissue partition coefficient
PW	O'Flaherty model plasma-well perfused tissue partition coefficient
RBA	relative bioavailability
RBC	red blood cell
RBCONC	red blood cell Pb concentration
RRBC	rate transfer of Pb from red blood cells to diffusible plasma
RT	respiratory tract
SAB	Science Advisory Board
SOF	Other Soft Tissues
SSC	standardized sensitivity coefficient
ST	soft tissue
TRW	technical review workgroup
ULIC	upper large intestine contents
VBLC	blood volume fraction of body weight
VBONE	bone volume
VK	kidney volume
VL	liver volume
VR	ventilation rate
XRF	X-ray fluorescence
WBODY	body weight
WBONE	bone weight

CHAPTER 1. INTRODUCTION AND HISTORY OF ALL AGES LEAD MODEL

1.1. INTRODUCTION

The All Ages Lead Model (AALM) is a tool for quantitatively relating human lead (Pb) exposures from environmental media that occur over the life time to Pb levels and concentrations in blood, other body tissues, and excreta. The primary intended use of the model is for computational Pb toxicology and risk assessment. As such, the primary audience for the AALM is intended to be risk assessors and researchers, especially those engaged in site-based risk assessments. This technical support document is intended for users seeking a deeper understanding of the equations and technical foundations of the AALM. For more general information on the model and information specific to using the user interface, consult the User's Guide.

The AALM represents an extension of research and regulatory models previously developed by EPA such as the Integrated Exposure Uptake Biokinetics (IEUBK) Model for Pb in Children which simulates exposure-blood Pb concentration relationships occurring from birth to age 7 years (Hogan et al., 1998; White et al., 1998; Zaragoza and Hogan, 1998). The AALM also incorporates Pb modeling concepts explored in models developed in other research efforts, including those of Leggett (Pounds and Leggett, 1998; Leggett, 1993; Leggett et al., 1993), O'Flaherty (O'Flaherty et al., 1998; O'Flaherty, 1998, 1995, 1993, 1991a, b, c) and others (U.S. EPA, 2006; Maddaloni et al., 2005).

As discussed in Section 1.2, the AALM has been implemented in several platforms over the course of its development. The AALM was first developed and implemented in Visual C+ (AALM.C) by U.S. EPA's Office of Research and Development (ORD). Subsequently, ORD implemented the AALM in Advance Continuous Simulation Language, ACSL®, a.k.a. acslX, (AALM.CSL) to further develop and evaluate the model. In a parallel effort, EPA's Office of Chemical Safety and Pollution Prevention (OCSPP) was developing a biokinetic Fortran model (ICRPv005.FOR) with similar capabilities to the AALM.CSL being developed by ORD. From 2015 through 2019, EPA's ORD and OCSPP have coordinated efforts to advance Pb biokinetic modeling and produced a version of the AALM software implemented in Fortran with a Microsoft Excel user interface. As discussed in Section 1.1.1, the AALM version 2.0 (Fortran executable with Excel user interface) underwent an independent federal advisory committee peer review in 2019-2020. Based on peer review comments, the AALM version 3.0 (i.e., the current version of the AALM) was developed from 2020 through 2023 to address all necessary revisions (Tier 1 peer review recommendations) and many suggested revisions (Tier 2 peer review recommendations).

This document, in Chapter 2, describes in detail the conceptual and computational structure of the current Fortran version of the AALM (i.e., version 3.0), including an inventory and explanation of all parameters, variables, and expressions used in the model to calculate Pb intakes and Pb tissue and excreta levels and/or concentrations. Chapter 2 has two primary subsections. The initial primary section (exposure model) describes components of the Fortran code that relate environmental and diet Pb exposures to rates of Pb intake. This code expands all time-varying exposure and physiology variables into complete timeseries covering the simulation. This is followed by a section that provides a detailed description of model components that relate Pb intakes to Pb levels and concentrations in body tissues and excreta. Appendices A and B provide a complete listing of equations and parameters used in the model, respectively, that are directly pertinent to calculations of Pb intakes and Pb levels and concentrations in

body tissues and excreta. Appendices C and D provide a complete list of parameter names and default values used in the model.

Chapter 3 describes the development and evaluation of AALM.FOR, which became the AALM v2.0. This chapter describes the process of harmonizing two model versions [AALM.CSL and OCSPP's biokinetic model in Fortran (ICRPv005.FOR)], evaluating the differing biokinetics for the two versions against available human data, and selection of final model parameters for use in AALM.FOR. The side-by-side comparisons of AALM.CSL and AALM.FOR provided a quality assurance opportunity to ensure code was implemented and operating as expected, i.e., the mathematical relationships posited by the model were correctly translated into computer code and its operation was free of numerical errors. Model parameter optimization and sensitivity analyses discussed in Chapter 4 provides the basis for parameters in AALM.CSL that were ultimately used in AALM.FOR. These analyses were not repeated using AALM.FOR since it provides identical estimations to AALM.CSL. Model evaluations in Chapter 3 compare AALM.CSL and AALM.FOR against the same datasets used in Chapter 4 as well as some additional datasets for striking workers and children.

Chapter 4 describes the ORD development and evaluation of AALM.CSL. The AALM.CSL version implemented both the Leggett model (Leggett, 1993) and O'Flaherty model (O'Flaherty, 1995, 1993). The chapter begins with a comparison of the Leggett and O'Flaherty model structures and then provides a comparison of estimated blood and bone concentrations of Pb between the models. Sensitivity analyses are subsequently provided that were utilized to determine the most influential biokinetic parameters in the models. An evaluation and optimization biokinetics models against observations is provided. A biokinetic parameter controlling Pb binding to red blood cells Pb concentrations was adjusted to align the AALM.CSL results more closely with the IEUBK model for children without adversely affecting the good model agreement and predictive capability for infants or adults.

1.1.1. Quality Assurance and Peer Review

The use of quality assurance (QA) and peer review helps ensure that EPA conducts high-quality science that can be used to inform policymakers, industry, and the public. Quality assurance activities performed by EPA ensure that the Agency's environmental data are of sufficient quantity and quality to support the Agency's intended use. Detailed QA Project Plans (QAPPs) have been developed as a requirement for contracted technical support during the development of the AALM. The AALM is classified as providing Influential Scientific Information (ISI), which is defined by the Office of Management and Budget (OMB) as scientific information the agency reasonably can determine will have or does have a clear and substantial impact on important public policies or private sector decisions (Bolton, 2004). OMB requires the Agency to subject ISI to peer review prior to dissemination. To meet this requirement, EPA often engages the Scientific Advisory Board (SAB) as an independent federal advisory committee to conduct peer reviews. The SAB released a call for peer review panel nominations on November 1, 2018 (83FR54923). Fourteen peer review panel members were chosen to create a balanced panel based on factors such as technical expertise, knowledge, experience, and absence of any real or perceived conflicts of interest. The SAB review of the AALM version 2.0 and associated documentation consisted of a two-day public meeting in October 17-18, 2019 and teleconferences on April 23 and June 23, 2020. The final review report was transmitted to the EPA Administrator on August 3, 2020. SAB provided Tier 1 recommendations (necessary revisions), Tier 2 recommendations (suggestions), and Tier 3 recommendations (future considerations) to create a new version of the AALM for public release in a

timely manner. Both peer review comments provided by the SAB panel and their public deliberations were considered in the development of the final AALM version 3.0. The AALM version 3.0 responds to all of SAB's Tier 1 necessary revisions and incorporates some of their Tier 2 suggestions.

This report was prepared by EPA with assistance from SRC. EPA has agency-wide QA program that is outlined in the EPA Environmental Information Quality Procedure, CIO 2105-P-01.3, and follows specification outlined in EPA Environmental Information Policy CIO 2105.3. Quality assurance for this research is documented in a Quality Assurance Project Plan (QAPP), entitled Advancing EPA's Biokinetic Modeling of LEAD and L-HEEAD 0033058-QP.

1.2. HISTORY OF THE AALM

The AALM was developed as a computational tool for estimating blood Pb concentrations associated with multimedia exposures to Pb that occur from birth through adulthood. The model is a substantial conceptual extension of an earlier model developed by EPA to estimate blood Pb concentrations in children, the IEUBK model (Hogan et al., 1998; White et al., 1998; Zaragoza and Hogan, 1998; U.S. EPA, 1994a, c, 1989). The IEUBK model has been widely used at Superfund sites to develop remedial objectives.

1.2.1. AALM.C

Development of the AALM implemented in Visual C (AALM.C) by the EPA National Center for Environmental Assessment (NCEA) began in 1999 to extend Pb exposure and biokinetics modeling capability of the IEUBK model to address a wider range of model applications in computational Pb toxicology and risk assessment; these include:

- Simulation of Pb biokinetics associated with multimedia exposures occurring within any age range from birth through adulthood (the IEUBK model is limited to birth to age 84 months);
- Simulation of Pb biokinetics in blood, bone, soft tissues, and excreta (in the IEUBK model, Pb levels in tissues and excreta are intermediary variables used to support the blood Pb simulation, and are not output variables);
- Simulation of Pb biokinetics in response to changes in Pb exposure that occur over periods of days (the IEUBK model exposure averaging time is typically ≥1 year and estimates quasi-steady state blood Pb concentrations); and
- Expansion of the exposure model to include multiple sources of exposure from air, drinking water, food, and indoor dust and soil.

Over the intervening years between initiation of the development of the IEUBK model in 1989 and its release for regulatory use (U.S. EPA, 1994b), several modeling approaches were reported for simulating Pb biokinetics of ages extending beyond early childhood. Two models in particular were influential in developing the structure of the AALM. The first was the Leggett model (Pounds and Leggett, 1998; Leggett, 1993), based on a biokinetic model originally developed for the International Commission on Radiological Protection (ICRP) that calculated radiation doses from environmentally important bone-seeking radionuclides, including radioisotopes of Pb (Leggett, 1992a, b, 1985). The original model was used to develop cancer risk coefficients for internal radiation exposures to Pb and other alkaline earth elements that have biokinetics similar to those of calcium (U.S. EPA, 1998; ICRP, 1993). The compartment structure, Pb transfer coefficients, and numerical integration method of the Leggett model

were adopted in the early versions of the AALM. The second model was the O'Flaherty model that simulates Pb exposure, uptake, and disposition in humans, from birth through adulthood (O'Flaherty, 2000; O'Flaherty et al., 1998; O'Flaherty, 1998, 1995, 1993, 1991a, b, c). Important features that distinguish the O'Flaherty model from the Leggett model are simulation of growth (the Leggett model simulates growth of blood volume only), bone formation, and resorption (the Leggett model simulates the "effects" of bone growth and resorption on Pb kinetics, but does not simulate bone growth and resorption explicitly). Uptake and release of Pb from trabecular bone and metabolically active cortical bone are functions of bone formation and resorption rates, respectively, and are simulated in the O'Flaherty model; this establishes a relationship between the age-dependence and the Pb kinetics in and out of bone, and allows for explicit simulation of the effects of bone formation (e.g., growth and loss, changes in bone volume, and bone maturation) on Pb uptake and release from bone. In contrast, the Leggett model represents age-dependence of bone Pb kinetics as age-dependent rate coefficients for transfer of Pb into and out of bone. Although the O'Flaherty model had a more physiologically accurate representation of bone growth and resorption, the Leggett model configuration for growth of the blood volume and bone Pb kinetics was used for early versions of the AALM.

In October of 2005, the EPA Science Advisory Board (SAB) reviewed a Visual C implementation of the AALM (AALMv1.05.C) and highlighted the need for expanded documentation and further evaluation of the model (U.S. EPA, 2007a). The SAB also identified a number of deficiencies, and suggested potential improvements. EPA expanded the documentation and evaluation of the AALM to include the following: (1) a Guidance Manual for the AALM that describes the conceptual basis and structure of the model (including all equations, parameters, and parameter values) (SRC, 2008); (2) review and evaluation of evidence supporting further extension and/or refinement of the model (SRC, 2009a); and (3) a comparative review of alternative modeling approaches (SRC, 2009b).

1.2.2. AALM.CSL

Research initiated by EPA NCEA in early 2013 expanded the AALM further to address deficiencies identified by the SAB and re-evaluated performance of the model. The AALM was migrated to acslX which removed the need to develop and maintain computer code for the numerical integration solution of the AALM biokinetics model, and made use of existing acslX code to implement the Leggett and O'Flaherty models (Lorenzana et al., 2005). An exposure model was developed in Excel which removed the need to develop *de novo* computer code for the exposure model, and allowed development of exposure scenarios in Excel without the requirement for a license or knowledge of acslX. Development of the acslX version of the AALM is described in Chapter 4. The latest version of the model is AALMv4.2.CSL (July 2015).

AALM.CSL included the user option to link the exposure model to either the Leggett or O'Flaherty biokinetics models. It also introduced several changes to both the Leggett and O'Flaherty biokinetics models including some new parameters and as well as revised parameter values. Some of these data used in the optimization were not available at the time the original models were developed. Optimization against a common set of data resulted in general convergence of AALM-LG.CSL and AALM-OF.CSL estimations for blood, bone, and soft tissue, and agreement with blood Pb estimations for children from the IEUBK model (Chapter 4).

1.2.3. AALM.FOR

In 2014, the EPA Office of Pollution Prevention and Toxics (OPPT) developed an implementation of the Leggett model (Pounds and Leggett, 1998; Leggett, 1993) biokinetics model to support the Agency's *Approach for Estimating Exposures and Incremental Health Effects from Lead Due to Renovation, Repair, and Painting Activities in Public and Commercial Buildings* (U.S. EPA, 2014b). The latest released version of the model, ICRPv005.FOR, has the capability of simulating Pb levels in body tissues (e.g., blood, bone, brain) and excreta at resulting from acute or chronic exposures to inorganic Pb that occur from birth through adulthood.

In developing ICRPv005.FOR, several changes were made to Leggett biokinetics model (see Table 3-1 in Chapter 3); however, up to ICRPv004.FOR, the biokinetics model was unchanged from Leggett (1993). The major changes included (1) age-dependent blood and tissue masses, adjustments to RBC uptake parameters, and adjustment of bone-to-plasma transfer rates. Collectively, updates made to ICRPv004.FOR to create ICRPv005.FOR resulted in lower estimated blood Pb concentrations for a given Pb intake in children, that more closely agreed with estimations from the IEUBK model [see Figure M-4 in (U.S. EPA, 2014a)]; and lower blood and bone Pb concentrations in adults [see Figure M-6 in (U.S. EPA, 2014a)]. ICRPv005.FOR was evaluated against data on blood and bone Pb levels in occupationally exposed adults reported in Nie et al. (2005), although some of these data have not been published. The conclusion from these evaluations was that the model tended to predict lower cortical bone Pb concentrations than observed and higher blood Pb concentrations [see Figures M-5 and M-6 in (U.S. EPA, 2014a)].

External peer review of the Approach for Estimating Exposures and Incremental Health Effects from Lead Due to Renovation, Repair, and Painting Activities in Public and Commercial Buildings (U.S. EPA, 2014b) resulted in several recommendations (Versar, 2015), including the need for further evaluation of ICRPv005.FOR. Based on these evaluations, ICRPv005.FOR was revised and parameter values updated to create AALM.FOR (Chapter 3). In the development of AALM.FOR, the model was evaluated with a larger set of observations in children and adults, including some data that had not been used in previous evaluations of ICRPv005.FOR, including all datasets used in the evaluation and development of the AALM.CSL (Chapter 4). AALM.FOR utilizes the same exposure and biokinetic parameter values as the AALM.CSL and, as a result, both models estimate the same blood and tissue Pb levels when the same exposure inputs are used in both models. Similar to the AALM.CSL, AALM.FOR utilizes a spreadsheet graphical user interface for setting exposure and biokinetics parameter model inputs and processing output. The major difference between the general architecture of the two models is that the biokinetics model of the AALM.FOR is implemented in Fortran, whereas, the biokinetics model of the AALM.CSL is implemented in acslX. The AALM.FOR model with an Excel User Interface was publicly released as the AALM version 2.0 and underwent an independent federal advisory committee peer review in 2019-2020 as discussed in Section 1.1.1. The AALM version 3.0 was developed from 2020 through 2023 to address peer review comments.

1.2.3.1 AALM.FOR changes between AALM version 2.0 and 3.0

The updated Fortran code includes changes to the lung section of the model. There are still four lung compartments, but the flows and variables are now defined differently. While there were no changes to the other 27 compartments or to the intercompartmental flows, there are three other changes of significance. First, the Fortran code now has a "front end" that evaluates all the external sources, growth

and physiological variables, and age-dependent rate constants on all the timesteps before beginning the biokinetics section. This takes advantage of vectorized evaluation which greatly speeds up the code's runtime. Second, the new AALM version 3.0 allows tracking of the contributions of up to 18 external Pb sources (3 for each of the 6 possible media) while the Pb resides in the lung or gastrointestinal (GI) tract compartments. Third, the new code explicitly checks the mass balance of Pb, both in total and by source. In test runs, over a full lifetime the mass balances extremely closely, often to better than one part in a million. Further, the new code can also handle more timesteps than the old code, which was limited to about 200,000 timesteps. Runs with over 10 million timesteps have been completed successfully. A typical run with 100 timesteps per day over a 90-year simulation takes under 30 seconds and could be even faster depending on available RAM.

Additionally, AALM v3.0 created new routines to allow for up to three sources with varied bioavailabilities within each media type (e.g., soil). The original code only allowed for a single bioavailability for each media type. The new routines conserve mass balance, i.e., nonbioavailable lead excreted in feces is tracked as part of the mass balance. These changes required extensive vector and array processing coding revisions to track up to 18 individual intake sources throughout simulated a lifetime. Because of these coding changes, processing times were improved with longer, more complex simulations now being possible.

Further, significant changes in the user interface were made between AALM versions 2.0 and 3.0. The user interface was overhauled to prioritize usability of the model while not removing model complexity or functionality. Many of these updates included reorganization of tabs and information, increased use of macros and automation to guide the user through the tool, and introduction of processes to eliminate how much the user needs to do to interact with the data. Further, the interface was updated to decrease visual clutter without content loss. To additionally facilitate user interaction with the model functionality was added to the User Interface allowing users to convert dust lead loading to concentration, visualize and revise growth curves, and to import and export simulation setups.

Finally, the User Guide was revised to match the updates made to the AALM v3.0 User Interface and was reorganized for increased functionality as a reference manual. This manual was also outfitted with example exposure scenarios. The example exposure scenarios leverage the ability to import simulation setups. With this feature, users can load examples exposure scenarios, run the simulations, and view results with confidence that the exposure conditions have been correctly implemented.

CHAPTER 2. THEORETICAL FRAMEWORK, PARAMETERS, AND EQUATIONS

2.1. OVERVIEW OF AALM STRUCTURE

The AALM Fortran code consists of two executable files: AALM_32.exe and AALM_64.exe. The former is a 32-bit Windows application and the latter is the 64-bit version. The AALM version 3.0 has been tested exclusively on computers with a Microsoft Windows operating systems. The AALM Fortran code and Excel Interface have not been used or tested on other systems (i.e., Apple, Linux) at this time. Both are referred to below as AALM.FOR. The code comprises two major submodels that simulate Pb exposure and Pb biokinetics, respectively. The exposure model described in Section 2.2 calculates rates of Pb intake (µg Pb/day) from ingestion or inhalation based on inputs for exposure concentrations in air, indoor dust, soil, and water; and Pb intakes (µg/day) from food or other sources. The exposure model simulates a hypothetical individual (subject), defined in terms of age, sex, and rates of contact with

environmental media (e.g., drinking water or indoor dust or soil ingestion rates). As the subject ages, a growth model updates body weight and selected physiological parameters, and the inhalation and ingestion rates may optionally vary with age.

The AALM biokinetics model described in Section 2.3 simulates kinetics of absorption of Pb into a central (diffusible blood plasma) compartment, transfers of Pb between the central compartment and various tissues, and transfers of Pb to excreta. Absorption of Pb from the respiratory tract is simulated as a first-order process governed by rate coefficients (d^{-1}) for absorption from each of four respiratory tract compartments. Absorption from the gastrointestinal tract is simulated as a first-order process governed by age-dependent absorption fractions and first-order rate coefficients for transfers of Pb within the gastrointestinal tract. Rates of absorption from inhaled and ingested Pb are summed to yield a total rate of transfer (µg Pb/day) to the central plasma compartment; these rates include Pb absorbed from intakes from exposures as well as Pb transferred to the gastrointestinal tract from the respiratory tract (i.e., mucociliary clearance), and from the liver (i.e., biliary secretion). Biokinetics model output variables are tissue Pb masses and concentrations, and Pb masses in excreta corresponding to the exposure and absorption scenarios constructed in the exposure and absorption models. Tissues represented in the model include red blood cells and blood plasma (including a pool of Pb in plasma that is bound to proteins), brain, cortical and trabecular bone, kidney, liver, and other soft tissues. Distinct excretory pathways represented in the model include feces, urine, sweat, and other routes (e.g., hair and nails, exfoliated skin). Transfers of Pb between compartments are simulated as first-order processes governed by first-order rate coefficients (d^{-1}) that are scaled for age.

The AALM architecture consists of two components: (1) an Excel workbook (*AALM.xlsm*)[1] that implements the exposure model and provides user access to all exposure and biokinetics parameters in the Fortran code; (2) a Fortran executable program that implements the biokinetics model. Input parameter values are selected by the user in *AALM.xlsm*. Macros pass the input parameter values to a comma-delimited (CSV) text file (*LeggettInput.txt*) which are imported into the AALM Fortran program. Output variables from the simulation are passed back via multiple CSV files which are read into the *AALM.xlsm* file with Excel macros.

AALM Fortran inputs and outputs are controlled and recorded in *AALM.xlsm* workbook. This workbook has several functions: (1) allows setting of input parameter values for AALM.FOR simulations; (2) macros in this workbook are used to pass data to and from Fortran; (3) allows plotting of AALM Fortran output data; and (4) provides a complete record of input values and results of each AALM Fortran simulation. Worksheets in *AALM.xlsm* allow the user to set exposure scenarios for Pb in air (*Air*), food (*Food*), indoor dust, (*Dust*), soil (*Soil*), drinking water (*Water*), and/or other ingestion intakes (*other*). Exposures can be discrete (i.e., a series of exposures at selected ages), and/or pulsed in a repeating frequency (e.g., 2 days/week for 3 months/year, for a selected age range). The AALM Fortran executable uses inputs from all exposure media when it creates biokinetics simulations. This allows construction of complex multi-pathway exposure scenarios having varying temporal patterns. Worksheets in *AALM.xlsm* also allow the user to set values for parameters that control Pb absorption and relative bioavailability in

[1] The User Interface typically includes a release date in the filename but is simply listed herein as "AALM.xlsm" where "xlsm" indicates it is a macro-enabled Excel workbook.

individual exposure media (*RBA*), and biokinetics (*Lung*, *Systemic*, *Sex*). All settings are recorded in the *AALM.xlsm* workbook and can be recalled to re-run the simulation.

2.2. EXPOSURE MODEL

2.2.1. General Structure of the Exposure Model

The exposure model of the AALM Fortran executable calculates rates of Pb intake from ingestion and inhalation pathways, for a hypothetical individual (subject) based on inputs for inhalation exposure to Pb in air, ingestion of Pb in food and water, incidental ingestion of Pb in indoor dust and soil, and from miscellaneous ingestion intakes (designated in the model as *other*). Intakes (μg Pb/day) derived from the exposure model are passed to the biokinetics model and provide the bases for calculating Pb masses in tissues and excreta for each age day simulated.

A list of all equations used in the code to calculate Pb intakes are presented in standard form in Table 2-1, and as they appear in the Fortran code in Appendix A. The parameters used in these equations are defined in Appendix C.

The Fortran code for the AALM v3.0 consists of two sections, for exposure and biokinetics. The first section reads the inputs and constructs timeseries for each exposure variable and time-varying physiological variable, for the entire simulation. The 64-bit version can handle a few hundred timesteps per day for a lifetime (potentially over 10 million timesteps). The 32-bit version can handle up to 12 timesteps per day for a lifetime, or more timesteps per day for a shorter simulation. The variables may change either in stepwise fashion (jumping to a new value at a given age) or else interpolated linearly between specified ages. At this stage, daily intakes are converted to intakes per timestep. The same timestep is used for the duration of the simulation.

The AALM v3.0 can handle up to 3 sources for each of 6 media: air, dust, soil, water, food, and other.[2] Up to the point of absorption into the blood, the Pb from each of these sources is tracked separately with its own mass-balance accounting. The mass-balance is applied to the sum over all sources, including all body compartments and excreta. Daily intake amounts by source (and total) are reported on the output file with the prefix "day_" followed by the run name, along with daily uptakes (into the blood) and daily losses. Up to 20 exposures at specific ages may be specified under either the stepwise or interpolated methods. In the latter case, these are the ages at which the linear interpolation changes slope.

Optionally, any or all sources may be subject to periodic masking if the user sets it. Each mask consists of 4 parameters, a source, period, first day masked, and last day masked. For example, the source might be dust source #2. The period is the number of days for the mask to repeat. The most common values are 7 (weekly repetition) or 365 (yearly repetition). Multiple masks may be applied to the same source, for example, weekly and yearly masks can be combined to create an exposure pattern only on certain days of the week during one season. When any mask is "on", it blocks that source. When not masked, the source has the same value as if no masks were present. Masks may be used with either stepwise or interpolated sources. The AALM User Guide should be consulted for specific examples of how this functionality is implemented in the Excel User Interface.

[2] The AALM v2.0 only allowed for one source per media. The AALM v2.0 only tracked the mass-balance of bioavailable Pb.

2.2.2. Parameters That Define a Hypothetical Individual

Age: There are two different time intervals in the code: the timestep and the day. There are always a whole number of timesteps in a day. Inputs such as sources are indexed by day number, with age=0 representing birth. Simulations begin on a user-specified birthday (e.g., age 10 years). The user interface measures age in years, defined as 365 days. In the example, timestep 0 corresponds to the start of the simulation which is the end of day 3650, and timestep 1 becomes the first of day 3651. The user also specifies the stopping age for the simulation (another birthday).

Sex: The sex specification links the subject to an appropriate sex-specific growth algorithm (O'Flaherty, 1995, 1993) described in Section 3.5.2.

Fetal Exposure: If the AALM.FOR simulation begins at birth, the neonatal tissue Pb masses assigned values based on the user-designated maternal blood Pb, as described in Section 2.3.11.

Physiology: The physiological variables are divided into two groups on separate tabs of the Excel interface: those constant in time and those that vary with age. For the latter, the user specifies a list of selected ages at which each time-varying physiological variable is to be specified in Excel. These values are passed to the Fortran code and are then interpolated to every timestep.

2.2.3 The AALM Fortran "front end" or exposure code

The exposure section of the code is also called the "front end" and it serves two functions. First, it evaluates the intake rate for each of the source subtypes on every timestep of the simulation. Second, it evaluates all the time-varying physiology including age-dependent compartmental loss rate constants on every simulation timestep. These steps are vectorized resulting in fast evaluation. It also helps with code QA/QC to be able to examine the timeseries separately from the biokinetic portion of the code to localize any possible errors or problems. As an example, for one million timesteps, the front end completes its task in about 10 seconds.

The general form of the equations for calculating Pb intakes from Pb concentrations is given in Equation 2.2-1 for air, dust, soil, or water:

$$IN_j = Pb_j \cdot f_j \cdot IR_{medium} \cdot M_{j1} \cdot M_{j2} \ldots / N \qquad \text{Eq. (2.2-1)}$$

where IN_j is the timeseries of Pb intake rate (µg Pb/timestep) for a specific environmental source j in a specific medium (e.g., one water source), Pb_j is the Pb concentration (e.g., µg Pb/L water) in that medium, f_j is the fraction of total intake of the medium for that source, IR_{medium} is the intake rate of the medium (e.g., L water/day), and N is the number of timesteps per day. The parameters Pb_j, f_j and IR_{medium} can be assigned age-dependent values through the interface, and furthermore, periodic masking (the M_{j1} and M_{j2}, etc.) may be applied. The details are as follows.

Age-dependent variables such as Pb_j, f_j and IR_{medium} can be specified at user-selected ages in the Excel interface. Up to 20 ages may be used, although 5-10 are more typical. The ages for concentration Pb_j values may be specified separately from those used for intake (the other two variables). To evaluate the variables between the specified ages, the user selects either the *stepwise* or *interpolation* options.

The stepwise option means that each age-specific value remains in effect (as a constant) until the next specified age is reached. If the first specified age is greater than the starting simulation age, that value is extended back to the simulation start. If a source of zero is desired at the start, specify that directly at the start age. This method has the advantage of being easy to understand, and the resulting values are straightforward to check.

The interpolation option connects all the age-specific values using piecewise linear interpolation. The timeseries all appear to be continuous, although technically these are also stepwise at the timestep level, since the model assumes all inputs are unchanging over each timestep but can jump to another value at the next timestep. With potentially a million timesteps or more in a simulation, the changes per timestep are extremely small when using interpolation. Like the stepwise method, if the simulation period extends beyond the specified ages at which values are given, the value at the first (or last) specified age is used. For example, suppose two ages are used for some variable, with the value set to 3 at age 1 and to 4 at age 11. If the simulation runs from birth to age 15, then the value of 3 is used from birth to age 1 year (for 12 months), then a linear increase at a rate of 0.1 per year until age 11, then it remains at 4 from age 11 to 15. In this method the slope can change at each specified age.

The three variables Pb_j, f_j and IR_{medium} in 2.2-1 are filled in separately, whether stepwise or interpolation is used (the same choice of method applies to all media). In the case of the source fractions f_j there is an additional constraint: the fractions must sum to one for each media. If there are N source subtypes for that medium (N can range from 1 to 3 unless that medium is not used) then the first (N-1) are read from the input file, then filled in either stepwise or interpolated, then the fraction for source N is set to one minus the sum of the others on each timestep.

If masks are used, these are also filled in on every simulation timestep. Each mask is periodic with a source number *j*, a period, a start day, and end day. The start and end days cannot exceed the period. Within each period from the start day to the end day (inclusive) the mask has a value of zero, otherwise it is one. This pattern is repeated each period until the simulation ends. This creates a daily timeseries for the mask, which is converted to a timestep timeseries, then all the timeseries are multiplied together. Multiple masks may be applied to the same source so, for example, it is possible to create weekly periodic patterns for selected times of the year (another mask with an annual period). Note that masks may be used with either stepwise or interpolated sources, and the source may vary over time when it is not being masked.

Equation 2.2-1 is used to obtain the source *j* intake IN_{j} on every timestep. Again, this is very fast because the different timesteps do not affect each other computationally and all timesteps may be evaluated using vectorized code, that is, equation 2.2-1 is applied effectively in parallel to the values on each timestep.

For food and other sources, the above method is modified. Basically, the medium contact rate and the fractions are wrapped into the Pb concentration term as

$$IN_{\mathrm{j}} = Pb_j \cdot \mathrm{M}_{j1} \cdot \mathrm{M}_{j2} \ldots / \mathrm{N} \qquad \text{Eq. (2.2-2)}$$

Here Pb_j has units of (µg Pb/day) while IN_j is in (µg Pb/timestep). For food, a variety of foods are eaten each day with very different Pb content. It is beyond the scope of this model to categorize hundreds of foods, so a combined Pb intake must be specified. The same logic applies to the other source category because it is a catch-all for everything not otherwise specified, and the details of how such sources may be subdivided are outside the scope of this model.

Even without masks and with N=1, Equation 2.2-2 is more than just an identity operation, because Pb_j is specified in the interface only at selected ages. By contrast, IN_j is a timeseries with a value on every simulation timestep. In between the specified ages (where 2.2-2 applies exactly), the values are calculated using either the stepwise or interpolation logic. Any masks applied to "food" or "other" will use the same logic as masks for the other four media types.

Equations used in the AALM to calculate Pb inhalation and ingestion intake rates are presented in Tables 2-1 and 2-2 and in Appendix A and parameters are defined in Appendix C. The tables present the equations in symbolic form whereas Appendix A presents them as they appear in the Fortran code. For readability, tables are provided at the end of this chapter and appendices are provided at the end of the document.

As is the case for the source intakes, the front end also computes a full simulation timeseries for all the time-varying physiology, including growth variables (body and organ weights and volumes), and age-dependent deposition fractions and rate constants. The term "constants" is used here because these determine the rates of first-order loss processes (that is, exponential rate constants). These are taken to be constants within each timestep, although they can have different values on other timesteps. For these physiological variables interpolation is always used; there is no stepwise method available because the human body does not generally change abruptly (unlike source strengths).

2.3. BIOKINETICS

2.3.1. Computational Structure of the AALM Biokinetics Model

The biological model is a compartmental flow model with time-integrated outflow calculated on each timestep for each compartment. This time integration assumes first-order rate loss constants fixed for the duration of each timestep. Intakes to each compartment are assumed to be uniform throughout the timestep, whether these are intakes from external sources or flows from other compartments. Under these assumptions the integrated outflow can be computed exactly.

The AALM code reports Pb masses (µg) in tissues for each simulation timestep and it also reports daily summaries of intake, uptake, and excretion. The tissue masses are used to calculate secondary variables such as blood Pb concentration. Lead masses in each biokinetics compartment are computed by stepwise integration applied to a series of differential equations that represent the rate of change in Pb mass in each compartment. The underlying assumptions for flow are:

1) inflows are spread evenly over the timestep on which they occur,
2) outflows are first-order processes proportional to the mass currently in the compartment, with a rate constant that does not change within any timestep.
3) outflows are integrated over each timestep and summarized as a flow (FL) term,

4) if the outflow is divided among multiple destinations, the fraction going to each is proportional to the rate constant for the flow to that destination,

5) outflows are subtracted from the contents of the *from* compartment at the end of each timestep, but they are not added to another compartment until the next timestep.

The last of these assumptions avoids any problems with not knowing inflows on the current timestep until other outflows have been determined, which would lead to a large coupled system of equations. The consequence is that some Pb mass in the body is "in transit", having been subtracted from one compartment but not yet added to another. Therefore, the explicit mass balance calculations must include these flow terms. Inflows and outflows have units of (Pb mass/timestep).

The general form of the differential equations used in the biokinetics model is as follows (Equation 2.3-1) for all compartments:

$$\frac{dY_j}{dt} = -R_j \cdot Y_j(\mathrm{t}) + P_j \qquad \text{Eq. (2.3-1)}$$

where dY_j/dt is the rate of change in Pb mass in compartment j with time (e.g., the derivative, units of µg/day), R_j is the first-order rate constant for Pb leaving the compartment (units of 1/day), Y_j(t) is the Pb mass (µg) at time t, and P_j is the rate of transfer of Pb into compartment j (µg Pb/day). Initial compartmental Pb masses at the start of the simulation are supported in the Fortran code but currently the interface supplies them only for simulations starting at birth.

Equation 2.3-1 is solved for each state variable (e.g., compartment) on each timestep. All compartments are evaluated on the current timestep before proceeding to the next timestep. Assuming R_j and P_j remain constant for any compartment j over the timestep, then the following equation (2.3-2) is an exact solution at any subsequent time (Leggett, 1993; Leggett et al., 1993):

$$\mathrm{Y}(t + \Delta t) = \left(\mathrm{Y(t)} - \frac{P}{R}\right) e^{-\mathrm{R}\,\Delta t} + \frac{\mathrm{P}}{R} \qquad \text{Eq. (2.3-2)}$$

Let Y(t) be the compartmental Pb mass at the start of a timestep of length Δt. Then $\mathrm{Y}(t + \Delta t)$ is the corresponding mass at the end of that time step. The original Leggett code computed the time-integrated Pb mass in each compartment (*YINT*) at each time step using (Equation 2.3-3):

$$YINT(t + \Delta t) = \left(Y(t) - \frac{P}{R}\right) \cdot \frac{1 - e^{-R\,\Delta t}}{R} + \frac{\mathrm{P}\,\Delta t}{R} \qquad \text{Eq. (2.3-3)}$$

The current code (i.e., AALM v3.0 versus v2.0) does not directly use this approach anymore, as it has been replaced by a "flow" variable that represents the Pb mass lost from the compartment on each timestep. By mass conservation, this flow must be (Equation 2.3-4):

$$\mathrm{FL}(t+\Delta t) = \mathrm{Y(t)} + P\,\Delta t - Y(t+\Delta t) \qquad \text{Eq. (2.3-4)}$$

Basically, the compartment starts with Pb mass Y(t) and the total inflow over the timestep is $P\Delta t$. This must equal the amount remaining in the compartment at the end, plus the total outflow. Equation 2.3-4 therefore enforces mass balance. On the next timestep (always of the same size Δt), this flow becomes the inflow to the downstream compartment. Since the inflow variable P is a flow rate (as opposed to a mass), the P for the downstream compartment on the next timestep is:

$$\mathrm{P}(t+\Delta t) = \mathrm{FL}(t+\Delta t)/\Delta t \qquad \text{Eq. (2.3-5)}$$

If the outflow from a compartment is divided among multiple destination compartments, then the flow is allocated proportionally to each destination, based on the ratio of intercompartmental flow rate variables. For example, with the outflow divided between two destinations with relative flow rates of 2 and 1, the first destination receives twice that of the second (that is, 2/3 of the outflow goes to the first destination, with 1/3 going to the second destination).

It is easily verified by combining equations 2.3-2 through 2.3-4 that the new FL variables are equivalent to the old Leggett code variables of the form (YINT · R) which were used in place of P Δt. However, the new FL variables are simpler to calculate and simpler to use and are subject to less rounding error when checking mass balance.

As a practical matter, the flow masses (FL variables) are subtracted from each compartment at the end of each timestep, but they are not added to the downstream compartments until the next timestep. This avoids the need for finding iterative solutions. When calculating the total mass of Pb in the body (for mass balance calculations) it is necessary to sum all the compartmental Pb mass plus all the intercompartmental flows (that is, all the Y variables plus all the FL variables).

2.3.2. Compartment Structure of the AALM.FOR Biokinetics Model

The structure of the AALM.FOR biokinetics model is derived from the Leggett (1993) model. The model includes a central exchange compartment (diffusible blood plasma), 4 lung compartments, 26 other body compartments, and 4 elimination pools. The central exchange compartment is named "PLAS" and represents the *diffusible* Pb in plasma, distinguished from a *bound* pool "PROT" in plasma representing Pb bound to plasma proteins. Lead is absorbed from the gastrointestinal tract and/or respiratory tract into PLAS. From here the Pb may travel to bone, brain, kidney, liver, red blood cells (RBC), and other soft tissues. Absorbed Pb is excreted in urine, sweat, and in a combined pathway "hair" representing hair, nails, and exfoliated skin. Unabsorbed ingested Pb is excreted in feces along with a fraction of absorbed Pb transferred to the gastrointestinal tract from diffusible plasma and liver (i.e., bile pathway). For inhalation, there is effectively a fifth loss pathway because Pb not deposited in the airways is assumed to be exhaled and is quantified for mass balance purposes. Ingestion and inhalation intakes, uptakes into the

plasma, and the five excretion pathways are all summarized daily over the simulation and written to an output file. Default values (see Appendix D) assigned to all parameters in the biokinetics model are intended to represent average values expected in a population of healthy individuals.

Transfers of Pb between compartments are assumed to follow first-order kinetics governed by rate coefficients (d^{-1}), where each rate coefficient represents a fractional Pb loss rate. The computed Pb masses in tissues and tissue masses (g) and/or volumes (dL) are used to calculate Pb concentrations in tissues. A conceptual representation of equations used in the AALM.FOR to calculate Pb masses and concentrations in tissues are presented in Table 2-2. Rate coefficients for exchange among compartments are provided in Table 2-3. A more comprehensive and accurate presentation of the equations as they appear in the code is presented in Appendix A. General concepts that underlie equations used for calculating Pb masses and concentrations are presented in the sections that follow. For readability, tables are provided at the end of this chapter and appendices appear at the end of this document.

2.3.2.1. Deposition Fractions in Lung Compartments

Three of the lung compartments, the extra-thoracic (ET), tracheo-bronchial (TB), and alveolar (ALV) have user-assigned source-specific deposition fractions on the input file. These are applied to the air intake, thus the deposition rate (effective intake) for lung compartment *k* from air source *j* is

$$P_{j\,k}(\mathrm{t}) = \mathrm{IN}_j(\mathrm{t}) \cdot \mathrm{Dep}_k \qquad \text{Eq. (2.3-6)}$$

The inhalation intake timeseries for source j is $\mathrm{IN}_j(\mathrm{t})$ and it has units of (µg Pb/timestep), as does $P_{j\,k}(\mathrm{t})$. The three deposition fractions Dep_k are unitless, constant over the simulation, and sum to 0.40 based on Leggett (1993) as further discussed in Section 2.3.3.1. The remaining 0.60 is assumed to be exhaled. The difference between the air intake and the lung deposition is recorded and daily sums of both are reported on the "day_" output file. The interstitial compartment (Int) is the fourth lung compartment, but it always has a deposition fraction of zero. It can receive Pb from ALV and can pass Pb to PLAS.

2.3.2.2. Losses from the Plasma Compartment

The outflow from the diffusible plasma compartment PLAS is split among 15 other compartments. The destination compartments are assigned deposition fractions with the prefix T (for example, TOKDN1 for kidney compartment #1). These T variables should sum to one, approximately. The transfer rate from the central compartment to compartment j is:

$$R_{PLAS\to j} = T_{PLAS\to j} \cdot RPLAS \qquad \text{Eq. (2.3-7)}$$

where $R_{PLAS\to j}$ is the flow rate coefficient from diffusible plasma to compartment *j* (d^{-1}), $T_{PLAS\to j}$ is the plasma deposition fraction for compartment *j*, and *RPLAS* is the rate coefficient for transfer of Pb from diffusible plasma to all receiving compartments (with default value 2000 d^{-1}). The actual Pb loss from the plasma is given by the sum of the $R_{PLAS\to j}$ over all the compartments j. This may differ from RPLAS if the fractions do not sum to one. Note that the deposition fraction variables on the input file

generally have the prefix "TO", but the ones in equation 2.3-7 have prefix "T". The distinction is due to certain adjustments described in the next section.

2.3.2.3. Age Scaling of Rate Coefficients and Deposition Fractions

Values for deposition fractions and rate coefficients are age-dependent and are assigned values for specific ages. Values between ages are interpolated. The input values for deposition fractions from diffusible plasma (designated with the prefix TO; e.g., TOBONE) are scaled in the biokinetics model to account for two factors: (1) growth of bone surface area and resulting age-dependence of deposition of Pb to bone surface, which changes the deposition fractions to other tissues; and (2) non-linear uptake of Pb from diffusible plasma to RBCs, which changes the RBC deposition fraction as the RBC Pb concentration increases. Scaled deposition fractions designated with the prefix *T* (e.g., TBONE). An age adjustment (*AGESCL*) restrains the deposition fractions (and total outflow) from diffusible plasma to soft tissues to the fraction not deposited to extravascular fluid (TEVF) or bone (TBONE). The age adjustment for bone surface takes the form (Equations 2.3-8 and 2.3-9):

$$AGESCL = \frac{1-TEVF-TBONE}{1-TEVF-TBONEL} \qquad \text{Eq. (2.3-8)}$$

Since as listed in Table D-1, TEVF = 0.5 and TBONEL=0.08, Eq. 2.3-8 can be reduced to:

$$AGESCL = \frac{0.50-TBONE}{0.42}$$

$$T_{PLAS\rightarrow j} = AGESCL \cdot TO_{PLAS\rightarrow j} \qquad \text{Eq. (2.3-9)}$$

Here *TEVF* is the deposition fraction to the extravascular fluid (see description of central compartment and bone Pb kinetics), *TBONE* is the deposition fraction to bone surface (see Table D-1), and *TBONEL* is the limiting adult value for the bone deposition fraction (as defined in Time Dependent Parameters for 25 years and greater). The variable $TO_{PLAS\rightarrow j}$ is the input value for the deposition fraction from diffusible plasma to compartment *j*, before adjustment for bone surface area. For example, at 1 year of age, AGESCL is 0.8476 (i.e., [0.50 – 0.144] / 0.42), where TBONE was obtained from Table D-1. Thus, the age-independent input value for TORBC (the deposition fraction from plasma to RBC) of 0.25 is age adjusted by multiplying by AGESCL so that the age-adjusted deposition fraction from plasma to RBC is 0.212 at 1 year. This adjustment (i.e., multiplication by AGESCL) is done for age-independent user inputs of TOFECE, TOKDN1, TOKDN2, TOLVR1, TORBC, TOPROT, TOSWET, and TOURIN. Although TOBRAN, TOSOF0, TOSOF1, and TOSOF2 are age-scaled deposition fractions, they are also further age adjusted by multiplication with AGESCL. This is all the plasma loss terms except for TBONE and TEVF.

Uptake of Pb into RBCs is simulated as a capacity-limited process, in which the deposition fraction to RBCs (*TRBC*) decreases with increasing RBC Pb concentration above a limiting threshold (see description of RBC compartment in Section 2.3.4.3). The decrease in RBC deposition fraction as the RBC concentration approaches the limiting value results in greater Pb available for deposition to other

tissues. This change is accounted for in the model by adjusting the deposition fractions to other tissues by the factor *CF* (Equation 2.3-10):

$$CF = \frac{1-TOORBC}{1-TRBC} \qquad \text{Eq. (2.3-10)}$$

where TRBC is the deposition fraction to RBCs below the limiting RBC Pb concentration, and TOORBC is the deposition fraction to RBCs above the limiting RBC Pb concentration. The adjustment factor, CF, increases as the RBC Pb concentration approaches saturation, and deposition fractions to other tissues (TOPLAS→j) are proportionately increased. Note that CF may differ on each timestep and is the only time-varying flow variable that is not calculated in advance (in the first stage of the Fortran code).

Once the outflow from the plasma has been apportioned as in 2.3-7, the Pb losses from the plasma are apportioned into the corresponding FL variables, which are the masses being transferred on that timestep from the plasma to each of the 15 destination compartments.

2.3.2.4. Growth of Blood and Tissues for Calculation of Pb Concentrations

The AALM biokinetics equations are used to compute Pb masses in each tissue compartment. Concentrations of Pb in selected tissues are calculated as the quotient of Pb mass and tissue volumes (e.g., dL blood) or masses (e.g., g kidney, cortical bone, trabecular bone, skeleton). Tissue volumes and masses are calculated based on growth equations and parameters from O'Flaherty's studies (O'Flaherty, 1995, 1993) (see Table 2-1 Equations D1–D10). Tissue volumes and masses are functions of body weight (Equation 2.3-11):

$$WBODY = WBIRTH + \frac{WCHILD \cdot AGEYEAR}{HALF + AGEYEAR} + \frac{WADULT}{1 + KAPPA \cdot e^{-LAMBDA \cdot WADULT \cdot AGEYEAR}} \qquad \text{Eq. (2.3-11)}$$

Each of the variables (except AGEYEAR, which is computed) on the right-hand-side of 2.3-11 may be altered in the Excel interface. Equation 2.3-11 calculates body weight as the sum of three growth phases: (1) pre-natal which achieves birth weight; (2) rapid (hyperbolic) post-natal growth that occurs before age 10 years; and (3) logistic growth beginning at puberty and continuing into early adulthood. *WBODY* is the body weight at any given age (*AGEYEAR*), *WBIRTH* is the body weight at birth, *WCHILD* is the maximum body weight gain achieved during early hyperbolic growth phase, *HALF* is the age at which body weight is one half of *WCHILD*, *WADULT* is the maximum adult body weight gain achieved during logistic growth, and *KAPPA* and *LAMBDA* are empirically derived logistic parameters. The resulting maximum body weight in achieved during the lifetime adulthood is the sum of WBIRTH, WCHILD and WADULT; 56.5 kg for females and 76.5 kg for males. The body weight parameters enable simulation of different growth patterns within each growth phase, including distinct patterns for males and females. The growth simulations are show in in Figure 2-2. Note the parameter values in the body growth equation represent body weight growth patterns observed in human populations at the time the parameters were evaluated (O'Flaherty 1993). Alternative parameter values can be adopted to simulate other growth patterns of interest (e.g., modern body weight growth patterns in the U.S. general population). The effect of these changes on the body weight growth curve can be visualized in the Growth Parameters user

interface of the AALM. If the body weight growth parameters are modified, consideration should also be given to re-examining the equations that simulate the body weight-dependent growth of volumes of other tissues (e.g., bone, liver, kidney). For example, volumes of some tissues may correlate more strongly with lean body mass than with total body weight including adipose. More recent increases in average body weight in the United States derive primarily from increased body fat rather than increased average lean body mass (Hales et al. 2020).

Volume growth of blood (*AMTBLD*) is a linear function of body weight (Equation 2.3-12):

$$AMTBLD = VBLC \cdot WBODY \cdot 10 \qquad \text{Eq. (2.3-12)}$$

Here *VBLC* is the blood volume (in dL) expressed as a fraction of body weight (*WBODY*). VBLC is the ratio in (L/kg) and the factor of 10 converts from liters to deciliters.

Plasma and RBC volumes are functions of blood volume and age-dependent hematocrit (*BLDHCT*). The latter is modelled using two input variables: HCTB (hematocrit at birth) and HCTA (adult hematocrit). The age dependence is given by Equation 2.3-13:

$$BLDHCT(AGEYEAR) = HCTB + (HCTA - HCTB)\ Exp(-13.9\ AGEYEAR) \qquad \text{Eq. (2.3-13)}$$

BLDHCT represents the volume fraction of the blood that is red blood cells (RBC), while the remainder (the fraction 1-BLDHCT) is plasma. Volume growth of kidney (*VK*) and liver (*VL*) are power functions of body weight (Equations 2.3-14 and 2.3-15).

$$KIDWT = 1050 \cdot VKC \cdot (WBIRTH + WADULT + WCHILD) \cdot \left(\frac{WBODY}{WBIRTH+WADULT+WCHILD}\right)^{0.84} \qquad \text{Eq. (2.3-14)}$$

$$LIVWT = 1050 \cdot VLC \cdot (WBIRTH + WADULT + WCHILD) \cdot \left(\frac{WBODY}{WBIRTH+WADULT+WCHILD}\right)^{0.85} \qquad \text{Eq. (2.3-15)}$$

Here *VKC* and *VLC* are volume ratios in units of (L/kg) to body weight (*WBODY*). These are not linear in body weight, but instead use the above regressions on the growth equation parameters. Kidney and liver weights (*KIDWT*, *LIVWT*) are in grams and each equation includes a factor of 1050 g/L which represents tissue density.

The growth of bone volume (*VBONE)* and weight (WBONE) are calculated as a power functions of body weight, with cortical bone volume (*CVBONE*) assigned 0.8 of total bone volume (VBONE, Equations 2.3-16 to 2.3-18), and trabecular bone volume (TVBONE) is the remainder. The factor of 1000 converts from kg to grams.

$$WBONE = 1000 \cdot 0.0290 \cdot WBODY^{1.21} \quad \text{Eq. (2.3-16)}$$

$$VBONE = 1000 \cdot 0.0168 \cdot WBODY^{1.188} \quad \text{Eq. (2.3-17)}$$

$$CVBONE = 0.8 \cdot VBONE \quad \text{Eq. (2.3-18)}$$

Similarly, cortical bone is assumed to comprise 80% of total bone weight, while trabecular bone accounts for the other 20%. The masses and volumes of compartments are age-dependent which means that small changes occur on every timestep. Like other physiological variables, these are evaluated in the Fortran "front-end" because that process can be vectorized over timesteps and therefore becomes very fast. The older Leggett code updated these variables on each timestep. The downside to vectorization is that is requires more memory, but that is not an issue in modern computers.

Because the compartmental masses and volumes do not remain fixed, it would be problematic to use Pb concentrations in the flow equations. The biokinetic model uses Pb mass exclusively, although outflow rates R may be specified as age-dependent to account for changes in the organs. The code solves for the compartmental Pb mass over the entire simulation, then calculates the relevant Pb concentrations when preparing the output files by dividing by the appropriate volumes.

2.3.2.5. Age Dependencies of Parameter Values

Biokinetics parameters that are assumed to change with age are assigned values for specific ages. These assignments are made as arrays of parameter values and corresponding ages (year), beginning with birth (age = 0 years). The Excel tab "Time Dep Phys Params" summarizes these inputs. Parameter values at timesteps between the designated ages are calculated by linear interpolation in the Fortran front end.

2.3.3. Absorption

The AALM model simulates Pb absorption from inhalation and ingestion. In the AALM, absorption represents the transfer of Pb intake (µg Pb intake/day), computed in the exposure model, to a rate of entry of Pb into the diffusible plasma compartment of the biokinetics model (µg Pb absorbed/day). Absorption from each exposure pathway is simulated as a first-order processes governed by absorption fractions and/or first-order rate coefficients (d^{-1}).

Each of the (up to) 18 source subtypes is given its own relative bioavailability (RBA), which reflects the gut absorption rate relative to Pb in water. For the lung compartments, each air subtype is also given its own absorption rate constants for direct uptake into the blood plasma. Some of the inhaled Pb may be transferred to the GI tract by mucociliary transport (see next section), after which the RBA values for air become relevant.

2.3.3.1. Absorption from the Respiratory Tract

The respiratory tract is simulated as three compartments (ET, TB, and ALV) into which inhaled Pb is deposited and from which Pb is absorbed into the diffusible plasma compartment. A fourth respiratory tract compartment, the interstitium, can only receive material that is deposited in the ALV region and subsequently cleared to the interstitium. In the AALM v3.0, Pb deposition and absorption are assigned the following values:

Compartment	ET	TB	ALV
Deposition Fraction (unitless)	0.200	0.159	0.040
Rate Coefficient (day^{-1})	7.68	1.94	0.347
$t_{1/2}$ (hour)	2.17	8.58	47.9

The division of the respiratory tract into these three regions (or compartments) is intended to facilitate the future use of deposition fractions calculated using the Multi-Path Particle Dosimetry model (MPPD; Version 3.04, ©2016) or a subsequent version.[3] This capability will allow the AALM to be applied to a wide range of inhalation exposure scenarios including exposure to resuspended dusts in the ambient environment and exposures in occupational settings.

In the AALM v3.0, however, the three-compartment model simulates the multi-phase absorption kinetics of inhaled Pb observed in studies of human exposures to Pb particulates as described by Leggett (1993). The elimination of Pb from the lungs into the blood was described by Leggett (1993) as a four-compartment exponential decay (fraction, half-time; 0.20, 1 hr; 0.35, 3 hr; 0.35, 9 hr; and 0.10, 48 hr). Herein, it is simulated by a three-compartment exponential decay (fraction, half-time; 0.50, 2.17 hr; 0.40, 8.58 hr; 0.10, 47.9 hr) with a goodness of fit of 1.00 between the four-compartment and three-compartment estimations from the time of aerosol inhalation until 160 hours post inhalation when lung retention became less than 1%.[4] In both AALM v2.0 and now in v3.0, the fraction associated with each exponential decay phase is multiplied by 0.40 to obtain the deposition fraction in each lung compartment.

The ET compartment has a deposition fraction and two out flows, to PLAS and stomach compartments, with units of (1/day). The first of these flow rates is the plasma absorption rate from the ET compartment and the second represents mucociliary transport. The TB also has a deposition fraction and two flows, to PLAS and to the ET compartments. The ALV compartment has a deposition fraction and three flows: to PLAS, TB, and to the interstitial (INT) compartment. The INT compartment has zero deposition from air and has one outflow rate, to PLAS, which at this time in AALM v3.0 is set zero as placeholder for a rate to be entered in a future version of the AALM. All these variables (three deposition fractions and eight outflow rate constants) may be specified separately for each of the 3 air source subtypes. The logic is that these subtypes may have distinct particle size distributions, and the larger particles take longer to disintegrate and thus lower flow rates. At this time in AALM v3.0, the default exchanges among respiratory compartments are set zero as placeholders for exchange rates among lung compartments to be entered in a future release.

[3] The MPPD model can be used to calculate particle deposition and clearance in multiple species. A description of the model, recent model improvements, and advancements incorporated into the MPPD model are provided by Miller et al. (2016). For additional information about the MPPD model (Version 3.04) or to obtain a copy, the reader is referred to: http://www.ara.com/products/mppd.htm.

[4] The goodness of fit was calculated as one minus the model sum of squares error (SSE) divided by the total sum of squares (SSY). The SSE equals the residual sum of squares (i.e., the sum of squared original [4-compartment] minus new [3-comparment] estimated values). The SSY equals the total sum of squares (i.e., the sum of squared original values minus average of original values).

The lung absorption/elimination kinetics of Leggett (1993) were based largely on the Chamberlain et al. (1978) study of human subjects inhaling clean (not excessively carbonaceous due to a fuel rich mixture) automotive exhaust from combustion of fuel containing ^{203}Pb-labeled tetraethyllead. As such, the original Leggett (1993) lung kinetics and those used in both AALM v2.0 and v3.0 are most appropriate for airborne Pb prior to the phase-out of leaded gasoline, in part, because the size of airborne Pb has shifted from <2.5 µm prior to the phase-out of leaded gasoline to somewhere between 2.5 µm and 10 µm after the phase-out (Cho et al., 2011). It is anticipated that a future version of the AALM will offer lung kinetics based on the form and size of inhaled Pb particulates.

2.3.3.2. Absorption from the Gastrointestinal Tract

In AALM.FOR, the gastrointestinal tract is simulated as four compartments representing: (1) stomach contents (STOM); (2) small intestine contents (SIC); (3) upper large intestine contents (ULIC); and (4) lower large intestine contents (LLIC). Intake for each Pb ingestion source (see Equation C1 in Table 2-1) enters the stomach and is passed, in series, to the small intestine, upper large intestine, lower large intestine, and feces at rates represented by first-order rate coefficients. Absorption of Pb from the gastrointestinal tract is assumed to occur in the small intestine. It is represented by an absorption fraction (*AF1*), representing the fraction of Pb mass in the small intestine that is transferred to the diffusible plasma compartment. Each of the above rates and variables is repeated for each source. For the gut absorption, the user may choose to implement data from Equation 2.3-19 based on an expression from O'Flaherty's studies (O'Flaherty, 1995, 1993):

$$\mathrm{F1}(\mathrm{AGE}_{YEAR}) = AF_{C1} - \frac{AF_{C2}}{1+30 \cdot \mathrm{Exp}(-AGE_{YEAR})} \qquad \text{Eq. (2.3-19)}$$

Values for AF_{C1} and AF_{C2} were assigned values of 0.4 and 0.28, respectively based on fitting simulations to data on blood Pb concentration in children (Sherlock and Quinn, 1986; Ryu et al., 1983) and adults (Rabinowitz et al., 1976) who ingested Pb in formula or food, respectively, as described in Chapter 4. These parameter values produce a decrease in the absorption fraction from a value of 0.39 at birth to a value of 0.12 at age 8 years (Figure 2-3). This age pattern of higher absorption fraction in infants and children is generally consistent with observations made in mass balance studies in infants and children (Ziegler et al., 1978; Alexander et al., 1974) and in isotope studies of Pb absorption in adults (Watson et al., 1986; James et al., 1985; Heard and Chamberlain, 1982; Rabinowitz et al., 1980). The adult value for the absorption fraction (12%) is close to estimates for soluble Pb from a human pharmacokinetics study, which ranged from 6 to 11% [Rabinowitz et al. (1976); see Figure 3.10]. The AALM default value for soil Pb RBA is 60% which yields an absorption fraction for soil Pb of 7% (i.e., 0.12 × 60% = 7.2%) in adults. This value is close to an estimate of the meal-weighted absorption fraction for soil Pb of approximately 8.4% (Maddaloni et al., 2005), based on results of a soil ingestion study in which a small group of adults ingested a soil collected from the Bunker Hill (Idaho) site which has been shown to have an average Pb RBA of approximately 66% (von Lindern et al., 2016).

Rate equations describing the rates of change of Pb mass (µg) in gastrointestinal tract contents are presented in Table 2-2 (Equations E1–E12).

In addition to intake of Pb from ingestion of environmental media, the stomach also receives Pb from the respiratory tract (i.e., mucociliary clearance). This amount equals the Pb mass lost from the extra-thoracic compartment via flow to the stomach.

The small intestine receives Pb from the stomach as well as from liver (i.e., biliary secretion) and diffusible plasma (Table 2-2 Equation E3). The liver is divided into two compartments, LVR1 and LVR2. The former divides its outflow among 3 compartments: LVR2, the plasma, and the small intestine, governed by the fractions H1toH2, H1toBL, and H1TOSI, which must sum to one. The small intestine is one of the 15 compartments that receives Pb from the diffusible plasma, with its rate determined by the physiological constant TOFECE.

Given that the fraction of the loss from the small intestine that is absorbed into the diffusible plasma is AF1, the remaining fraction (1-AF1) goes to the upper large intestine. The fraction AF1 is source and age dependent. The age dependence comes from that of the variable F1 on the time-varying physiology tab of the interface. The source dependence comes from the RBA values.

$$AF1_j(\mathrm{t}) = \mathrm{F1(t)} \cdot \mathrm{RBA}_j \qquad \text{Eq. (2.3-20)}$$

The RBA_j may be set separately for each source subtype *j*, including air (where it affects only the inhaled Pb subject to mucociliary transport into the GI tract). If the age dependence in 2.3-19 is to be implemented, it should be applied to F1(t) in the user interface, as it is no longer hard-coded. That is one of the time-dependent physiological variables, all of which are evaluated at the same set of ages. All these variables are linearly interpolated between the specified ages.

The Pb masses from the 3 air subtypes are tracked throughout the lungs until they are absorbed into the plasma. The 18 subtypes are tracked throughout the GI tract, up to and including fecal elimination, but they are combined once absorption into the plasma has occurred. It is necessary to keep the Pb masses separate to be able to apply the differing RBA_j to each source when calculating absorption.

2.3.4. Vascular and Extravascular Fluid

2.3.4.1. Diffusible Plasma

The AALM represents Pb in the vasculature as three compartments: (1) diffusible plasma (PLAS); (2) protein-bound plasma (PROT); and (3) red blood cells (RBC). Inflows to PLAS from the small intestine come from up to 18 sources, 3 air sources from each of the 4 lung compartments (12 terms) and 14 other compartments. These are summed together on each timestep to obtain the inflow P. After this point, the contributions of individual sources can no longer be traced, but total Pb mass conservation is still tracked.

The outflows from the diffusible plasma are divided among 15 compartments in the Leggett code: RBC, PROT, small intestine (SI), extra-vascular fluid (EVF), 3 types of soft tissue (SOF0, SOF1, and SOF2), the brain (BRAN), cortical and trabecular bone surfaces (CSUR and TSUR), liver (LVR1), two kidney compartments (KDN1, KDN2), urine (URIN) and sweat (SWET). In the AALM v3.0 the flow directly to the urine is kept at zero, forcing it to pass through the bladder first. Thus, the model has only 14 compartments receiving Pb from PLAS.

The rate coefficient for transfer of Pb from PLAS to all receiving compartments (*RPLAS*) has default value 2000 day^{-1} ($t_{1/2}$≈0.5 min; ln(2)/rate constant), although the user may change it. This is faster than one timestep, but due to the exact integration in equations 2.3-2 through 2.3-4, this does not introduce numerical error. This rate constant is subdivided into deposition fractions that represent the fractions of the total transfer assigned to each receiving compartment C. Deposition fractions change with age. Mass balance is maintained by ensuring that the value for RPLAS used in each time step (RPLS) is adjusted by the sum of the values for each deposition fractions in the same time step (Equation 2.3-21a).

$$RPLS = TSUM \cdot \text{RPLAS} \qquad \text{Eq. (2.3-21a)}$$

The Pb masses transferred are the product of the deposition fraction (T_C), an adjustment factor for variable deposition fraction to RBCs (*CF*, from Equation 2.3-10), and the rate of total outflow of Pb from PLAS (called "outplas") and are given by (Equation 2.3-21b):

$$FL_{PLAS \to C} = T_C(\text{t}) \cdot \text{CF(t)} \cdot outplas \qquad \text{Eq. (2.3-21b)}$$

The $T_C(\text{t})$ are evaluated on every timestep in the front end of the Fortran code, as described in section 2.2. These variables do not depend on the amount of Pb in the body and can be calculated using vector processing. The factor CF(t) does depend on the Pb mass and must be re-evaluated every timestep. Apart from the outputs (Pb masses and flows), CF(t) is the only time-varying quantity that must be evaluated this way.

2.3.4.2. Bound Pb in Plasma

Lead in the bound plasma compartment represents Pb reversibly bound to plasma proteins (PROT). Bound Pb in plasma is confined to the vascular fluid. Reversible binding is simulated as first-order transfers between compartments, with no maximum capacity for binding (Table 2-2, Equation F5). The transfer rate ratio establishes the equilibrium for binding. Based on Leggett (1993), these values for adults are 0.8 day^{-1} for transfer to the bound compartment and 0.139 day^{-1} ($t_{1/2}$ = 5.0 day) for transfer from the bound compartment, providing an equilibrium ratio (bound/free) of approximately 6. Values for children are similar, but the transfer to the bound compartment is slightly slower. In terms of the model variables, given RPLAS=2000, then TOPROT=0.0004 (since the product should be 0.8) and RPROT=0.139. All R variables have units of (1/day) and TOPROT is unitless.

2.3.4.3. Red Blood Cells

Lead in red blood cells (RBC) is governed by a deposition fraction for uptake (*TOORBC*) from PLAS, and loss rate constant (RRBC) back to PLAS. Uptake of Pb in RBCs is assumed to be limited by a maximum Pb concentration in RBCs (*SATRAT*, µg Pb/dL RBC volume). Deposition fractions to all other tissues increase proportionally by the factor *CF* (from Equation 2.3-10).

First, the volume of RBC/blood volume ratio is given by HEMAT (Eq 2.3-22):

$$HEMAT = HCTA + (HCTB - HCTA) \cdot Exp(-13.9 \cdot AGE_{YEAR}) \qquad \text{Eq. (2.3-22)}$$

Here HCTB is the hematocrit value at birth, while HCTA is the adult value. These are entered with the time-independent physiological parameters in the interface. AGE_{YEAR} is the age of the simulated person in years. The Pb mass in RBC is converted to a concentration (Eq 2.3-23):

$$RBCONC = YRBC/(HEMAT \cdot BLDVOL) \quad \text{Eq. (2.3-23)}$$

Above a threshold concentration in red blood cells (*RBCNL*, µg Pb/dL RBC volume), the deposition fraction (and corresponding rate coefficient) for transfer from diffusible plasma to RBCs (*TOORBC*) declines (Equation 2.3-24)

$$\text{TOORBC} = \text{TRBC} * (1 - \left(\frac{\text{RBCONC-RBCNL}}{\text{SATRAT-RBCNL}}\right)^{\text{power}}) \quad \text{Eq. (2.3-24)}$$

The value of "power" is adjustable in the interface, but the default value is 1.5 and should not be changed without good reason. Once TOORBC has been evaluated, the adjustment factor for the alternate PLAS loss terms is computed (Eq. 2.3-25):

$$CF = \frac{1-TOORBC}{1-TRBC}, \quad \text{if RBCONC>RBCNL, else CF=1} \quad \text{Eq. (2.3-25)}$$

The combination of the variables TOORBC and CF ensure that the outflow from PLAS remains the same as it would be without saturation effects. Values for rate coefficients for transfer in and out of the RBC, *SATRAT* (350 µg Pb/dL RBC) and *RBCNL* (20 µg Pb/dL RBC) result in rapid uptake of Pb into RBCs (adult $t_{1/2}$≈2 min in adults, 2-3 min in children) and replicate the non-linear relationship between plasma and red blood observed in adults (Smith et al., 2002; Manton et al., 2001; Bergdahl et al., 1999; Bergdahl et al., 1998; Bergdahl et al., 1997). The values for *RBCNL* and *RRBC* used in Equations C17 and C18 of Table 2-2 were adjusted upward from the values assigned in Leggett (1993) to provide improved fit to plasma-whole blood Pb relationships in adults and to harmonize blood Pb estimations in young children with the IEUBK model at the ages of 1, 5, and 10 years (see Chapter 4).

2.3.4.4. Extravascular Fluid

Lead in diffusible plasma exchanges with Pb in an extravascular fluid (EVF) compartment (Table 2-2 Equation H1-H2). The conceptual basis for including the EVF compartment is to allow simulation of the dynamics of Pb in plasma of efflux of Pb from plasma and return to the plasma during the first minutes following intravenous injection of Pb that has been observed following intravenous injection of Pb, as summarized in Leggett (1993) based on various experimental studies (Heard and Chamberlain, 1984; Booker et al., 1969; Hursh and Suomela, 1968; Stover, 1959). Efflux of Pb from the plasma is assumed to occur immediately after its entrance into plasma and prior to binding of Pb to plasma proteins ($t_{1/2}$≈1 day, adults) and uptake into RBCs (adult $t_{1/2}$≈2 min, adults). Uptake of Pb into RBCs subsequently provides a driving force for return of Pb to the plasma. These dynamics are simulated as rapid exchanges of Pb between the diffusible plasma and EVF compartments. For all ages, rate coefficients for transfers to and from the EVF, based on Leggett (1993), are 1000 day^{-1} ($t_{1/2}$≈1 min) and 333 day^{-1} ($t_{1/2}$≈3 min). These values produce a rapid efflux of Pb to the EVF compartment and return to diffusible plasma, with an equilibrium ratio for EVF/diffusible plasma Pb mass of approximately 3. The corresponding volume of distribution for the rapidly exchanging EVF compartment of three times diffusible plasma is consistent with observations made for the distribution of calcium, summarized in Leggett (1993) based on Harrison et al. (1967) and (Hart and Spencer, 1976).

2.3.5. Skeleton

2.3.5.1. General Structure of Bone Model

A major concept underlying the AALM simulation of bone Pb kinetics is that Pb kinetics behavior in bone resembles that of calcium and similar bone accumulating elements (e.g., strontium). Observations that formed the bases for the Leggett (1993) bone Pb model included experimental studies of the kinetics of Pb, calcium, and strontium in humans, non-human primates, and dogs [e.g., (Heard and Chamberlain, 1984; Lloyd et al., 1975; Cohen et al., 1970)]. The AALM.FOR simulates Pb biokinetics in bone as a combination of three processes: (1) relatively rapid exchange of Pb between diffusible plasma and surfaces of cortical and trabecular bone; (2) slower exchange of Pb at bone surfaces with an *exchangeable* Pb pool in bone volume; and (3) slow transfer of a portion of Pb in bone volume to a *non-exchangeable* pool that is released from bone to diffusible plasma only when bone is resorbed (Figure 2-4). These features are represented in the AALM.FOR as six bone subcompartments; three each for cortical and trabecular bone, representing bone surface, exchangeable Pb in bone volume, and non-exchangeable Pb in bone volume (CSUR, CDIF, and CVOL, respectively for cortical bone, or TSUR, TDIF and TVOL for trabecular bone. Cortical and trabecular bone volume are assumed to account for 80% and 20% of total bone volume, respectively (Leggett, 1993). Transfers of Pb in and out of the bone surface compartment are assumed to be relatively rapid: values for $t_{1/2}$ are approximately 0.01 day for transfer from plasma-to-bone surface; and 1.4 days for return from bone surface to plasma and transfer from bone surface to exchangeable bone volume (Leggett, 1993). Transfer from bone surface is faster in children ($t_{1/2} \approx 1.1$ days). Return of Pb from the exchangeable bone volume to bone surface is slower ($t_{1/2} \approx 37$ days); however, the dominant transfer processes determining long-term accrual of bone Pb burden (≈90% of body burden) are the slower rate coefficients for transfer of Pb from the non-exchangeable compartments of trabecular and cortical bone to diffusible plasma (adult $t_{1/2} \approx 1.9$ and 12 years, respectively). Bone transfer coefficients vary with age (faster in children) to reflect age-dependence of bone turnover. The slow, non-exchangeable, bone volume compartment is assumed to be much more labile in infants and children than in adults (e.g., cortical $t_{1/2} \approx 42$ days at birth, 677 days at 15 years, and 4220 days at ≥25 years; trabecular $t_{1/2} \approx 42$ days at birth, 363 days at 15 years, and 703 days at ≥25 years). Other physiological states that affect bone turnover and, therefore, bone Pb kinetics, such as pregnancy and menopause, could be accommodated with adjustments to tissue (e.g., bone) transfer coefficients.

2.3.5.2. Cortical and Trabecular Bone Surface

Cortical and trabecular bone surfaces exchange Pb with diffusible plasma and the exchangeable compartment of bone volume (Table 2-2, Equations K2 and K8). Bone *surfaces*, in this context, represent surfaces of bone in contact with the plasma (e.g., Haversian and Volkmann canals) and/or involved in bone production and resorption (e.g., endosteal and periosteal surfaces for cortical bone, resorption cavities, surfaces of trabecular bone). Deposition of Pb in bone surface is considered to reflect (and be in proportion to) rates of incorporation of calcium in bone that occur during growth, modeling, and remodeling of bone. Rates change with age, reflecting periods of more intense growth (e.g., infancy, pre-adolescence). In the AALM.FOR, bone Pb kinetics have the following three general characteristics. First, transfers are relatively rapid: adult $t_{1/2} \approx 0.01$ day for plasma-to-bone surface, adult $t_{1/2} \approx 1.4$ days for bone surface to plasma. Second, rates of transfer are age-dependent with highest rates during infancy (0–1 years) and adolescence (10–15 years), during periods of rapid bone growth. In infancy, transfer of Pb to bone surface accounts for approximately 24% of total flow of Pb out of the diffusible plasma (8% in

adults). And third, relative fractions of transfer from diffusible plasma to cortical and trabecular bone is also age-dependent, decreasing from 80% of total transfer going to cortical bone during infancy, to approximately 44% in adults.

2.3.5.3. Cortical and Trabecular Bone Volume

Bone volume compartments are subdivided into cortical (80%) and trabecular bone (20%), with each further subdivided into *exchangeable* and *non-exchangeable* subcompartments (Table 2-2, Equations K3, K5, K9, and K11). Exchangeable and non-exchangeable compartments represent Pb pools in bone volume having different rates and mechanisms of turnover. Lead in the exchangeable compartment is assumed to be subject to heteroionic exchange with other bone minerals (e.g., calcium) and/or diffusion of Pb into osteons (Leggett, 1993). Lead that enters the non-exchangeable compartment remains there, unless subject to bone resorption. Turnover of Pb in the non-exchangeable compartment reflects bone turnover rates.

Lead enters bone volume from bone surface. In the AALM, exchanges of Pb between bone surface and bone volume have the following three characteristics. First, the transfer to bone volume is faster (adult $t_{1/2}$≈1.4 days) compared to return to bone surface (adult $t_{1/2}$≈37 days), resulting in accumulation of Pb in bone volume, relative to bone surface. Second, transfer rates from bone surface to bone volume are constant ($t_{1/2}$≈2 days) up through adolescence, and slower than in adults ($t_{1/2}$≈1.4 days). And third, transfer rates between bone volume and bone surface are assumed to be similar for cortical and trabecular bone.

A portion of the Pb that enters bone from bone surface becomes associated with deep bone mineral deposits that can be mobilized during periods of bone resorption (including that which occurs during bone modeling associated with growth). In the AALM, kinetics of Pb in this non-exchangeable pool have the following six characteristics. First, transfer of Pb from the exchangeable compartment to the non-exchangeable compartment is relatively faster ($t_{1/2}$≈30 days) than transfer to surface bone ($t_{1/2}$≈37 days). Second, the transfer rate to the non-exchangeable compartment is independent of age. Third, transfer to the non-exchangeable compartments of cortical and trabecular bone occur at the same rates. Fourth, transfer of Pb out of the non-exchangeable compartment returns Pb directly to the diffusible plasma. Fifth, rates of transfer from the non-exchangeable compartment reflect bone turnover rate and are relatively slow (adult $t_{1/2}$≈12 years for cortical bone, adult $t_{1/2}$≈1.9 years for trabecular bone) compared to rates of removal of Pb from the exchangeable compartment. And sixth, age-dependent changes in bone turnover rates give rise to movement of Pb out of the non-exchangeable compartments that declines with increasing age:

AGE	**100 d**	**1 yr**	**5 yr**	**10 yr**	**15 yr**	**≥25**
Cortical $t_{1/2}$ (yr)	0.12	0.33	0.62	1.1	1.9	12
Trabecular $t_{1/2}$ (yr)	0.12	0.33	0.52	0.72	1.0	1.9

Discussed in Chapter 4, values for *RCORT* and *RTRAB* in Equations K6 and K12 of Table 2-2, and *FLONG* (Equation G1-G4) were adjusted to improve agreement between predicted and observed elimination kinetics of Pb from bone in adults (Nilsson et al., 1991).

2.3.6. Liver

The AALM simulates Pb kinetics in liver as the combination of three properties. First, there is relatively rapid exchange between Pb in diffusible plasma and a *fast* compartment in liver (LVR1). Second, slower transfer of Pb from the *fast* liver compartment to a *slow* compartment in liver (LVR2), which can release Pb to the diffusible plasma. And third, there is transfer of Pb from the fast liver compartment to the small intestine (i.e., biliary secretion). This configuration gives rise to Pb kinetics following a single absorbed dose that result in a relatively rapid initial uptake of Pb in liver, followed by a slow decline in liver Pb burden, consistent with experimental studies conducted in humans, non-human primate, and dogs (Leggett, 1993), based on several studies (Heard and Chamberlain, 1984; Lloyd et al., 1975; Cohen et al., 1970). With chronic dosing, liver Pb levels increase to approximately 10% of total body burden in early childhood and decline to 2% by age 40 years.

Rate equations for transfers of Pb in and out of the liver are presented in Table 2-2 (Equations M1 to M4). In the AALM, kinetics of Pb in liver have the following four general characteristics. First, transfer to the fast liver compartment (LRV1) from diffusible plasma is relatively rapid (adult $t_{1/2}$≈0.01 day) and accounts for approximately 4% of total transfer of Pb from diffusible plasma. Second, transfers from the LVR1 to diffusible plasma and to the small intestine are assumed to occur at approximately the same rate ($t_{1/2}$≈22 days) and is slower than uptake from diffusible plasma, resulting in Pb accumulates in the fast pool. Third, Pb in the fast liver compartment is slowly transferred to the slow liver pool (LVR2, $t_{1/2}$≈100 day). Fourth, rates of return of Pb from the slow compartment to diffusible plasma are age-dependent, with half-times decreasing from $t_{1/2}$≈1000 days at birth to 500 days at age 5 years, increasing to approximately 1200 days at age ≥10 years. This results in increasing rate of accumulation of Pb in the slow compartment with age, with chronic dosing. As discussed in Chapter 4, the value for *RLIV2* in Equation M3 of Table 2-2 was adjusted from the value reported in Leggett (1993) to improve agreement between predicted and observed soft tissue-bone Pb ratios (Barry, 1975).

Biliary secretion of Pb is simulated as transfer of Pb from the fast liver compartment (LVR1) to the small intestine (Table 2-2, see Note 1 to Equation M1). The biliary contribution to the small intestine Pb contents is given by Equation 2.3-26:

$$FL_{LVR1\rightarrow SIC} = H1TOSI \cdot FL_{LVR1} \qquad \text{Eq. (2.3-26)}$$

where *H1TOSI* is the fraction of Pb of the LVR1 outflow FL_{LVR1} that goes to the small intestine. A value of 0.45 is the default for *H1TOSI*, but this may be altered in the interface. This value is the rate constant from LVR1 to the small intestine divided by the sum of rate constants for movement from LVR1 to the small intestine, plasma, and LVR2 (Leggett, 1993).

2.3.7. Kidney

Like the liver, kidney Pb kinetics exhibit multiple components that include an initial phase of rapid uptake of Pb following a single dose of Pb, followed by a slow decline in kidney Pb burden, with long-term retention of <1% of the body burden during chronic dosing. The AALM code simulates Pb kinetics in kidney as the combination of two parallel processes: (1) relatively rapid transfer between Pb from diffusible plasma to a *fast* compartment in kidney (KDN1), a portion of which is excreted in urine

(*urinary path*); and (2) slower exchange Pb between diffusible plasma and a *slow* compartment in kidney (KDN2). This configuration gives rise to Pb kinetics following a single absorbed dose that result in a relatively rapid initial uptake of Pb in kidney, followed by a slow decline in kidney Pb burden. With chronic dosing, kidney Pb levels increase to approximately 2% of total body burden in early childhood and decline progressively 0.2–0.3% after age 40 years.

Rate equations for transfers of Pb in and out of kidney are presented in Table 2-2 (Equations L1 to L4). In the AALM, kinetics of Pb in kidney have the following four general characteristics. First, transfer from the diffusible plasma to the fast (urinary path) kidney compartment (KDN1) is relatively rapid ($t_{1/2}$≈0.02 day) and accounts for approximately 2.5% of total transfer of Pb from diffusible plasma. Second, transfer from the fast compartment of kidney (KDN1) to bladder urine is slower than uptake from diffusible plasma ($t_{1/2}$≈5 days). As a result, Pb accumulates in the fast compartment. Third, transfer of Pb from diffusible plasma to the slow kidney compartment (KDN2) is approximately 100 times slower than that to the fast compartment (adult $t_{1/2}$≈2 days), receiving approximately 0.04% of the total transfer out of the diffusible plasma). and fourth, rates of return of Pb from the slow compartment (KDN2) to diffusible plasma are age-dependent, with half-times increasing from $t_{1/2}$≈1000 days until age 5 years and to 3648 days at age ≥10 years. This results in increasing rate of accumulation of Pb in the slow compartment with age, with chronic dosing.

The value for *TKDN1* in Equation C4 of Table 2-2 was adjusted (see Chapter 4) from the value reported in Leggett (1993) to improve agreement between predicted and observed plasma-to-urine clearance in adults (Araki et al., 1986; Manton and Cook, 1984; Manton and Malloy, 1983; Chamberlain et al., 1978). The value for *RKDN2* in Equation L4 of Table 2-2 was adjusted (see Chapter 4) from the value reported in Leggett (1993) to improve agreement between predicted and observed soft tissue-bone Pb ratios reported by Barry (1975).

All the kidney modeling variables, including the inflow constants TOKDN1 and TOKDN2 and the outflows RKDN1 and RKDN2 may be entered through the user interface.

2.3.8. Brain

In the AALM, the brain is treated as a homogenous compartment (Table 2-2, Equations J1 and J2). This assumption is a gross simplification of more complex, non-uniform distribution of Pb in brain tissues (Grandjean, 1978). Nevertheless, the simplification has little consequence of overall kinetics of Pb, since brain constitutes a relatively small site of deposition (Barry, 1981; Barry, 1975; Lloyd et al., 1975; Cohen et al., 1970). In the AALM, the brain is assumed to receive approximately 0.05% total outflow of Pb from the diffusible plasma up to age 1 year and 0.015% at ages ≥5 years (Leggett, 1993). Transfer rates into brain (adult $t_{1/2}$≈2.3 day) and from brain to diffusible plasma ($t_{1/2}$≈730 day) result in brain Pb burdens that are 0.1–0.2% of body burden, with chronic dosing. Transfer rates into brain are age-dependent and are highest during the first year ($t_{1/2}$≈1 day) and decrease ($t_{1/2}$≈2–3 days) at ages ≥5 years. The age-dependence in transfer rates contribute to a peak in the Pb mass in brain (≈0.8% of body burden) between ages 3–4 years, with chronic exposure.

2.3.9. Other Soft Tissues

In the AALM, soft tissues not explicitly simulated as distinct compartments (e.g., muscle, skin, etc.) are lumped into a single compartment (Other Soft Tissue, SOF). This compartment is assumed to comprise

three subcompartments that are characterized with relatively *fast*, *intermediate*, or *slow* exchange kinetics with diffusible plasma (Table 2-2, Equations I1 to I6), and no exchanges between subcompartments. The fast compartment (*SOF0*) receives approximately 8-9% of the outflow of Pb from diffusible plasma (adult $t_{1/2}$≈0.004 day, child $t_{1/2}$ 0.5-1 day), with slower return of Pb to the diffusible plasma ($t_{1/2}$≈0.33 day). The intermediate compartment (*SOF1*) receives approximately 0.5-1% of the outflow from diffusible plasma (adult $t_{1/2}$≈0.07 day, child $t_{1/2}$ 0.04-0.06 day), with slower return kinetics (adult $t_{1/2}$≈167 day). The slow compartment (*SOF2*) receives approximately 0.1% of the total outflow of Pb from diffusible plasma (adult $t_{1/2}$≈0.35 day, child $t_{1/2}$ 0.400.6 day), with slower return ($t_{1/2}$≈1800 day). This configuration results in approximately 9% of the Pb body burden residing in the combined subcompartments that comprise the other soft tissue compartment during early childhood followed by a decrease to approximately 3% by age 40 years. A pathway for elimination of Pb to hair, nails, and exfoliated skin is assigned to the intermediate soft tissue compartment (Table 2-2, see Note 1 to the I equations).

2.3.10. Excretion

The AALM simulates excretion of absorbed Pb as five separate pathways representing urine, secretion from liver to small intestine (e.g., biliary), secretion from diffusible plasma to small intestine, sweat, and other routes (e.g., hair, nails, exfoliated skin as described in Section 2.3.9). The urinary pathway includes excretion of Pb deposited from the diffusible plasma into the fast kidney compartment (KDN1, Table 2-2, Equation C6). This pathway contributes approximately 2.5% of total outflow of Pb from the diffusible plasma. The corresponding plasma clearance (L plasma/day) is approximately 2.4 L/day at age 1 year and 20 L/day at age ≥25 years, and blood clearance (L blood/day) is approximately 0.05 L/day at age 1 year and 0.07 L/day at age ≥25 years. The urinary pathway contributes approximately 45% of total excretion of absorbed Pb in adults and approximately 80% up at ages ≤ 12 years. The AALM.FOR also includes rate coefficient for direct transfer of Pb from plasma to urine (*TURIN* in Equation C14 of Table 2-2). Improved agreement between predicted and observed plasma-to-urine clearance in adults was achieved with adjustments to the parameter *TKDN1* (Equation C4 of Table 2-2). Because values assigned to *TURIN* did not improve the fit to observations, the direct excretion pathway was nulled by setting *TURIN* to zero.

The fecal excretion pathway in the AALM.FOR includes the unabsorbed fraction of Pb that enters the small intestine from three sources (Table 2-2 Equation E3): (1) ingestion; (2) transfer from the liver (biliary secretion, Table 2-2 Equation notes to section M); and (3) transfer from diffusible plasma. Biliary secretion contributes approximately 32% of total excretion of absorbed Pb in adults (55% up to age 12 years) and transfer from plasma contributes approximately 11% (18% at age ≤12 years).

Sweat is simulated as a direct transfer out of diffusible plasma and accounts for approximately 6% in of total excretion of absorbed Pb in adults and approximately 11% at ages ≤12 years (Table 2-2, Equation N3). All other pathways of Pb excretion, not simulated with specific pathways, are accounted for in transfer of Pb from the intermediate soft tissue compartment (SOF1; Table 2-2 see notes to section I). These pathways include losses to hair, nails, and exfoliated skin and, combined, account for approximately 6% of total excretion of absorbed Pb in adults and 12% at ages ≤12 years.

2.3.11. Neonatal Pb

Lead masses in all compartments at birth are assigned values based on a value for maternal blood Pb concentration (Table 2-2, Equations B1–B7). The general equation for the neonatal distribution of Pb masses is in the form (Equation 2.3-24):

$$Y_i = \frac{YF_i \cdot BLDMOT \cdot BRATIO \cdot 3}{RBCin} \qquad \text{Eq. (2.3-27)}$$

Here *Yi* is the Pb mass (µg) in tissue *i* at birth, YF_i is the fraction of total body burden in tissue *i* at birth (input variables with suffix "in" like Bonin, Branin, Hepin, etc.), *BLDMOT* is the maternal blood Pb concentration (µg/dL), *BRATIO* is the fetal/maternal blood Pb concentration ratio, and *RBCin* is the fraction of body burden in RBCs at birth. The value 3 in the numerator represents the assumed blood volume (dL) at birth. Tissue compartments assigned values at birth are: brain, kidney (*KDN2*), liver (*LVR2*), RBC, soft tissue (*SOF0*), and non-exchangeable bone volume (80% cortical, 20% trabecular).

2.3.12. Chelation

The original Leggett model included parameters to simulate the effect of chelation therapy on internal Pb kinetics. However, the AALM v3.0 of the model does not support this option.

TABLE 2-1. EXPOSURE AND GROWTH EQUATIONS OF AALM FORTRAN CODE

No.		**Equation**
A		**Pb Intake from source j (µg/timestep)**
A	1	$IN_j = Pb_j \cdot f_j \cdot IR_{medium} \cdot M_{j1} \cdot M_{j2} \ldots / N$ j = source index for air, dust, soil, water
A	2	$IN_j = Pb_j \cdot M_{j1} \cdot M_{j2} \ldots / N$ j = source index for food, other
		Notes: 1) All variables except N (timesteps per day) are time dependent. 2) Input variable defined at user-specified ages (up to 100 ages). 3) Timesteps are filled in by the front end, either stepwise or interpolation. 4) 6 media, maximum of 3 sources per medium, for 18 sources maximum. 5) Masks M_{j1}, M_{j2}, etc. are optional, each periodically blocks intake for one source. 6) Each of the 6 media can support up to 9 masks.
		Pb deposited in lung compartment k (µg/timestep)
B	1	$P_{j\,k}(t) = IN_j(t) \cdot Dep_k$ j = air source index
		Notes: 1) Only 3 lung compartments (ET, TB, ALV) have deposition. 2) With maximum of 3 air sources, up to 9 lung intake timeseries.
C		**Pb Intake from Ingestion**
C	1	$Ingest(t) = \sum_j IN_j(t)$ j = all non-inhalation sources

No.		Equation
		Notes: 1) Up to 15 ingestion sources. 2) While some inhaled Pb is transferred to the gut, this does not count as ingestion.
D		**Growth Equations**
D	1	$\mathrm{AGE}_{YEAR} = \mathrm{AGE}/365$
D	2	$WBODY = \mathrm{WBIRTH} + \frac{WCHILD \cdot \mathrm{AGE}_{YEAR}}{(HALF + \mathrm{AGE}_{YEAR})} + \frac{WADULT}{(1 + KAPPA \cdot \mathrm{Exp}(-13.9 \cdot \mathrm{AGE}_{YEAR}))}$
D	3	$BLDVOL = \mathrm{WBODY} \cdot \mathrm{VBLC} \cdot 10$
D	4	$WGTSUM = \mathrm{WBIRTH} + \mathrm{WCHILD} + \mathrm{WADULT}$
D	5	$KIDWT = 1050 \cdot \mathrm{VKC} \cdot \mathrm{WGTSUM} \cdot \left(\frac{WBODY}{WGTSUM}\right)^{0.84}$
D	6	$LIVWT = 1050 \cdot \mathrm{VLC} \cdot \mathrm{WGTSUM} \cdot \left(\frac{WBODY}{WGTSUM}\right)^{0.85}$
D	7	$BONEWT = 1000 \cdot 0.0290 \cdot (\mathrm{WBODY})^{1.21}$
D	8	$BONEVOL = 1000 \cdot 0.0168 \cdot (\mathrm{WBODY})^{1.188}$
D	9	$CORTWT = 0.8 \cdot \mathrm{BONEWT}$
D	10	$TRABWT = 0.2 \cdot \mathrm{BONEWT}$

TABLE 2-2. BIOKINETICS EQUATIONS OF AALM FORTRAN CODE

No.		Equation
A		**General Timestep Equations for all Compartments**
A	1	$\mathrm{Y}(t+\Delta t) = \left(\mathrm{Y(t)} - \frac{P}{R}\right)\, e^{-\mathrm{R}\,\Delta t} + \frac{\mathrm{P}}{R}$
A	2	$\mathrm{FL}(t+\Delta t) = \mathrm{Y(t)} + P\,\Delta t - Y(t+\Delta t)$
A	3	$\mathrm{P}(t+\Delta t) = \mathrm{FL}(t+\Delta t)/\Delta t$
A	Notes	1) The Pb mass (μg) within each compartment is Y. 2) The inflow rate (assumed uniform over a timestep) of Pb (μg/day) is P. 3) The Pb outflow rate constant is R (1/day). 4) The outflow Pb mass (μg) on each timestep is FL. 5) Outflow on one timestep becomes an inflow on the next timestep. 6) Every simulation timestep Δt is the same size.
B		**Pb Masses at Birth**
B	1	$YRBC = BLDMOT \cdot BRATIO \cdot 3$
B	2	$YBRAN = BRANIN * YRBC \;/\; RBCIN$
B	3	$YKDN2 = RENIN * YRBC \;/\; RBCIN$
B	4	$YLVR2 = HEPIN * YRBC \;/\; RBCIN$
B	5	$YSOF2 = SOFIN * YRBC \;/\; RBCIN$
B	6	$YCVOL = 0.8 * BONIN * YRBC \;/\; RBCIN$
B	7	$YTVOL = 0.2 * BONIN * YRBC \;/\; RBCIN$
C		**Age-scaling of Diffusible Plasma-to-tissue Deposition Fractions**
C	1	$AGESCL = \frac{1 - TEVF - TBONE}{1 - TEVF - TBONE(AGEmax)}$
C	2	$TBRAN = AGESCL \cdot TOBRAN(t)$
C	3	$TFECE = AGESCL \cdot TOFECE$
C	4	$TKDN1 = AGESCL \cdot TOKDN1$
C	5	$TKDN2 = AGESCL \cdot TOKDN2$
C	6	$TLVR1 = AGESCL \cdot TOLVR1$
C	7	$TPROT = AGESCL \cdot TOPROT$
C	8	$TRBC = AGESCL \cdot TORBC$
C	9	$TSOF0 = AGESCL \cdot TOSOF0(t)$
C	10	$TSOF1 = AGESCL \cdot TOSOF1(t)$
C	12	$TSOF2 = AGESCL \cdot TOSOF2(t)$

No.		Equation
C	13	$TSWET = AGESCL \cdot TOSWET$
C	14	$TURIN = AGESCL \cdot TOURIN$
C	15	$HEMAT = HCTA + (HCTB - HCTA) \cdot Exp(-13.9 \cdot AGE_{YEAR})$
C	16	$RBCONC = YRBC/(HEMAT \cdot BLDVOL)$
C	17	$\text{TOORBC} = \text{TRBC} * (1 - \left(\frac{\text{RBCONC-RBCNL}}{\text{SATRAT-RBCNL}}\right)^{\text{power}})$, if RBCONC>RBCNL
C	18	$CF = \frac{1-TOORBC}{1-TRBC}$, if RBCONC>RBCNL, else CF=1
D		**Respiratory Tract (RT)**
D	1	ET, k=1: $P_j = P_{j\,1} + FL_{j,TB\rightarrow \text{ET}} \,/\, \Delta t$
D	2	ET, k=1: $R_j = R_{j,ET\rightarrow PLAS} + R_{j,ET\rightarrow STOM}$
D	3	TB, k=2: $P_j = P_{j\,2} + FL_{j,ALV\rightarrow \text{TB}} \,/\, \Delta t$
D	4	TB, k=2: $R_j = R_{j,TB\rightarrow PLAS} + R_{j,TB\rightarrow \text{ET}}$
D	5	ALV, k=3: $P_j = P_{j\,3}$
D	6	ALV, k=3: $R_j = R_{j,ALV\rightarrow PLAS} + R_{j,ALV\rightarrow TB} + R_{j,ALV\rightarrow INT}$
D	7	INT, k=4: $P_j = FL_{j,ALV\rightarrow INT} \,/\, \Delta t$
D	8	INT, k=4: $R_j = R_{j,INT\rightarrow PLAS}$
D	9	$FL_{k\rightarrow PLAS} = \sum_j FL_{j,k\rightarrow PLAS}$
D	10	$UP_{LUNG} = \sum_j FL_{k\rightarrow PLAS}$
D	Notes	1) Each lung equation above is evaluated separately for each air source *j*.
E		**Gastrointestinal Tract (GI) – Stomach (STOM)**
E	1	$P_j = IN_j$ for j not an air source (4−18) $P_j = FL_{j,ET\rightarrow STOM} \,/\, \Delta t$ for j an air source (1−3)
E	2	$R_j = R_{STOM}$
E	Notes	1) The outflow rate constant is the same for all source types. 2) Outflow goes to small intestine and is tracked by source.
E		**Gastrointestinal Tract (GI) – Small Intestine (SI)**
E	3	$P_j = FL_{j,STOM\rightarrow SI} \,/\, \Delta t$ for j = 1 to 18 $P_0 = (FL_{\,LVR1\rightarrow SI} + FL_{\,PLAS\rightarrow SI}) \,/\, \Delta t$ for j=0

No.		Equation
E	4	$R_j = R_{SI}$
E	Notes	3) 18 external sources plus source 0 for Pb coming from liver or plasma 4) Loss rate is the same for all sources. 5) Loss fraction going to PLAS is $(\mathrm{F1(t)} \cdot \mathrm{RBA}_j)$, the remainder goes to ULI. 6) The loss fractions vary by source. For source 0, RBA=1.
E		**Gastrointestinal Tract (GI) – Upper Large Intestine (ULI)**
E	5	$P_j = FL_{j,SI\rightarrow\mathrm{ULI}} \ / \Delta t$ for j = 0 to 18
E	6	$R_j = R_{ULI}$
E		**Gastrointestinal Tract (GI) – Lower Large Intestine (LLI)**
E	7	$P_j = FL_{j,ULI\rightarrow\mathrm{LLI}} \ / \Delta t$ for j = 0 to 18
E	8	$R_j = R_{LLI}$
E	Notes	7) Each GI compartment has a Y_j for Pb from each source j (from 1 to 18). 8) Each GI compartment except STOM also has a j=0 term, 9) Each compartment also has a combined Y for the sum over all j.
E		**Uptake into PLAS from Gastrointestinal Tract (GI)**
E	9	$UP_j = FL_{j,SI} \cdot \mathrm{F1} \cdot \mathrm{RBA}_j$
E	10	$FL_{j,SI\rightarrow\mathrm{ULI}} = FL_{j,SI} \cdot (1 - \mathrm{F1} \cdot \mathrm{RBA}_j)$
E	11	$UP_{GI} = \sum_{j=0}^{18} UP_j$
E	12	$UP_{ING} = \sum_{j=4}^{18} UP_j$
E	Notes	10) The total GI tract uptake is the sum of UP_j from j=0 to 18 11) The ingestion uptake is the sum not including j=0 or air sources (j=1-3) 12) These uptakes are per timestep (µg Pb/timestep). 13) Uptakes reported on the daily output file are sums over the timesteps each day.
F		**Blood – Plasma (Diffusible) (PLAS)**
F	1	$P = UP_{GI} + UP_{LUNG} + \sum_k FL_{k\rightarrow PLAS} \ / \Delta t$
F	2	$TSUM = \sum_C T_C$
F	3	$R = RPLAS \cdot TSUM$
F	4	$FL_{PLAS\rightarrow C} = FL_{PLAS} \cdot T_C \cdot \mathrm{CF} \ / \ TSUM$

No.		Equation
F	Notes	1) The T_C are the "T" variables in equations C2 – C14. 2) TSUM is evaluated in the front end, without accounting for RBC saturation. 3) CF is defined in equation C18. 4) When TRBC is reduced by saturation effects, then CF>1. 5) The CF adjustment in F4 is not applied to RBC but applied to all the others. Equation F4 uses TOORBC (C17), whereas F2 uses TRBC (C8). 6) The compartments *k* supplying Pb to PLAS are listed in C2 – C14. 7) FL_{PLAS} is the total Pb mass lost from the plasma on this timestep, computed from A1 and A2 using P and R from F1 and F3. 8) The compartments *C* receiving Pb from PLAS: RBC, PROT, SI, EVF, SOF0, SOF1, SOF2, BRAN, CSUR, TSUR, LVR1, KDN1, KDN2, BLAD, SWET. 9) While still present in the code, the bladder BLAD receives nothing directly from PLAS, the Pb in urine now all comes from KDN1.
F		**Blood – Plasma – Protein Bound (PROT)**
F	5	$P = FL_{\text{PLAS}\rightarrow\text{PROT}} \ / \Delta t$
F	6	$R = RPROT$
F		**Blood – Red Blood Cell (RBC)**
F	7	$P = FL_{\text{PLAS}\rightarrow\text{RBC}} \ / \Delta t$
F	8	$R = RRBC$
G		**Blood and Other Concentrations (output variables)**
G	1	$C_{BLOOD} = (Y_{PLAS} + Y_{PROT} + Y_{RBC})/BLDVOL$
G	2	$C_{PLAS} = (Y_{PLAS} + Y_{PROT})/BLDVOL$
G	3	$C_{KIDNEY} = (Y_{KDN1} + Y_{KDN2})/KIDWT$
G	4	$C_{LIVER} = (Y_{LVR1} + Y_{LIVR2})/LIVWT$
G	5	$C_{CORT} = (Y_{CSUR} + Y_{CDIF} + Y_{CVOL})/CORTWT$
G	6	$C_{TRAB} = (Y_{TSUR} + Y_{TDIF} + Y_{TVOL})/CORTWT$
G	7	$C_{BONE} = (Y_{CSUR} + Y_{CDIF} + Y_{CVOL} + Y_{TSUR} + Y_{TDIF} + Y_{TVOL})/BONEWT$
G	Notes	1) The denominators are timeseries that depend on body weight WBODY and were evaluated on all timesteps in the Fortran front end. 2) The concentrations do not affect the biokinetics, so equation G1-G7 are evaluated once each, after the loop over timesteps has been completed, using the timeseries variables Y_x for the compartmental Pb masses.
H		**Extravascular Fluid (EVF)**
H	1	$P = FL_{\text{PLAS}\rightarrow\text{EVF}} \ / \Delta t$
H	2	$R = REVF$

No.		Equation
I		**Soft Tissue: Fast transfer (SOF0)**
I	1	$P = FL_{\text{PLAS}\rightarrow\text{SOF0}} \ / \Delta t$
I	2	$R = RSOF0$
I		**Soft Tissue: Intermediate transfer (SOF1)**
I	3	$P = FL_{\text{PLAS}\rightarrow\text{SOF1}} \ / \Delta t$
I	4	$R = RSOF1$
I	Notes	1) The outflow from SOF1 is split, with a fraction S2HAIR going to HAIR and the remainder going back to PLAS.
I		**Soft Tissue: Slow transfer (SOF2)**
I	5	$P = FL_{\text{PLAS}\rightarrow\text{SOF2}} \ / \Delta t$
I	6	$R = RSOF2$
J		**Brain (BRAN)**
J	1	$P = FL_{\text{PLAS}\rightarrow\text{BRAN}} \ / \Delta t$
J	2	$R = RBRAN$
K		**Bone – Cortical Bone Surface (CSUR)**
K	1	$P = (FL_{\text{PLAS}\rightarrow\text{CSUR}} + FL_{\text{CDIF}\rightarrow\text{CSUR}}) \ / \Delta t$
K	2	$R = RCS2B + RCS2DF$
K		**Bone – Exchangeable Cortical Bone (CDIF)**
K	3	$P = FL_{\text{CSUR}\rightarrow\text{CDIF}} \ / \Delta t$
K	4	$R = RDIFF$
K	Notes	1) The outflow from CDIF is split with a fraction FLONG going to CVOL and the remainder going to CSUR.
K		**Bone – Non-Exchangeable Cortical Bone Volume (CVOL)**
K	5	$P = FL_{\text{CDIF}\rightarrow\text{CVOL}} \ / \Delta t$
K	6	$R = RCORT$
K		**Bone – Trabecular Bone Surface (TSUR)**
K	7	$P = (FL_{\text{PLAS}\rightarrow\text{TSUR}} + FL_{\text{TDIF}\rightarrow\text{TSUR}}) \ / \Delta t$
K	8	$R = RTS2B + RTS2DF$
K		**Bone – Exchangeable Trabecular Bone (TDIF)**
K	9	$P = FL_{\text{TSUR}\rightarrow\text{TDIF}} \ / \Delta t$
K	10	$R = RDIFF$

No.		Equation
K	Notes	2) The rate constant is the same variable for both TDIF and CDIF. 3) The outflow is split with a fraction FLONG going to TVOL, with the remainder going to TSUR.
K		**Bone – Non-Exchangeable Trabecular Bone (TVOL)**
K	11	$P = FL_{\text{TDIF}\rightarrow\text{TVOL}} \ / \Delta t$
K	12	$R = RTRAB$
L		**Kidney – Compartment 1 (fast, urinary path) (KDN1)**
L	1	$P = FL_{\text{PLAS}\rightarrow\text{KDN1}} \ / \Delta t$
L	2	$R = RKDN1$
L		**Kidney – Compartment 2 (slow path) (KDN2)**
L	3	$P = FL_{\text{PLAS}\rightarrow\text{KDN2}} \ / \Delta t$
L	4	$R = RKDN2$
L		**Bladder (BLAD)**
L	5	$P = (FL_{\text{KDN1}\rightarrow\text{BLAD}} + FL_{\text{PLAS}\rightarrow\text{BLAD}}) \ / \Delta t$
L	6	$R = RBLAD$
L	Notes	1) The outflow from KDN1 goes to BLAD. 2) The outflow from KDN2 goes to PLAS. 3) The outflow from BLAD exits the body as urine.
M		**Liver – Fast Compartment 1 (LVR1)**
M	1	$P = FL_{\text{PLAS}\rightarrow\text{LVR1}} \ / \Delta t$
M	2	$R = RLVR1$
M		**Liver – Slow Compartment 2**
M	3	$P = FL_{\text{LVR1}\rightarrow\text{LVR2}} \ / \Delta t$
M	4	$R = RLVR2$
M	Notes	1) The outflow from LVR1 is split into 3 parts: a fraction H1toH2 to LVR2, fraction H1toSI to small intestine, and fraction H1toBl to PLAS. 2) The interface should check that the above fractions sum to one. 3) The outflow from LVR2 goes entirely to PLAS.
N		**Exit pathways – (URIN, FECE, SWET, HAIR)**
N	1	$Y_{URIN}(t + \Delta t) = Y_{URIN}(t) + FL_{\text{BLAD}\rightarrow\text{URIN}}(t)$
N	2	$Y_{FECE}(t + \Delta t) = Y_{FECE}(t) + FL_{\text{LLI}\rightarrow\text{FECE}}(t)$
N	3	$Y_{SWET}(t + \Delta t) = Y_{SWET}(t) + FL_{\text{PLAS}\rightarrow\text{SWET}}(t)$
N	4	$Y_{HAIR}(t + \Delta t) = Y_{HAIR}(t) + FL_{\text{SOF1}\rightarrow\text{HAIR}}(t)$

No.		Equation
N	Notes	1) Each exit pathway accumulates losses over the simulation. 2) Hair is a generic name that includes hair, fingernails, toenails, as well as skin dander that is sloughed off. 3) The purpose of tracking accumulated losses is to check mass balance (see below).
O		**Mass balance calculations – Air sources (j=1 to 3)**
O	1	$SOURCE_j(T) = \sum_{t=0}^{T} IN_j(t)$
O	2	$NONDEP_j(T) = (1 - DEP_j) \cdot \sum_{t=0}^{T} IN_j(\mathrm{t})$
O	3	$INTAKE_j(T) = SOURCE_j(T) - NONDEP_j(T)$
O	4	$GITRACT_j(T) = Y_{j,STOM} + Y_{j,SI} + Y_{j,ULI} + Y_{j,LLI} + FL_{j,STOM\rightarrow SI} + FL_{j,SI\rightarrow PLAS} + FL_{j,SI\rightarrow ULI} + FL_{j,ULI\rightarrow \mathrm{LLI}} + FL_{j,LLI\rightarrow \mathrm{FECE}}$
O	5	$LUNGS_j(T) = Y_{j,ET} + Y_{j,TB} + Y_{j,ALV} + Y_{j,INT} + FL_{j,TB\rightarrow ET} + FL_{j,ALV\rightarrow \mathrm{TB}} + FL_{j,ALV\rightarrow INT} + FL_{j,ET\rightarrow \mathrm{STOM}} + FL_{j,ET\rightarrow \mathrm{PLAS}} + FL_{j,TB\rightarrow \mathrm{PLAS}} + FL_{j,ALV\rightarrow \mathrm{PLAS}} + FL_{j,INT\rightarrow \mathrm{PLAS}}$
O	6	$ABSORB_j(T) = \sum_{t=0}^{T-\Delta t} \left(FL_{j,ET\rightarrow \mathrm{PLAS}} + FL_{j,TB\rightarrow \mathrm{PLAS}} + FL_{j,ALV\rightarrow \mathrm{PLAS}} + FL_{j,INT\rightarrow \mathrm{PLAS}}\right)$
O	7	$ELIM_j(T) = \sum_{t=0}^{T-\Delta t} FL_{j,LLI\rightarrow \mathrm{FECE}}$
O	8	$SUM_j(T) = LUNGS_j(T) + GITRACT_j(T) + ABSORB_j(T) + ELIM_j(T)$
O	Notes	1) $INTAKE_j(T)$ is the time integrated Pb intake from air source j 2) $SUM_j(T)$ is the Pb mass still in the body, absorbed into PLAS, or eliminated. 3) For mass balance, $INTAKE_j(T)$ should equal $SUM_j(T)$ at all times T.
O		**Mass balance calculations – non-Air sources (j=4 to 18)**
O	9	$INTAKE_j(T) = \sum_{t=0}^{T} IN_j(t)$
O	10	$GITRACT_j(T) = Y_{j,STOM} + Y_{j,SI} + Y_{j,ULI} + Y_{j,LLI} + FL_{j,STOM\rightarrow SI} + FL_{j,SI\rightarrow PLAS} + FL_{j,SI\rightarrow ULI} + FL_{j,ULI\rightarrow \mathrm{LLI}} + FL_{j,LLI\rightarrow \mathrm{FECE}}$
O	11	$ABSORB_j(T) = \sum_{t=0}^{T-\Delta t} FL_{j,SI\rightarrow \mathrm{PLAS}}$
O	12	$ELIM_j(T) = \sum_{t=0}^{T-\Delta t} FL_{j,LLI\rightarrow \mathrm{FECE}}$
O	13	$SUM_j(T) = GITRACT_j(T) + ABSORB_j(T) + ELIM_j(T)$

No.		Equation
O	Notes	4) $INTAKE_j(T)$ is the time integrated Pb intake from non-air source j 5) $SUM_j(T)$ is the Pb mass still in the GI tract, absorbed into PLAS, or eliminated. 6) For mass balance, $INTAKE_j(T)$ should equal $SUM_j(T)$ at all times T.
O		**Mass balance calculations for all Pb**
O	14	$START = YRBC(0) + YBRAN(0) + YSOF0(0) + YKDN2(0) + YLVR2(0) + YCVOL(0) + YTVOL(0)$
O	15	$INTAKE(T) = \sum_{j=1}^{18} INTAKE_j(T)$
O	16	$COMPART(T) = \sum_{k=1}^{31} Y_k(T)$
O	17	$FLOWS(T) = \sum_{m=1}^{55} FL_m(T)$
O	18	$ELIM(T) = YURIN(T) + YFECE(T) + YSWET(T) + YHAIR(T)$
O	Notes	7) START is the Pb present at birth 8) There are (up to) 18 sources, 31 compartments and 55 intercompartmental flows. 9) The total Pb "available" at time T is START + INTAKE(T). 10) The total Pb in the body is COMPART(T) + FLOWS(T) 11) The total Pb eliminated from the body up to time T is ELIM(T) 12) If START + INTAKE(T) = COMPART(T) + FLOWS(T) + ELIM(T) then Pb mass has been conserved. This should be true at all times T, but an explicit comparison is made only at the end of the simulation. If it holds then, it must hold at earlier times, as it is very improbable that a discrepancy would occur and then later be cancelled by an equal and opposite discrepancy.

See Appendix B for parameter name definitions and descriptions. Generally, prefix R indicates a rate loss constant from a compartment, prefix T indicates deposition fractions from plasma into a compartment, and prefix Y indicates Pb mass in a compartment. Also see text (Section 2.3) for discussion of equations.

TABLE 2-3. RATE COEFFICIENTS FOR PB TRANSFERS IN AALM

Pathway	100 days	1 year	5 years	10 years	15 years	≥25 years
Plasma-D to EVF	1000	1000	1000	1000	1000	1000
Plasma-D to RBCs	310	424	443	382	313	500
Plasma-D to Plasma-B	0.495	0.678	0.709	0.611	0.501	0.800
Plasma-D to Urinary Bladder	0	0	0	0	0	0
Plasma-D to Small Intestine	7.43	10.2	10.6	9.17	7.51	12.0
Plasma-D to Trab Surf	96.0	57.6	56.8	89.5	132	89.0
Plasma-D to Cort Surf	384	230	199	268	341	71.0
Plasma-D to Liver 1	49.5	67.8	70.9	61.1	50.1	80.0
Plasma-D to Kidney 1	31.0	42.4	44.3	38.2	31.3	50.0
Plasma-D to Kidney 2	0.495	0.678	0.709	0.611	0.501	0.800
Plasma-D to ST0	103	141	148	128	105	177
Plasma-D to ST1	12.4	17.0	17.7	15.3	12.5	10.0
Plasma-D to ST2	1.24	1.70	1.77	1.53	1.25	2.00
Plasma-D to Brain	0.557	0.763	0.266	0.229	0.188	0.300
Plasma-D to Sweat	4.33	5.93	6.20	5.35	4.38	7.00
RBCs to Plasma-D	0.462	0.785	0.499	0.195	0.139	0.139
EVF to Plasma-D	333	333	333	333	333	333
Plasma-B to Plasma-D	0.139	0.139	0.139	0.139	0.139	0.139
Cort Surf to Plasma-D	0.35	0.35	0.35	0.35	0.35	0.50
Trab Surf to Plasma-D	0.35	0.35	0.35	0.35	0.35	0.50
Cort Surf to Exch Vol	0.65	0.65	0.65	0.65	0.65	0.50
Trab Surf to Exch Vol	0.65	0.65	0.65	0.65	0.65	0.50
Cort Exch Vol to Surf	0.00924	0.00924	0.00924	0.00924	0.00924	0.00924
Trab Exch Vol to Surf	0.00924	0.00924	0.00924	0.00924	0.00924	0.00924
Cort Exch Vol to Nonexch Vol	0.0139	0.0139	0.0139	0.0139	0.0139	0.0139

Pathway	100 days	1 year	5 years	10 years	15 years	≥25 years
Trab Exch Vol to Nonexch Vol	0.0139	0.0139	0.0139	0.0139	0.0139	0.0139
Cort Nonexch Vol to Plasma-D	0.0161 [a]	0.00576	0.00308	0.00178	0.00102	0.00016
Trab Nonexch Vol to Plasma-D	0.0161 [a]	0.00576	0.00362	0.00264	0.00191	0.00099
Liver 1 to Plasma-D	0.0312	0.0312	0.0312	0.0312	0.0312	0.0312
Liver 1 to Small Intestine	0.0312	0.0312	0.0312	0.0312	0.0312	0.0312
Liver 1 to Liver 2	0.00693	0.00693	0.00693	0.00693	0.00693	0.00693
Liver 2 to Plasma-D	0.000693	0.000693	0.001386	0.000570	0.000570	0.000570
Kidney 1 to Urinary Bladder	0.139	0.139	0.139	0.139	0.139	0.139
Kidney 2 to Plasma-D	0.000693	0.000693	0.000693	0.000190	0.000190	0.000190
ST0 to Plasma-D	2.08	2.079	2.079	2.079	2.079	2.079
ST1 to Plasma-D	0.00416	0.00416	0.00416	0.00416	0.00416	0.00416
ST1 to Excreta	0.00277	0.00277	0.00277	0.00277	0.00277	0.00277
ST2 to Plasma-D	0.00038	0.00038	0.00038	0.00038	0.00038	0.00038
Brain to Plasma-D	0.00095	0.00095	0.00095	0.00095	0.00095	0.00095

[a] 0.0204 d^{-1} at birth.

Coefficients are in units of d^{-1}. Coefficients from diffusible plasma (Plasma-D) are derived from the product of scaled deposition fractions and the rate coefficient for transfer from the diffusible plasma to all receiving compartments (RPLS, 2000 d^{-1}), from Equation 2.3-9.

Cort, cortical bone; Exch, exchangeable; EVF, extravascular fluid; Nonexch, nonexchangeable; Plasma-D, diffusible plasma; Plasma-B, Pb-bound in plasma; RBC, red blood cell; Surf, surface; ST0, ST1, and ST2, soft tissues with fast, moderate, and slow exchange rates, respectively; Trab, trabecular bone; vol, volume.

FIGURE 2-1. STRUCTURE OF AALM.FOR BIOKINETICS MODEL.

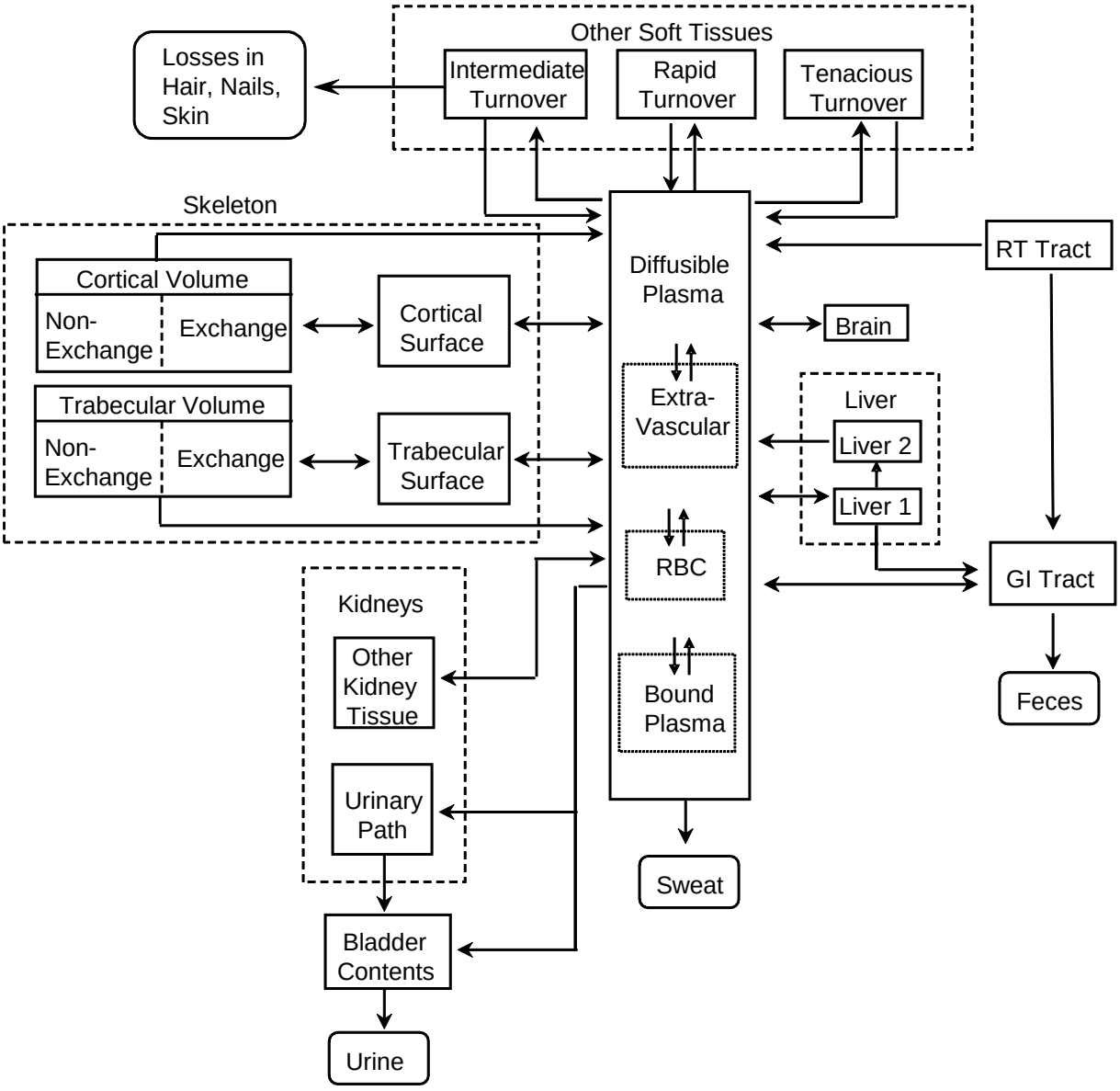

Based on Leggett (1993). Lines with arrows represent Pb transfers.

FIGURE 2-2. BODY AND TISSUE GROWTH IN THE AALM.

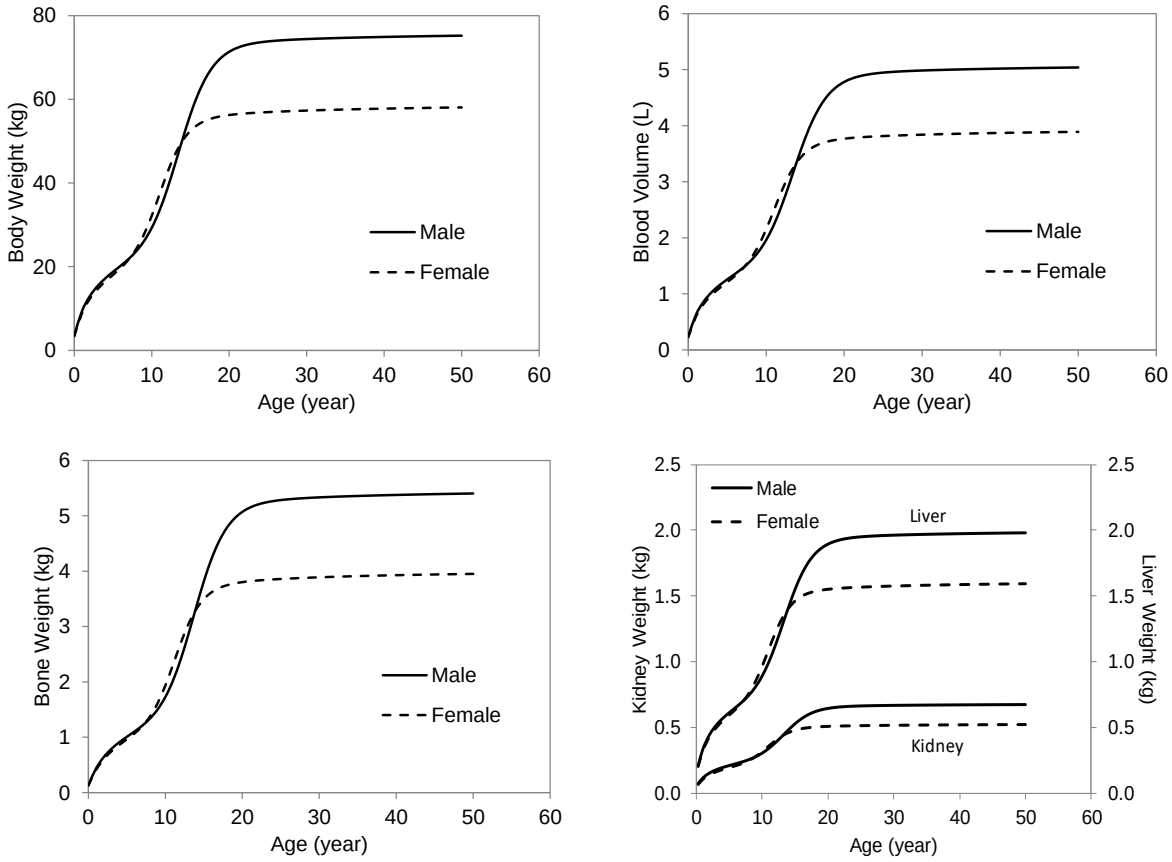

FIGURE 2-3. GASTROINTESTINAL ABSORPTION OF PB AS OPTIMIZED IN AALM.

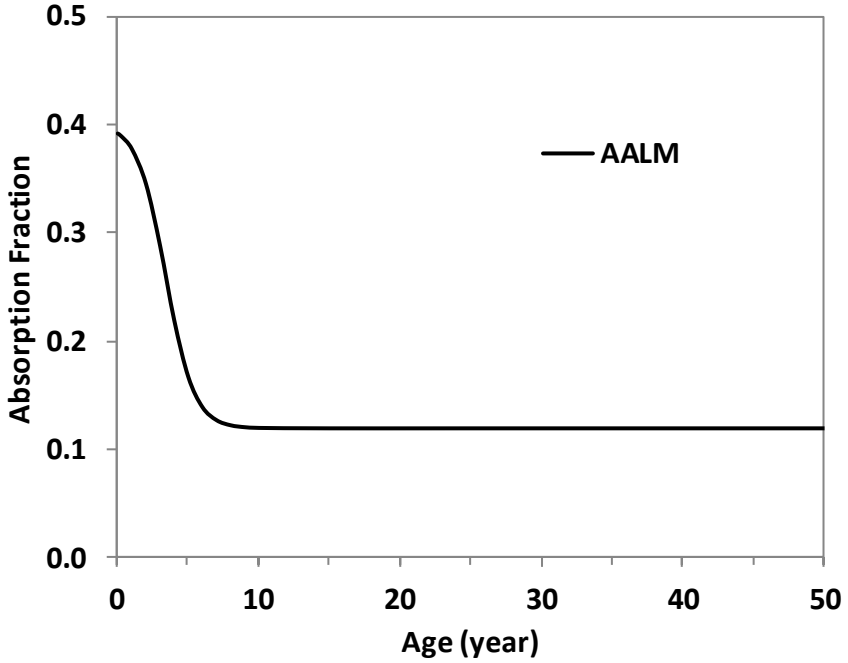

Optimization based on Ryu et al. (1983), Sherlock and Quinn (1986), Rabinowitz et al. (1976) and Maddaloni et al. (2005).

FIGURE 2-4. STRUCTURE OF AALM BONE MODEL.

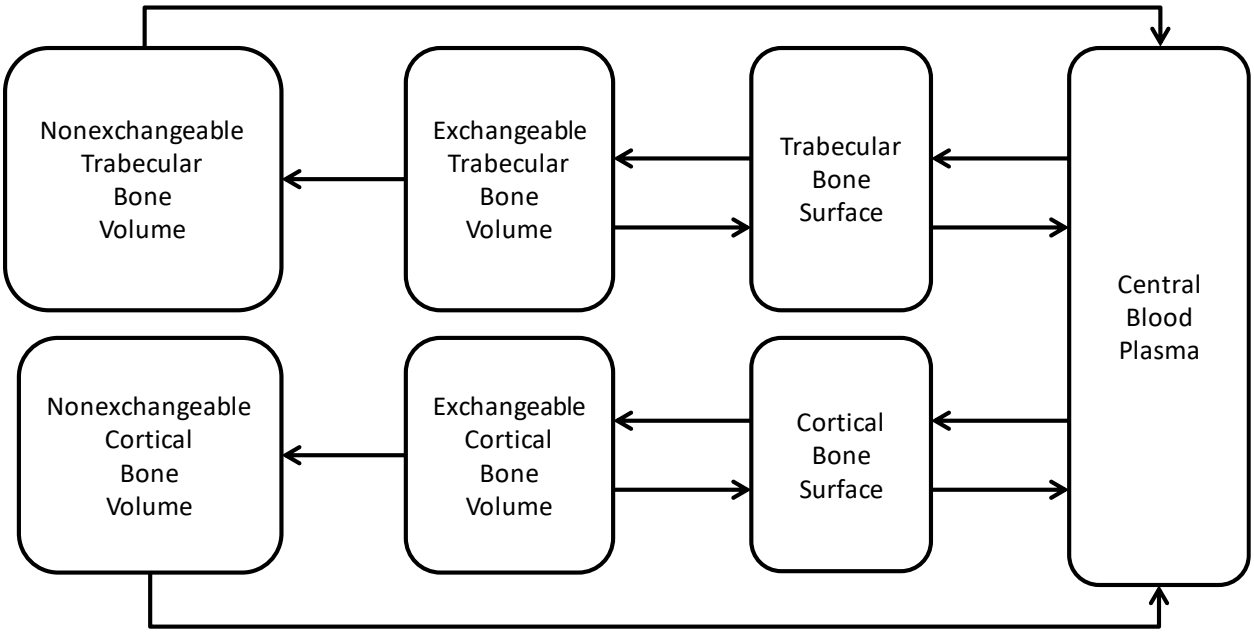

This figure is based on Leggett (1993).

CHAPTER 3. EVALUATION AND DEVELOPMENT OF THE FORTRAN BASED AALM

3.1. INTRODUCTION AND OJBECTIVES OF THIS ANALYSIS

In 2014, EPA released the report Framework for Identifying and Evaluating Lead-Based Paint Hazards from Renovation, Repair, and Painting Activities in Public and Commercial Buildings (U.S. EPA, 2014c) which described how EPA could identify and evaluate hazards in public and commercial buildings. The framework report was followed by a more detailed Approach for Estimating Exposures and Incremental Health Effects due to Lead During Renovation, Repair and Painting Activities in Public and Commercial Buildings (U.S. EPA, 2014b) and appendices (U.S. EPA, 2014a). The latter report describes in greater detail an approach to estimating potential environmental concentrations, Pb body burdens, and incremental health effects related to exposure to Pb from renovations of public and commercial buildings. A key element in the approach was a Monte Carlo Analysis of Pb exposure scenarios and predicted blood and bone Pb concentrations in children and adults. Blood and bone Pb were estimated using an implementation of the Leggett (Pounds and Leggett, 1998; Leggett, 1993) biokinetics model (Leggett Fortran Model, LFM). Several modifications were made to the LFM to improve its performance and facilitate the Monte Carlo Analysis. The results of these modifications produced ICRPv005.FOR, also referred to as Leggett Model Version 5 (https://www.epa.gov/lead/approach-estimating-exposures-and-incremental-health-effects-lead-due-renovation-repair-and). In developing ICRPv005.FOR, several changes were made to the Leggett biokinetics model (Table 3-1). ICRPv005.FOR performed well when evaluated using the NHANES data for children and occupational Pb smelter data for adults, indicating good agreement with both these measured data sources and IEUBK model estimates. As part of the response to peer review comments on the approach, EPA undertook the analyses described in another report (Versar, 2015).

In the months following EPA OPPT's release of the Approach for Estimating Exposures and Incremental Health Effects due to Lead During Renovation, Repair and Painting Activities in Public and Commercial Buildings document, EPA ORD NCEA completed a beta test version of the All Ages Lead Model (AALM.CSL; v. 4.2, July 2015) which also implemented an updated and expanded version of the Leggett model (Pounds and Leggett, 1998; Leggett, 1993) in Advanced Continuous Simulation Language (ACSL; a.k.a. acslX). The development of AALM.CSL included calibration and evaluation of model performance that are described in Chapter 4 using several data sets that were of potential value for further evaluations of the ICRPv005.FOR model. EPA was also interested in exploring differences in the structures and estimations of blood and bone Pb from the two models. In part, to determine if one or the other model might offer advantages for applications in estimating Pb body burdens related to public and commercial building renovations as well as other potential research and regulatory applications of the models for estimating exposure-body burden relationships.

This chapter summarizes results of analyses undertaken by EPA to explore differences in the structures and estimations of blood and bone Pb between AALM.CSL and ICRPv005.FOR. The specific objectives of these analyses were as follows:

- Conduct further evaluations of ICRPv005.FOR and AALM.CSL;
- Modify the models as needed, based on the outcome of these evaluations; and

- Harmonize the two models so that the models estimate similar blood and bone Pb levels for similar exposure inputs.

A detailed description of the structure of the AALM version 3.0 (Fortran executable with Excel User Interface) is provided in Chapter 2.

Within this chapter, Section 3.2 compares estimations of blood and bone Pb concentrations obtained from the models. Section 3.3 describes the outcomes of comparisons of model estimations to observations. Section 3.4 discusses data needs for potential further refinement and evaluation of the models. Section 3.5 summarizes conclusions from the model comparisons, model harmonization and responses to peer review comments on approaches to blood and bone Pb modeling.

The AALM (Fortran executable with Excel User Interface) was publicly released as the AALM version 2.0 and underwent an independent federal advisory committee peer review in 2019-2020 as discussed in Section 1.1.1. Based on peer review comments, the AALM version 3.0 (i.e., the current version of AALM again using a Fortran executable with Excel user interface) was developed from 2020 through 2023 to address all necessary revisions (Tier 1 recommendations) and many suggested revisions (Tier 2 recommendations). Section 3.6 of this chapter provides a sensitivity analysis for the AALM version 3.0.

3.2. MODEL ESTIMATIONS OF BLOOD AND BONE PB

Differences in the parameter values used in ICRPv005.FOR and AALM.CSL biokinetics models (Table 3-2) resulted in different estimations of blood and tissue Pb levels for similar Pb exposure assumptions. Ultimately it was decided to harmonize the two models and a Fortran version (AALM.FOR) of AALM.CSL was created. Thus, Table 3-2 essentially provides the changes in ICRPv005.FOR that were required to create AALM version 2.0 in Fortran. The AALM version 2.0 in Fortran and AALM.CSL implementations are structurally identical and have only few differences in parameter values and computational schemes that do not affect simulations of blood and bone Pb concentrations (Table 3-3). The most important changes made to ICRPv005.FOR to create AALM include the following: (1) Growth parameters from O'Flaherty (1995, 1993) were adopted in AALM, this results in identical age profiles for blood volumes and tissue masses between the models (see Chapter 2, Figure 2-2); and (2) GI absorption parameters from AALM.CSL were adopted in AALM (see Section 4.7.1 and Figure 4-13). The GI absorption fraction is 0.39 at birth and decreases to 0.12 at age 8 years (Figure 3-1). All other parameter values (e.g., transfer rates and deposition fractions) from AALM.CSL were adopted in the Fortran version of the AALM v2.0.

Two types of comparisons were made of ICRPv005.FOR and AALM: (1) age profiles for blood and tissue Pb levels following an exposure to a constant Pb intake (µg/day) were simulated and compared; and (2) dose-response relationships between ingested dose and Pb levels were compared by simulating a series of increasing Pb intakes. In either type of simulation, parameters that control Pb absorption and growth were set to the same values, so that differences in blood and tissue Pb levels could be attributed entirely to differences in the simulation of systemic (post-absorption) biokinetics.

3.2.1. Constant Pb Intake

Figures 3-2 and 3-3 show simulations of the accrual and elimination of Pb in blood and bone, respectively, in children and adults. Exposures were simulated as a constant baseline Pb intake (5 µg/day) with a period of elevated intake (40 µg/day in children and 105 µg/day in adults). This exposure

results in estimated blood Pb concentrations ≤5 µg/dL, which is well below the concentration at which saturation of uptake into RBCs significantly affects blood Pb levels. Several differences are evident from these comparisons:

- The harmonized Fortran version of the AALM and AALM.CSL produce identical estimations of blood and bone Pb concentrations.
- The AALM estimates higher blood and bone Pb concentrations than ICRPv005.FOR. The difference is more pronounced in the adult simulation (Figure 3-2).
- The AALM estimates a slower approach to a quasi-state state blood Pb concentration than ICRPv005.FOR and slower elimination and return to baseline (Figure 3-2). The difference is more pronounced in the adult simulation. The AALM estimates a return to baseline over a period of decades in adults; whereas, ICRPv005.FOR estimates a return to baseline within one year.
- The pattern of decline in blood Pb concentration following an abrupt decrease in Pb intake is also different in the AALM and ICRPv005.FOR. Both models estimate multi-phasic elimination of Pb from blood in children (Figure 3-2A); however, the AALM estimates an early rapid phase, followed by a slower phase; whereas, ICRPv005.FOR estimates a slower early phase, followed by more rapid phase.
- The AALM estimates similar cortical and trabecular bone Pb concentrations in children; whereas, ICRPv005.FOR estimates trabecular bone Pb concentrations that are approximately 25% of cortical bone (Figure 3-3A, 8C).
- The AALM and ICRPv005.FOR estimate higher Pb concentrations in adult trabecular bone, compared to cortical bone, and slower accrual and elimination kinetics in cortical bone (Figure 3-3 B, D).
- The AALM estimates faster elimination of Pb from adult cortical bone compared to ICRPv005.FOR (Figure 3-3B).

3.2.2. Dose-Response for Blood and Bone Pb

Although both the AALM and ICRPv005.FOR model are mathematically linear models (i.e., all compartment Pb masses are defined with linear differential equations), they estimate curvilinear dose-response relationships for blood Pb resulting from a saturable capacity of RBCs to take up Pb. Dose-response relationships estimated from AALM.CSL, AALM.FOR[5] and ICRPv005.FOR are shown in Figures 3-4 for blood and 3-5 for bone, in children (age 2 years) and adults (age 30 years). In the AALM, curvature in the intake-blood Pb relationship is negligible at blood Pb concentrations <10 µg/dL. Both models estimate linear dose-response relationships for bone Pb.

3.3. COMPARISONS OF MODEL ESTIMATIONS TO OBSERVATIONS

Peer reviewers of Approach for Estimating Exposures and Incremental Health Effects due to Lead During Renovation, Repair and Painting Activities in Public and Commercial Buildings (U.S. EPA, 2014b)

[5] AALM.FOR is used throughout the remainder of this chapter as well as its tables and figures to indicate the Fortran version of the AALM, which was released publicly as AALM v2.0.

suggested that data be used to evaluate blood and bone Pb estimations in adults from Hattis (1981) and Nie et al. (2005), including additional unpublished Nie et al. data.

Data that were available from the Nie study consisted of three longitudinal blood and bone XRF measurements for 209 adult Pb workers. The measurements were made in 1991, 1999 and 2008. This period included a nine-month strike (July 1990 to May 1991), during which exposures at the plant were interrupted. The available data also included birth dates and dates of hire. There were no data on actual exposures at the plant. Although attempts were made to reconstruct exposures so that blood and bone Pb concentrations could be estimated and compared to observations, ultimately, it was concluded that the data were not suitable for model evaluations because of the uncertainty in the exposures that preceded the blood and bone Pb measurements and that occurred during the measurement period. Exposures prior to 1991, including the period of the strike, had to be reconstructed with no basis for verification other than the observed blood and bone Pb measurements. In one reconstruction attempted, each subject was assumed to have an age-intake profile that estimated an age-blood Pb profile that was similar to the central estimates from the NHANES survey that corresponded to the subject's age date. Added to this background intake was a constant occupational intake (except during the strike) that was calibrated to achieve a good fit to the weighted MSE for observed bone Pb (tibia and calcaneus) and blood Pb (relative weights: cortical bone 3, trabecular bone 2, blood 1). This fitting procedure resulted in good agreement between cortical and trabecular bone Pb estimated from ICRPv005.FOR and corresponding observations ($r^2 > 0.8$). However, a good fit to the observations could be expected for a wide range of biokinetics parameter settings; therefore, these data would not allow a determination of whether ICRPv005.FOR or the AALM would perform better at estimating the observations.

Data that were available from the Hattis study were much more suitable for model evaluation. These data included blood Pb concentrations in 57 workers at hire and prior to and following a nine-month strike. Although pre-hire exposures were unknown, it was possible to calibrate the post-hire and pre-strike exposures to achieve agreement with blood Pb concentrations at the time of hire and just prior to the strike, and then estimate without further calibration the post-strike blood Pb. Agreement between post-strike observations and estimations would be sensitive to biokinetics parameter settings that control blood Pb elimination rates. Therefore, these data were used to compare performance of ICRPv005.FOR and AALM. The outcome of this comparison indicated that the AALM performed better at estimating the Hattis observations than ICRPv005.FOR (described in detail in Section 3.3.1). Based on these evaluations, a Fortran version of the AALM (AALM.FOR) was developed and additional evaluations of AALM.FOR and AALM.CSL were conducted. These evaluations are described in Sections 3.3.2 to 3.3-10.

Goodness of fit of model predictions to observations were evaluated three approaches: (1) visual inspection of observed and predicted values; (2) inspection of standardized residuals (Equation 3-1); and (3) r^2 for the least-squares linear regression of observed and predicted values.

$$Standardized\ Residual = \frac{Predicted - Observed}{Standard\ Deviation\ of\ Observed\ Mean} \qquad \text{Eq. (3-1)}$$

Standardized residuals $\leq \pm 2$ and $r^2 > 0.70$ were considered acceptable fit to the observations.

3.3.1. Pb Elimination Kinetics in Workers with Dose Reconstruction (Hattis Data)

The Hattis data set used in this analysis included the following data on 57 adult Pb workers: (1) duration of employment prior to strike (Days_prestrike); (2) blood Pb concentration prior to start of employment (BLL_start); (3) blood Pb just prior to a nine-month strike (BLL_prestrike); and (4) blood Pb on return to work, following strike (BLL_poststrike). The 57 subjects comprised a subset of the 66 subjects in the dataset described in Hattis (1981). Subjects were excluded from the analysis if pre-strike blood Pb was >75 µg/dL, post-strike blood Pb was < blood Pb at date of hire, or post-strike blood Pb was > pre-strike blood Pb. In the absence of information on pre-employment Pb exposures, pre-hire Pb intake was simulated as a constant ingestion intake (µg/day/kg body weight) that would result in a estimated blood Pb concentration at age 20 years that was similar to BLL_start (±1 µg/dL). Pre-strike occupational exposure was simulated as a constant ingestion intake (µg/day) that would result in a estimated blood Pb concentration at age = (20 years + duration of strike) that was similar to BLL_start (±1 µg/dL). During the strike (assumed to be 270 days in duration), ingestion intake reverted to the pre-hire Pb intake.

An example of a simulation for a single subject from the Hattis data is shown in Figure 3-6 for AALM.CSL. In this simulation, the pre-hire Pb intake and pre-strike exposure intake were calibrated to estimate blood Pb concentrations similar to the observations made at the time of hire and at the start of the strike. In this case, the estimated post-strike blood Pb concentration (18.5 µg/dL) was within 10% of the observed (17.0 /dL). A pseudo first-order elimination rate (d^{-1}) and $t_{1/2}$ were estimated from the observed blood Pb concentrations at the beginning and end of the strike as follows (Equations 3-2 and 3-3):

$$k = \ln\left(\frac{BLL\ pre-strike}{BLL\ post-strike}\right)/270 \qquad \text{Eq. (3-2)}$$

$$t_{1/2} = \frac{\ln(2)}{k} \qquad \text{Eq. (3-3)}$$

The $t_{1/2}$ calculated from the blood Pb concentrations estimated from the model and observations were 371 days and 320 days, respectively. The calculated values for $t_{1/2}$ do not reflect the actual elimination kinetics of Pb from blood in this subject, or estimated from the AALM, because both would be expected to be multi-phasic over the 270-day interval. However, it serves as a convenient metric for comparing model performance when applied to the entire set of 57 subjects.

Both ICRPv005.FOR and AALM.CSL were successfully calibrated to the blood Pb concentrations measured at time of hire and just prior to the strike (r^2 = 1.0). Estimated and observed post-strike blood Pb concentrations were also correlated, but showed substantially more variability that could not be accounted for by the models, as expected for model estimations (r^2 = 0.47; Figure 3-7).

Figure 3-8 shows the distribution of calculated $t_{1/2}$ values for the Hattis subjects. Summary statistics for the evaluation are presented in Table 3-4. The median $t_{1/2}$ estimated from the observations was 633 days (GSD 2.4). The median from AALM.CSL was 483 days (GSD 1.6) and the median from ICRPv005.FOR was 274 days (GSD 1.6). The average difference between the individual observed and estimated $t_{1/2}$ values was -5% for AALM.CSL and -37% for ICRPv005.FOR. AALM.FOR estimated $t_{1/2}$ (median 465 days, GSD 1.6; percent difference -8%) that were similar to AALM.CSL estimation.

3.3.2. Pb Elimination Kinetics in Workers with Dose Reconstruction (Nilsson et al., 1991)

Nilsson et al. (1991) reported longitudinal data on blood and finger bone Pb concentrations in 14 Pb workers for period ranging from 8–18 years following cessation of their occupational exposures. The median blood Pb concentration at the end of exposure was approximately 45 µg/dL. The decline in bone Pb concentration was described by a first-order model with a single rate constant. Estimates of elimination half-times for each individual were reported. The group median was 16 years (95% CI: 12, 23). The decline in blood Pb was described by a tri-exponential model with the following parameters.

Parameter	Unit	C1 (95% CI)	C2 (95% CI)	C3 (95% CI)
$t_{1/2}$	year	34 day (29, 41)	1.2 year (0.85, 1.8)	13 year (10, 18)
C	µg/dL	10.2	12.6	22.8

AALM simulations were run for a constant Pb intake from birth to age 60 years, to achieve a terminal blood Pb concentration of approximately 45 µg/dL (2000 µg/day), followed by 20 years without exposure. A first-order exponential rate was estimated for the decline in cortical bone Pb concentrations estimated for 20 years following cessation of exposure. Figure 3-9 compares rates of elimination of Pb from bone and blood with the corresponding empirical models derived for the Pb workers (Nilsson et al., 1991). Elimination rates of Pb from bone estimated from the optimized models are within the 95% CI of the empirical model and yield standardized residuals that range within the -2, 2, criteria ($r^2 = 0.99$). Elimination half-times estimated for bone Pb (16 years) were identical to estimates from Nilsson et al. (1991). Although elimination rates from blood estimated by the optimized models are approximately at the confidence limits of the empirical model, the initial model divergence is due largely to the slower elimination kinetics observed during the first 5 years following cessation of exposure; after which the models converge on the empirical model ($r^2 = 0.96$). Half-times estimated for the period 5 to 20 years after exposure were 1.25 years, similar to values estimated for C2 (1.2 year) from Nilsson et al. (1991).

3.3.3. Blood Pb Accrual and Elimination Kinetics in Adults with Known Pb Doses (Rabinowitz et al., 1976)

Rabinowitz et al. (1976) conducted a pharmacokinetics study in which four adults ingested daily doses of [207Pb] nitrate for periods up to 124 days. Concentrations of 207Pb in blood, urine, and feces were then monitored during and following cessation of exposure, and data on daily intakes and blood concentrations for each subject were reported. Absorption fractions for Pb were estimated for each individual based on mass balance in feces.

Figure 3-10 compares observed and estimated blood 207Pb concentrations from AALM.FOR and AALM.CSL. Gastrointestinal absorption fractions were set in both models to the estimates for each individual reported in Rabinowitz et al. (1976). No other changes were made to parameter values. Both models estimated the rise and decline in blood Pb concentrations in temporal patterns that agreed with observations. Values for r^2 for AALM estimations are 0.99, 0.98, 0.92, and 0.97 for Subjects A, B, D, and E, respectively.

3.3.4. Post-mortem Soft Tissue-to-Bone Pb Ratio (Barry, 1975)

Four studies provide data for measurements of post-mortem soft tissue and bone Pb concentrations (Gerhardsson et al., 1995; Barry, 1981; Barry, 1975; Gross et al., 1975). Gerhardsson et al. (1995) reported only soft tissue Pb concentrations; whereas, the other three studies reported soft tissue and bone Pb concentrations that can be used to estimate the ratios. Barry (1981) and Barry (1975) reported data for children and adults in age brackets. The data from Barry (1975) was used as the primary source to optimize parameters for kidney/bone and liver/bone Pb ratios as a function of age. Barry (1975) reported data on tibia Pb concentrations that are simulated as cortical bone concentrations in the AALM models. Since Barry (1975) reported group mean tissue concentrations (not ratios in autopsy cases), the mean tissue-to-bone ratios were approximated from the group means. Figure 3-11 compares estimated and observed kidney/bone and liver/bone Pb ratios in adults. Values for r^2 for kidney/bone estimations (of average of male and female ratios) were 0.95. Values for r^2 for liver/bone estimations were 0.96 and 0.93 for AALM, respectively.

3.3.5. Plasma-to-Bone Pb Ratio in Workers (Hernández-Avila et al., 1998; Cake et al., 1996)

Two studies provide data to evaluate the relationship between plasma or serum blood Pb and bone Pb concentrations (Hernández-Avila et al., 1998; Cake et al., 1996). Cake et al. (1996) measured paired serum, tibia, and calcaneus Pb concentrations in 49 adult male Pb workers, and reported corresponding linear regression parameters. Hernández-Avila et al. (1998) measured paired plasma, tibia and patella Pb concentrations in 26 adults (20 female) who had no known occupational exposures to Pb. These data can be used to derive corresponding linear regression parameters for the log-transformed plasma Pb. Individual subject data were digitized from Figure 1 of Hernández-Avila et al. (1998), and linear regression parameters derived for the untransformed plasma Pb concentrations, in order to compare these with the linear regression parameters from Cake et al. (1996).

Bone Pb/plasma Pb slopes at age 50 years were estimated from the AALM for a series of simulations in which Pb intake was varied from 1 to 1000 µg/day. Table 3-5 and Figure 3-12 compare estimated and observed slopes based on data from Cake et al. (1996) and Hernández-Avila et al. (1998). The bone/plasma ratios estimated from the AALM were within the 95% CI of the Cake et al. (1996) estimates and were also within the 95% CI of the Hernández-Avila et al. (1998) for tibia.

3.3.6. Plasma Pb – Blood Pb Relationship (Meta-data)

Six studies provided data on individual human subjects that can be used to evaluate the relationship between plasma Pb and blood Pb concentrations. Measurements of plasma Pb were made using either inductively coupled plasma mass spectrometry (Smith et al., 2002; Bergdahl et al., 1999; Bergdahl et al., 1998; Hernández-Avila et al., 1998; Bergdahl et al., 1997; Schütz et al., 1996) or stable isotope dilution with thermal ionization mass spectrometry (Manton et al., 2001). In all of these studies, methods were employed to control for sample contamination, which is of particular importance in measurements of the low Pb levels found in plasma. Taken together, the observations from these reports varied over a wide range of blood Pb (approximately 0.34–94.8 µg/dL) and plasma Pb (approximately 0.0014–1.92 µg/dL) levels. These studies provided 406 individual measurements of plasma Pb and blood Pb, in adult workers as well as individuals with no known history of occupational exposure to Pb (U.S. EPA, 2003a). Only

one study provides similar data in children (Bergdahl et al., 1999). The observations in children do not appear to differ substantially from those for adults.

A best fit (least-squares) model for combined data from the above six studies was identified, and is presented in Equation 3-4:

$$Blood\ Pb = 87.0 \cdot Plasma\ Pb^{0.5} - 3.89 \quad (r^2=0.90) \qquad \text{Eq. (3-4)}$$

Figures 3-13 compares the observed and estimated plasma-whole blood Pb relationship in adults. Standardized residuals for the optimized models are within acceptable limits (-2, 2). The r^2 values for estimations are 0.99 and 0.98.

3.3.7. Blood Pb Elimination Kinetics in Infants with Known Doses (Sherlock and Quinn, 1986; Ryu et al., 1983)

Only two studies provide data on the relationships between Pb dose and blood Pb concentration in infants (Sherlock and Quinn, 1986; Ryu et al., 1983). In the Ryu et al. (1983) study, blood Pb concentrations were monitored in 25 formula-fed infants. From birth to age 111 days, infants were fed formula (packaged in cartons) that had a Pb concentration of approximately 20 µg/L. From age 112 to 195 days, a subset of the infants (n = 7) were switched to formula (packaged in cans) that had a Pb concentration of approximately 57 µg/L. Formula intakes were measured, and provided estimates of Pb intakes in each subject. Ryu et al. (1983) reported a table of individual Pb intakes, and presented a figure illustrating group mean blood Pb concentrations at various ages (these data were digitized for use in this analysis). Standard errors (or deviations) of mean blood Pb concentrations were not reported; however, as discussed below, based on Sherlock and Quinn (1986), standard errors may have been approximately 10% of the means. The parameter for maternal blood Pb concentration was set at 10 µg/dL, the reported maternal mean for the study. Lead absorption was not quantified in Ryu et al. (1983); therefore, the gastrointestinal absorption fraction during infancy was set to 40%, based on estimates from mass balance studies (Ziegler et al., 1978). No other changes were made to parameter values. Figure 3-14 compares estimated and observed blood Pb concentrations for the two exposure regimens (carton formula or carton followed by canned formula). Simulations are shown for the mean intake (12–20 µg/day) and ± 1 SD (10–18 µg/day, 15–22 µg/day). AALM.CSL and AALM.FOR simulations encompass most of the observations within ±1 SD of the mean intakes. If standard errors of mean blood Pb concentrations were 10% of the mean, standardized residuals for AALM estimations ranged from -3.7 to 0.15 for carton exposures (mean -1.2). The AALM captures the increase in blood Pb concentration associated with the switch the higher Pb intakes for canned formula and the overall temporal trends in the observations; r^2 for estimations were 0.85.

Sherlock and Quinn (1986) measured blood Pb concentration in 131 infants at age 13 weeks and estimated dietary intake of Pb for each infant based on Pb measurements made in duplicate diet samples collected daily during week 13. Sherlock and Quinn (1986) provided a plot of blood Pb means and standard errors for group mean dietary Pb intakes (these data were digitized for use in this analysis). The parameter for maternal blood Pb concentration was set at 18 µg/dL, the reported maternal geometric mean. The gastrointestinal absorption fraction was set at 40% for infants; the same value used in simulations of Ryu et al. (1983). Figure 3-15 compares estimated and observed blood Pb concentrations for the range of Pb intakes in the study. AALM.CSL and AALM.FOR models reproduce the general shape of the observed curvilinear dose-blood Pb relationship; the apparent plateau observed at the higher end of the dose range, however, it is achieved at higher doses in the models (>800 µg/day). Although the

model results for the plateau contributed to high residuals at the highest Pb intake (>200 µg/day), standardized residuals for lower Pb doses ranged from -4.8 to 1.5 (mean -2.3). The overall dynamics of increasing blood Pb with increasing Pb dose was estimated with $r^2 = 0.95$. One possible explanation for the higher plateaus in the dose-blood Pb relationship estimated from both models is that the models may estimate higher saturation levels of Pb in RBCs than actually occurred in the infants in the Sherlock and Quinn (1986) study. Parameter values for RBC uptake are based on data collected on adults, and have not been optimized for infants due to an absence of good supporting data (see Section 3.3.6).

3.3.8. Blood Pb Elimination Kinetics in Infants with Dose Reconstruction (ATSDR)

Agency for Toxic Substances and Disease Registry (ATSDR) made available for this analysis longitudinal blood Pb data in children following intervention in response to measurement of an elevated blood Pb concentration. The data included dates of birth and dates and results of repeated Pb measurements in 12 females and 12 males. Interventions included interruption of the exposure which allows an evaluation of elimination kinetics of blood Pb. However, other interventions may have also been conducted but were not documented in the data made available for this analysis. Intervention is likely to have included chelation therapy in children whose blood Pb concentration exceeded 45 µg/dL. Chelation would be expected to have affected rates of decline in blood Pb concentration during the first 1-3 weeks following the diagnosis of elevated blood Pb. The longitudinal blood Pb data available for longer periods would reflect post-chelation kinetics and are suitable for evaluating model estimations of blood Pb elimination kinetics.

Since actual exposures to Pb were unknown for each child, the exposures leading up to the first blood Pb measurements were reconstructed as a constant baseline Pb intake (µg/day) that resulted in a blood Pb concentration of 5 µg/dL at age 6 months. Selection of 5 µg/dL as the target for the baseline simulation is supported by the observations that that average terminal blood Pb concentration was 5.5 µg/dL (±2.4 SD, n = 24). Some children had blood Pb concentrations reported prior to an episode of elevated blood Pb concentrations; the mean was 5.3 µg/dL (±2.4 SD, n = 4). Another uncertainty is the reconstruction of the level and duration of the elevated exposure that occurred prior to the detection of the elevated blood Pb. Since there was no information about the exposure level or duration, these parameters were calibrated to the blood Pb observations to achieve optimal residuals and r^2 for the estimations. Examples of successful exposure constructions are shown in Figures 3-16 to 3-18. Although, there is considerable uncertainty about the reconstructed exposures, in each case, the AALM simulated the blood Pb elimination kinetics from observations well beyond the expected period of chelation. Figure 3-18 shows one of the few cases in which a baseline blood Pb measurement was available prior to the elevated exposure. The timing of this baseline measurement considerably decreases the uncertainty about the duration of the elevated exposure. Since the baseline measurement was made at age 450 days and first elevated blood Pb was measured at age 810 days, the duration was likely to have been no more than 360 days. The optimized duration (age day 600 – 800) and exposure level (13,000 ppm Pb in dust) provided a good fit to the observed elimination kinetics (r^2 0.81). The simulations shown in Figures 3-16 to 3-18 are examples of one approach to reconstructing the Pb exposures that occurred prior to the blood Pb observations.

3.3.9. Comparison to IEUBK Model for Pb in Children

Figure 3-19 compares estimations of the AALM v2.0 and the IEUBK model v1.1 for a continuous dust Pb intake of 10 µg/day.[6] In both models, the relative bioavailability (RBA) for Pb in dust was assumed to be 60%. This corresponds to an absolute bioavailability of approximately 20% at age 2 years in the AALM and 30% in the IEUBK model. At age 2 years the IEUBK model estimates a blood Pb concentration of 1.18 µg/dL; the AALM estimates 1.25 µg/dL.

3.3.10. Comparison to Adult Lead Methodology

Figure 3-20 and Table 3-6 compare estimations of adult blood Pb concentrations from the Adult Lead Methodology and AALM, for an exposure to 1000 ppm. In both models, the RBA for Pb in dust was assumed to be 60%. This corresponds to an absolute bioavailability of approximately 4.8% in the AALM and 12% in the Adult Lead Methodology. The Adult Lead Methodology estimates a blood Pb concentration of 2.9 µg/dL; the AALM estimates 3.1 µg/dL at age 30 years (mid-point for age range in the Adult Lead Methodology, 17-45 years).

3.4. DATA NEEDS FOR FURTHER REFINEMENT OF THE AALM V2.0

The AALM.FOR model (publicly released as AALM v2.0) discussed in this chapter demonstrates the considerable advancements that have been made since a development of ICRPv005.FOR in terms of its capability and evaluation estimations of Pb body burdens, including blood Pb concentrations in children and blood and bone Pb concentrations in adults. Blood Pb concentrations in adults estimated from the AALM are very similar to estimations from the EPA Adult Lead Methodology (ALM) for the same soil Pb concentrations. Estimations for infants are similar between the AALM and the IEUBK. Work done for the release of the AALM v2.0 was responsive to comments received on both models from peer reviews conducted in 2005 and 2014 (see Section 3.5).

Recommendations for data to reduce uncertainty in the estimations obtained from AALM.FOR and AALM.CSL, and improve the consistency among all model estimations include the following:

- *Further verify AALM estimations.* Additional observations in humans should be identified that can serve to evaluate the performance of the optimized AALM (and that were not used in the optimization). Ideally, these would be blood and/or bone Pb measurements in people for whom Pb intakes are known with reasonable certainty. Ethical concerns typically preclude Pb dosing experiments; therefore, Pb doses must be estimated with accurate tools such as duplicate diet surveys or dietary recalls and information on Pb levels in diet and other relevant exposure media. Types of data that would be valuable for model validation include: (1) blood soft tissue or bone Pb levels in children or adults for whom Pb dosage is known or can be reliable estimated from exposure data; (2) changes in blood, soft tissue or bone Pb levels in children or adults following and abrupt change (increase or decrease) in Pb exposure; (3) steady state (or quasi-steady state)

[6] As of May 2021, the IEUBK v2.0 is the most current version. New comparisons between the AALM and IEUBK v2.0 were are not provided here since the biokinetic parameters in the IEUBK model were not changed between v1.1 and v2.0. Although default exposure and intake parameters were changed between IEUBK v1.1 and v2.0, this does not affect the relative fold-differences between AALM and IEUBK predicted blood Pb concentrations when the media exposure and intake parameters are matched.

blood/soft tissue blood/bone Pb ratios in children or adults; (4) urinary Pb clearance from blood or plasma in children or adults; and (5) plasma/whole blood concentration ratios in children.

- *Evaluate and document the empirical basis for exposure model parameters.* Most of the exposure parameter values in the AALM serve as placeholders and should be replaced by users with values for specific receptor populations for which an empirical basis can be provided.
- *Further refine the gastrointestinal tract model*. AALM.FOR allows the user to input values for RBA of Pb in exposure media. This is important for risk assessment applications because the absorption fraction Pb is known to vary with the environmental medium in which it is contained (e.g., Pb in soil can have a lower absorption fraction than Pb dissolved in water). However, in the 2019 version of AALM.FOR, the RBA adjustment is applied to the media-specific Pb intake rather than to the absorption fraction (*F1*) in the small intestine. In this configuration, Pb that is not absorbed when RBA is <1 does not appear in feces. This resulted in an underestimation of fecal Pb excretion and a negative mass balance (excretion < intake). This issue was resolved in the AALM version 3.0 which adjusts the absorption fraction by RBA and provides a more accurate representation of medium-specific absorption and excretion of Pb. This is similar to the modeling approach to RBA that was contained in AALM.CSL.
- *Further refine the respiratory tract (RT) model*. The 2019 version of AALM.FOR uses a 4-compartment RT model from the Leggett (1993) model in which Pb intake to the RT represents the deposited dose (µg Pb deposited in the RT per day), which must be calculated outside of AALM.FOR for a given set of assumptions regarding the air Pb concentration (µg/m^3), inhaled particle size and minute (day) and volume day volume (m^3/day). As described in Section 2.3.3.1, the division of the respiratory tract into three regions (ET, TB, and ALV) in the AALM v3.0 is intended to facilitate the future use of deposition fractions calculated using the Multi-Path Particle Dosimetry model (MPPD) or another model. It is anticipated that a future model release will use inputs of air Pb concentration, particle size and Pb species would be more useful for applications to simulating air Pb exposures. This could be similar to the simplified version of the ICRP (1994) model that was implemented in the beta test version of AALM.CSL (v. 4.2, July 2015).
- *Refinement of the bone mineral model*. The AALM includes calculations for converting concentrations of Pb in bone wet weight to concentration per g bone mineral by dividing the wet weight concentration by the ash fraction of bone. This conversion is important for comparing model estimations of bone Pb concentrations with bone X-ray fluorescence (XRF) data, which is typically reported in units of Pb per g bone mineral. In AALM.CSL, bone ash fractions were assumed to be 0.55 and 0.50 for cortical and trabecular bone, respectively (ICRP, 1996). In ICRPv005.FOR, the bone ash fractions were assumed to be 0.55 for cortical bone and 0.18 for trabecular bone. AALM.CSL values have been adopted for AALM.FOR and the different values for trabecular bone have not been reconciled. Further research that could provide a stronger empirical basis for these values would improve confidence in simulations of XRF observations.

3.5. CONCLUSIONS AND IMPLICATIONS FOR MODELING LEAD BODY BURDENS

The 2019 version of AALM.FOR (publicly released as AALM v2.0 in September 2019) represents a substantial update to ICRPv005.FOR used in the Approach for Estimating Exposures and Incremental Health Effects due to Lead During Renovation, Repair and Painting Activities in Public and Commercial

Buildings (U.S. EPA, 2014b) and appendices (U.S. EPA, 2014a) . The updates include new parameters for simulating physiological growth and gastrointestinal absorption, as well as updated parameters that govern rates of exchange of Pb between plasma, RBCs, bone, kidney and liver (Table 3-2). AALM.FOR estimates blood, bone and soft tissue Pb levels that are identical AALM.CSL and provides an alternative Fortran platform to acslX, which is no longer commercially supported, for implementing the AALM.

3.5.1. Evaluation of AALM Performance

AALM.FOR (publicly released as AALM v2.0 in September 2019) was evaluated with a larger set of observations in children and adults, including some data that had not been used in previous evaluations of ICRPv005.FOR. Data on Pb dose-blood Pb relationships is limited to a three studies; one of adults in which five male subjects were administered known doses of a stable Pb isotope for periods of 2 to 6 months (Rabinowitz et al., 1976) and two studies of infants in which Pb ingestion doses were estimated from dietary (formula) Pb measurements and exposures were for approximately 3 months [n=25, (Ryu et al., 1983)] and [n=131, (Sherlock and Quinn, 1986)]. No data were available on dose-blood Pb concentration relationships in older children or adolescents for whom Pb ingestion doses were known with certainty. Several studies have reconstructed Pb intakes in children from exposure models supported by measurements of environmental exposure concentrations (Dixon et al., 2009; TerraGraphics, 2004; Malcoe et al., 2002; Hogan et al., 1998; Lanphear et al., 1998; Bornschein et al., 1985). However, these studies were not considered in these evaluations.

Although limited in size, these evaluations suggest that AALM.FOR can provide an accurate estimation of dose-blood Pb relationships when actual doses are known or can be calculated with certainty. In general, AALM.FOR estimated the observed blood Pb concentrations and dynamics in infants and adults in response to changing Pb dosing (see Figures 3-10, 3-14). AALM.FOR also estimated quasi-steady state blood Pb concentrations in infants across a range of ingestion doses of Pb (Figures 3-15). The model estimated a higher plateau for the dose-blood Pb relationship than was observed in infants (Figure 3-15), however, this difference would be of quantitative significance only at intakes resulting in blood Pb concentrations >30 µg/dL. These evaluations show that the model reliably estimates both quasi-steady state blood Pb concentrations as well the rates of change Pb that occur with a change in exposure.

AALM.FOR also estimated the observed relationships between plasma and whole blood Pb concentrations in adults (Figure 3-13). Transfer out of RBCs in AALM.FOR is age-dependent and faster in children than in adults. The validity of the age-dependence was not rigorously explored in this analysis. What little data there are on plasma-blood Pb relationships in children does not suggest an appreciable difference in the relationship for children and adults (Bergdahl et al., 1999). Since the age-dependence could not be rigorously evaluated it is retained in AALM.FOR. AALM.FOR also estimated the observed relationships between plasma and bone Pb concentrations in adults (Figure 3-12) and between kidney, liver and bone Pb concentrations in children and adults based on post-mortem data (Figure 3-11). This suggests that the model accurately estimates the ratios of the exchange kinetics (rates into tissue and out to plasma) that give rise to the age-dependent distribution of Pb between bone and soft tissue.

AALM.FOR estimated the observed changes in blood Pb concentrations in children and adults for reconstructed exposures estimated based on observed blood Pb measurements (Figures 3-8, 3-9, 3-16 to 3-18). These evaluations indicate that the model accurately estimates observed elimination kinetics of Pb from blood in children and adults, and bone in adults. AALM.FOR estimates more rapid elimination of

Pb from bone in children compared to adults (Figure 3-3). This is consistent with more active bone growth and turnover of bone mineral during childhood which should contribute to more volatile bone Pb stores (O'Flaherty, 1995; Leggett, 1993). However, the kinetics of bone Pb in children estimated by the model have not been quantitatively verified as no data were available on kinetics of elimination of Pb from bone in children.

Collectively, the above observations provide added confidence for applications of AALM.FOR for estimating Pb body burdens associated with long-term steady state exposures or short-term intermittent exposures, such as those associated with public and commercial building renovations.

3.5.2. Response to Peer Review of ICRPv005.FOR

The updates made to ICRPv005.FOR and further evaluations of ICRPv005.FOR and AALM.FOR (publicly released as AALM v2.0 in September 2019) address several comments made by peer reviewers of the *Approach for Estimating Exposures and Incremental Health Effects due to Lead During Renovation, Repair and Painting Activities in Public and Commercial Buildings* (Versar, 2015; U.S. EPA, 2014b). These are summarized below.

Rationale for selecting the Leggett model over the O'Flaherty model. Peer reviewers suggested that performance of the Leggett and O'Flaherty models be evaluated and that a stronger rationale be provided for selecting the Leggett model for applications to public and commercial renovation assessments. This report does not specifically address performance of the O'Flaherty model; however, the model was extensively evaluated Chapter 4. The latter report described the development and evaluation of AALM.CSL which includes modules that implement biokinetics models based on either the Leggett model (AALM-LG.CSL) or O'Flaherty model (AALM-OF.CSL). A conclusion of the latter report was that AALM-LG.CSL provided superior agreement to the Rabinowitz et al. (1976) observations compared to AALM-OF.CSL. This conclusion supports selection of the Leggett model as the basis for AALM.FOR and for applications of AALM.FOR, rather than the O'Flaherty model, to assessments of public and commercial building renovations. Additional considerations that support use of AALM.FOR were: (1) the need for Monte Carlo applications of the model which require sufficient computational speed afforded by the Fortran code; and (2) limited future availability of an acslX program to run AALM.CSL, because acslX is no longer being commercially supported.

Accounting for sex differences in biokinetics. The peer reviewers suggested that the model should simulate sex differences in Pb biokinetics. The analyses described in this report could not evaluate sex differences in biokinetics because there are no data on dose-body burden relationships in humans that would allow such evaluations. ICRPv005.FOR was updated in creating AALM.FOR to include algorithms that control growth of the body, volumes of plasma and blood and masses of bone and soft tissues AALM.FOR includes parameters to simulate male or female growth. AALM.FOR was shown to estimate elimination kinetics of Pb from blood in male and female children when exposures were reconstructed (Figure 3-16 to 3-17), and soft tissue-bone Pb relationships in males and females (Figure 3-11).

Evaluation of relationship between plasma-whole blood Pb concentrations. The peer reviewers suggested that the model should be evaluated for accurately estimating the plasma-blood Pb concentration ratio. A meta-dataset of observations of plasma-blood Pb concentrations in children and adults was assembled for evaluation of model performance. In all of these studies, methods were employed to

control for sample contamination, which is of particular importance in measurements of the low Pb levels found in plasma. The dataset used in the evaluation included paired observations of plasma and whole blood Pb concentration for 409 adults (Smith et al., 2002; Bergdahl et al., 1999; Bergdahl et al., 1998; Hernández-Avila et al., 1998; Bergdahl et al., 1997; Schütz et al., 1996). The relationship between plasma and whole blood Pb concentrations estimated from AALM.FOR agreed with observations (Figure 3-13). Only one study provides similar data in children (Bergdahl et al., 1999). Based on these data, the plasma-blood relationships in children and adults do not appear to differ substantially.

Accounting for relative bioavailability (RBA) of ingested Pb. The peer reviewers suggested that RBA of Pb in dust/soil needs to be included as part of the ingestion calculations. This has been included in AALM.FOR. However, by making RBA an adjustment on the ingested dose, rather than the gastrointestinal absorption fraction, the RBA adjustment will result in an underestimation of fecal Pb excretion and a negative mass balance (excretion < intake) if RBA is <1 (see Sections 2.2.3). An error in the Pb intake-excretion mass balance will not affect the simulation internal kinetics of Pb or body burdens (e.g., blood or bone concentrations), although, it may be noteworthy for some research applications. Further refinement of the model at some point in the future to make the RBA an adjustment to the absorption fraction in the small intestine is discussed in Section 3.4.

Revaluation of model estimations of blood Pb kinetics in the Rabinowitz et al. (1976) *study.* The peer reviewers suggested that the model should be revaluated with the Rabinowitz et al. (1976) data to ensure that changes made to the model in creating ICRPv005.FOR did not degrade performance of the model to accurately simulate these observations. AALM.FOR estimated blood Pb concentrations and the temporal pattern of the rise and decline in blood Pb concentrations observed in the Rabinowitz et al. (1976) subjects (Figure 3-10).

Evaluation of model performance for Hattis data. The peer reviewers suggested that the model be evaluated for estimating blood Pb concentrations in a cohort of workers described in Hattis (1981). These data included blood Pb concentrations in workers measured at the date of hire and prior to and following a nine-month strike. Although pre-hire exposures were unknown, it was possible to calibrate the post-hire and pre-strike exposures to achieve agreement with blood Pb concentrations at the time of hire and just prior to the strike, and then estimate without further calibration the post-strike blood Pb. After calibration to the blood Pb concentrations measured at time of hire and just prior to the strike ($r^2 = 1.0$), AALM.FOR estimated rates of decline in blood Pb concentration (pseudo first-order $t_{1/2}$) for individual subjects and for the group median that agreed with the observations (Table 3-4).

Evaluation of model performance for the Nie et al. data. The peer reviewers suggested that the model be evaluated for estimating blood and bone Pb concentrations in a cohort of workers described in Nie et al. (2005) including use of some unpublished Nie et al. data. These data were used in an analyses of an implementation of the Leggett model developed by California EPA (CalEpa, 2013). There were no data on actual exposures experienced by the workers in this cohort. As described in Section 3.3, the Nie et al. data were reviewed and evaluated. Although attempts were made to reconstruct exposures so that blood and bone Pb concentrations could be estimated and compared to observations, ultimately, it was concluded that the data were not suitable for model evaluations because of the uncertainty in the exposures that preceded the blood and bone Pb measurements and that occurred during the measurement period.

Evaluation of model performance for intermittent exposures. Renovations of public and commercial buildings can result in elevated Pb exposures that may persist for several days to several months. Therefore, assessment methods applied to renovation-related exposure scenarios must be able to estimate blood and bone Pb levels that might occur as a result of short-term or intermittent exposures to children or adults. Several evaluations described in this report suggest that AALM.FOR can be expected to reliably estimate blood Pb kinetics associated with short-term or intermittent exposures. (1) AALM.FOR estimated the rate of accrual and elimination of Pb from blood in adult subjects who were exposed to Pb over periods of 2-6 months (Figure 3-10). (2) The model estimated the increase in blood Pb that was observed in infants who were abruptly switched to a higher Pb level diet following approximately 100 days of ingesting a lower Pb level diet (Figure 3-14). (3) The model estimated the rate of decline in blood Pb that was observed following interventions to decrease elevated exposures that occurred over periods of 200 – 400 days (Figures 3-16 to 3-18). (4) The model estimated the decrease in blood Pb concentrations that occurred in Pb workers following a nine-month strike (Table 3-4).

3.5.3. Summary

Collectively, the updates made to ICRPv005.FOR to create AALM.FOR (publicly released as AALM v2.0 in September 2019) and evaluations of AALM.FOR provide increased confidence in applying a biokinetics modeling approach to support estimations of blood Pb concentrations and Pb body burdens following a variety of potential Pb exposure scenarios. Although the AALM.FOR predicts Pb amounts in compartments such as the brain, these predictions should be viewed as hypothetical with no evaluations being possible. AALM.FOR offers an improved modeling tool for estimating exposure-body burden relationships for intermittent as well as chronic Pb exposures.

3.6 SENSITIVITY ANALYSIS OF AALM

3.6.1. Background

A sensitivity analysis was conducted of the newest Fortran implementation of the AALM (i.e., AALM version 3.0). There were two categories analyzed:

1. low_ing: low-level ingestion source
2. high_ing: high-level ingestion source

3.6.2. Methods

The AALM model was run 99 times for each scenario (combination of inputs), of which there were two (high or low source) for ingestion. The 99 runs consist of one base run, plus two runs (adjust up or adjust down) for each of the 49 input variables that were examined. Each AALM run provides information for two ages (5 and 30 years) for all five output variables (Ablood, Abone, Akidney, Aliver, and Asoft). The total for the sensitivity analysis is 198 AALM model runs (2 scenarios × 99 runs each), each producing 60 MB of output.

From this data, each scenario (2 for ingestion) produces 980 elasticities (2 ages and 2 adjustment directions, for each combination of 49 input variables and 5 output variables). The “raw” elasticities were tabulated in Excel files created from the model output. As the high source and low source runs are analyzed together there is effectively only one input scenario, while there are 8 elasticities (for 2 sources, 2 ages, and 2 adjustment directions) for each of the 49×5=245 combinations of input and output variables. Only summary data are presented here.

3.6.2.1 Age-dependent Inputs

Some of the physiological inputs (such as rate constants) to AALM are age-dependent. Therefore, it is expected that some pathways for Pb in the body would be more important at some ages than at others. The elasticities in part measure the importance of specific physiological inputs in determining the amount of Pb accumulating in various compartments. Thus, these elasticities should exhibit age dependence.

The age-dependent inputs that were also part of the sensitivity analysis were:

1. FLONG – Age-scaled fraction of total transfer from the exchangeable bone directed to non-exchangeable bone.
2. GSCAL –Age-scaling factor for gastrointestinal tract transfer.
3. RBLAD – Age-scaled transfer rate from urinary bladder to urine.
4. RBRAN – Age-scaled transfer rate from brain to diffusible plasma.
5. RCORT – Age-scaled transfer rate from non-exchangeable cortical bone to diffusible plasma.
6. RCS2B – Age-scaled transfer rate from cortical bone surface to exchangeable cortical bone.
7. RCS2DF – Age-scaled transfer rate from cortical bone surface to diffusible plasma.
8. RDIFF – Age-scaled transfer rate from the exchangeable bone, including transfer to surface and non-exchangeable bone.
9. RKDN2 –Age-scaled transfer rate from kidney compartment 2 to diffusible plasma.
10. RLVR2 – Age-scaled transfer rate from the slow liver compartment 2 to diffusible plasma.
11. RRBC – Age-scaled transfer rate from RBC to diffusible plasma.
12. RTRAB – Age-scaled transfer rate from non-exchangeable trabecular bone to diffusible plasma.
13. RTS2B – Age-scaled transfer rate from surface trabecular bone to exchangeable trabecular bone.
14. RTS2DF – Age-scaled transfer rate from trabecular bone surface to diffusible plasma.
15. TBONE – Age-scaled deposition fraction from diffusible plasma to surface bone.
16. TFRAC – Bone deposition-scaled fraction of diffusible plasma-to-bone deposition that goes to trabecular surface bone; 1 TFRAC is the fraction that goes to cortical surface bone.
17. TOBRAN – Age-scaled deposition fraction from diffusible plasma to brain.
18. TOSOF0 – Age-scaled deposition fraction from diffusible plasma to soft tissue compartment 0.
19. TOSOF1 – Age-scaled deposition fraction from diffusible plasma to soft tissue compartment 1.
20. TOSOF2 – Age-scaled deposition fraction from diffusible plasma to soft tissue compartment 2.

Since many of the pathways in the physiological model are in competition with each other, many of the variables that are not explicitly age-dependent will be in competition with age-dependent ones and therefore their elasticities will also change with age.

3.6.2.2. Age-independent Inputs

The age-independent inputs that were part of the sensitivity analysis were:

1. H1TOBL – Fraction of transfer out of liver compartment 1 to diffusible plasma.
2. H1TOH2 – Fraction of transfer out of liver compartment 1 to liver compartment 2.
3. H1TOSI – Fraction of transfer out of liver compartment 1 to the small intestine.
4. POWER – Exponent for RBC deposition.
5. RBCNL – Threshold concentration in RBC for non-linear deposition from diffusible plasma to RBC.
6. RKDN1 – Transfer rate from kidney compartment 1 to urinary pathway.
7. RLLI – Transfer rate from lower large intestine to feces.

8. RLVR1 –Transfer rate out of the liver compartment 1, including to small intestine and diffusible plasma.
9. RPLAS – Total transfer rate from diffusible plasma to all compartments.
10. RPROT – Transfer rate from bound plasma to diffusible plasma.
11. RSIC – Transfer rate from small intestine to upper large intestine.
12. RSOF0 – Transfer rate from soft tissue compartment 0 to diffusible plasma.
13. RSOF1 – Transfer rate from soft tissue compartment 1 to diffusible plasma.
14. RSOF2 – Transfer rate from soft tissue compartment 2 to diffusible plasma.
15. RSTMC – Transfer rate from stomach to small intestine.
16. RULI – Transfer rate from upper large intestine to lower large intestine.
17. S2HAIR – Deposition fraction from soft tissue compartment 1 to other excreta.
18. SATRAT – Maximum (saturating) concentration of lead in RBC.
19. SIZEVT – Relative volume of the EVF compartment compared to plasma (EVF/Plasma).
20. TBONEL – Terminal value of age-scaled deposition fraction from diffusible plasma to surface bone.
21. TEVF – Deposition fraction from diffusible plasma to extravascular fluid.
22. TOFECE – Deposition fraction from diffusible plasma directly to the small intestine (not including the transfer from biliary secretion, specified by RLVR1).
23. TOKDN1 – Deposition fraction from diffusible plasma to kidney compartment 1.
24. TOKDN2 – Deposition fraction from diffusible plasma to kidney compartment 2.
25. TOLVR1 – Deposition fraction for Pb from diffusible plasma to liver compartment 2.
26. TOPROT – Deposition fraction from diffusible plasma to protein-bound plasma.
27. TORBC – Deposition fraction from diffusible plasma to RBCs, below non-linear threshold.
28. TOSWET – Deposition fraction from diffusible plasma to sweat.
29. TOURIN – Deposition fraction for Pb from diffusible plasma to urine.

3.6.2.3. Endpoints

As noted above, within each case, a "base" AALM run was performed first. Then two more runs were made for each analysis variable, one run with that input raised by 1% from its base value, and the other with it lowered by 1% from its base value. A total of 49 analysis variables were studied, resulting in 99 runs for each of the 20 cases. The output reported the effects on five response variables or endpoints:

1. Ablood – mass of Pb in blood
2. Abone – mass of Pb in bone
3. Akidney – mass of Pb in kidneys
4. Aliver – mass of Pb in liver
5. Asoft – mass of Pb in soft tissues

AALM reports the above variables daily from birth to the age at which the simulation is stopped (up to 90 years). For these analyses, it was agreed that two sets of sensitivity indices should be computed for each case, one for a child and one for an adult. A single point in time could be used but would have the possibility of being unusual or affected by transient changes. Therefore, it was agreed that the indices would compare the averages over a full year in the two runs (one baseline and the other adjusted). For the child, this average is from age 5 to 6, for the adult it is from age 30 to 31.

3.6.2. Interpreting Elasticities

Each input variable has eight cases to consider, which are all combinations of three settings: age (5 or 30 years), variable adjustment direction (down or up from base case), and source strength (low or high). An

elasticity of one represents a change in output of the same relative size as the variable adjustment, with positive elasticity meaning the same direction and negative meaning the opposite direction. All elasticities are rounded to the nearest 0.0001, meaning that a change in input of X percent results in a change in output of (X/10000) percent. Due to modeling uncertainties, increments smaller than this are not meaningful.

The sensitivity analysis uses five statistics:

1. Direction of effect
   Some output variables have positive correlation with the input while others have negative correlation. The algebraic sign of the elasticity matches the sign of the correlation. All eight scenarios must have the same direction or else it is reported as zero.
2. Size of elasticities
   Here the largest (in absolute value) of the eight elasticities is reported for each variable.
3. Asymmetry between up and down elasticities
   Asymmetry is defined as

   asym = abs(elasticity (variable adjusted up) + elasticity (variable adjusted down))

   If the elasticities are equal and opposite, then asym=0. The largest of the four cases is reported.
4. Source strength effects
   The absolute value of the difference between the low source and high source elasticities is calculated, and the largest (of the four cases) is reported.
5. Age differences
   The absolute value of the difference between the 5-year and 30-year elasticities is calculated, and the largest (of the four cases) is reported.

3.6.3. Ingestion

3.6.3.1. Results

The sensitivity analysis had 49 input variables and five output variables (Ablood, Abone, Akidney, Aliver, and Asoft) each having five statistics (for direction, size, asymmetry, source difference, and age difference) reported. The full dataset for ingestion forms a 49 (row) × 25 (column) table. The results for the amounts of Pb in blood, bone, kidney, liver, and soft tissues are provided in Tables 3-7, 3-8, 3-9, 3-10, and 3-11, respectively.

Some of the input variables have all elasticities equal to zero. This can be due to two causes: either there is no effect at all (for example, TOURIN is always set to zero, so the "up" and "down" adjustments leave it unchanged) or else some effect exists but it is smaller than half the roundoff value. In Tables 3-6 through 3-11 absolute values have been taken so there are no negative entries. Negative elasticities represent an output going down when the input goes up, or vice versa.

The elasticities were barely affected by source strength ("Delta source" in Tables 3-6 through 3-11). Every "Delta source" value was below 0.002. This indicates that (at these source strengths) the response is linear, and the elasticity does not vary with source strength. It is known that at very high concentrations, red blood cell saturation occurs which should affect the elasticities, but that is not seen in the cases examined.

The asymmetry was small in general, with all values below 0.026. For Ablood, the largest asymmetry was 0.0200 when RRBC, the rate of chemical loss from red blood cells, was varied. All other input variables had asymmetries below 0.005 for Ablood. For Abone, the largest asymmetry was 0.0115 for

RCORT, the rate of loss from cortical bone. For Akidney, the largest was 0.0210 for RKDN2, the rate of loss from the kidney to the bladder. For Aliver, the largest was 0.0257 for RLVR2, the rate of loss from the liver to the intestines. For Asoft, the largest asymmetry was 0.0142 for RSOF2, the rate of loss from soft tissue to the blood. These values are all small and all are loss rates for the relevant organs. These values are summarized below in Table 3-12.

The age-dependence ("Delta age" in Tables 3-6 through 3-11) of the elasticities was intermediate in size, for some variables at least. For Ablood the largest age effect was 0.1096 for TFRAC, and a total of 12 variables had age effects over 0.01. For Abone the largest was 0.3916 for TFRAC and 16 variables had effects over 0.01. For Akidney the largest was 0.7052 for RKDN2 and 17 variables had effects over 0.01. For Aliver the largest age effect was 0.4439 for RLVR2 and 18 variables has effects over 0.01. For Asoft the largest age effect was 0.5837 for RSOF2 and 16 variables had effects over 0.01. It is notable that the variables with the largest age effects also were the ones with the largest asymmetries, although the latter were consistently much smaller. These values are summarized in Table 3-13.

The direction of the elasticities is reported under the heading "Direction" in Tables 3-6 through 3-11. A value of 1 means that in all eight cases the output moved in the same direction as the input. A value of -1 means that in all eight cases the output moved in opposite direction to the input. If a mix of directions occurred, or an input variable had no effect at all on the output, then "direc" is set to zero. Note that the direction is computed before rounding, so some elasticities reported as zero (after rounding to 0.0001) still have positive or negative directions.

The directions of the largest elasticities were consistent and in line with expectations. For Ablood, TORBC has positive direction while RRBC has negative direction. Since RBC is effectively a storage compartment for Pb in the blood, increasing its inflow raises blood lead, while increasing outflow lowers blood lead. For other physiological variables the effects on Ablood were more complicated because of interactions and feedback effects. In some cases (such as RLVR2) the direction is age-dependent, being positive up to age 25, then negative up to ~ 35, after which RLVR2 had virtually no effect on Ablood. The reason for this age-dependent effect is not immediately clear but has been successfully replicated and so does not appear to be an error.

While not all directions are explained here, another example is as follows. The variable FLONG reflects the fraction of Pb flow into bone that goes into long-term storage. Evidently, given equal intake of Pb, more long-term storage should mean that Abone is higher while other compartments have less Pb. This is reflected in Abone having a positive elasticity for FLONG, while the others (Ablood, Akidney, Aliver, and Asoft) all have negative directions for FLONG.

3.6.3.2. Discussion

The main consideration regarding the elasticity indices is their size. Since there are eight cases, there are also eight sizes. To simplify, the "size" is defined as the largest of the eight elasticities in absolute value. Differences among the eight values are measured by asymmetry, delta source, and delta age.

For Ablood, TOBRC and RRBC have the largest elasticities, with the former being 0.9996 and the latter 1.0098. These are both close to one, meaning that an X% change in input results in an X% change in Ablood. The next three variables ranked by size are TOKDN1, H1TOBL, and TOLVR1. All are in the range of 0.3 to 0.5 in absolute value. As expected, H1TOBL is positive (since it represents flow into the blood, while the others are negative (these are flows out of the blood).

For Abone, TBONE and RCORT have the largest elasticities (1.1403 and 0.708, respectively). Elasticities greater than one are unusual and reflect positive feedback which amplifies an effect. In this

case it might be due to the renormalization of the sum of the specific blood loss terms (for consistency with RPLAS), in which an increase in TBONE effectively reduces flows elsewhere. While this is one possible explanation, others may exist, and detailed analysis would be needed to confirm any of them.

For Akidney, the two largest elasticities are 1.117 for RKDN2 and 0.8333 for TOKDN2, with the next four largest being H1TOBL, TOLVR1, TOKDN1, and RKDN1. All except for TOLVR1 directly involve the kidneys. TOLV1 has a negative direction as befits an alternative pathway to the kidneys for Pb to exit the blood. Note that KDN2 has Pb outflow only back into the blood, while KDN1 directs its Pb outflow to the bladder (and then it leaves the body). The variable Akidney is the total Pb mass in KDN1 and KDN2 combined. While a larger TOKDN2 value increases Akidney (as expected), a larger TOKDN1 reduces Akidney (as indicated by the negative direction). This makes sense as the Pb flowing into the kidneys as a result of TOKDN1 will soon leave the body, reducing the overall body burden of Pb and ultimately reducing kidney burden as well.

The analysis of Aliver resembles that of Akindey. Aliver is the sum of Pb mass in LVR1 and LVR2. The Pb in LVR2 can exit only to the blood. The Pb in LVR1 is split in 3 ways, with part going to the small intestine and then exiting the body. The largest elasticities are RLVR2 (1.1461), H1TOH2 (0.9561), and TOLVR1 (0.7165). As expected, RLVR2 has a negative direction, while the other two are positive. The next largest elasticity is TOKDN1 which is negative, reflecting that flow to the kidneys is an alternative to flow to the liver, for blood Pb.

For Asoft, which represents Pb in soft tissues, the largest elasticities are TOSOF2 (0.7711), RSOF2 (0.7567), and RSOF1 (0.4962). The first has a positive direction (as do TOSOF1 and TOSOF0, although they are smaller in size), while RSOF2 and RSOF1 have negative direction. The variables TOKDN1 and TOLVR1 are moderate in size and have negative direction, reflecting their roles as removal pathways for blood Pb. TBONE also removes Pb from the blood, but its size is smaller and its direction is inconsistent across the 8 cases because Pb entering the bone does not reduce the body burden and nearly all will eventually return to the blood.

3.6.4. Conclusion

A very large number of cases were examined in this sensitivity analysis and very few elasticities exceeded one, which would indicate disproportionate model influence from the given variable. The largest elasticity of all was 1.146, indicative of a modest positive feedback effect. Many elasticities were zero or negligible on the five outputs examined here (Ablood, Abone, Akidney, Aliver, and Asoft), although these inputs may have larger elasticities on other outputs not examined (for example, RBLAD would affect the Pb in the bladder and the overall body burden of Pb, but it did not affect any of the five outputs examined). Elasticities depended very little on source strength, age, or direction of input adjustment.

Overall, this sensitivity analysis produced consistent results with no obvious outliers that need further explanation. This does not constitute a proof that the entire AALM model code is working correctly, but it does support the belief that the parts of the code relevant to the determination of the variables examined here are behaving as expected.

TABLE 3-1. CHANGES MADE TO ICRPV004.FOR TO CREATE ICRPV005.FOR

ICRPv004.FOR[a]	ICRPv005.FOR	Output/Functionality Affected
Adult kidney mass	Age-dependent kidney mass based on ICRP (2002)	Age-dependent kidney Pb concentrations
Adult bone mass	Age-dependent bone mass based on ICRP (2002)	Age-dependent bone Pb concentrations
Constant hematocrit	Age-dependent hematocrit based on ICRP (2002)	Age-dependent RBC and plasma volumes
Constant trabecular bone fraction (20%)	Age-dependent trabecular bone fraction from Table M-1 of U.S. EPA (2014a)	Age-dependent cortical and trabecular bone Pb concentrations
RBC Pb saturation threshold (25 µg/dL blood) and maximum (350 µg/dL RBC)	RBC Pb saturation threshold (0 µg/dL blood) and maximum (270 µg/dL RBC)	Pb uptake– blood Pb relationship
Transfer rate from (d^{-1}) plasma to RBC birth–10 years: • birth: 0.462 • 0.27 y: 0.462 • 1 y: 0.462 • 5 y: 0.277 • 10 y: 0.139	Transfer rate from (d^{-1}) plasma to RBC birth–10 years: • birth: 0.562 • 0.27 y: 0.562 • 1 y: 0.562 • 5 y: 0.277 • 10 y: 0.277	Plasma– RBC Pb relationship in children
Deposition fraction from RBC to diffusible plasma (0.24)	Deposition fraction from RBC to diffusible plasma: • birth: 0.20 • 0.27 y: 0.20 • 1 y: 0.20 • 5 y: 0.21 • 10 y: 0.22 • ≥15 y: 0.22	Plasma– RBC Pb relationship in children
Transfer rate (d^{-1}) from non-exchangeable cortical bone to diffusible plasma: • birth: 0.00822 • 0.27 y: 0.00822 • 1 y: 0.00288 • 5 y: 0.00154 • 10 y: 0.00089 • 15 y: 0.000512 • ≥25 y: 0.000082	Transfer rate (d^{-1}) from non-exchangeable cortical bone to diffusible plasma: • birth: 0.0102 • 0.27 y: 0.00822 • 1 y: 0.00288 • 5 y: 0.00154 • 10 y: 0.00089 • 15 y: 0.000512 • 18 y: 0.000370 • 24 y: 0.000082 • ≥30 y: 0.000041	Bone to plasma Pb kinetics, in late adolescence (age 15–19 years) and adults (≥30 years)

ICRPv004.FOR[a]	ICRPv005.FOR	Output/Functionality Affected
Transfer rate (d^{-1}) from non-exchangeable trabecular bone to diffusible plasma: • birth: 0.00822 • 0.27 y: 0.00822 • 1 y: 0.00288 • 5 y: 0.00181 • 10 y: 0.00132 • 15 y: 0.000956 • ≥25 y: 0.000493	Transfer rate (d^{-1}) from non-exchangeable trabecular bone to diffusible plasma: • birth: 0.0102 • 0.27 y: 0.00822 • 1 y: 0.00288 • 5 y: 0.00181 • 10 y: 0.00132 • 15 y: 0.000956 • 18 y: 0.000781 • 24 y: 0.000493 • 30 y: 0.000247 • 40 y: 0.000247 • 45 y: 0.000274 • 55 y: 0.000301 • 65 y: 0.000329 • 75 y: 0.000356	Bone-to-plasma Pb transfer kinetics (age 15–18 years), adults (≥25 years)

Based on (U.S. EPA, 2014a, b).

[a]ICRPv004.FOR is an implementation of the Leggett (1993) model.

TABLE 3-2. DIFFERENCES IN ICRPV005.FOR AND AALM.FOR (AALM V2.0) BIOKINETICS

ICRPv005.FOR	AALM.FOR (AALM v2.0)	Output/Functionality Affected
Age-dependent blood and plasma volumes based on ICRP (2002)	Age-dependent blood and plasma volumes based on O'Flaherty (1995, 1993)	Age-dependent blood Pb concentration
Age-dependent bone mass based on ICRP (2002)	Age-dependent bone mass based on O'Flaherty (1995, 1993)	Age-dependent cortical and trabecular bone Pb concentration
Age-dependent trabecular bone fraction based from Table M-1 of U.S. EPA (2014a)	Age-dependent cortical and trabecular bone masses based on O'Flaherty (1995, 1993)	Age-dependent cortical and trabecular bone Pb concentration
Age-dependent kidney mass based on ICRP (2002)	Age-dependent kidney mass based on O'Flaherty (1995, 1993)	Age-dependent kidney Pb concentration
Adult liver mass	Age-dependent liver mass based on O'Flaherty (1995, 1993)	Age-dependent liver Pb concentration
Age-dependent absorption fraction (*F1*): • birth: 0.45 • 0.27 y: 0.45 • 1 y: 0.30 • 5 y: 0.30 • 10 y: 0.30 • 15 y: 0.30 • ≥25 y: 0.15	Age-dependent absorption fraction (*F1*): • birth: 0.39 • 0.27 y: 0.39 • 1 y: 0.38 • 5 y: 0.17 • ≥10 y: 0.12	Absorption fraction for ingested Pb
Absorption fraction for ingested Pb not adjusted for RBA	Media-specific ingestion intakes adjusted for RBA	Intake-fecal mass balance
RBC Pb saturation threshold: 0 µg/dL blood) Maximum: 270 µg/dL RBC	RBC Pb saturation threshold: 20 µg/dL blood) Maximum: 350 µg/dL RBC)	Pb uptake–blood Pb relationship
Transfer rate (d^{-1}) from non-exchangeable cortical bone to diffusible plasma (RCORT): • birth: 0.0102 • 0.27 y: 0.00822 • 1 y: 0.00288 • 5 y: 0.00154 • 10 y: 0.00089 • 15 y: 0.00512 • ≥25 y: 0.0000822	Transfer rate (d^{-1}) from non-exchangeable cortical bone to diffusible plasma (RCORT): • birth: 0.0204 • 0.27 y: 0.01644 • 1 y: 0.00576 • 5 y: 0.00308 • 10 y: 0.00178 • 15 y: 0.00124 • ≥25 y: 0.0001644	Shorter retention of Pb in cortical bone
Transfer rate (d^{-1}) from non-exchangeable trabecular bone to diffusible plasma (RTRAB): • birth: 0.0102 • 0.27 y: 0.00822	Transfer rate (d^{-1}) from non-exchangeable trabecular bone to diffusible plasma (RTRAB): • birth: 0.0204 • 0.27 y: 0.01644	Shorter retention of Pb on trabecular bone

ICRPv005.FOR	AALM.FOR (AALM v2.0)	Output/Functionality Affected
• 1 y: 0.00288 • 5 y: 0.00181 • 10 y: 0.00132 • 15 y: 0.000956 • ≥25 y: 0.000493	• 1 y: 0.00576 • 5 y: 0.00362 • 10 y: 0.00264 • 15 y: 0.001912 • ≥25 y: 0.000986	
Fraction of total transfer from the exchangeable bone directed to non-exchangeable bone (FLONG): 0.2	Fraction of total transfer from the exchangeable bone directed to non-exchangeable bone (FLONG): 0.6	Longer retention of Pb in cortical and trabecular bone
Transfer rate (d^{-1}) from liver compartment 2 to diffusible plasma (RLVR2): • birth: 0.00693 • 0.27 y: 0.00693 • 1 y: 0.00693 • 5 y: 0.00693 • 10 y: 0.00190 • 15 y: 0.00190 • ≥25 y: 0.00190	Transfer rate (d^{-1}) from liver compartment 2 to diffusible plasma (RLVR2): • birth: 0.000693 • 0.27 y: 0.000693 • 1 y: 0.000693 • 5 y: 0.001386 • 10 y: 0.000570 • 15 y: 0.000570 • 25 y: 0.000570 • 30 y: 0.001425 • 40 y: 0.003040 • 60 y: 0.003420 • 90 y: 0.00380	Longer retention of Pb in liver
Transfer rate (d^{-1}) from kidney compartment 2 to diffusible plasma (RKDN2): • birth: 0.00693 • 0.27 y: 0.00693 • 1 y: 0.00693 • 5 y: 0.00693 • 10 y: 0.00190 • 15 y: 0.00190 • ≥25 y: 0.00190	Transfer rate (d^{-1}) from kidney compartment 2 to diffusible plasma (RKDN2): • birth: 0.000693 • 0.27 y: 0.000693 • 1 y: 0.000693 • 5 y: 0.000693 • 10 y: 0.000190 • 15 y: 0.000190 • 25 y: 0.000190 • 30 y: 0.000950 • ≥40 y: 0.00190	Longer retention of Pb in kidney
Deposition fraction from diffusible plasma to kidney compartment 2 (TKDN2): 0.0002	Transfer rate (d^{-1}) from kidney compartment 2 to diffusible plasma (TKDN2): 0.0004	Faster transfer from diffusible plasma to kidney at all ages
Deposition fraction from diffusible plasma to kidney compartment 1 (TKDN1): 0.02	Deposition fraction from diffusible plasma to kidney compartment 1 (TKDN1): 0.025	Faster transfer from diffusible plasma to kidney at all ages
Deposition fraction from diffusible plasma to urine (TOURIN): 0.015	Deposition fraction from diffusible plasma to urine (TOURIN): 0	All urinary excretion occurs from kidney

TABLE 3-3. DIFFERENCES BETWEEN AALM.FOR (AALM V2.0) AND AALM.CSL

AALM.FOR (AALM v2.0)	AALM.CSL	Output/Functionality Affected
Numerical integration time steps controlled by user input	Numerical integration time steps controlled by user Gear (1971) algorithm	Numerical integration error
Media-specific ingestion intakes adjusted for RBA	GI tract absorption fraction adjusted for media-specific RBA	Fecal Pb mass balance
4-compartment RT model that requires user inputs for deposition rate (µg/day)	12-compartment model that accepts user inputs for air concentration, particle size and absorption class	Simulations of Pb deposition and absorption of inhaled Pb

TABLE 3-4. BLOOD LEAD ESTIMATIONS FROM THE AALM FOR 57 SUBJECTS IN THE HATTIS DATASET

		Hattis		ICRPv005		AALM.CSL		AALM.FOR	
		Mean	SD	Mean	SD	Mean	SD	Mean	SD
BLL at hire	µg/dL	20	7	20	7	20	7	20	7
BLL at strike	µg/dL	48	11	49	13	48	11	48	11
BLL after strike	µg/dL	33	9	23	7	31	7	31	7
BLL half-time	days	1027	1433	312	184	553	370	523	314
BLL half-time delta				-0.37	0.59	-0.05	0.54	-0.08	0.52

		Hattis		ICRPv005		AALM.CSL		AALM.FOR	
		GM	GSD	GM	GSD	GM	GSD	GM	GSD
BLL half-time	days	633	2.4	274	1.6	483	1.6	465	1.6

	Hattis		ICRPv005.FOR		AALM.CSL		AALM.FOR	
	Mean	SD	Mean	SD	Mean	SD	Mean	SD
BLL at hire (µg/dL)	20	7	20	7	20	7	20	7
BLL at strike (µg/dL)	48	11	49	13	48	11	48	11
BLL after strike (µg/dL)	33	9	23	7	31	7	31	7
BLL half-time (d)	1027	1433	312	184	553	370	523	314
BLL half-time delta (d)			-0.37	0.59	-0.05	0.54	-0.08	0.52

	Hattis		ICRPv005.FOR		AALM.CSL		AALM.FOR	
	GM	GSD	GM	GSD	GM	GSD	GM	GSD
BLL half-time (d)	633	2.4	274	1.6	483	1.6	465	1.6

AALM.CSL, the July 2015 version of the AALM implemented in acslX; AALM.FOR, the AALM implemented in Fortran and publicly released as AALM v2.0 in September 2019; ICRPv005.FOR, the Leggett model implemented in Fortran as released by OPPT in 2014.

TABLE 3-5. COMPARISON OF ESTIMATED AND OBSERVED PLASMA PB/BONE PB SLOPES

Model	Study	Bone	Estimated Slope	Observed Slope	SE	95%CL	Residual
AALM	CA96	Cortical	0.037	0.052	0.013	0.027, 0.077	-1.16
AALM	CA96	Trabecular	0.040	0.041	0.007	0.027, 0.054	-0.16
AALM	HE98	Cortical	0.037	0.036	0.011	0.014, 0.058	0.12
AALM	HE98	Trabecular	0.040	0.025	0.004	0.017, 0.033	3.67

CA96, Cake et al. (1996); HE98, Hernández-Avila et al. (1998); AALM is version 2.0

TABLE 3-6. COMPARISON OF ALM AND AALM ESTIMATIONS OF BLOOD PB CONCENTRATIONS IN ADULTS

Parameter	Description	Units	ALM	AALM
PbS	Soil lead concentration	µg/g or ppm	1000	1000
BKSF	Biokinetic Slope Factor	µg/dL per µg/day	0.4	NA
PbB_0	Baseline Blood Pb	µg/dL	1.5	1.5
IR_S	Soil Ingestion Rate	g/day	0.050	0.05
$AF_{S, D}$	Absorption Fraction	--	0.12	0.072
$EF_{S, D}$	Exposure Frequency	days/yr	219	219
$AT_{S, D}$	Averaging Time	days/yr	365	365
PbB_{adult}	Blood Pb Concentration	µg/dL	2.9	2.9

ALM, Adult Lead Methodology. See Figure 3-20 for AALM v2.0 input parameter values.

TABLE 3-7. AALM V3.0 SENSITIVITY COEFFICIENTS FOR BLOOD

Variable	Direction	Size	Asymmetry	Delta Source	Delta Age
FLONG [a]	-1	0.0324	0.0003	0.0001	0.0014
GSCAL [a]	0	0	0	0	0
H1TOBL	1	0.3361	0.0022	0.0002	0.0241
H1TOH2	1	0.0975	0.0002	0.0001	0.0296
H1TOSI	0	0	0	0	0
POWER	0	0	0	0	0
RBCNL	0	0	0	0	0
RBLAD [a]	0	0	0	0	0
RBRAN [a]	0	0.0013	0	0	0.0014
RCORT [a]	1	0.0532	0.0016	0.0003	0.0238
RCS2B [a]	1	0.0252	0.0005	0.0002	0.0173
RCS2DF [a]	-1	0.0252	0.0001	0.0002	0.0169
RDIFF [a]	-1	0.0222	0.0003	0.0002	0.0125
RKDN1	0	0	0	0	0
RKDN2 [a]	0	0.0029	0	0	0.0054
RLLI	0	0	0	0	0
RLVR1	-1	0.0009	0	0	0.0008
RLVR2 [a]	0	0.0209	0.0004	0	0.0413
RPLAS	-1	0.0011	0	0	0.0008
RPROT	-1	0	0	0	0
RRBC [a]	-1	1.0098	0.0200	0	0.0009
RSIC	0	0	0	0	0
RSOF0	-1	0.0002	0	0	0.0002
RSOF1	-1	0.0027	0	0	0.0022
RSOF2	1	0.0062	0	0	0.0054
RSTMC	0	0	0	0	0
RTRAB [a]	0	0.0109	0.0003	0.0001	0.0216
RTS2B [a]	0	0.0013	0	0	0.0025
RTS2DF [a]	0	0.0014	0	0	0.0026
RULI	0	0	0	0	0
S2HAIR	-1	0.0712	0.0001	0	0.0286
SATRAT	0	0	0	0	0
SIZEVF	1	0	0	0	0
TBONE [a]	0	0.0472	0.0014	0.0005	0.0651
TBONEL	0	0	0	0	0

Variable	Direction	Size	Asymmetry	Delta Source	Delta Age
TEVF	1	0.0584	0.0018	0.0001	0.0554
TFRAC [a]	1	0.1186	0.0004	0	0.1096
TOBRAN [a]	1	0.0006	0	0	0.0005
TOFECE	-1	0.1118	0.0003	0.0001	0.0083
TOKDN1	-1	0.4672	0.0042	0.0002	0.0349
TOKDN2	0	0.0064	0	0	0.0085
TOLVR1	-1	0.3128	0.0019	0.0001	0.0019
TOPROT	1	0	0	0	0
TORBC	1	0.9996	0	0	0.0009
TOSOF0 [a]	1	0.0002	0	0	0.0002
TOSOF1 [a]	-1	0.0656	0.0001	0	0.0239
TOSOF2 [a]	-1	0.0086	0	0	0.0085
TOSWET	-1	0.0652	0.0001	0	0.0048
TOURIN	0	0	0	0	0
Maximum		1.0098	0.02	0.0005	0.1096

[a] Age-dependent parameter

TABLE 3-8. AALM V3.0 SENSITIVITY COEFFICIENTS FOR BONE

Variable	Direction	Size	Asymmetry	Delta Source	Delta Age
FLONG [a]	1	0.4767	0.0048	0.0001	0.2379
GSCAL [a]	0	0	0	0	0
H1TOBL	1	0.3062	0.0018	0.0002	0.008
H1TOH2	1	0.074	0.0001	0.0001	0.017
H1TOSI	0	0	0	0	0
POWER	0	0	0	0	0
RBCNL	0	0	0	0	0
RBLAD [a]	0	0	0	0	0
RBRAN [a]	0	0.0016	0	0	0.002
RCORT [a]	-1	0.708	0.0115	0.0005	0.1212
RCS2B [a]	-1	0.4202	0.0043	0.0002	0.0574
RCS2DF [a]	1	0.4189	0.0041	0.0002	0.0614
RDIFF [a]	-1	0.2162	0.0042	0.0002	0.1634
RKDN1	0	0	0	0	0
RKDN2 [a]	1	0.0024	0	0	0.0014
RLLI	0	0	0	0	0
RLVR1	-1	0.0004	0	0	0.0002
RLVR2 [a]	0	0.023	0.0004	0	0.0255
RPLAS	-1	0	0	0	0
RPROT	-1	0	0	0	0
RRBC [a]	1	0.0017	0	0	0.001
RSIC	0	0	0	0	0
RSOF0	-1	0.0001	0	0	0.0001
RSOF1	-1	0.0014	0	0	0.0012
RSOF2	1	0.0051	0.0001	0	0.0038
RSTMC	0	0	0	0	0
RTRAB [a]	-1	0.1715	0.0035	0.0001	0.0253
RTS2B [a]	-1	0.1051	0.0012	0	0.0135
RTS2DF [a]	1	0.1043	0.001	0	0.0143
RULI	0	0	0	0	0
S2HAIR	-1	0.0669	0.0001	0	0.0165
SATRAT	0	0	0	0	0
SIZEVF	1	0	0	0	0
TBONE [a]	1	1.1403	0.0041	0.0007	0.0156

Variable	Direction	Size	Asymmetry	Delta Source	Delta Age
TBONEL	0	0	0	0	0
TEVF	1	0.2095	0.0063	0.0002	0.0348
TFRAC [a]	-1	0.4085	0.0009	0	0.3916
TOBRAN [a]	0	0.0003	0	0	0.0005
TOFECE	-1	0.1018	0.0002	0.0001	0.0028
TOKDN1	-1	0.4257	0.0035	0.0002	0.012
TOKDN2	0	0.0026	0	0	0.0034
TOLVR1	-1	0.3061	0.0018	0.0001	0.0062
TOPROT	1	0	0	0	0
TORBC	-1	0.0017	0	0	0.001
TOSOF0 [a]	1	0.0001	0	0	0.0001
TOSOF1 [a]	-1	0.0646	0.0001	0	0.0163
TOSOF2 [a]	0	0.0096	0	0	0.0105
TOSWET	-1	0.0594	0.0001	0	0.0016
TOURIN	0	0	0	0	0
Maximum		1.1403	0.0115	0.0007	0.3916

[a] Age-dependent parameter

TABLE 3-9. AALM V3.0 SENSITIVITY COEFFICIENTS FOR KIDNEY

Variable	Direction	Size	Asymmetry	Delta Source	Delta Age
FLONG [a]	-1	0.0551	0.0005	0.0001	0.0105
GSCAL [a]	0	0	0	0	0
H1TOBL	1	0.314	0.0019	0.0002	0.0463
H1TOH2	1	0.0789	0.0001	0	0.0351
H1TOSI	0	0	0	0	0
POWER	0	0	0	0	0
RBCNL	0	0	0	0	0
RBLAD [a]	0	0	0	0	0
RBRAN [a]	0	0.0015	0	0	0.0016
RCORT [a]	1	0.1004	0.002	0.0003	0.0403
RCS2B [a]	1	0.0481	0.0005	0.0002	0.0103
RCS2DF [a]	-1	0.0477	0.0004	0.0002	0.0097
RDIFF [a]	0	0.0166	0.0004	0.0001	0.0277
RKDN1	-1	0.2511	0.005	0.0006	0.0807
RKDN2 [a]	-1	1.117	0.021	0.0019	0.7052
RLLI	0	0	0	0	0
RLVR1	0	0.0009	0	0	0.001
RLVR2 [a]	0	0.0189	0.0003	0	0.0235
RPLAS	0	0	0	0	0
RPROT	0	0	0	0	0
RRBC [a]	1	0.002	0	0	0.0008
RSIC	0	0.0001	0	0	0.0001
RSOF0	0	0.0001	0	0	0.0001
RSOF1	0	0.0031	0.0001	0	0.0042
RSOF2	1	0.0041	0.0001	0	0.0023
RSTMC	0	0	0	0	0
RTRAB [a]	1	0.0243	0.0005	0.0001	0.0169
RTS2B [a]	1	0.0119	0.0001	0.0001	0.006
RTS2DF [a]	-1	0.0118	0.0001	0.0001	0.0059
RULI	0	0	0	0	0
S2HAIR	-1	0.058	0.0001	0.0001	0.0085
SATRAT	0	0	0	0	0
SIZEVF	0	0	0	0	0
TBONE [a]	-1	0.1396	0.001	0.0007	0.1172

Variable	Direction	Size	Asymmetry	Delta Source	Delta Age
TBONEL	0	0	0	0	0
TEVF	0	0.0276	0.0008	0.0001	0.0422
TFRAC [a]	1	0.1055	0.0003	0	0.0998
TOBRAN [a]	0	0.001	0	0	0.0012
TOFECE	-1	0.1044	0.0002	0.0001	0.0152
TOKDN1	-1	0.267	0.0021	0.0002	0.1426
TOKDN2	1	0.8333	0	0.0008	0.0853
TOLVR1	-1	0.3045	0.0018	0.0003	0.0199
TOPROT	0	0	0	0	0
TORBC	-1	0.0019	0	0	0.0008
TOSOF0 [a]	0	0.0001	0	0	0.0001
TOSOF1 [a]	-1	0.0619	0.0001	0.0001	0.0142
TOSOF2 [a]	-1	0.0095	0	0	0.0091
TOSWET	-1	0.0609	0.0001	0	0.0088
TOURIN	0	0	0	0	0
Maximum		1.117	0.021	0.0019	0.7052

[a] Age-dependent parameter

TABLE 3-10. AALM V3.0 SENSITIVITY COEFFICIENTS FOR LIVER

Variable	Direction	Size	Asymmetry	Delta Source	Delta Age
FLONG [a]	-1	0.0452	0.0005	0.0001	0.0012
GSCAL [a]	0	0	0	0	0
H1TOBL	1	0.3288	0.0021	0	0.0603
H1TOH2	1	0.9561	0.0016	0.0004	0.0469
H1TOSI	0	0	0	0	0
POWER	0	0	0	0	0
RBCNL	0	0	0	0	0
RBLAD [a]	0	0	0	0	0
RBRAN [a]	0	0.0015	0	0	0.0017
RCORT [a]	1	0.1014	0.002	0.0003	0.0586
RCS2B [a]	1	0.0473	0.0005	0.0002	0.0162
RCS2DF [a]	-1	0.047	0.0004	0.0002	0.0158
RDIFF [a]	0	0.0159	0.0004	0.0001	0.0285
RKDN1	0	0	0	0	0
RKDN2 [a]	0	0.0019	0	0	0.0022
RLLI	0	0	0	0	0
RLVR1	-1	0.1358	0.0027	0.0002	0.0009
RLVR2 [a]	-1	1.1461	0.0257	0.0016	0.4439
RPLAS	0	0	0	0	0
RPROT	0	0	0	0	0
RRBC [a]	1	0.0019	0	0	0.0012
RSIC	0	0.0001	0	0	0.0001
RSOF0	0	0.0001	0	0	0.0001
RSOF1	0	0.0032	0.0001	0	0.004
RSOF2	1	0.004	0	0	0.0031
RSTMC	0	0	0	0	0
RTRAB [a]	0	0.0246	0.0005	0.0001	0.0276
RTS2B [a]	1	0.0117	0.0001	0	0.0109
RTS2DF [a]	-1	0.0116	0.0001	0	0.0108
RULI	0	0	0	0	0
S2HAIR	-1	0.0581	0.0001	0	0.0128
SATRAT	0	0	0	0	0
SIZEVF	0	0	0	0	0
TBONE [a]	0	0.1352	0.0011	0.0006	0.1767

Variable	Direction	Size	Asymmetry	Delta Source	Delta Age
TBONEL	0	0	0	0	0
TEVF	0	0.0615	0.0018	0.0001	0.074
TFRAC [a]	1	0.1276	0.0004	0	0.122
TOBRAN [a]	0	0.0011	0	0	0.0012
TOFECE	-1	0.1094	0.0002	0	0.0198
TOKDN1	-1	0.4572	0.004	0.0001	0.0832
TOKDN2	0	0.004	0	0	0.0068
TOLVR1	1	0.7165	0.0043	0.0006	0.0263
TOPROT	0	0	0	0	0
TORBC	-1	0.0019	0	0	0.0012
TOSOF0 [a]	0	0.0001	0	0	0.0001
TOSOF1 [a]	-1	0.062	0.0001	0	0.0181
TOSOF2 [a]	-1	0.0097	0	0	0.0096
TOSWET	-1	0.0638	0.0001	0	0.0116
TOURIN	0	0	0	0	0
Maximum		1.1461	0.0257	0.0016	0.4439

[a] Age-dependent parameter

TABLE 3-11. AALM V3.0 SENSITIVITY COEFFICIENTS FOR SOFT TISSUES

Variable	Direction	Size	Asymmetry	Delta Source	Delta Age
FLONG [a]	-1	0.0513	0.0005	0.0001	0.0083
GSCAL [a]	0	0	0	0	0
H1TOBL	1	0.3203	0.002	0.0001	0.046
H1TOH2	1	0.0823	0.0001	0.0001	0.0352
H1TOSI	0	0	0	0	0
POWER	0	0	0	0	0
RBCNL	0	0	0	0	0
RBLAD [a]	0	0	0	0	0
RBRAN [a]	0	0.0015	0	0	0.0016
RCORT [a]	1	0.0948	0.002	0.0002	0.0411
RCS2B [a]	1	0.0426	0.0006	0.0001	0.0072
RCS2DF [a]	-1	0.0423	0.0004	0.0001	0.0068
RDIFF [a]	0	0.0119	0.0003	0.0001	0.0233
RKDN1	0	0	0	0	0
RKDN2 [a]	1	0.002	0	0	0.0019
RLLI	0	0	0	0	0
RLVR1	0	0.0006	0	0	0.0007
RLVR2 [a]	0	0.0198	0.0003	0	0.0259
RPLAS	0	0	0	0	0
RPROT	0	0	0	0	0
RRBC [a]	1	0.0017	0	0	0.0007
RSIC	1	0.0001	0	0	0.0001
RSOF0	-1	0.0129	0.0003	0	0.0008
RSOF1	-1	0.4962	0.0104	0.0003	0.2766
RSOF2	-1	0.7567	0.0142	0.0003	0.5837
RSTMC	1	0	0	0	0
RTRAB [a]	1	0.0227	0.0005	0.0001	0.019
RTS2B [a]	1	0.0104	0.0001	0	0.0065
RTS2DF [a]	-1	0.0103	0.0001	0	0.0064
RULI	0	0	0	0	0
S2HAIR	-1	0.0599	0.0001	0	0.0124
SATRAT	0	0	0	0	0
SIZEVF	0	0	0	0	0
TBONE [a]	0	0.1216	0.0011	0.0004	0.1322

Variable	Direction	Size	Asymmetry	Delta Source	Delta Age
TBONEL	0	0	0	0	0
TEVF	0	0.047	0.0014	0.0001	0.0584
TFRAC [a]	1	0.1181	0.0003	0	0.1118
TOBRAN [a]	0	0.0008	0	0	0.0009
TOFECE	-1	0.1065	0.0002	0	0.0152
TOKDN1	-1	0.4453	0.0038	0.0002	0.0636
TOKDN2	0	0.0027	0	0	0.0054
TOLVR1	-1	0.3088	0.0019	0.0001	0.02
TOPROT	0	0	0	0	0
TORBC	-1	0.0017	0	0	0.0007
TOSOF0 [a]	1	0.0128	0	0	0.0008
TOSOF1 [a]	1	0.3987	0.0005	0.0004	0.2285
TOSOF2 [a]	1	0.7711	0.0001	0.0004	0.2534
TOSWET	-1	0.0621	0.0001	0	0.0088
TOURIN	0	0	0	0	0
Maximum		0.7711	0.0142	0.0004	0.5837

[a] Age-dependent parameter

TABLE 3-12. SUMMARY OF THE AALM V3.0 VARIABLES WITH THE GREATEST ELASTICITY ASYMMETRY FOR EACH ENDPOINT

Endpoint	Greatest Asymmetry	Asymmetrical Variable	Variable definition
Ablood	0.0200	RRBC	The rate of chemical loss from red blood cells
Abone	0.0115	RCORT	The rate of loss from cortical bone
Akidney	0.0210	RKDN2	The rate of loss from the kidney to the bladder
Aliver	0.0257	RLVR2	The rate of loss from the liver to the intestines
Asoft	0.0142	RSOF2	The rate of loss from soft tissue to the blood

TABLE 3-13. SUMMARY OF THE AALM V3.0 VARIABLES WITH THE GREATEST AGE-DEPENDENT ELASTICITY ASYMMETRY FOR EACH ENDPOINT

Endpoint	Greatest Asymmetry	Asymmetrical Variable	Variable definition
Ablood	0.1096	TFRAC	Bone deposition-scaled fraction of diffusible plasma-to-bone deposition that goes to trabecular surface bone
Abone	0.3916	TFRAC	Bone deposition-scaled fraction of diffusible plasma-to-bone deposition that goes to trabecular surface bone
Akidney	0.7052	RKDN2	The rate of loss from the kidney to the bladder
Aliver	0.4439	RLVR2	The rate of loss from the liver to the intestines
Asoft	0.5837	RSOF2	The rate of loss from soft tissue to the blood

FIGURE 3-1. GASTROINTESTINAL ABSORPTION OF PB IN THE (LEGGETT, 1993) MODEL AND AALM V2.0, OPTIMIZED TO (RYU ET AL., 1983).

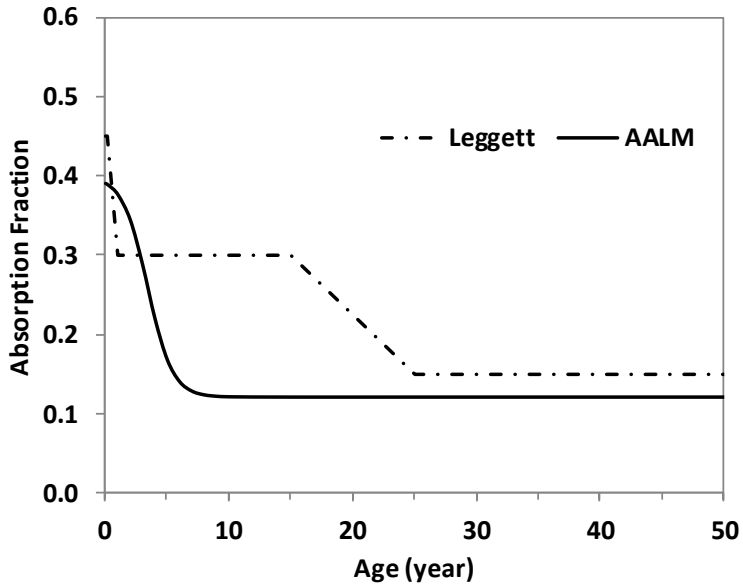

FIGURE 3-2. COMPARISON OF ACCRUAL AND ELIMINATION KINETICS OF BLOOD PB IN CHILDREN (A) AND ADULTS (B) ESTIMATED FROM AALM.CSL, AALM.FOR AND ICRPV005.FOR.

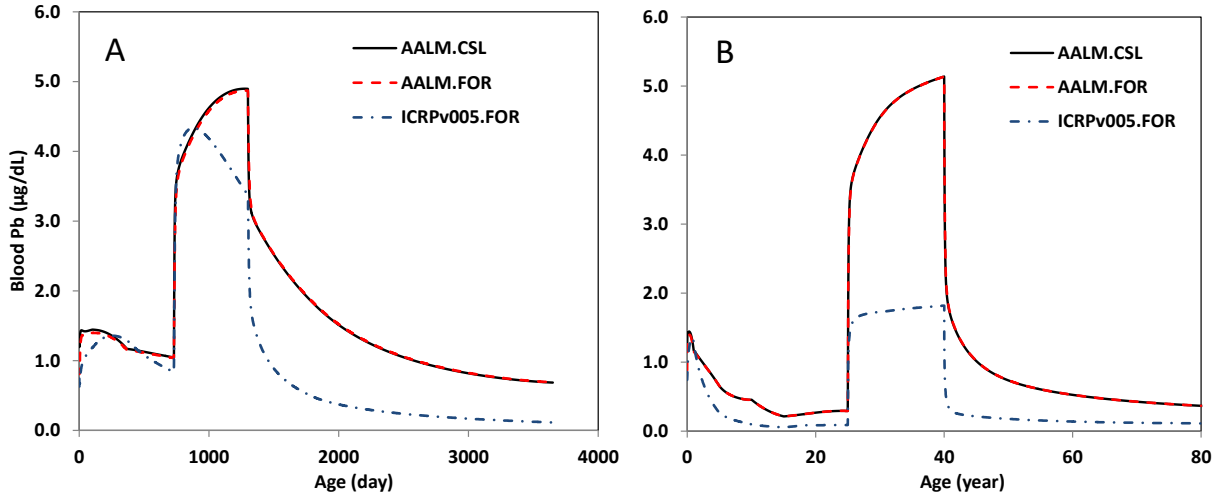

The simulated Pb exposure was a constant baseline intake (5 µg/day) beginning at birth. In the child simulation, a period of elevated intake of (40 µg/day) began on day 720 and ended on day 1300. In the adult simulation, a period of elevated intake of (105 µg/day) began at age 25 years and ended at age 40 years. AALM.CSL, the July 2015 version of the AALM implemented in acslX; AALM.FOR, the AALM implemented in Fortran and publicly released as AALM v2.0 in September 2019; ICRPv005.FOR, the Leggett model implemented in Fortran as released by OPPT in 2014.

FIGURE 3-3. COMPARISON OF ACCRUAL AND ELIMINATION KINETICS OF CORTICAL BONE (A, B) AND TRABECULAR BONE (C, D) PB IN CHILDREN (A, C) AND ADULTS (B, D) ESTIMATED FROM AALM.CSL, AALM.FOR AND ICRPV005.FOR.

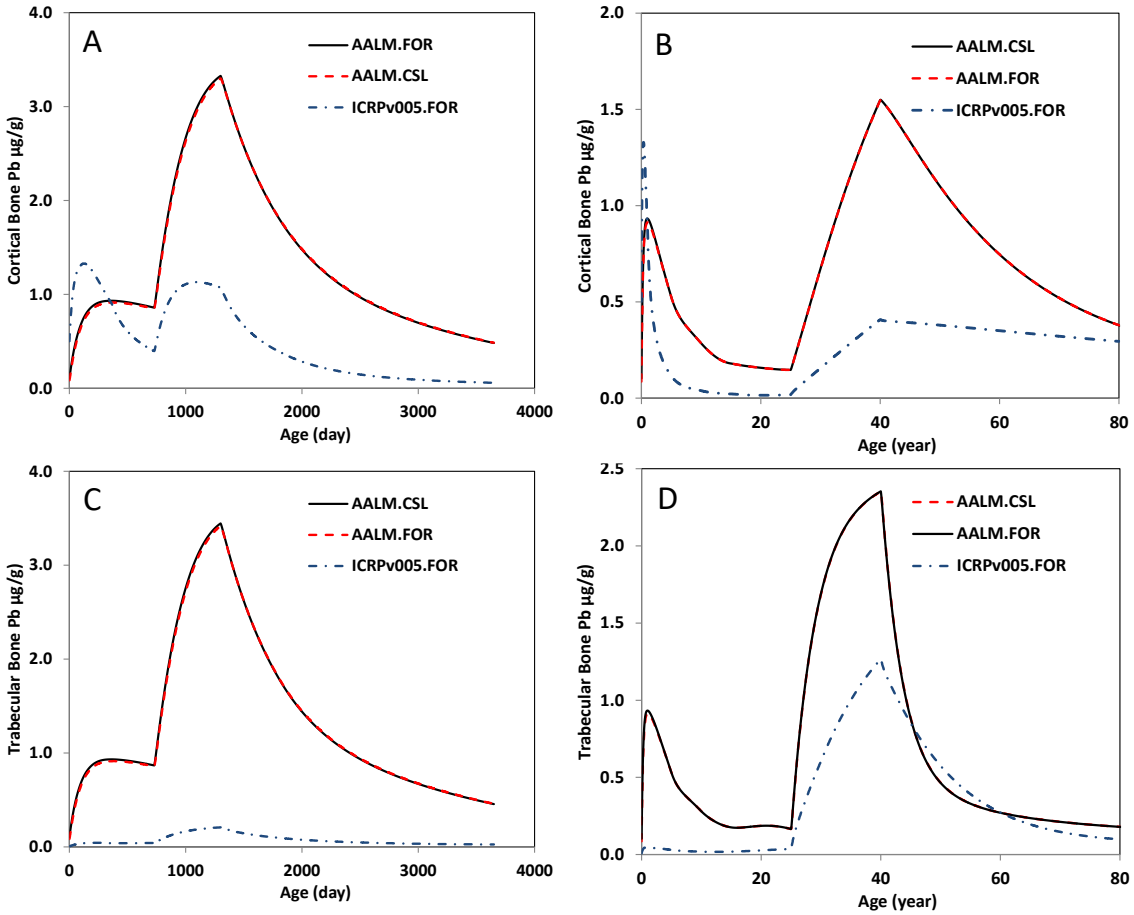

The simulated Pb exposure was a constant baseline intake (5 µg/day) beginning at birth. In the child simulation, a period of elevated intake of (40 µg/day) began on day 720 and ended on day 1300. In the adult simulation, a period of elevated intake of (105 µg/day) began at age 25 years and ended at age 40 years. AALM.CSL, the July 2015 version of the AALM implemented in acslX; AALM.FOR, the AALM implemented in Fortran and publicly released as AALM v2.0 in September 2019; ICRPv005.FOR, the Leggett model implemented in Fortran as released by OPPT in 2014.

FIGURE 3-4. COMPARISON OF RELATIONSHIPS BETWEEN PB INTAKE (G/DAY) AND BLOOD PB IN CHILDREN (A) AND ADULTS (B) ESTIMATED FROM AALM.CSL, AALM.FOR AND ICRPV005.FOR.

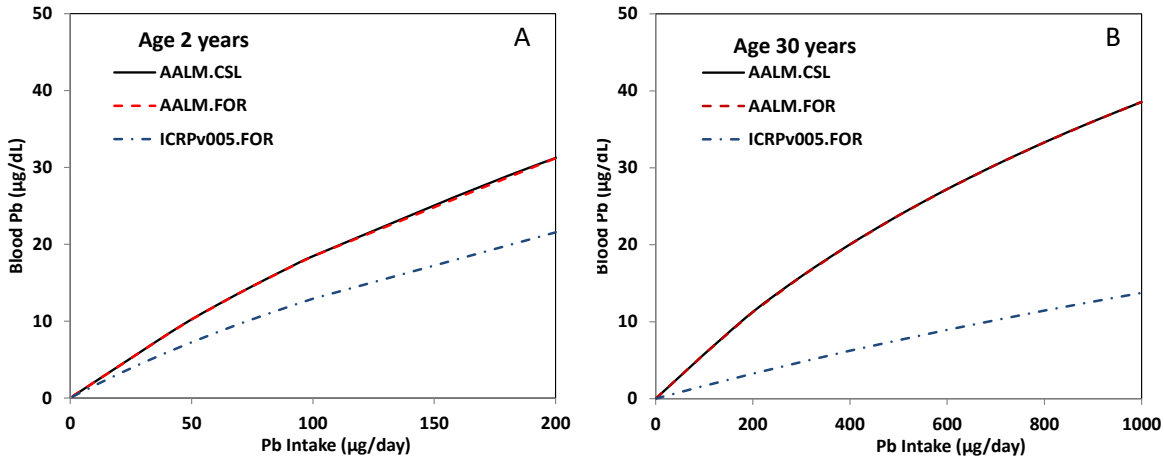

AALM.CSL, the July 2015 version of the AALM implemented in acslX; AALM.FOR, the AALM implemented in Fortran and publicly released as AALM v2.0 in September 2019; ICRPv005.FOR, the Leggett model implemented in Fortran as released by OPPT in 2014.

FIGURE 3-5. COMPARISON OF RELATIONSHIPS BETWEEN PB INTAKE (G/DAY) AND CORTICAL (A, B) AND TRABECULAR (C, D) BONE PB IN CHILDREN (A, C) AND ADULTS (B, D) ESTIMATED FROM AALM.CSL, AALM.FOR AND ICRPV005.FOR.

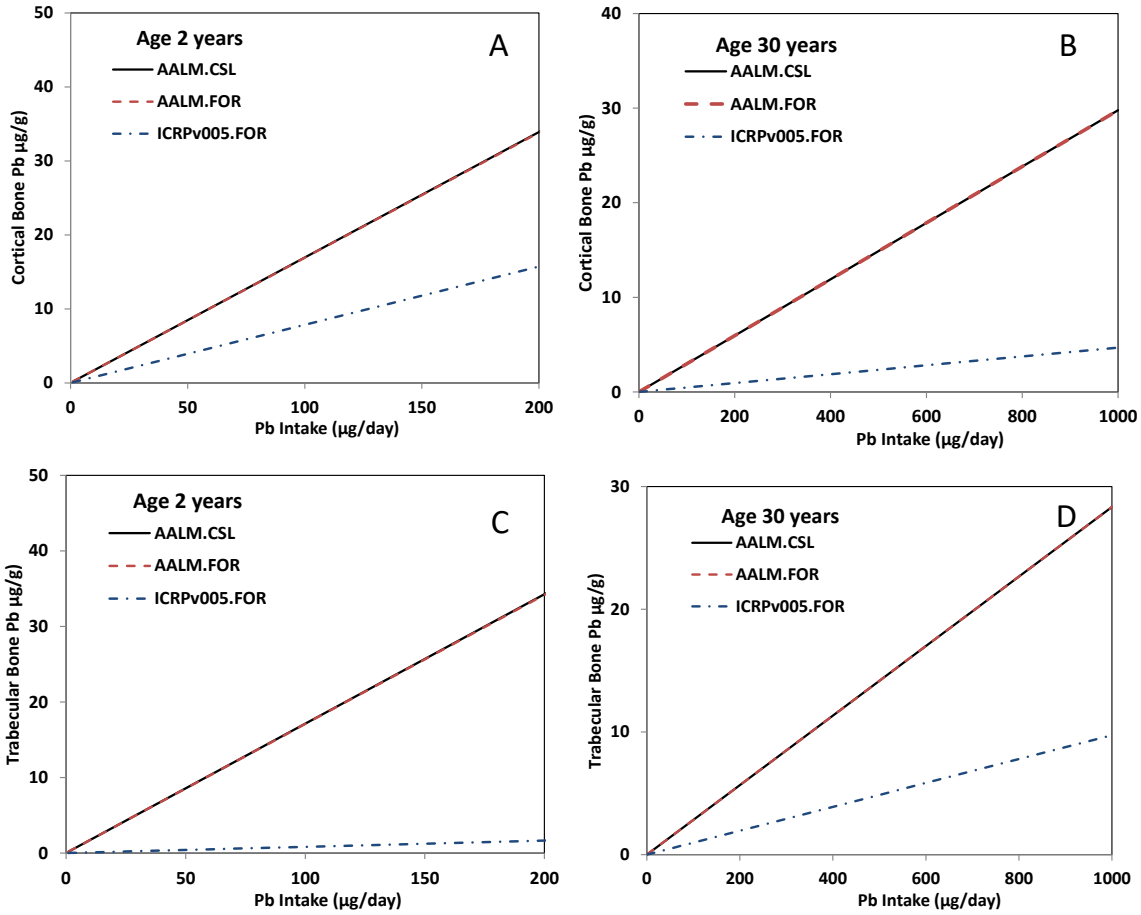

AALM.CSL, the July 2015 version of the AALM implemented in acslX; AALM.FOR, the AALM implemented in Fortran and publicly released as AALM v2.0 in September 2019; ICRPv005.FOR, the Leggett model implemented in Fortran as released by OPPT in 2014.

FIGURE 3-6. AALM.CSL SIMULATION OF OBSERVATIONS FOR HATTIS COHORT SUBJECT 5.

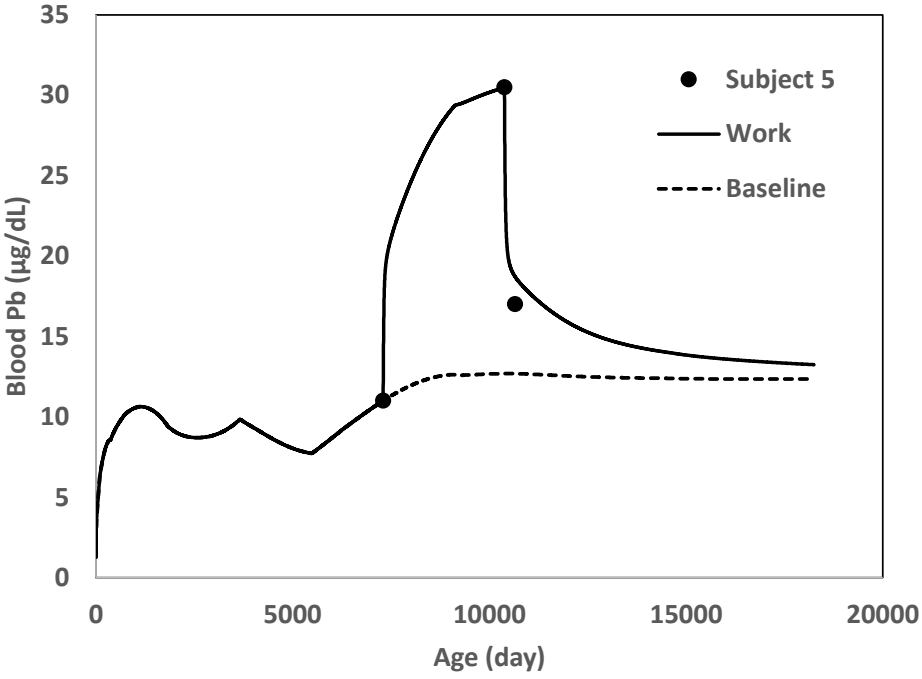

Age		AALM BLL (µg/dL)	Observed BLL (µg/dL)	Ratio (Pred./Obs.)
7300	days	10.6	11.0	0.96
10384	days	30.6	30.5	1.00
10654	days	18.5	17.0	1.09
k	day^{-1}	0.00187	0.00216	0.86
$t_{1/2}$	day	372	320	1.16

The subject (unknown age and sex) experience an occupational exposure that was interrupted by 9-month strike. Pre-strike exposures were reconstructed as a constant Pb ingestion (µg/kg/day) that resulted in a pre-hire blood Pb that was within 1 µg/dL of the reported pre-hire blood Pb (11 µg/dL) for the subject. Pre-strike exposures were reconstructed as a constant Pb ingestion (µg/day), for the reported pre-strike employment durations (3084 days), that resulted in a pre-strike blood Pb that was within 1 µg/dL of the reported pre-strike blood Pb (30.5 µg/dL) for the subject. During the 9-month strike (assumed to be 270 days), exposure reverted to the per/kg baseline level. The elimination half-time from blood was calculated from pre-strike and post-strike blood Pb concentrations, assuming a first-order elimination. The elimination half-time estimated from the observed blood Pb data is 320 days. The half-time estimated from the AALM.CSL is 372 days.

FIGURE 3-7. COMPARISON OF ICRPV005.FOR (TOP) AND AALM.FOR (BOTTOM) ESTIMATIONS AND OBSERVED BLOOD PB CONCENTRATIONS AFTER THE STRIKE FOR 57 SUBJECTS IN THE HATTIS COHORT.

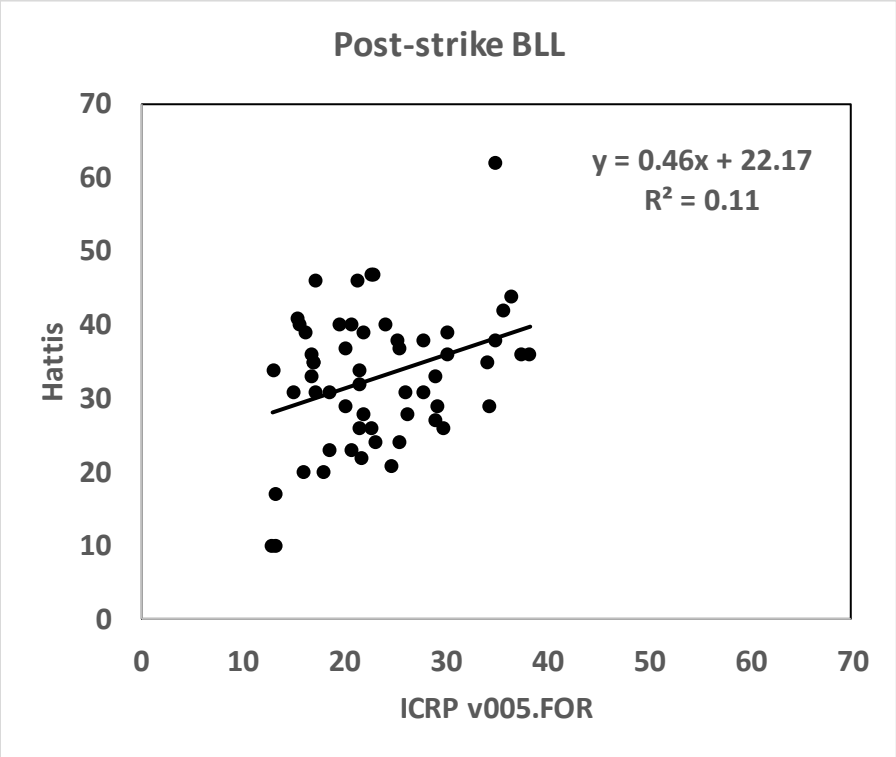

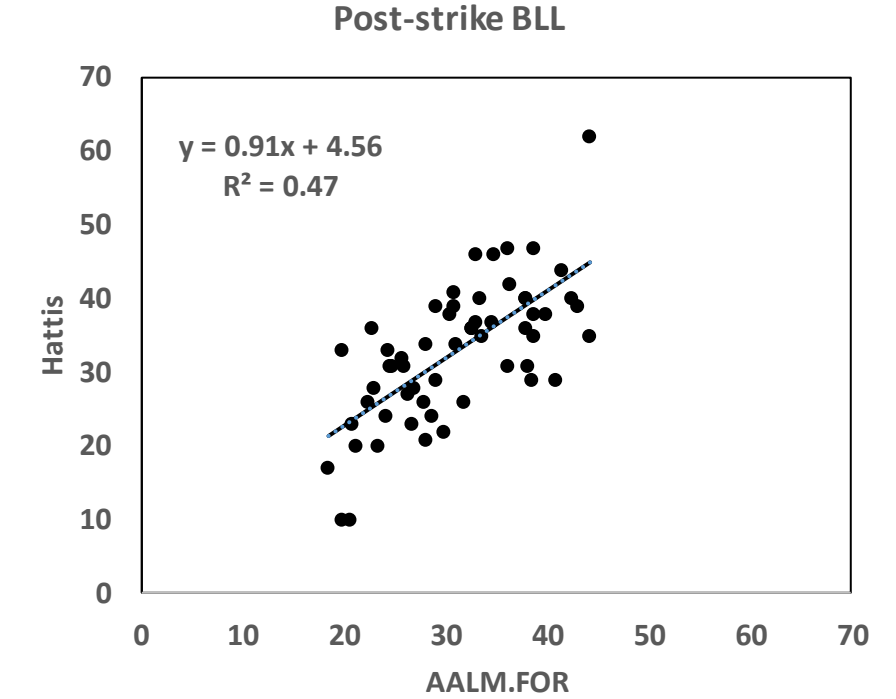

FIGURE 3-8. AALM.CSL, AALM.FOR AND ICRPV005.FOR SIMULATIONS OF BLOOD PB ELIMINATION HALF-TIME FOR 57 SUBJECTS IN THE HATTIS COHORT.

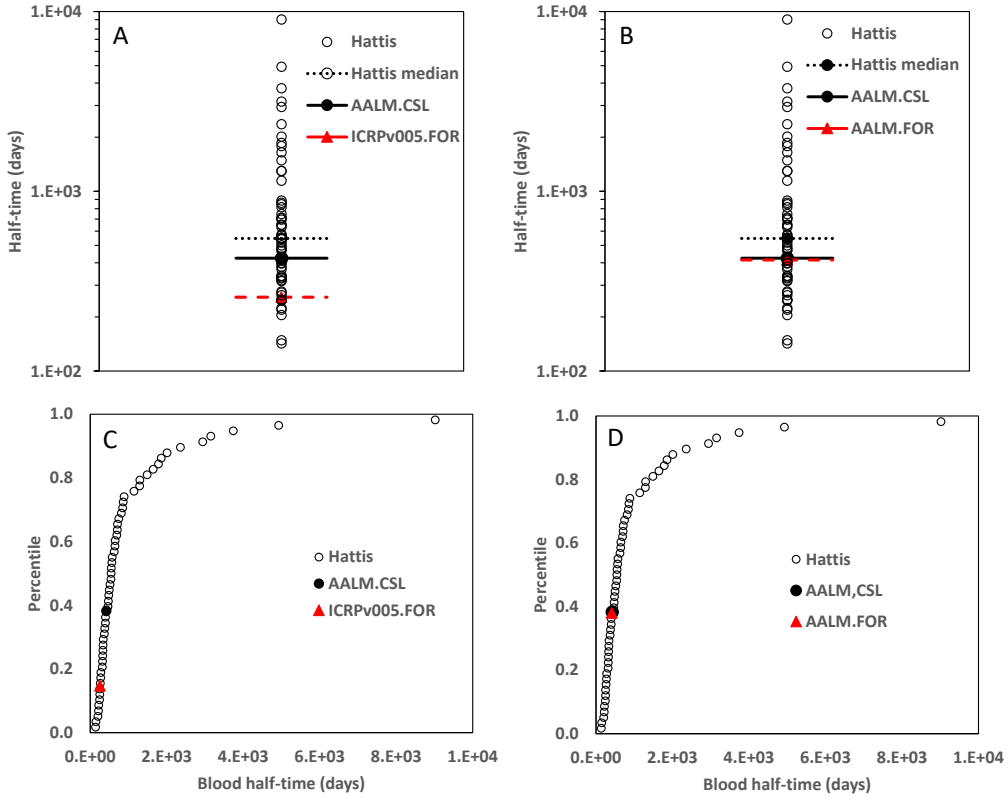

Panel A compares the half-times estimated for the observations with medians estimated from the AALM.CSL and ICRPv005.FOR. Panel C displays the same data as percentiles of the half-times estimated from the observations for AALM.CSL and ICRPv005.FOR. Panels B and D display the corresponding plots comparing AALM.CSL and AALM.FOR. Half-times were calculated as follows: half-time = ln(2)/[ln(pre-strike/post-strike)/270]. AALM.CSL, the July 2015 version of the AALM implemented in acslX; AALM.FOR, the AALM implemented in Fortran and publicly released as AALM v2.0 in September 2019.

FIGURE 3-9. AALM.CSL AND AALM.FOR SIMULATIONS OF ELIMINATION KINETICS OF PB FROM BLOOD (A) AND BONE (B).

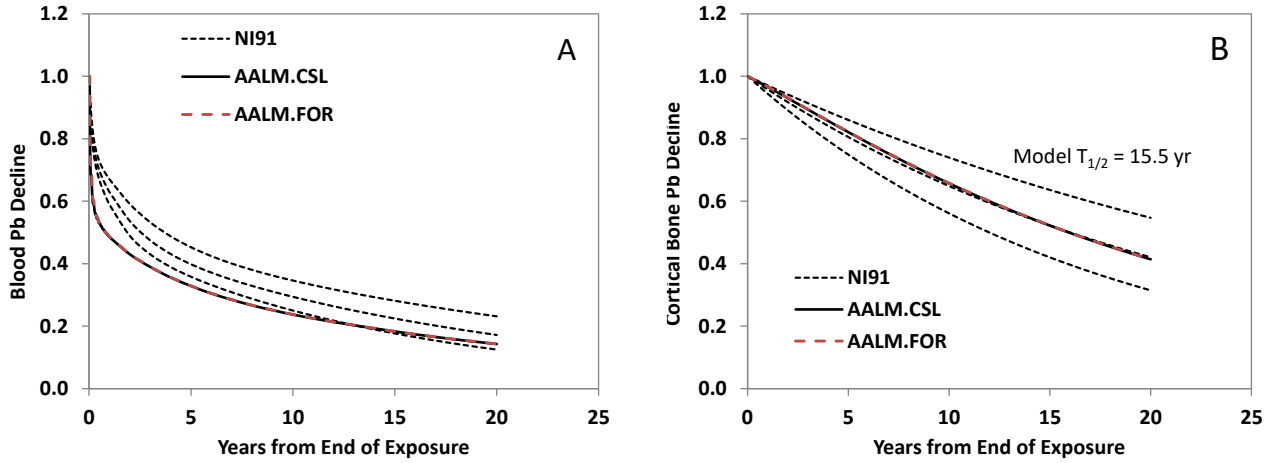

Dotted lines show the elimination from based on the median and upper and lower 95% confidence limits of the tri-exponential model retired Pb workers (n = 14, median age 60 years at time of retirement) reported in Nilsson et al. (1991). AALM.CSL, the July 2015 version of the AALM implemented in acslX; AALM.FOR, the AALM implemented in Fortran and publicly released as AALM v2.0 in September 2019.

FIGURE 3-10. AALM.CSL AND AALM.FOR SIMULATIONS OF BLOOD PB CONCENTRATIONS IN INDIVIDUALS WHO RECEIVED INGESTION DOSES OF [^{202}PB]-NITRATE (RABINOWITZ ET AL., 1976).

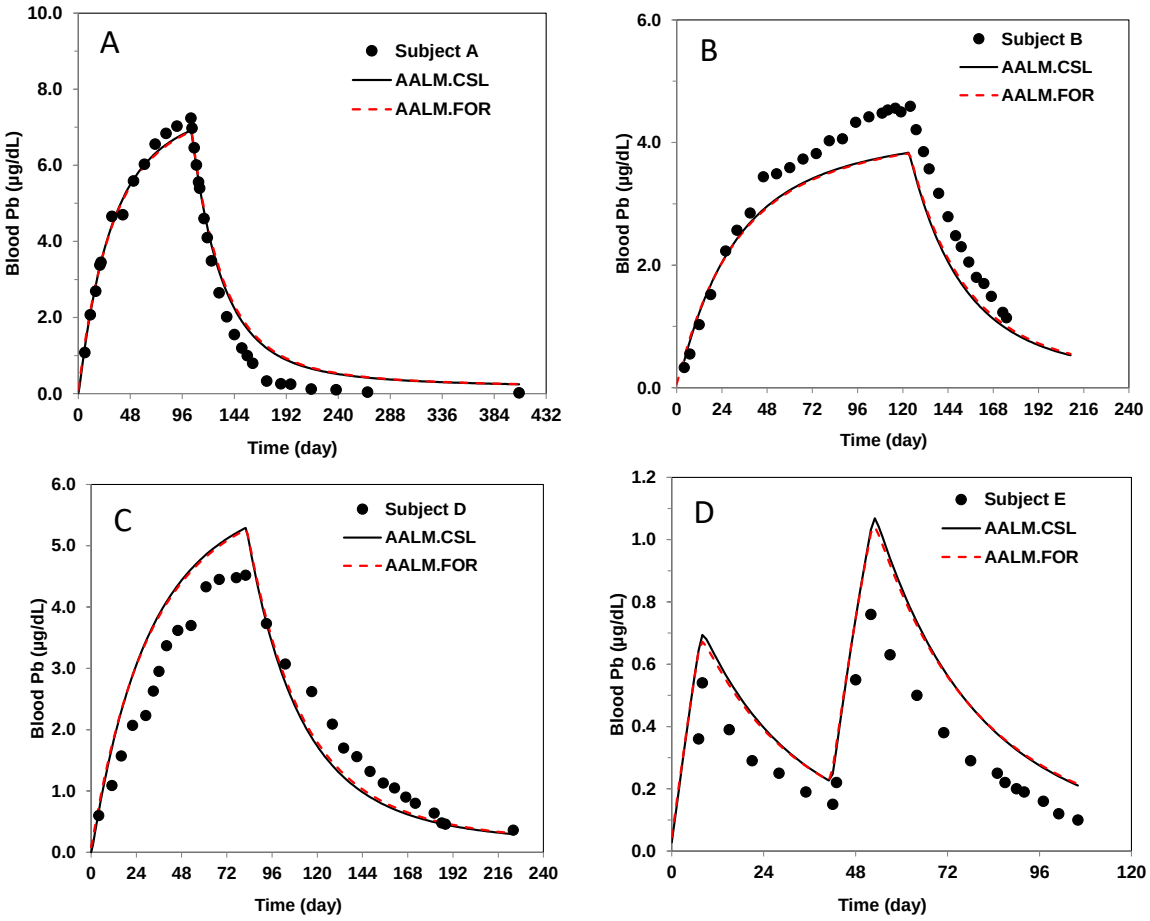

Subject A received 204 µg/day for 104 days, Subject B received 185 µg/day for 124 days, Subject D received 105 µg/day for 83 days, and Subject E received 99 µg/day for on days 1–8 and days 42–51. Estimated absorption fractions were 8.5% for Subject A, 6.5% for Subject B, 10.9% for Subject D and 9.1% for Subject E. AALM.CSL, the July 2015 version of the AALM implemented in acslX; AALM.FOR, the AALM implemented in Fortran and publicly released as AALM v2.0 in September 2019.

FIGURE 3-11. AALM AND LFM SIMULATIONS OF POST-MORTEM SOFT TISSUE/TIBIA PB RATIOS.

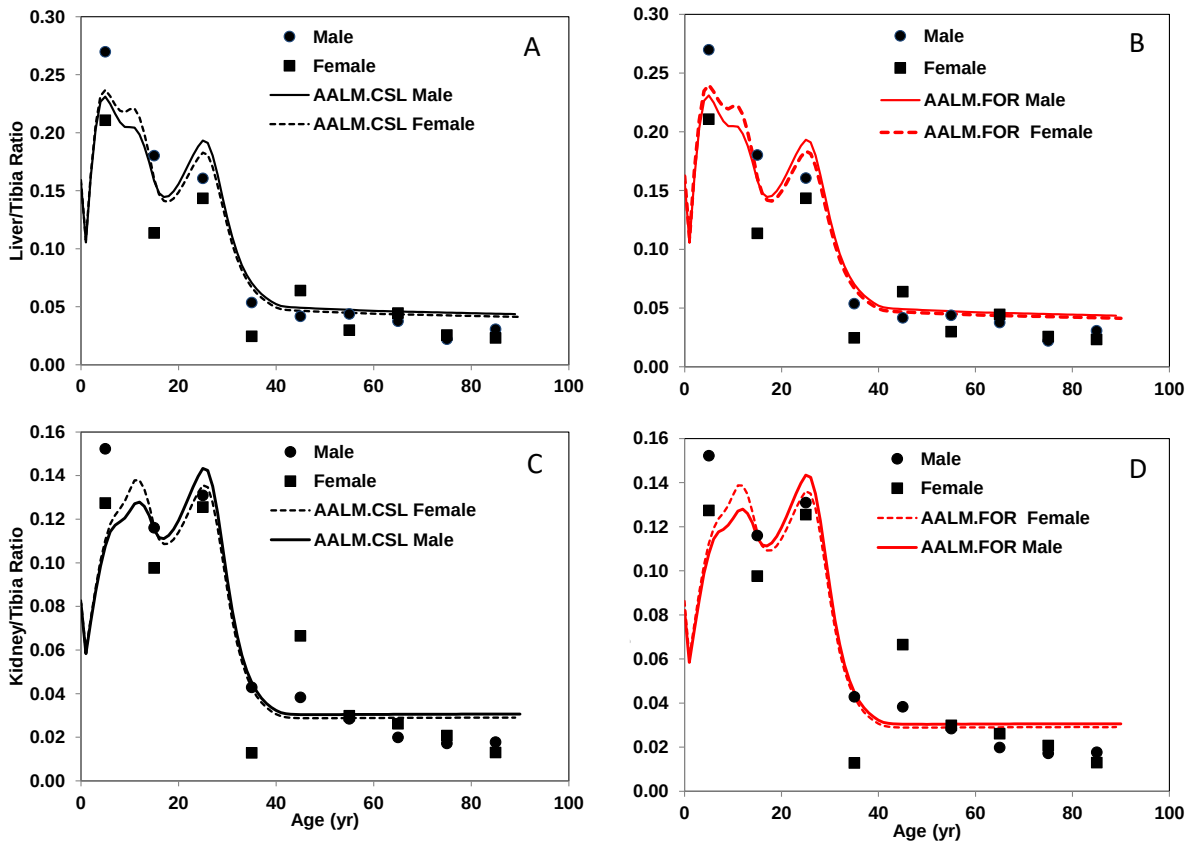

Shown are means for 9 (liver, A and B) and 8 (kidney, C and D) individual estimated from the AALM.CSL (A, C) or AALM.FOR (B, D), based on Barry (1975). AALM.CSL, the July 2015 version of the AALM implemented in acslX; AALM.FOR, the AALM implemented in Fortran and publicly released as AALM v2.0 in September 2019.

FIGURE 3-12. AALM.CSL AND AALM.FOR SIMULATIONS OF PLASMA PB/BONE PB RATIO IN ADULTS.

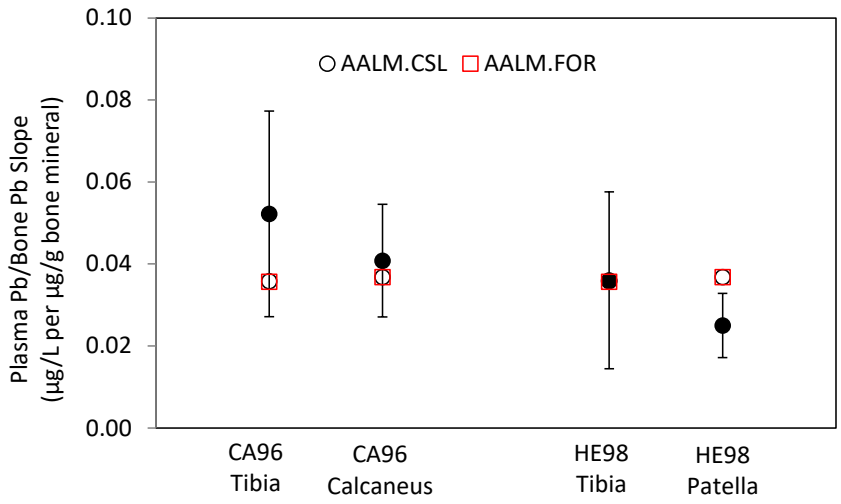

Observations are means and 95% CIs, based on CA96, Cake et al. (1996); HE98, Hernández-Avila et al. (1998). AALM.CSL, the July 2015 version of the AALM implemented in acslX; AALM.FOR, the AALM implemented in Fortran and publicly released as AALM v2.0 in September 2019.

FIGURE 3-13. SIMULATION OF WHOLE BLOOD AND PLASMA PB IN ADULTS.

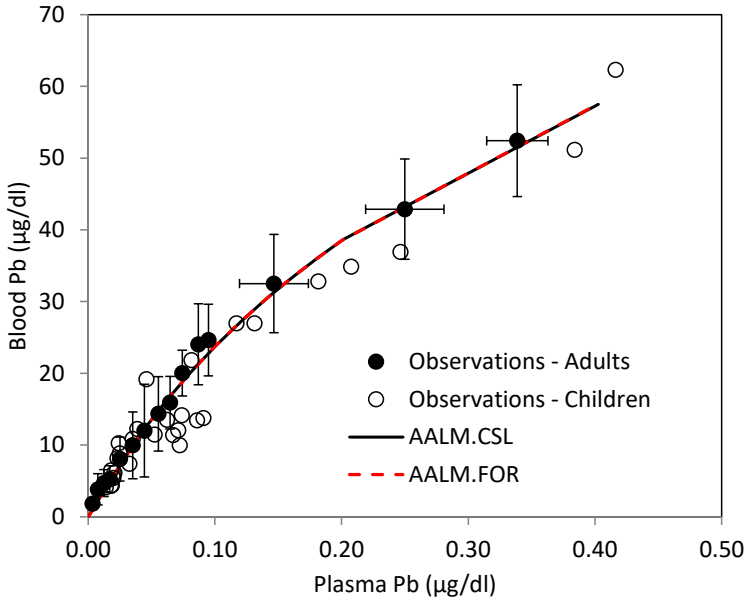

Combined data for adult individuals (N = 406) from all studies were quantized into ranges of plasma Pb; shown are mean and standard deviations for ranges (Smith et al., 2002; Bergdahl et al., 1999; Bergdahl et al., 1998; Hernández-Avila et al., 1998; Bergdahl et al., 1997; Schütz et al., 1996). The r^2 for estimations and observatiosn was 0.99. Data for children (n = 29) are are overlayed on the adult data (Bergdahl et al., 1999). AALM.CSL, the July 2015 version of the AALM implemented in acslX; AALM.FOR, the AALM implemented in Fortran and publicly released as AALM v2.0 in September 2019.

FIGURE 3-14. AALM.CSL (A) AND AALM.FOR (B) SIMULATIONS OF FORMULA-FED INFANTS FROM (RYU ET AL., 1983).

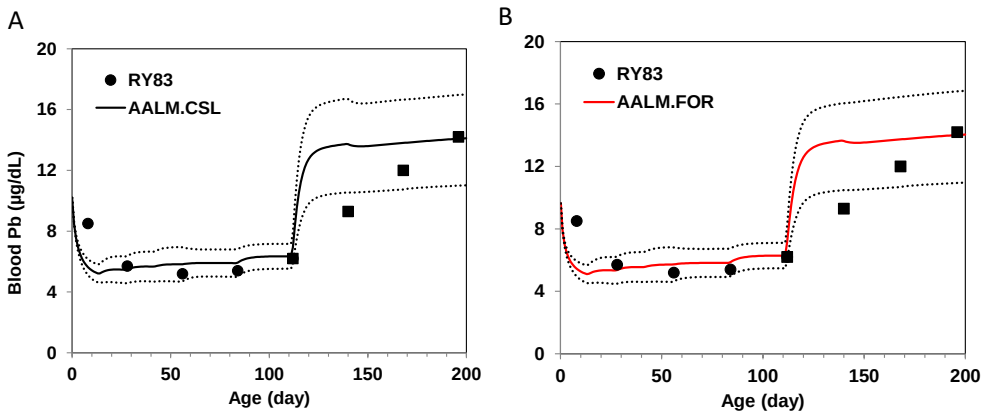

Data (RY83) are from infants fed formula from cartons (12–20 µg/day) from age 8–196 days (closed circles, n=25) and then a subset (closed squares, n = 7) that were switched to formula from cans at age 112 days (60–63 µg/day). Solid lines show simulations of the mean Pb intakes; dotted lines show simulations of ±1 SD of mean intakes. AALM.CSL, the July 2015 version of the AALM implemented in acslX; AALM.FOR, the AALM implemented in Fortran and publicly released as AALM v2.0 in September 2019.

FIGURE 3-15. AALM.CSL AND AALM.FOR SIMULATIONS OF FORMULA-FED INFANTS.

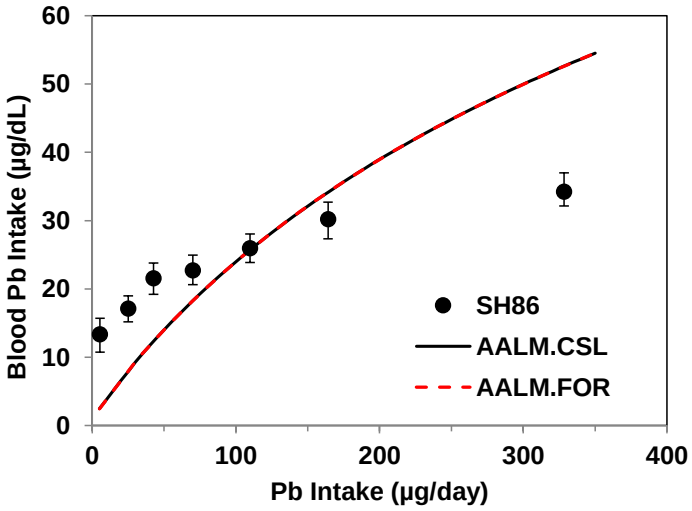

Data are for 131 infants, age 91 days from Sherlock and Quinn (1986). AALM.CSL, the July 2015 version of the AALM implemented in acslX; AALM.FOR, the AALM implemented in Fortran and publicly released as AALM v2.0 in September 2019.

FIGURE 3-16. AALM V2.0 SIMULATION OF SUBJECT 48490 (FEMALE).

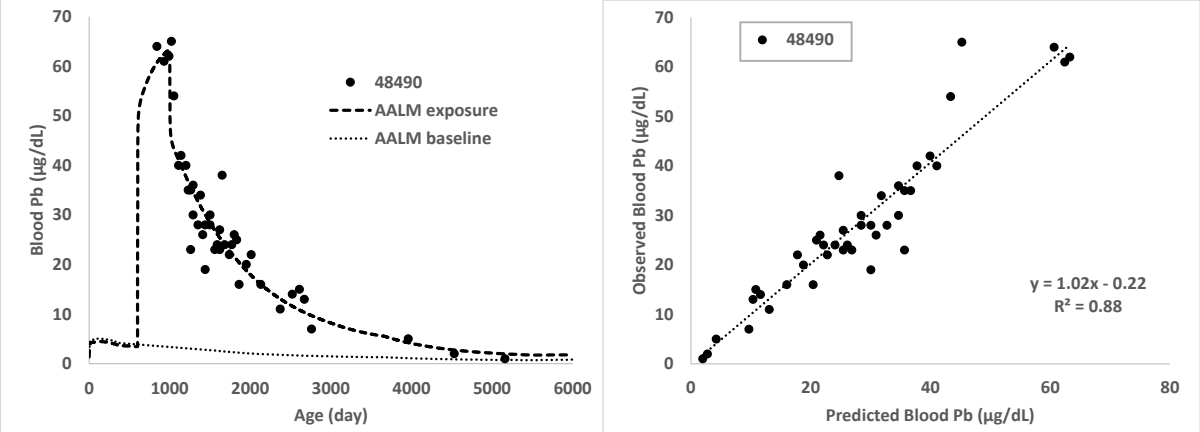

Baseline (15 µg/day) was set to achieve a 6-month BLL of approximately 5 µg/dL, consistent with data for other subjects. Exposure to 22,000 ppm dust Pb (RBA = 0.6) began on age day 600 and continued to age day 1000. Data provided by ATSDR.

FIGURE 3-17. AALM V2.0 SIMULATION OF SUBJECT 3030 (MALE).

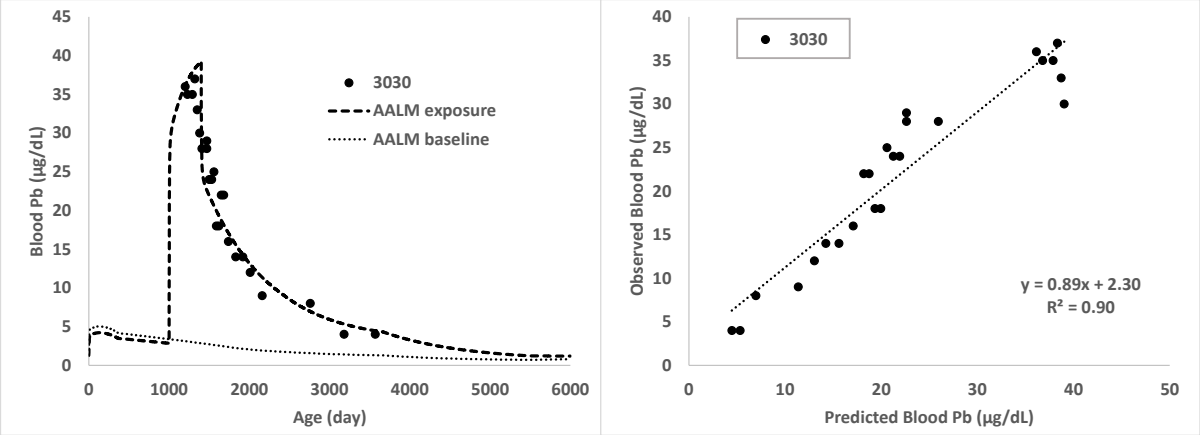

Baseline (15 µg/day) was set to achieve a 6-month BLL of approximately 5 µg/dL, consistent with data for other subjects. Exposure to 11,000 ppm dust Pb (RBA = 0.6) began on age day 1000 and continued to age day 1400. Data provided by ATSDR.

FIGURE 3-18. AALM V2.0 SIMULATION OF SUBJECT 87350 (FEMALE).

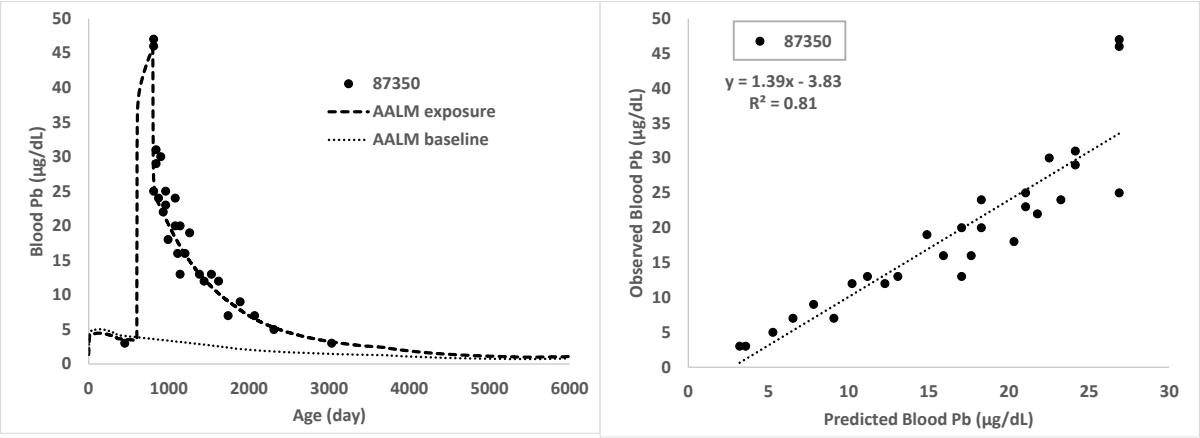

Baseline (15 µg/day) was set to achieve a 6-month BLL of approximately 5 µg/dL, consistent with data for other subjects. Exposure to 13,000 ppm dust Pb (RBA = 0.6) began on age day 600 and continued to age day 800. Data provided by ATSDR.

FIGURE 3-19. COMPARISON OF BLOOD PB ESTIMATIONS OF AALM V2.0 AND IEUBK MODEL.

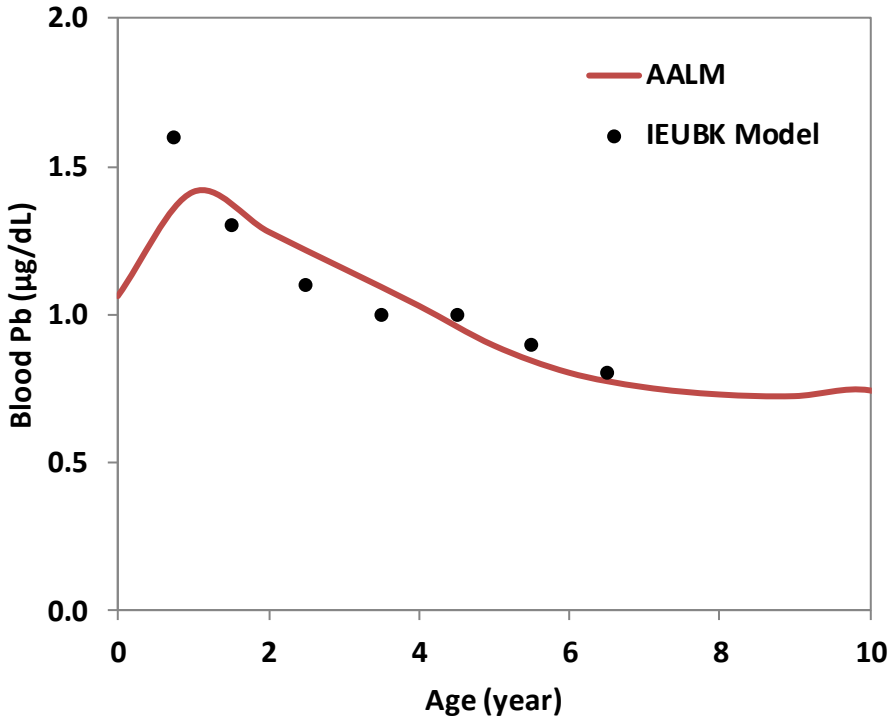

Maternal blood Pb was assumed to be 1 µg/dL. Exposure was to Pb in soil (RBA = 0.6) at a constant intake (10 µg/day). Absorption parameters were: AF1 C1=0.40 (AF1=0.39 at birth), AF1 C2=0.28 (AF1=0.12 at age ≥10 years). The average AF1 for age 0-7 years was 0.26.

FIGURE 3-20. COMPARISON OF BLOOD PB ESTIMATIONS OF AALM V2.0 AND ALM.

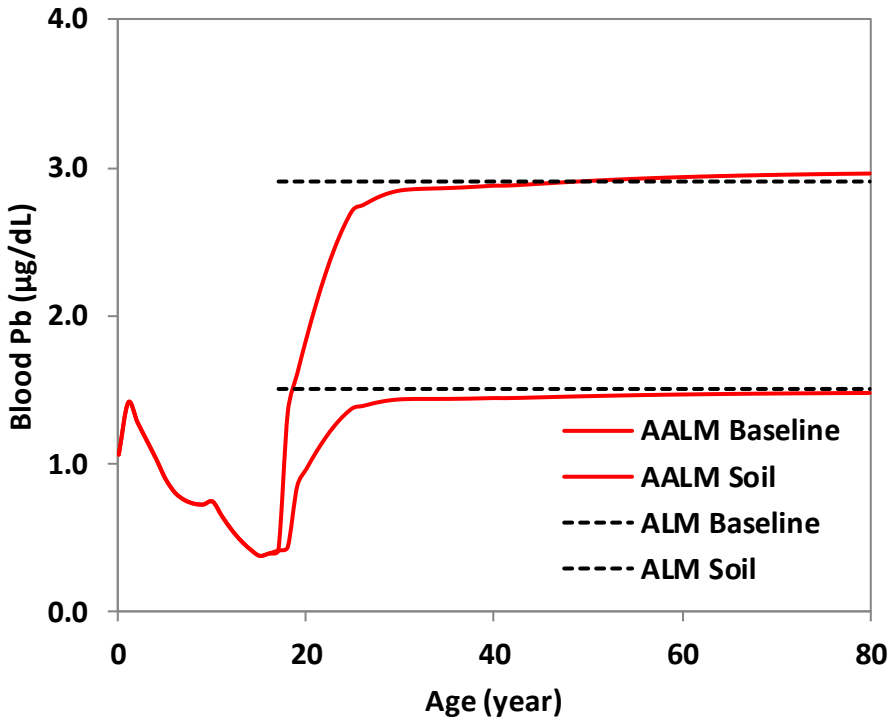

AALM input parameters:

OTHER Baseline Pb=6 µg/day

OTHER Pulse Pb=12 µg/day

OTHER Pulse start= 6205 day (17 years)

OTHER RBA = 1

SOIL baseline Pn = 0 µg/day

SOIL Pulse Pb=600 µg/g (1000*219/365)

SOIL IRs = 0.05 at age ≥15 years

SOIL RBA = 0.6

AF1 C1=0.40 (AF1=0.39 at birth), AF1 C2=0.28 (AF1=0.12 at age ≥10 years)

CHAPTER 4. EVALUATION AND DEVELOPMENT OF AALM.CSL

4.1. INTRODUCTION

This chapter summarizes developments in the AALM that were initiated in early 2013 by EPA's Office of Research and Development (ORD)/National Center for Environmental Assessment (NCEA). Six major objectives have been realized in this most recent effort, and are described in this report including: (1) recoding of the AALM biokinetics models from Visual C to the more robust kinetic model development software, Advance Continuous Simulation Language, ACSL® (acslX); (2) addition of a user friendly, flexible, and transparent exposure model interface implemented in Microsoft Excel®(Excel); (3) capability to run either the Leggett (AALM-LG) or O'Flaherty (AALM-OF) biokinetics models from the same exposure model interface, and with the same exposure and absorption conditions; (4) a more realistic RT model representation in both the Leggett and O'Flaherty biokinetics models compared with earlier versions; (5) accessible and transparent output for easy comparison of the estimations from the Leggett and O'Flaherty biokinetics models; and (6) an evaluation and optimization of the Leggett and O'Flaherty biokinetics models against a common set of observations that lead to the version of the AALM in acslX (AALM.CSL v.4.2, July 2015).

Section 4.2 provides a brief overview the functional structure of AALM.CSL. Section 4.3 compares the structures of the two biokinetics models contained in the AALM.CSL (AALM-LG, AALM-OF). Section 4.4 describes the outcomes of model runs that compare estimations of blood and tissue Pb levels obtained from the AALM-LG and AALM-OF. Section 4.5 presents the results of sensitivity analyses coefficients (SSCs) conducted from the AALM.CSL biokinetics models. Section 4.6 presents the conclusions from the model comparison. Section 4.7 presents results of an empirical evaluation and optimization of the AALM-LG and AALM-OF. Section 4.8 provides conclusions and discusses implications of performance of the optimized models for model applications. Section 4.9 discusses differences between the AALM.CSL model output and the IEUBK model for similar exposures, identifies AALM model parameter changes that resolve the differences, and provides a rationale for changes in the parameter values. Section 4.10 outlines the next steps to be taken, and the data needed to further develop and evaluate the AALM.CSL.

4.2. OVERVIEW OF AALM.CSL STRUCTURE

The AALM estimates blood and tissue Pb masses (µg) and concentrations (µg/g) resulting from exposures to Pb in air, drinking water, surface dust, food, or miscellaneous Pb ingestion pathways. The AALM exposure module allows the user to simulate multi-pathway exposures that are constant or that vary in time increments as small as one day; and that occur at any age from birth to 90 years. The user can select to run a Pb biokinetics simulation based on either the Leggett (AALM-LG) or O'Flaherty (AALM-OF) biokinetics models. The ICRP Human Respiratory Tract Model [HRTM; (ICRP, 1994)] deposition and absorption parameters are used in both the AALM-LG and AALM-OF. The user can select gastrointestinal absorption fractions for any age values as well as values for relative bioavailability (RBA) of Pb from all ingestion pathways.

The AALM software architecture consists of three components: (1) a macro-enabled Excel workbook (INPUT&OUTPUT.xlsm) that implements the exposure model and provides user access to all exposure and biokinetics parameters in the AALM; (2) an acslX program that implements a Leggett-based

biokinetics model (AALM-LG.csl); and (3) an acslX program that implements an O'Flaherty-based biokinetics model (AALM-OF.csl).

The data flow for AALM simulations is shown in Figure 4-1. The AALM simulation is implemented in acslX with AALM_LG.csl (or AALM_OF.csl). Input parameter values are selected by the user in a macro-enabled INPUT&OUTPUT Excel file (.xlsm). Macros in the INPUT&OUTPUT Excel file pass the input parameter values to a comma-delimited (CSV) text file (INPUT.DAT). Data in INPUT.DAT are imported into the AALM acslX program with acslX m-file scripts. Output variables from the simulation are passed from acslX to a CSV file (OUTPUT.DAT) and are read into the INPUT&OUTPUT Excel file with Excel macros.

AALM inputs and outputs are controlled and recorded in the *INPUT&OUTPUT.xlsm* workbook. This workbook has several functions: (1) allows setting of input parameter values for AALM simulations; (2) macros in this workbook are used to pass data to and from acslX; (3) allows plotting of AALM output data; and (4) provides a complete record of input values and results of each AALM simulation.

Worksheets in *INPUT&OUTPUT.xlsm* allow the user to set exposure scenarios for Pb in air (*Air*), surface dust, (*Dust*), drinking water (*Water*), food (*Food*) and/or other ingestion intakes (*Other*). Exposures can be discrete (i.e., a series of exposures at selected ages), and/or pulsed in a repeating frequency (e.g., 2 days/week for 3 months/year, for a selected age range). The AALM uses inputs from all exposure media when it creates biokinetics simulations. This allows construction of complex multi-pathway exposure scenarios having varying temporal patterns. Worksheets in *INPUT&OUTPUT.xlsm* also allow the user to set values for parameters that control Pb absorption and relative bioavailability in each medium (*RBA*), and biokinetics (*Lung*, *Systemic*, *Sex*). All settings are recorded in the *INPUT&OUTPUT.xlsm* workbook and can be recalled to re-run the simulation.

The two biokinetics models in the AALM have been modified from the originally reported Leggett (1993) and O'Flaherty (1995, 1993) models. The important modifications include: (1) removal of all exposure components (moved to the Excel implementation); (2) implementation of a simplified version of the ICRP HRTM (ICRP, 1994) in both biokinetics models; (3) implementation of the O'Flaherty model growth algorithms in both biokinetics models to enable output of Pb concentrations in tissues in both models, and to unify blood and tissue volumes; and (4) implementation of relative bioavailability factors for ingested Pb from each exposure medium.

4.3. COMPARISON OF STRUCTURES OF AALM-LG AND AALM-OF BIOKINETICS MODELS

The AALM has two systemic biokinetics modules, one that is based on the Leggett (1993) model (AALM-LG) and the other based on the O'Flaherty (1995, 1993) model (AALM-OF). Figures 4-2 and 4-3 show the structures of both models. Table 4-1 summarizes some of the major differences between the two modules. The most important difference is the way each model simulates Pb kinetics in bone. Both models represent kinetics of Pb in bone that are influenced by changes in the rates of bone turnover (bone formation and resorption). In general, the major features of bone Pb kinetics in both models are as follows: (1) relatively rapid transfers of Pb between plasma and bone forming surfaces; (2) increased bone Pb uptake during periods of bone growth; (3) incorporation of Pb into bone matrix and release of Pb from bone matrix during bone resorption; (4) maturation of bone associated with lower rates of bone turnover and related decreased mobility of Pb in bone matrix; and (5) more rapid turnover of trabecular

bone Pb, relative to mature cortical bone. However, these processes are parameterized very differently in the two models.

AALM-LG simulates bone as a multi (6)-compartment system (see Figure 4-4) consisting of 3 cortical and 3 trabecular compartments that are distinguished by different Pb transfer rates: (1) relatively rapid exchange of Pb between diffusible plasma and surfaces of cortical and trabecular bone; (2) slower exchange of Pb at bone surfaces with an exchangeable Pb pool in bone volume; and (3) slow transfer of a portion of Pb in bone volume to a non-exchangeable pool that is released from bone to diffusible plasma only when bone is resorbed. Bone growth and maturation are simulated by age-dependent adjustments in rate coefficients for Pb transfers from plasma-to-bone surfaces, and from bone matrix to plasma. This approach simulates outcomes of the bone formation and resorption with bone Pb kinetics parameters, rather than simulating the underlying physiology of bone formation and resorption directly with parameters that govern formation and resorption.

AALM-OF simulates bone formation, resorption, and maturation of bone explicitly, and links these processes to uptake and release of Pb from bone (see Figure 4-5). In AALM-OF, bone turnover in cortical and trabecular bone is simulated with parameters that govern age-dependent bone formation and resorption of bone. Two phases of bone turnover are simulated. In juvenile bone, formation and resorption rates in cortical and trabecular bone are relatively high (high bone turnover) and formation dominates, resulting in bone growth, which ceases at age 25 years. In mature bone, formation and resorption rates are slower and bone formation rate equals resorption rate, resulting in remodeling, but no net growth of bone. Transfers of Pb into and out of trabecular bone are governed by age-dependent rates of bone formation and resorption, respectively. Cortical bone is assumed to consist of two regions: (1) metabolically active cortical bone in which Pb transfers are governed solely by rates of bone formation and resorption; and (2) mature cortical bone in which Pb undergoes exchange with bone calcium. The later process is simulated as bidirectional radial diffusion of Pb in between eight concentric shells of cortical bone.

The approach to modeling bone in AALM-OF (i.e., bone Pb kinetics as a function of bone physiological parameters) offers two major advantages: (1) inclusion of parameters that control bone physiology (e.g., growth, volume, maturation) supports simulation of changes to bone mineral metabolism that might affect bone production, growth, or maturation (e.g., disease, nutrition, menopause, weightlessness), and estimations of the effects that these changes might have on bone Pb kinetics. An analogous simulation in the AALM-LG requires direct knowledge (or assumptions) of the effects of these changes on bone Pb transfer coefficients; and (2) advances in the knowledge of bone physiology (e.g., metabolism, growth, resorption, disease) and of bone kinetics for other elements (e.g., calcium, strontium) can be incorporated into the model to improve the parameterization and parameter values of the model, and its capability to simulate and estimate bone growth, volume, and maturation. In contrast, specialized studies for all the different age-related scenarios would be needed to improve values for the less physiologically representation of bone Pb kinetics in the AALM-LG model based on compartment transfer rates that change with age.

4.4. COMPARISON OF AALM-LG AND AALM-OF ESTIMATIONS OF BLOOD AND TISSUE PB

Differences in the structures of the Leggett and O'Flaherty biokinetics models would be expected to result in different estimations of blood and tissue Pb levels for similar Pb exposure assumptions (Maddaloni et al., 2005). The revised AALM provides a convenient platform for comparing the models, because it

allows both to be run using the same exposure and absorption settings. Two types of comparisons were made of AALM-LG and AALM-OF: (1) age profiles for blood and tissue Pb levels following an exposure to a constant Pb intake (µg/day) were simulated and compared; and (2) dose-response relationships between ingested dose and Pb levels were compared by simulating a series of increasing Pb intakes. In either type of simulation, parameters that control Pb absorption and growth were set to the same values (defaults for AALM-OF), so that differences in blood and tissue Pb levels could be attributed entirely to differences in the simulation of systemic (post-absorption) biokinetics.

4.4.1. Comparison of Model Estimations for Constant Pb Intake

Figures 4-6 thru 4-9 show results of the simulations for a constant ingestion of 5 µg Pb/day beginning at birth and extending to age 30 years. This exposure results in estimated blood Pb concentrations less than 5 µg/dL, which is well below the concentration at which saturation of uptake into RBCs significantly affects blood Pb levels. Figure 4-6 shows the age profiles for selected output variables (µg Pb in blood, bone, soft tissue and total body). Figure 4-7 shows the differences expressed relative to the AALM-LG (arbitrarily selected as the reference for presentation of the results). A negative value in Figure 4-7 indicates that the estimation from AALM-OF is less than that from AALM-LG. For example, -0.65 in Figure 4-7 indicates that the AALM-OF blood Pb estimation is less than the AALM-LG estimation, and the magnitude of the difference is 65% relative to the AALM-LG value. Figure 4-8 compares estimated cumulative urinary and fecal Pb excretion. Figure 4-9 compares elimination rates following cessation of exposure.

Several differences between the models are evident from these comparisons.

- AALM-OF predicts lower blood Pb levels prior to age 10 years (64–65%), after which, the models begin to converge on similar blood Pb levels, with adult estimations from the AALM-OF exceeding AALM-LG by approximately 20%.
- AALM-OF estimates lower bone Pb levels in children prior to age 10 years (63–68%), after which, the models begin to converge on similar bone Pb levels, with adult estimations from the AALM-OF exceeding AALM-LG by approximately 18%.
- AALM-OF estimates lower soft tissue Pb levels (all tissues combined, excluding bone) at all ages (59–92%).
- Both models estimate similar accumulation of Pb over the lifetime, reflected in similar total body burdens (agreement is within 10%).
- With cessation of exposure, both models estimate rapid declines of Pb in blood ($t_{1/2}$ = 30–50 days) and soft tissue, with a slower decline in bone Pb ($t_{1/2}$ 10–20 years).
- Both models estimate multiple rates of decline in blood Pb. In adults, the half-time for the first 50 days following cessation of exposure is approximately 36 days in AALM-LG and 46 days in AALM-OF. The half-time for the period 5–20 years following cessation of exposure is 12.7 years in AALM-LG, and 10.9 years in AALM-OF. The slow phase results from transfer of bone Pb to blood.

- Both models estimate a more rapid decline in bone Pb in children compared to adults following cessation of exposure. The two models estimated similar half-times for bone Pb elimination in children ($t_{1/2}$ = 3.00 [AALM-LG], 2.24 years [AALM-OF]).
- Although both models estimate slower elimination of Pb from bone in adults, AALM-OF estimates a more rapid decline ($t_{1/2}$ = 12.6 year) than AALM-LG ($t_{1/2}$ = 19.7 year).
- AALM-OF estimates a higher rate of urinary excretion of Pb compared to AALM-LG. Fecal excretion is identical in both models because it is dominated by unabsorbed Pb and gastrointestinal absorption parameters were set to the same values in both models for the comparison simulations.

Amounts of Pb in tissues are converted to Pb concentrations in both models by dividing Pb masses by age-dependent values for tissue weights. The latter are estimated in both models from the body growth and tissue growth models developed by O'Flaherty (1995). The blood and bone Pb concentrations estimated for an exposure to 5 µg Pb/day are shown in Figure 4-10. Differences in the model estimations of tissue Pb masses are reflected in the tissue Pb concentrations. The magnitudes of the differences between models (i.e., ratio AALM-LG/AALM-OF) are the same for Pb masses and concentrations, because both models use the same tissue growth algorithms, which estimate the same tissue volumes and weights.

4.4.2. Comparison of Estimated Dose-Response for Blood and Tissue Pb

Although both AALM-LG and AALM-OF are mathematically linear models (i.e., all state variables are defined with linear differential equations), they estimate curvilinear dose-response relationships for blood Pb resulting from a saturable capacity of red blood cells (RBC) to take up Pb. Dose-response relationships estimated from AALM-LG and AALM-OF are shown in Figures 4-11 and 4-12, for children (age 5 years) and adults (age 30 years), respectively. Although curvature of the dose-response relationship for blood derives from saturation of uptake of Pb in RBCs, the two models use different computational approaches to model the saturable uptake. AALM-LG simulates binding of Pb in red blood cells with rate coefficients for transfer of Pb from plasma to RBCs (child and adult, $t_{1/2}$ = 0.0014 days), and from RBCs to plasma (child $t_{1/2}$ = 2.5 days, adult $t_{1/2}$ = 5 days). This results in a rapid uptake, slower release, and accumulation of RBC Pb. The plasma-blood concentration ratio is governed, in part, by the ratio of these transfer coefficients (plasma to RBC/RBC to plasma). The higher ratio in children (i.e., exit rate is faster) results in higher plasma-RBC concentration ratios in children. Above a non-linear, threshold Pb concentration in red blood cells (60 µg/L), the rate constant for transfer into RBCs declines with increasing intracellular concentration, approaching zero (no uptake) at a saturating concentration of 350 µg/dL RBC (see Equation 4-1).

$$TOORBC = TORBC \cdot [1 - \left(\frac{RBCCONC - RBCNL}{SATRAT - RBCNL}\right)]^{1.5} \qquad \text{Eq. (4-1)}$$

where *TOORBC* is the deposition fraction from diffusible plasma to red blood cells; TORBC the age-scaled deposition fraction from diffusible plasma to red blood cells below non-linear threshold; *RBCCONC* the red blood cell Pb concentration (µg/dL RBC volume); *RBCNL* the non-linear uptake kinetics threshold concentration (µg Pb/dL RBC volume); and *SATRAT* the maximum capacity of the red blood cell compartment (µg Pb/dL RBC volume).

AALM-OF simulates a binding equilibrium (rather than kinetics) in which Pb in plasma achieves instantaneous equilibrium with unbound Pb in RBCs, which is in equilibrium with bound Pb. Binding parameters include a maximum capacity (270 µg Pb/dL RBC) and half-saturation concentration (0.75 µg/dL RBC), with the relationship represented as follows (see Equation 4-2):

$$CB = (1 - HCT) \cdot CP + HCT \cdot CP \cdot \left\{G + \frac{BIND}{KBIND + CP}\right\} \qquad \text{Eq. (4-2)}$$

where *CB* is the blood Pb concentration (µg/dL), *CP* the plasma Pb concentration (µg/dL); *HCT* is the hematocrit; *G* the ratio of unbound RBC Pb to plasma Pb; *BIND* the maximum capacity of RBC binding (µg/dL); and *KBIND* the half-saturation coefficient (µg/dL). One advantage of this approach is that the parameters BIND and KBIND have a direct empirical basis, as they have been estimated from data on Pb concentrations in plasma and RBCs [e.g., (Bergdahl et al., 1998; O'Flaherty, 1993)]. However, a disadvantage is that it represents plasma-RBC kinetics as essentially being instantaneous; whereas, observations made following injection of radiolead suggest that kinetics may be slower and more complex [see Leggett (1993) for discussion of these observations].

The different parameterizations of RBC saturation are evident in the relationships between plasma and blood Pb estimated from the two models. In both models, the plasma-blood concentration ratio increases with increasing blood Pb concentration, as the RBC approaches saturation. In AALM-OF, the plasma-blood Pb ratio below saturation remains nearly constant with age (0.007); whereas, in AALM-LG, the plasma:blood ratios are higher in children compared to adults. AALM-LG estimates a plasma-blood ratio that declines from 0.01 at age 1 year to 0.003 at ages beyond 10 years (below saturation).

The AALM estimates the non-linear relationship between plasma and whole blood Pb concentrations observed in studies in which methods were employed to control for sample contamination, which is of particular importance in measurements of the low Pb levels found in plasma (see discussion of Figure 3-13). The dependency of the RBC deposition fraction (TOORBC) on RBC Pb concentration results in the blood Pb concentration being independent of the hematocrit.

Both models estimate linear dose-response relationships for bone Pb, and for all other tissue Pb. The estimated dose-response relationships for bone are more similar in adults, whereas AALM-LG estimates a steeper dose-response relationship for bone in children. The steeper dose-response relationship for bone Pb in children occurs in AALM-LG even though the elimination rates from bone are similar in both models. This suggests that the differences between model results for bone Pb is related to the rates of deposition of Pb in bone, rather than to differences in rates of bone Pb elimination.

4.5. SENSITIVITY ANALYSIS OF AALM-LG AND AALM-OF

Relative to the AALM-LG, AALM-OF estimates lower amounts and concentrations of Pb in blood in children, higher amounts and concentrations of Pb in blood in adults, and lower amounts and concentrations of Pb in soft tissues in at all ages. Numerous individual parameters or combinations of parameters could contribute to these differences. AALM-LG has 39 parameters and AALM-OF has 35 parameters that collectively determine the biokinetics of absorbed Pb in each model to varying degrees. These parameters and their nominal values are presented in Tables 4-2 (AALM-LG) and 4-3 (AALM-OF). A univariate sensitivity analysis was conducted to determine the effect of each parameter

on estimations of Pb in blood, bone, and soft tissues.[7] The sensitivity analysis consisted of running each model before and after perturbing values for single parameters by a factor of 0.01, in the up and down directions. Parameter sensitivities were assessed by comparing standardized sensitivity coefficients (see Equation 4-3):

$$SSC = f'(x) = \frac{ABS[f(x+\Delta x) - f(x-\Delta)]}{2\Delta x} \cdot \frac{x}{f(x)} \qquad \text{Eq. (4-3)}$$

where *SSC* is the standardized sensitivity coefficient; *f(x)* the output variable (e.g., blood Pb) at parameter value *x*; and Δ the perturbation of *x* (e.g., 0.01x). Values for SSC were determined for blood, bone, and soft tissue Pb at ages selected to represent children (5 years) or adults (30 years).

4.5.1. Sensitivity Analysis of AALM-LG

SSCs were derived for all input parameters to AALM-LG other than those that control Pb absorption or growth. Separate sensitivity analyses were run to determine parameter sensitivity of the total amount of Pb in blood, bone, liver, kidney, or other soft tissues, in children (age 5 years) and adults (age 30 years). SSCs are displayed in order of highest to smallest value for adults in Tables 4-4 thru 4-8. Larger values of SSC indicate larger effects of the parameter on blood Pb. For example, blood Pb is most sensitive to the value of the parameter *TEVF*, the deposition fraction for Pb transfer from diffusible plasma to the extravascular fluid (see Table 4-4). The value 8.38 indicates that a 1% change in *TEVF* results in an 8.38% change in blood Pb. Influential parameters have SSCs that exceed 0.1 (>0.1% change in tissue Pb per 1% change in the input parameter).

In the discussion that follows, input parameter values are expressed as their equivalent first-order transfer rates (day^{-1}) shown in Table 4-2 and their corresponding approximate first-order half-times ($t_{1/2}$, day). In AALM-LG, the central distribution compartment is diffusible plasma, which exchanges Pb with other tissue compartments. Input parameters that control transfers of Pb from tissues to diffusible plasma are expressed as first-order rates. Input parameters that control transfers from diffusible plasma to tissues are expressed as deposition fractions. Deposition fractions represent the fractional apportionment of the total outflow of Pb from diffusible plasma (Leggett, 1993). First-order rates are derived in the AALM-LG as the product of deposition fraction and total outflow of Pb from the diffusible plasma compartment (*RPLAS*, see Equation 4-4).

$$REFV = TEFV \cdot RPLAS \qquad \text{Eq. (4-4)}$$

where *REFV* is the transfer rate from diffusible plasma to the extravascular fluid (day^{-1}); *TEFV* the deposition fraction for transfer to the extravascular fluid; and *RPLAS* the total rate of transfer of Pb to all tissues (day^{-1}). The nominal value for *RPLAS* is 2000 day^{-1}. If the deposition fraction for *TEFV* is 0.5, the corresponding transfer rate for *TEFV* is 1000 day^{-1} (0.5×2000 day^{-1}). Values for transfer rates corresponding to deposition fractions are presented in Table 4-2, so that they can be directly compared to

[7] This approach to sensitivity analysis does not consider potential interactions between parameters. Sensitivity coefficients measured in univariate analyses may be larger or smaller than SSCs measured in multivariate analyses (i.e., when multiple parameters are varied simultaneously).

the return transfer rates from tissue to diffusible plasma. The values for the corresponding depositions fractions can be calculated from Equation 4-4.

4.5.1.1. Influential Parameters Common to All Tissues

Several parameters had relatively large influences (SSC > 0.1) across all or most of the tissues that were included in the sensitivity analysis and dominate Pb biokinetics in the AALM-LG. These parameters are *TEVF*, *TORBC*, *TOSOF0*, *TOLVR1*, *H1TOBL*, and *TBONE*.

The parameter *TEVF* controls the rate of transfer of Pb from diffusible (non-bound) plasma to the extravascular space. The nominal value for the rate is 1000 day^{-1} ($t_{1/2}$ = 1.0 min) or approximately one half of the total transfer rate out of diffusible plasma to all tissues (2000 day^{-1}). The return rate to diffusible plasma is 333 day^{-1} ($t_{1/2}$ = 3.0 min). This results in a rapid exchange of Pb in diffusible plasma with the extravascular fluid, with an equilibrium ratio in which the extravascular fluid contains approximately 3 times the amount of Pb in diffusible plasma. The extravascular fluid serves as a rapid exchange reservoir that contributes to plasma Pb. Increasing or decreasing the value of *TEVF* increases or decreases, respectively, the amount of Pb in plasma and, thereby, blood Pb and the amount of Pb available for distribution to other tissues. The prominence of *TEVF* in the SSCs for all tissues may also result from its use in age-scaling of deposition fractions in the model. Deposition fractions for all tissues other than bone are scaled as function of *TEVF* and *TBONE* (the deposition fraction to bone surfaces) (see Equation 4-5).

$$AGESCL = \frac{1-TEVF-TBONE(t)}{1-TEVF-TBONEL} \qquad \text{Eq. (4-5)}$$

where *TBONEL* is the terminal value for *TBONE* as defined in the Time Dependent Parameters for 25 years and greater. The *AGESCL* adjustment restrains the deposition fractions (and total outflow) from diffusible plasma to soft tissues to the fraction not deposited to extravascular fluid or bone. This allows the bone deposition fraction (TBONE) to vary with age without disruption mass balance of transfer of Pb to soft issues. As a result of its use to scale deposition fractions to soft tissues, changes to *TEVF* affects Pb kinetics of RBC, kidney, liver, and other soft tissues.

The parameters *TORBC* and *RRBC* control the transfer rates of Pb into and out of RBCs, respectively. The nominal values in adults are 480 day^{-1} ($t_{1/2}$ = 2.1 min) and 0.139 day^{-1} ($t_{1/2}$ = 5.0 day). The equilibrium ratio (*TORBC/RRBC*) is approximately 3450, which results in accumulation of Pb in the RBC, relative to plasma, and Pb in red blood cells being the dominant contributor to blood Pb. Increasing the transfer rate into red blood cells (*TORBC*), without a change in the return rate (*RRBC*) increases blood Pb, whereas, increasing the transfer rate out of red blood cells (*RRBC*), makes more Pb available to the diffusible plasma compartment for distribution to other tissues, and decreases blood Pb.

AALM-LG has three soft tissue compartments, representing fast (*SOF0*), moderate (*SOF1*), and slow (*SOF2*) kinetic pools of Pb in soft tissues other than blood, kidney, or liver. The parameter *TOSOF0* controls the rate of transfer from diffusible plasma to the fast compartment. The nominal value in adults is 178 day^{-1} ($t_{1/2}$ = 5.6 min) and the return rate is 2.08 day^{-1} ($t_{1/2}$ = 8.0 hours). Similar to the extravascular fluid, this soft tissue compartment provides an exchange reservoir to support plasma and blood Pb, as well as Pb available for distribution to other tissues.

The parameters *TOLVR1* and *H1TOBL* control the transfer of Pb from diffusible plasma to liver and the return to plasma, respectively. Nominal values are 80 day^{-1} ($t_{1/2}$ = 12.5 min) for transfer to liver and 0.03

day^{-1} ($t_{1/2}$ = 23.1 day) for return. Similar to the rapid exchange soft tissue compartment, this liver compartment provides a reservoir to support plasma and blood Pb.

The parameter *TBONE* controls the transfer rate from diffusible plasma to surface bone, the only pathway for entrance of Pb into bone where it can be sequestered into slower kinetic pools of bone volume. The nominal values are 89 day^{-1} and 71 day^{-1} ($t_{1/2}$ = 11.2 min, 14.1 min) for trabecular and cortical bone, respectively. The return value from both types of bone is 0.5 day^{-1} (14 day). More than 90% of the Pb body burden resides in bone, as a result, the transfer to bone affects Pb levels in all other tissues. The terminal value of *TBONE* (*TBONEL*) is also used in the age-scaling of deposition fractions to all tissues other than bone (see Equation 4-5). This is reason why it shows up as an influential parameter across all tissues.

4.5.1.2. Sensitivity Analysis of AALM-LG Blood Pb Estimations

AALM-LG SSCs for blood Pb (*ABLOOD*) are shown in Table 4-4. The most influential parameters on blood Pb (SSCs > 0.1) are *TEFV*, *TORBC*, *TOSOF0*, *RRBC*, *TOLVR1*, *H1TOBL*, and *TBONE*. These parameters have SSCs > 0.1 across all tissues (see Section 4.5.1.1).

4.5.1.3. Sensitivity Analysis of AALM-LG Bone Pb Estimations

AALM-LG SSCs for bone Pb (*ABONE*) are shown in Table 4-5. The most influential parameters on bone Pb (SSCs > 0.1) are *TEFV*, *TORBC*, *TBONE*, *TOSOF0*, *FLONG*, *RCS2DF*, *TOLVR1*, *H1TOBL*, and *RTS2DF*. The bone model in AALM-LG includes three sub-compartments for cortical and trabecular bone that represent fast (surface bone), moderate (exchangeable), and slow (non-exchangeable) Pb pools (see Figure 4-4). The slow compartment contains most (>90%) of the Pb in bone and, therefore, is the major determinant of the amount of Pb in bone. The parameter *FLONG* controls the rate of transfer of Pb from the moderate to the slow compartment. Lead enters the moderate and slow bone compartments from surface bone, which is in direct exchange with plasma. The parameter *TBONE* controls the rate of transfer of Pb to bone surfaces; nominal values are 89 day^{-1} and 71 day^{-1} ($t_{1/2}$ = 11.2 min, 14.1 min) for trabecular and cortical bone, respectively. The parameters *RCS2DF* and *RTS2DF* control the rate of return of Pb from bone surface to plasma (0.5 day^{-1}, $t_{1/2}$ = 1.4 day).

4.5.1.4. Sensitivity Analysis of AALM-LG Liver Pb Estimations

The most influential parameters on liver Pb (SSCs > 0.1) are *TEFV*, *TORBC*, *TOSOF0*, *TOLVR1*, *H1TOH2*, *RLVR2*, *H1TOBL*, and *RLVR1* (see Table 4-6). The liver model in AALM-LG includes two sub-compartments representing fast (H1) and slow (H2) pools. Lead in the fast compartment exchanges with plasma and delivers Pb into the slow compartment and to bile. Transfer of Pb into the fast compartments controlled by the parameter *TOLVR1* (80 day^{-1}, $t_{1/2}$ = 11.2 min) and return to plasma is controlled by *RLVR1* (0.0312 day^{-1}, $t_{1/2}$ = 22.2 day). Transfer of Pb from the fast to the slow compartment is controlled by *H1TOH2* (0.00693 day^{-1}, $t_{1/2}$ = 100 day) and transfer to bile is controlled by *H1TOBL* (0.0312day^{-1}, 22.2 day). Return of Pb to plasma is controlled by *RLVR2* (0.0019 day^{-1}, $t_{1/2}$ = 365 day).

4.5.1.5. Sensitivity Analysis of AALM-LG Kidney Pb Estimations

The most influential parameters on kidney Pb (SSCs > 0.1) are *TEFV*, *TORBC*, *TOSOF0*, *RKDN2*, *TOKDN1*, *TOKDN2*, *RKDN2*, *TOLV1*, and *H1TOBL* (see Table 4-7). The kidney model in AALM-LG includes two sub-compartments representing urinary route through the kidney (RK1) and a storage compartment that exchanges with plasma (RK2) pools. Transfer of Pb into kidney is controlled by the

parameters *TOKDN1* (40 day^{-1}, $t_{1/2}$ = 25 min) and *TOKDN2* (0.4 day^{-1}, $t_{1/2}$ = 1.7 day). Return of Pb to plasma is controlled by the parameter *RKDN2* (0.0019 day^{-1}, $t_{1/2}$ = 365 day).

4.5.1.6. Sensitivity Analysis of AALM-LG Other Soft Tissue Pb Estimations

The most influential parameters on other soft tissue Pb (SSCs > 0.1) are *TEFV*, *TORBC*, *TOSOF0*, *RSOF2*, *TOSOF2*, *TOLVR1*, *H1TOBL*, *TOSOF1*, and *RSOF1* (see Table 4-8). AALM-LG has three soft tissue compartments, representing fast (SOF0), moderate (SOF1), and slow (SOF2) kinetic pools of Pb in soft tissues other than blood, kidney, or liver. Transfer into each compartment is controlled by parameters TOSOF0 (178 day^{-1}, $t_{1/2}$ = 5.6 min), *TOSOF1* (10 day^{-1}, 1.7 hours), and *TOSOF2* (2 day^{-1}, $t_{1/2}$ = 8.3 hours). Return of Pb to plasma is controlled by parameters *RSOF0* (2.08 day^{-1}, $t_{1/2}$ = 8.0 hours), *RSOF1* (0.00416 day^{-1}, $t_{1/2}$ = 167 day), and *RSOF2* (0.00038 day^{-1}, 1824 day).

4.5.2. Sensitivity Analysis of AALM-OF

SSCs were derived for all input parameters to AALM-OF other than those that control Pb absorption or growth. Separate sensitivity analyses were run to determine parameter sensitivity of the total amount of Pb in blood, bone, liver, kidney, or poorly perfused and well-perfused tissues, in children (age 5 years) and adults (age 30 years). Input parameter values for AALM-OF are presented in Table 4-3. This is a mix of parameters for Pb, and parameters that control bone formation and resorption rates that determine transfer of Pb in and out of deep bone. SSCs for each tissue are displayed in order from highest to smallest value for adults in Tables 4-9 thru 4-14.

4.5.2.1. Influential Parameters Common to All Tissues

Three parameters had large influences (SSC > 0.1) across all, or most, of the tissues that were included in the sensitivity analysis, and dominate Pb kinetics in the AALM-OF. These parameters are C1, C2, and C3. Urinary excretory clearance of Pb from plasma is simulated in AALM-OF as a function of glomerular filtration rate (GFR). The parameters *C1*, *C2*, and *C3* are unitless parameters in the function that simulates GFR as a function of age. Changes to these parameters alter the rate of removal of Pb from plasma to urine and, thereby, the amount of Pb in blood and available for distribution to other tissues.

4.5.2.2. Sensitivity Analysis of AALM-OF Blood Pb Estimations

The most influential parameters on blood Pb (SSCs > 0.1) are *C1*, *C2*, *BIND*, *KBIND*, and *C3* (see Table 4-9). Uptake of Pb into RBCs is simulated in AALM-OF as a binding equilibrium between plasma Pb and RBC Pb (see Section 2.2). The parameters *BIND* (2.7 mg/L) and *KBIND* (0.0075 mg/L) are the maximum binding capacity of the RBCs, and the half-saturation concentration of Pb for binding, respectively. Changing *BIND* or *KBIND* affects the amount of Pb sequestered in RBCs, and the amount of Pb available to the plasma compartment for distribution to other tissues. Increasing *BIND* increases RBC binding, and increases blood Pb. Increasing *KBIND* increases the plasma Pb concentration needed to achieve a given RBC Pb concentration, and decreases blood Pb.

4.5.2.3. Sensitivity Analysis of AALM-OF Bone Pb Estimations

The most influential parameters on bone Pb (SSCs > 0.1) are *C1*, *C2*, *R0*, *RAD8*, *EXPO*, and *C3* (see Table 4-10). The parameter *R0* controls the clearance of Pb from bone into the vascular sites in bone (canaliculi) where exchange with plasma occurs. The nominal value is 5E-7 cm^3/day. Increasing *R0* decreases bone Pb. The parameter *RAD8* is the radius of the deepest (eight of 8) diffusion shells in mature cortical bone. This parameter determines the diffusion volume (2.14E-3 cm) and, thereby, the

clearance of Pb from the deepest bone compartment. Increasing *RAD8* decreases bone Pb. The parameter *EXPO* is a unitless exponent constant in the function that simulates the age-dependency of the bone volume participating in adult remodelling. During adult remodelling, bone formation and resorption rates are slower than during child and adolescent growth periods. As a result, exchange of Pb between deep bone deposits and plasma is slower in mature bone than during growth.

4.5.2.4. Sensitivity Analysis of AALM-OF Liver Pb Estimations

The most influential parameters on liver Pb (SSCs > 0.1) are *C1*, *C2*, *PL*, and *C3* (see Table 4-11). Exchange of Pb between plasma and liver is simulated in AALM-OF as a flow-limited process determined by the liver/plasma partition coefficient and blood flow to the liver. The parameter *PL* is the liver/plasma partition coefficient (*PL* = 50). The nominal value is 50. Increasing *PL* increases liver Pb.

4.5.2.5. Sensitivity Analysis of AALM-OF Kidney Pb Estimations

The most influential parameters on kidney Pb (SSCs > 0.1) are *C1*, *C2*, *PK*, and *C3* (see Table 4-12). Similar to liver, exchange of Pb between plasma and kidney is simulated in AALM-OF as a flow-limited process determined by the kidney/plasma partition coefficient (*PK* = 50) and blood flow to the kidney. Increasing *PK* increases kidney Pb.

4.5.2.6. Sensitivity Analysis of AALM-OF Poorly Perfused Tissue Pb Estimations

The most influential parameters on poorly perfused tissue Pb (SSCs > 0.1) are *C1*, *C2*, *PP*, and *C3* (see Table 4-13). Exchange of Pb between plasma and poorly perfused tissue is simulated in AALM-OF as a flow-limited process determined by the tissue/plasma partition coefficient (*PP* = 2.0) and blood flow to the tissue. Increasing *PP* increases poorly perfused tissue Pb.

4.5.2.7. Sensitivity Analysis of AALM-OF Well-Perfused Tissue Pb Estimations

The most influential parameters on well-perfused tissue Pb (SSCs > 0.1) are *C1*, *C2*, *PW*, and *C3* (see Table 4-14). Exchange of Pb between plasma and well-perfused tissue is simulated in AALM-OF as a flow-limited process determined by the tissue/plasma partition coefficient (*PW* = 50) and blood flow to the tissue. Increasing *PW* increases well-perfused tissue Pb.

4.6. CONCLUSIONS FROM MODEL COMPARISONS AND SENSITIVITY ANALYSES

Table 4-15 lists the dominate parameters causing major differences between estimations from AALM-LG and AALM-OF and corresponding parameter values that had the highest SSCs for each estimation. Data may exist for some of the significant parameters that would allow evaluation and/or optimization of parameter values. AALM-OF parameters *C1* and *C2* control GFR, and thereby, urinary clearance of Pb from plasma. Abundant data exist on rates and age (i.e., body size) dependence of glomerular filtration in humans [e.g., (Peters, 2004; Peters et al., 2000)]. Data on urinary clearance of Pb in humans also exist that may be useful for evaluating model estimations [e.g., (Diamond, 1992)].

AALM-OF parameters *BIND* and *KBIND* and AALM-LG parameters *TORBC* and *RRBC* control uptake of Pb into RBCs and, thereby, influence plasma Pb and its distribution to tissues. These parameters can be evaluated against data from studies in which levels of Pb in plasma and whole blood (and/or RBCs) have been measured in humans with methods that ensure sampling of plasma Pb without contamination with Pb from lysed red cells [e.g., (U.S. EPA, 2003a)].

Direct empirical evaluation of AALM-OF and AALM-LG parameters that control bone Pb may not be feasible because of lack of data to directly estimate parameter values. However, optimization of influential parameters that control bone Pb levels and relationships between blood and bone Pb may be feasible with data from long-term monitoring studies of blood and bone, where exposure to Pb was abruptly changed [e.g., retired Pb workers; see (U.S. EPA, 2013)].

Similarly, direct empirical evaluation of AALM-OF tissue-plasma partition coefficients, and AALM-LG transfer rates and deposition fractions that control Pb levels in liver, kidney, and other soft tissues may not be feasible because of lack of data to directly estimate parameter values. However, it may be possible to optimize these parameters against data from cadaver studies in which the distribution of Pb body burden in bone and soft tissue has been measured.

4.7. EVALUATION AND OPTIMIZATION OF THE AALM

Although the sensitivity analyses described in Section 4.5 provides some insight regarding the parameters that contribute to differences in estimations from the two models; a more important objective is to determine what set of parameters provides the most accurate representation of observations of Pb kinetics in humans. Extensive documentation of the development and calibration of the Leggett and O'Flaherty models has been reported (O'Flaherty, 2000; O'Flaherty et al., 1998; O'Flaherty, 1998, 1995; Leggett, 1993; O'Flaherty, 1993). New data have become available since the development of the models (U.S. EPA, 2013). Important objectives for further development of the AALM are: (1) collect and re-examine all available data for utility in model evaluation, optimization, and validation; (2) conduct a comprehensive evaluation of the models against a common set of data; (3) optimize influential parameters identified in Section 4.5 that can be informed by the observation data sets; and (4) validate the model against a set of observations not utilized in optimization of the models.

Searches for studies of the toxicokinetics of Pb in humans that provide data that might be useful for estimated model parameter values were conducted. Three types of data were of particular interest: (1) blood, tissue, or excreted Pb paired with measured Pb intakes and/or exposures; (2) temporal patterns of blood, tissue, or excreted Pb following an abrupt change in Pb intake or exposure; and (3) paired data for blood and tissues or excreted Pb (e.g., urine/blood or tissue/blood ratios). Based on the available data retrieved and processed from the searches as well as considerations of the results of comparisons of the two models, a stepwise optimization approach was developed, in which specific outputs of the models were evaluated against observations in humans, and key parameters were optimized to achieve agreement with the observations (see Table 4-16).

Optimization was achieved using maximum likelihood (MLE) algorithms available in acslX (e.g., Nelder Mead) or if this was not possible, by visual inspection. Optimizations were evaluated by inspection of residuals (Equation 4-6) and the r^2 for the least-squares linear regression of observed and predicted values.

$$Residual = \frac{Predicted - Observed}{Standard\ Deviation\ of\ Mean} \qquad \text{Eq. (4-6)}$$

The optimization objectives were residuals $\leq \pm 2$ and $r^2 > 0.70$.

Most pertinent to the AALM.FOR model are the changes made to the Leggett (1993) model to create the AALM-LG model, based on the evaluations described below. These changes are summarized in Table 4-22.

4.7.1. Unification of Simulation of GI Absorption and Growth

A goal of the optimization was to determine if AALM-LG and AALM-OF would converge on similar estimations for post-absorption kinetics of blood and tissue Pb concentrations. To remove effects of differences in absorption and growth parameters in the two biokinetics modules, the GI absorption and growth parameters from the O'Flaherty (1995, 1993) model were adopted for both AALM sub-models. The resulting AALM GI absorption model is a continuous function (Equation 4-7) that simulates an age-dependent decline in the absorption fraction (AF_{Age}), from the value in infancy to the value in adults.

$$AF_{Age} = AF_{C1} - \frac{AF_{C2}}{1+30 \cdot e^{-Age}} \quad \text{Eq. (4-7)}$$

The settings (AF_{C1} = 0.60, AF_{C2} = 0.52) result in AF = 0.58 at birth and AF = 0.08 in adults (see Figure 4-13, OF default). As discussed in Section 4.7.8, AF_{C1} was set to 0.40 for infants based on Ryu et al. (1983). An AF_{C2} of 0.28 keeps the AF for adults at 0.12 (see Figure 4-13, AALM), which aligns with the Adult Lead Methodology (U.S. EPA, 2003b).

Tissue growth in the AALM is simulated as a function of body weight, which is age-dependent (see Figure 4-14). Tissue Pb concentrations are calculated as the Pb mass (µg) divided by the tissue weight (g). Concentrations of Pb in bone wet weight are converted to concentration per gram bone mineral by dividing the wet weight concentration by the ash fraction of bone. This conversion was used to compare model estimations with bone X-ray fluorescence (XRF) data, which is typically reported in units of Pb per g bone mineral. Bone ash fractions were assumed to be 0.55 and 0.50 for cortical and trabecular bone, respectively (ICRP, 1996).

4.7.2. Optimization of Plasma Pb – Blood Pb Relationship

Six studies provided data on individual human subjects that can be used to evaluate the relationship between plasma Pb and blood Pb concentrations. Measurements of plasma Pb were made using either inductively coupled plasma mass spectrometry (Smith et al., 2002; Bergdahl et al., 1999; Bergdahl et al., 1998; Hernández-Avila et al., 1998; Bergdahl et al., 1997; Schütz et al., 1996) or stable isotope dilution with thermal ionization mass spectrometry (Manton et al., 2001). In all of these studies, methods were employed to control for sample contamination, which is of particular importance in measurements of the low Pb levels found in plasma. Taken together, the observations from these reports varied over a wide range of blood Pb (approximately 0.34–94.8 µg/dL) and plasma Pb (approximately 0.0014–1.92 µg/dL) levels. These studies provided 406 individual measurements of plasma Pb and blood Pb, in adult workers as well as individuals with no known history of occupational exposure to Pb (U.S. EPA, 2003a). Only one study provides similar data in children (Bergdahl et al., 1999). The observations in children do not appear to differ substantially from those for adults.

A best fit (least-squares) model for combined data from the above six studies was identified, and is presented in Equation 4-8:

$$Blood\ Pb = 87.0 \cdot Plasma\ Pb^{0.5} - 3.89 \ (r^2 = 0.90) \quad \text{Eq. (4-8)}$$

AALM-OF parameters KBIND and BIND were optimized (Nelder Mead) against this data set in the AALM-OF function relating plasma Pb and blood Pb (Equation 4-9):

$$CB = (1 - HCT) \cdot CP + HCT \cdot CP \cdot \left(\frac{G+BIND)}{KBIND+CP}\right) \quad \text{Eq. (4-9)}$$

AALM-LG parameter RBCNL was optimized by visual inspection (it was not possible to derive an independent expression for the plasma Pb and blood Pb relationship because relevant parameters control rate constants for transfer of Pb between plasma and RBC compartments).

Figures 4-15 compares the observed and estimated whole blood and plasma Pb in adults relationship. Residuals for the optimized models are within acceptable limits (-2, 2). The r^2 values for estimations are 0.99 and 0.98.

4.7.3. Optimization of Plasma-to-Urine Pb Clearance

Four studies provide data to derive estimates of the Pb plasma-to-urine clearance rate (L/day) (Araki et al., 1986; Manton and Cook, 1984; Manton and Malloy, 1983; Chamberlain et al., 1978). Clearance estimates from these studies are reported in Diamond (1992). These estimated clearance rates are based on measurements made in a total of 32 ("normal" subjects). The mean of the estimates from the four studies is 18 L/day ± 4 (SD).

Rentschler et al. (2012) reported individual subject data on urinary excretion of Pb (µg/g creatinine) and plasma Pb concentration in in five cases of Pb poisoning (blood Pb>80 µg/dL). The cases were followed for periods up to 800 days. If assumptions are made about body weight (not reported) and established associations between creatinine excretion and lead body mass, clearance rates can be estimated from these data. The estimated mean plasma clearance was 43 L/day ±13 (SD) (range: 32–64 L/day). Lead poisoning may have been a contributing factor to the relatively high clearances based on Rentschler et al. (2012). Therefore, for the purpose of model optimization, 18 L/day was selected as the representative value for plasma-to-urine clearance.

In AALM-OF, urinary excretion of Pb is an age-dependent fraction of GFR. Parameters for the GFR function were modified to achieve an adult GFR of approximately 170 L/day/1.73m^2 (120 mL/min/1.73 m^2 body surface area (ICRP, 2002, 1975), with infant (<1 year) values 30% of the adult value (Dewoskin and Thompson, 2008). AALM-OF parameters C2 and C3 were optimized in a function relating age and total Pb excretory clearance (FRX) as shown in Equation 4-10.

$$FRX = C1 - C2/(1 + C3 \cdot e^{-AGE}) \qquad \text{Eq. (4-10)}$$

AALM-LG parameters TKDN1 and TOURIN were optimized by visual inspection.

Figure 4-16 compares predicted and observed urinary clearance in adults. No data are available to evaluate the different age patterns for urinary clearance estimated by AALM-LG and AALM-OF.

4.7.4. Optimization of Soft Tissue-to-Bone Pb Ratio

Four studies provide data for measurements of post-mortem soft tissue and bone Pb concentrations (Gerhardsson et al., 1995; Barry, 1981; Barry, 1975; Gross et al., 1975). Gerhardsson et al. (1995) reported only soft tissue Pb concentrations; whereas, the other three studies reported soft tissue and bone Pb concentrations that can be used to estimate the ratios. Barry (1981) and Barry (1975) reported data for children and adults in age brackets. The data from Barry (1975) was used as the primary source to optimize parameters for kidney/bone and liver/bone Pb ratios as a function of age.

Barry (1975) reported data on tibia Pb concentrations that are simulated as cortical bone concentrations in the AALM models. Since Barry (1975) reported group mean tissue concentrations (not ratios in autopsy cases), the mean tissue-to-bone ratios were approximated from the group means.

In AALM-OF, uptake of Pb into kidney, liver, and other well-perfused tissue is assumed to be flow-limited and governed by blood flow and the tissue/plasma partition coefficients, PK, PL, and PW. Attempts to optimize these three parameters failed to accurately simulate the decline in the tissue/bone ratios estimated from the Barry (1975) observations. An improved fit was achieved when the constants PK, PL, and PW were allowed to vary with age according to the function shown in Equation 4-11.

$$PK = PKC \cdot (1 + e^{-PKA \cdot AGE)}) \qquad \text{Eq. (4-11)}$$

The parameters PKC and PKA (for kidney), PLC and PLA (for liver), and PWC and PWA (for other well-perfused) were optimized (Nelder Mead) against the tissue/cortical bone ratios derived from the data reported in Barry (1975).

AALM-LG parameters TOKDN2 and RKDN2 (for kidney) and RLVR2 (for liver) were optimized by visual inspection. It was not possible to use acslX parameter estimation functions because RKDN2 and RLVR2 are array variables.

Figure 4-17 compares estimated and observed kidney/bone and liver/bone Pb ratios in adults. Standard deviations of observed means were not available for calculating residuals because they were calculated from group mean tissue concentration reported in Barry (1975). Values for r^2 for kidney/bone estimations (of average of male and female ratios) were 0.95 and 0.77 for AALM-LG and AALM-OF, respectively. Values for r^2 for liver/bone estimations were 0.96 and 0.93 for AALM-LG and AALM-OF, respectively.

4.7.5. Optimization of Blood-to-Bone Pb Ratio

Two studies provide data to evaluate the relationship between plasma or serum blood Pb and bone Pb concentrations (Hernández-Avila et al., 1998; Cake et al., 1996). Cake et al. (1996) measured paired serum, tibia, and calcaneus Pb concentrations in 49 adult male Pb workers, and reported corresponding linear regression parameters. Hernández-Avila et al. (1998) measured paired plasma, tibia and patella Pb concentrations in 26 adults (20 female) who had no known occupational exposures to Pb. These data can be used to derive corresponding linear regression parameters for the log-transformed plasma Pb. Individual subject data were digitized from Figure 1 of Hernández-Avila et al. (1998), and linear regression parameters derived for the untransformed plasma Pb concentrations, in order to compare these with the linear regression parameters from Cake et al. (1996).

Bone Pb/Plasma Pb slopes at age 50 years were estimated from AALM-LG and AALM-OF from a series of simulations in which Pb intake was varied from 1 to 1000 µg/day. Table 4-17 and Figure 4-18 compare estimated and observed slopes based on data from Cake et al. (1996) and Hernández-Avila et al. (1998). Given the relatively low residuals for cortical bone, which were within the range -2 to 2, no further optimization for either model was needed for the respective parameters.

4.7.6. Optimization of Bone Pb Elimination Kinetics

Nilsson et al. (1991) reported longitudinal data on blood and finger bone Pb concentrations in 14 Pb workers for periods ranging from 8–18 years following cessation of their occupational exposures. The median blood Pb concentration at the end of exposure was approximately 45 µg/dL. The decline in bone Pb concentration was described by a first-order model with a single rate constant. Estimates of elimination half-times for each individual were reported. The group median was 16 years (95% CI: 12, 23). The decline in blood Pb was described by a tri-exponential model with the following parameters.

Parameter	Unit	C1 (95% CI)	C2 (95% CI)	C3 (95% CI)
$t_{1/2}$	year	34 day (29, 41)	1.2 year (0.85, 1.8)	13 year (10, 18)
C	µg/dL	10.2	12.6	22.8

AALM-OF simulations were run for a constant Pb intake from birth to age 60 years, to achieve a terminal blood Pb concentration of approximately 45 µg/dL (1000 µg/day), followed by 20 years without exposure. A first-order exponential rate was estimated for the decline in cortical bone Pb concentrations estimated for 20 years following cessation of exposure. The AALM-OF parameter R0 (coefficient for Pb diffusion out of bone mineral into canaliculus) was optimized (visual inspection) to achieve an elimination half-time from cortical cone of 16 years, the median value based on the Nilsson et al. (1991) results.

AALM-LG simulations were run for a constant Pb intake from birth to age 60 years, to achieve a terminal blood Pb concentration of approximately 45 µg/dL (2000 µg/day), followed by 20 years without exposure. A first-order exponential rate was estimated for the decline in cortical bone Pb concentrations estimated for 20 years following cessation of exposure. The AALM-LG parameters FLONG (fraction of total transfer from the exchangeable bone directed to non-exchangeable bone) and RCORT (transfer rate from non-exchangeable cortical bone to diffusible plasma) were optimized (visual inspection) to achieve an elimination half-time from cortical bone of 16 years, the median value based on the Nilsson et al. (1991) results. FLONG and RCORT are age-dependent arrays and were varied in the optimization by applying a constant (proportional) adjustment to all elements in the age array. The same adjustment factor was therefore applied to child and adult values, even though the optimization was made against data only for adults. The same adjustment factor was also applied to RTRAB (transfer rate from non-exchangeable cortical bone to diffusible plasma).

Figure 4-19 compares rates of elimination of Pb from bone and blood with the corresponding empirical models derived for Pb workers (Nilsson et al., 1991). Elimination rates of Pb from bone estimated from the optimized models are within the 95% CI of the empirical model and yield residuals that range within the -2, 2, criteria ($r^2 = 0.99$). Elimination half-times estimated for bone Pb (16 years) were identical to estimates from Nilsson et al. (1991). Although elimination rates from blood estimated by the optimized models are approximately at the confidence limits of the empirical model, the initial model divergence is due largely to the slower (AALM-LG) or faster (AALM-OF) elimination kinetics during the first 5 years following cessation of exposure; after which the models converge on the empirical model ($r^2 = 0.96$ AALM-LG; $r^2 = 0.99$ AALM-OF). Half-times estimated for the period 5 to 20 years after exposure were 1.25 years from AALM-LG and 1.06 years from AALM-OF, similar to values estimated for C2 (1.2 year) from Nilsson et al. (1991).

4.7.7. Evaluation of Blood Pb Elimination Kinetics in Adults

Rabinowitz et al. (1976) conducted a pharmacokinetics study in which four adults ingested daily doses of [^{207}Pb] nitrate for periods up to 124 days. Concentrations of ^{207}Pb in blood, urine, and feces were then monitored during and following cessation of exposure, and data on daily intakes and blood concentrations for each subject were reported. Absorption fractions for Pb were estimated for each individual based on mass balance in feces.

Figure 4-20 compares observed and estimated blood ^{207}Pb concentrations for the optimized AALM-LG and AALM-OF. Gastrointestinal absorption fractions were set in both models to the estimates for each individual reported in Rabinowitz et al. (1976). No other changes were made to parameter values. Although both models AALM-LG estimate a rise and decline in blood Pb concentrations, AALM-LG estimations are closer to the observations. Values for r^2 for AALM-LG estimations are 0.99, 0.98, 0.92, and 0.97 for Subjects A, B, D, and E, respectively. Values for r^2 for AALM-OF estimations range from 0.08 (Subject E) to 0.24 (Subjects A, B, and D). AALM-OF estimates slower accrual and decline of blood Pb, and lower peak blood Pb concentrations.

4.7.8. Evaluation of Blood Pb Elimination Kinetics in Infants

Only two studies provide data on the relationships between Pb dose and blood Pb concentration in infants (Sherlock and Quinn, 1986; Ryu et al., 1983). In the Ryu et al. (1983) study, blood Pb concentrations were monitored in 25 formula-fed infants. From birth to age 111 days, infants were fed formula (packaged in cartons) that had a Pb concentration of approximately 20 µg/L. From age 112 to 195 days, a subset of the infants (n = 7) were switched to formula (packaged in cans) that had a Pb concentration of approximately 57 µg/L. Formula intakes were measured, and provided estimates of Pb intakes in each subject. Ryu et al. (1983) reported a table of individual Pb intakes, and presented a figure illustrating group mean blood Pb concentrations at various ages (these data were digitized for use in this analysis). Standard errors (or deviations) of mean blood Pb concentrations were not reported; however, as discussed below, based on Sherlock and Quinn (1986), standard errors may have been approximately 10% of the means. The parameter for maternal blood Pb concentration was set at 10 µg/dL, the reported maternal mean for the study. Lead absorption was not quantified in Ryu et al. (1983); therefore, the gastrointestinal absorption fraction during infancy was set to 40%, based on estimates from mass balance studies (Ziegler et al., 1978). No other changes were made to parameter values. Figure 4-21 compares estimated and observed blood Pb concentrations for the two exposure regimens (carton formula or carton followed by canned formula). Simulations are shown for the mean intake (12–20 µg/day) and ± 1 SD (10–18 µg/day, 15–22 µg/day). AALM-LG encompasses most of the observations within ±1 SD of the mean intakes. AALM-OF estimations are higher than observations. If standard errors of mean blood Pb concentrations were 10% of the mean, residuals for AALM-LG estimations ranged from -3.7 to 0.15 for carton exposures (mean -1.2). Residuals for AALM-OF estimations ranged from -3.0 to 4.4 (mean 2.0). Both models capture the increase in blood Pb concentration associated with the switch the higher Pb intakes for canned formula and the overall temporal trends in the observations; r^2 for estimations were 0.85 and 0.76 for AALM-LG and AALM-OF, respectively.

Sherlock and Quinn (1986) measured blood Pb concentration in 131 infants at age 13 weeks and estimated dietary intake of Pb for each infant based on Pb measurements made in duplicate diet samples collected daily during week 13. Sherlock and Quinn (1986) reported a plot of blood Pb means and standard errors for group mean dietary Pb intakes (these data were digitized for use in this analysis). The parameter for maternal blood Pb concentration was set at 18 µg/dL, the reported maternal geometric mean. The gastrointestinal absorption fraction was set at 40% for infants; the same value used in simulations of Ryu et al. (1983). Figure 4-22 compares estimated and observed blood Pb concentrations for the range of Pb intakes in the study. Both models reproduce the general shape of the observed curvilinear dose-blood Pb relationship; the apparent plateau observed at the higher end of the dose range, however, is achieved at higher doses in the models (>800 µg/day AALM-LG, >600 AALM-OF). Although the model results for the plateau contributed to high residuals at the highest Pb intake (>200

µg/day), residuals for lower Pb doses ranged from -4.8 to 1.5 (mean -2.3) for AALM-LG and -4.3 to 2.2 (mean – 1.0) for AALM-OF. The overall dynamics of increasing blood Pb with increasing Pb dose was estimated with r^2 = 0.95 for AALM-LG and 0.98 for AALM-OF. One possible explanation for the higher plateaus in the dose-blood Pb relationship estimated from both models is that the models may estimate higher saturation levels of Pb in RBCs than actually occurred in the infants in the Sherlock and Quinn (1986) study. Parameter values for RBC uptake are based on data collected on adults, and have not been optimized for infants due to an absence of good supporting data (see Section 4.7.2).

4.8. CONCLUSIONS AND IMPLICATIONS OF PERFORMANCE OF OPTIMIZED MODELS

The initial configuration of the AALM biokinetics model was an acslX implementation of the Leggett (1993) and O'Flaherty (1995, 1993) models. The AALM.CSL (v. 4.2, July 2015) introduced several changes to both models, including new parameters (see Table 4-18), and has optimized parameter values against the same data sets. Some of the data used in the optimization were not available at the time the original models were developed. Optimization against a common set of data resulted in convergence of model estimations for blood, bone, and soft tissue (see Figures 4-23 and 4-24). The optimized AALM-LG and AALM-OF estimate similar blood, bone, and soft tissue Pb concentration (see Table 4-19). Evaluation of model estimations of blood Pb relationships at known ingestion doses of Pb was limited to data in a few adult subjects (Rabinowitz et al., 1976), and only two studies in infants (where Pb ingestion doses were estimated from dietary [formula] Pb measurements) (Sherlock and Quinn, 1986; Ryu et al., 1983). No data were available on blood Pb concentrations in children or adolescents, for whom Pb ingestion doses were known with certainty. Several studies have reconstructed Pb intakes in children from exposure models supported by measurements of environmental exposure concentrations (Dixon et al., 2009; TerraGraphics, 2004; Malcoe et al., 2002; Hogan et al., 1998; Lanphear et al., 1998; Lanphear and Roghmann, 1997; Bornschein et al., 1985). However, these studies were not considered for evaluation of the AALM biokinetics models since they would introduce exposure uncertainty into the evaluation.

Although limited in scope, these evaluations provide several insights into model performance. In general, the AALM, in both AALM-LG and AALM-OF configurations, estimated-observed blood Pb dynamics in infants and adults, in response to changing Pb dosing (see Figures 4-20 thru 4-22). In infants, observed blood Pb concentrations were on average within ±2 SE of the observed mean (mean residual range -2, 2). AALM-LG and AALM-OF estimate similar quasi-steady state blood Pb concentrations in infants (Figures 4-21 and 4-22). Both models estimate a higher plateau for the dose-blood Pb relationship than was observed in infants, however, this difference would be of quantitative significance only at intakes resulting in blood Pb concentrations >30 µg/dL.

AALM-OF estimates slower than observed blood Pb kinetics in adults compared to AALM-LG. This resulted in larger differences between estimated and observed blood Pb concentrations in controlled, short-term, exposure studies. More rapid blood Pb kinetics estimated by AALM-LG provided a closer agreement to observations (see Figure 4-20). Although short-term exposure studies revealed important differences in blood Pb kinetics estimated by AALM-LG and AALM-OF, both models estimate well the long-term elimination rates of Pb from bone following decades of exposure, and its effect on long-term elimination of Pb from blood, that have been observed in worker populations following cessation of exposure (see Figure 4-19).

Optimization exercises also revealed differences in model structure that are relevant to model applications. Attempts to optimize AALM soft tissue/bone lead ratios solely by adjusting tissue/plasma partition coefficients were unsuccessful. Improved performance was achieved by introducing age-dependence and larger values for partition coefficients. O'Flaherty (1995, 1993) assigned values of 50 to the kidney/plasma and liver/plasma partition coefficients. The optimized values are substantially higher; approximately 1350 for plasma/kidney, and 1600 for plasma/liver, in infants that progressively decrease with age to adult values of approximately 700 and 800 respectively. It is possible, and likely, that these large adjustments were necessary because the assumption of flow-limited transfer of Pb into and out of soft tissue Pb does not accurately reflect the complexities of age-dependent transport and retention of Pb in soft tissues. In support of this hypothesis, optimization of the bidirectional transfer coefficients that govern uptake and retention of Pb in kidney and liver successfully estimated observations made in infants, children and adults (see Figure 4-17).

AALM-LG and AALM-OF were also successfully optimized to estimate observed relationships between plasma and whole blood Pb concentrations in adults even though the two models use very different mathematical approaches to simulating uptake and retention of Pb in RBCs. AALM-OF simulates binding of Pb with RBCs as a saturable instantaneous equilibrium. AALM-LG simulates bidirectional transfer between plasma and RBCs, with saturable transfer into RBCs. Transfer out of RBCs in AALM-LG is age-dependent and faster in children than in adults. The validity of the age-dependence was not rigorously explored in this analysis. What little data there are on plasma-RBC relationships in children does not suggest an appreciable difference in the relationship for children and adults (Bergdahl et al., 1999). Since the age-dependence assumption could not be rigorously evaluated it is retained in AALM-LG.

The most substantial differences in the structures of AALM-LG and AALM-OF are in the simulation of bone Pb kinetics. In AALM-LG, bone Pb kinetics are represented as age-dependent rate coefficients for transfer of Pb into and out of bone. In AALM-OF, bone Pb kinetics are simulated as outcomes of a physiological model of bone formation and resorption. The physiological approach to bone metabolism implemented in AALM-OF allows the model to be used to explore relationships between bone metabolism and Pb kinetics. This is potentially useful for simulating Pb kinetics in various bone metabolism contexts associated with life stages [e.g., pregnancy and menopause, O'Flaherty (2000); diseases (e.g., bone wasting diseases); and environments (e.g., weightlessness)].

The AALM possesses several attributes (discussed in the following bullets) that make it attractive in human health risk assessment when estimating Pb internal dosimetry following real or hypothetical environmental exposures.

- Currently, human health risk assessment of Pb is conducted using two separate regulatory models, the IEUBK model for Lead in Children and Adult Lead Methodology. The IEUBK model has a terminal age of 7 years. The Adult Lead Methodology is limited to adults. The AALM provides a single physiological/compartmental model capable of estimating blood Pb concentrations at all ages from birth through adulthood. The AALM would replace or supplement the results of the two separate models, and would provide additional assessment capability for older children and adolescent subpopulations.
- The current regulatory model, the Adult Lead Methodology is a slope factor model in which biokinetics are represented as a single variable relating the linear slope of the change in blood Pb concentration per unit change of absorbed Pb (µg/day). The AALM offers a more mechanistic

approach to simulating Pb kinetics that can incorporate information on age, growth, life stage, and other physiological variables that may affect Pb kinetics.

- The AALM can simulate exposures in time steps as small as a single day. This allows estimations of blood Pb concentrations associated with acute or highly intermittent exposures. The IEUBK model and Adult Lead Methodology simulate quasi-steady state blood Pb concentration associated with exposures that have durations of >3 months. Shorter-term dynamics of blood Pb concentrations expected to occur with exposures that vary over days or weeks cannot be simulated with the IEUBK model or the ALM.
- The AALM can estimate concentrations of Pb in bone. This offers the potential for using estimates of bone Pb as an internal dosimeter in assessing health risk from exposure to environmental Pb. Bone Pb may be more suitable than blood Pb when estimating risk for certain effects of Pb such as hypertension (U.S. EPA, 2013).
- The RT model in the AALM provides a more realistic simulation of inhaled aerosols of Pb that incorporates information on air Pb concentrations, air Pb particle size, solubility, receptor activity levels (which determine inhalation volumes), and age. This capability of the AALM is a major improvement over the RT representation in the IEUBK model, which consists only of parameters for inhalation volumes, and a single parameter for the absorption fraction of inhaled Pb (from the lung and GI tract). The Adult Lead Methodology does not represent the RT.

4.9. CALIBRATING THE AALM TO THE IEUBK MODEL

Figure 4-25 compares estimations of the AALM.CSL and the IEUBK model version 1.1 for a continuous dust Pb intake of 10 µg/day.[8] In both models, the relative bioavailability (RBA) for Pb in dust was assumed to be 60%. This corresponds to an absolute bioavailability of approximately 20% at age 2 years in the AALM and 30% in the IEUBK model. At age 2-3 years the IEUBK model estimates a blood Pb concentration of 1.1 µg/dL; AALM-LG and AALM-OF estimate 2.1 and 2.8 µg/dL, respectively. The approximately 2-fold higher predicted blood Pb concentrations by AALM-LG relative to the IEUBK model was largely expected based on Table 3 of Pounds and Leggett (1998).

Table 4-20 compares estimations of adult blood Pb concentrations from the Adult Lead Methodology and AALM.CSL, for an exposure to 1000 ppm. In both models, the RBA for Pb in dust was assumed to be 60%. This corresponds to an absolute bioavailability of approximately 4.8% in the AALM and 12% in the Adult Lead Methodology. The Adult Lead Methodology estimates a blood Pb concentration of 2.9 µg/dL; AALM-LG and AALM-OF estimate 3.1 and 4.6 µg/dL at age 30 years (mid-point for age range in the Adult Lead Methodology, 17-45 years), respectively.

The optimized AALM discussed in Section 4.7 estimates blood Pb concentrations in children that are approximately 2-fold higher than the currently established regulatory IEUBK model based on the same Pb intakes (Figure 4-25). Data available for optimizing and evaluating performance of the Pb biokinetics

[8] As of May 2021, the IEUBK v2.0 is the most current version. New comparisons between the AALM and IEUBK v2.0 were are not provided here since the biokinetic parameters in the IEUBK model were not changed between v1.1 and v2.0. Although default exposure and intake parameters were changed between IEUBK v1.1 and v2.0, this does not affect the relative fold-differences between AALM and IEUBK predicted blood Pb concentrations when the media exposure and intake parameters are matched.

models are largely limited to data for Pb kinetics in adults. Only two studies have reported data on intake-blood Pb relationships in infants (Sherlock and Quinn, 1986; Ryu et al., 1983), and no data of this type are available for children in the age range 1-7 years, the age range simulated in the IEUBK model. Given the large uncertainties in the available data on intake-blood Pb relationships in children, the model differences in absolute terms are relatively small in the context of model capabilities (e.g., approximately 1–2 µg/dL in children for a dust Pb ingestion rate of 10 µg/day). These small differences in model estimates, however, could have implications to consider in making risk management decisions at contaminated sites, which are typically based on a "not-to-exceed" blood Pb concentration (U.S. EPA, 1994a).

The IEUBK model has a long, established history of use in risk assessment and support for soil clean-up goals at hazardous waste sites. Thus, it was deemed worthwhile to further evaluate the most sensitive AALM parameter values to determine which parameters values could be calibrated against the IEUBK model output for child blood Pb concentrations relative to Pb intake without altering the AALM model performance in simulating the infant and adult data.

This additional evaluation identified value changes for a single biokinetic parameter, *RRBC*, that were sufficient to align the AALM-LG results more closely with the IEUBK model results. The RRBC parameter controls the rate of return of Pb from RBCs to plasma. Support for adjusting this parameter is based on the following three arguments: (1) sensitivity analyses of the AALM-LG revealed that blood Pb estimations were highly sensitive to parameters controlling plasma-RBC Pb exchange rates (Section 4.5, Table 4-4), (2) the parameter *RRBC* value is derived from an age-dependent array that allows adjustment of the parameter value for children without altering values for infants or adults, precluding degradation of model performance in estimating Pb kinetics for infant and adult subpopulations; and (3) the RRBC parameter value for children remains uncertain and has no data support, however the upward adjustment needed for this parameter (i.e., faster outflow from RBCs) is consistent with assumptions that were made in the early development of the Leggett model, namely that removal half-times of Pb from RBCs are expected to be shorter in young children than in adults (Leggett, 1993). The *RRBC* parameter was adjusted upward until close agreement was achieved between blood Pb estimated by AALM-LG and the IEUBK model for a constant ingestion intake of 10 µg/day Pb in surface dust, and an RBA relative to soluble Pb = 0.60 (compare Figure 4-25 with 4-26).

Using the same rationale, red cell parameters in AALM-OF were adjusted to align the AALM-OF blood Pb estimations in children more closely with the IEUBK model results. Unlike the AALM-LG, which represents Pb exchanges between plasma and RBC with first-order rate coefficients, the AALM-OF represents binding of Pb in RBCs as an instantaneous binding equilibrium with plasma Pb controlled by two parameters, a half-saturation parameter (*KBIND*) and maximum binding capacity (*BIND*), both of which are constants and independent of age. Although, either of the two parameters could be adjusted, the half-saturation parameter (*KBIND*) was selected in order to keep the binding capacity unchanged, which is similar to the strategy used in resolving differences with AALM-LG.

As illustrated in Figure 4-26, adjustments to the RBC parameters in the AALM-LG and AALM-OF resulted in close agreement with child blood Pb profiles in children estimated by the IEUBK model. At age 2-3 years the IEUBK model estimates a blood Pb concentration of 1.1 µg/dL; AALM-LG and AALM-OF estimate 1.3 and 1.5 µg/dL, respectively, for a dust Pb intake of 10 µg/dL. Because the parameter adjustments were age-dependent and were restricted to children, the adjustments had no effect

on estimations of Pb kinetics in adults, and the revised AALM models performed similarly to the optimized version in estimating observed Pb kinetics in adults. Similarly, the adjustments made to the AALM RBC parameter values for the children subpopulation had minimal effect on the model estimations of blood Pb levels or kinetics in infants (see Figures 4-27 and 4-28). Blood and tissue Pb concentrations estimated by the revised AALM are presented in Table 4-21.

4.10. DATA NEEDS AND FURTHER EVALUATION OF THE AALM

The improvements in the AALM discussed in this report demonstrate the considerable advancements made in the AALM model capability and exposure interface, as well as the optimized parameters that control important model estimations (e.g., plasma/RBC ratios, soft tissue/bone ratios, plasma-to-urine clearance), and that have been optimized against the available data in infants and adults.

Of particular interest to risk assessment applications are estimations of blood and bone Pb, as these two biomarkers have been used extensively to establish dose-response relationships for health effects of Pb in humans (U.S. EPA, 2013). The two models estimate long-term accrual of Pb in blood and bone Pb levels in adults (ages >16 years), that differ by less than 20%. This agreement is remarkable, given the very different approaches used to simulate bone Pb, which is the major depot for Pb in the body. This magnitude of difference is less than observed inter-individual variability in blood and bone Pb measurements in humans (CDC, 2013; U.S. EPA, 2013; Hu et al., 2007). The two models also estimate similar blood Pb concentrations in children. At an earlier age of 2 years, however, blood Pb concentrations estimated from AALM-LG are approximately 25% lower than estimations from AALM-OF, however, data are limited, and additional data are likely to result in improvements in model performance.

Blood Pb concentrations in adults estimated from the AALM are very similar to estimations from the Adult Lead Methodology for the same soil Pb concentrations. Estimations for infants are similar between the AALM and the IEUBK. With the adjusted RBC parameter value, the AALM and IEUBK model estimate similar blood Pb concentrations in children for the same dust Pb intakes and RBA assumptions. Subject to further external peer review and verification of the AALM results, the agreement between the AALM, the IEUBK model, and the ALM supports the potential future use of the AALM in risk assessment applications to supplement or replace the IEUBK model and the ALM in supporting regulatory decisions. At present, however, the IEUBK model and the ALM remain the established methods that will be used for regulatory decisions.

Recommendations for data to reduce uncertainty in the AALM model results, and improve the consistency among all model estimations include the following:

- *Resolve differences between the AALM-LG and AALM-OF estimations of blood Pb kinetics.* AALM-OF estimates slower accrual and elimination of Pb from blood compared to AALM-LG, while AALM-LG more close reproduced blood Pb kinetics observed in the short-term Pb dosing studies of Rabinowitz et al. (1976). Additional data on blood Pb kinetics may serve to improve the optimization of both models, and resolve these differences. This will be important for application of either model to simulating blood Pb dynamics associated with short-term or highly variable exposures.

- *Evaluate and optimize AALM-OF bone metabolism parameters.* A literature search and review of newer data on rates of bone production and resorption may provide a basis for re-optimization of AALM-OF or its extension to include simulations of specific bone metabolism scenarios of interest to toxicology or risk assessment (e.g., pregnancy, osteomalacia [soft bone disease]).
- *Further verify AALM-LG and AALM-OF estimations.* Additional observations in humans should be identified that can serve to evaluate the performance of the optimized AALM (and that were not used in the optimization). Ideally, these would be blood and/or bone Pb measurements in people for whom Pb intakes are known with reasonable certainty. Ethical concerns typically preclude Pb dosing experiments; therefore, Pb doses must be estimated with accurate tools such as duplicate diet surveys or dietary recalls and information on Pb levels in diet and other relevant exposure media. Types of data that would be valuable for model validation include: (1) blood soft tissue or bone Pb levels in children or adults for whom Pb dosage is known or can be reliable estimated from exposure data; (2) changes in blood, soft tissue or bone Pb levels in children or adults following and abrupt change (increase or decrease) in Pb exposure; (3) steady state (or quasi-steady state) blood/soft tissue blood/bone Pb ratios in children or adults; (4) urinary Pb clearance from blood or plasma in children or adults; and (5) plasma/whole blood concentration ratios in children.
- *Evaluate and document the empirical basis for exposure model parameters.* Most of the exposure parameter values in the AALM.CSL serve as placeholders and should, in the future, be replaced with default values for specific receptor populations for which an empirical basis can be provided.
- *Further refine the RT model*. The AALM.CSL includes values for inhalation rates and deposition fractions for the general public, as defined by ICRP (1994). These values do not adequately represent many receptor populations of interest who have activity levels that differ from general population assumptions (e.g., workers). Additional parameter value matrices should be developed to represent selected receptor populations of interest.

Finally, the AALM has been developed with a relatively easy to use and versatile exposure interface, access to model parameters and values, and transparency of model code to support stakeholder use and evaluation internally and external to the Agency.

TABLE 4-1. SUMMARY OF MAJOR DIFFERENCES BETWEEN STRUCTURES OF AALM-LG AND AALM-OF

Model Component	AALM-LG	AALM-OF
GI tract	Four compartments representing stomach, small intestine, upper and lower large intestine	No GI tract compartment
Absorption from GI tract	First-order transfer from small intestine to blood	First-order transfer of ingested Pb to liver (portal blood)
Plasma	Two compartments representing diffusible (transferable to other tissues) and bound	One compartment in equilibrium with bound Pb in RBC
RBC	Binding represented with first-order rate transfer rates adjusted for saturating concentration	Binding represented with non-linear binding function (i.e., maximum and half-saturating concentration)
Kidney	Two compartments, first-order transfer rates	One compartment with flow-limited transfer
Liver	Two compartments, first-order transfer rates	One compartment with flow-limited transfer
Other soft tissue	Three compartments, first-order transfer rates	None
Poorly perfused tissue	None	One compartment with flow-limited transfer
Well-perfused tissue	None	One compartment with flow-limit transfer
Brain	One compartment, first-order transfer rates	None
Bone	Six compartments representing surface, exchangeable and non-exchangeable cortical and trabecular bone. Pb transfers governed by age-dependent first-order transfer rates	Transfer to and from metabolically active trabecular and cortical bone governed by age-dependent bone formation and resorption rates, respectively; transfer to and from mature cortical bone governed by radial diffusion
Sweat	First-order transfer from plasma to sweat	None
Miscellaneous excretory routes (e.g., hair)	First-order transfer from other soft tissues to other excretory routes	None

TABLE 4-2. AALM-LG INPUT PARAMETERS CONTROLLING POST-ABSORPTION PB KINETICS

No.	Transfer Pathway	Controlling Parameter(s)	Rate at Specified Age (day^{-1})					
			0-100 days	1 year	5 years	10 years	15 years	≥25 years
1	Plasma-D to EVF	TEVF	1000	1000	1000	1000	1000	1000
2	Plasma-D to RBCs	TORBC	310	424	443	382	313	500
3	Plasma-D to Plasma-B	TOPROT	0.495	0.678	0.709	0.611	0.501	0.800
4	Plasma-D to Urinary bladder	TOURIN	0	0	0	0	0	0
5	Plasma-D to Small intestine	TOFECE	7.439	10.2	10.6	9.17	7.51	12.0
6	Plasma-D to Trab surf	TOBONE (TFRAC)	96.04	57.6	56.8	89.5	132	89.0
7	Plasma-D to Cort surf	TBONE (1-TFRAC)	384	230	199	268	341	71.0
8	Plasma-D to Liver 1	TOLVR1	49.5	67.8	70.9	61.1	50.1	80.0
9	Plasma-D to Urinary path	TOKDN1	31.0	42.4	44.3	38.2	31.3	50.0
10	Plasma-D to Other kidney	TOKDN2	0.495	0.678	0.709	0.611	0.501	0.800
11	Plasma-D to ST0	TOSOF0	103	141	148	128	105	177
12	Plasma-D to ST1	TOSOF1	12.4	17.0	17.7	15.3	12.5	10.0
13	Plasma-D to ST2	TOSOF2	1.24	1.70	1.77	1.53	1.25	2.00
14	Plasma-D to Brain	TOBRAN	0.557	0.763	0.266	0.229	0.188	0.300
15	Plasma-D to Sweat	TOWET	4.33	5.93	6.20	5.35	4.38	7.00
16	RBCs to Plasma-D	RRBC	0.462	0.785	0.499	0.195	0.1390	0.1390
17	EVF to Plasma-D	RPLAS	334	333	333	333	333	333
18	Plasma-B to Plasma-D	RPROT	0.139	0.139	0.139	0.139	0.139	0.139
19	Cort surf to Plasma-D	RCS2DF	0.35	0.35	0.35	0.35	0.35	0.50
20	Trab surf to Plasma-D	RTS2DF	0.35	0.35	0.35	0.35	0.35	0.50

No.	Transfer Pathway	Controlling Parameter(s)	Rate at Specified Age (day^{-1})					
			0-100 days	1 year	5 years	10 years	15 years	≥25 years
21	Cort surf to Exch vol	RCS2B	0.65	0.65	0.65	0.65	0.65	0.50
22	Trab surf to Exch vol	RTS2B	0.65	0.65	0.65	0.65	0.65	0.50
23	Cort exch vol to Surl	RDIFF*(1-FLONG)	0.00924	0.00924	0.00924	0.00924	0.00924	0.00924
24	Trab exch vol to Surf	RDIFF*(1-FLONG)	0.00924	0.00924	0.00924	0.00924	0.00924	0.00924
25	Cort exch vol to Nonexch vol	RDIFF*FLONG	0.0139	0.0139	0.0139	0.0139	0.0139	0.0139
26	Trab exch vol to Nonexcn vol	RDIFF*FLONG	0.0139	0.0139	0.0139	0.0139	0.0139	0.0139
27	Cort nonexch vol to Plasma-D	RCORT	0.0161 [a]	0.00576	0.00308	0.00178	0.00102	0.00016
28	Trab nonexch vol to Plasma-D	RCORT	0.0161 [a]	0.00576	0.00362	0.00264	0.00191	0.00099
29	Liver 1 to Plasma-D	RLVR1	0.0312	0.0312	0.0312	0.0312	0.0312	0.0312
30	Liver 1 to Small intestine	H1TOSI	0.0312	0.0312	0.0312	0.0312	0.0312	0.0312
31	Liver 1 to Liver 2	H1TOH2	0.00693	0.00693	0.00693	0.00693	0.00693	0.00693
32	Liver 2 to Plasma-D	RLVR2	0.000693	0.000693	0.001386	0.000570	0.000570	0.000570
33	Urinary path to Urinary bladder	RBLAD	0.139	0.139	0.139	0.139	0.139	0.139
34	Other kidney to Plasma-D	RKDN2	0.000693	0.000693	0.000693	0.000190	0.000190	0.000190
35	ST0 to Plasma-D	RSOF0	2.08	2.08	2.08	2.08	2.08	2.08
36	ST1 to Plasma-D	RSOF1	0.00416	0.00416	0.00416	0.00416	0.00416	0.00416
37	ST1 to Excreta	S2HAIR	0.00277	0.00277	0.00277	0.00277	0.00277	0.00277
38	ST2 to Plasma-D	RSOF2	0.00038	0.00038	0.00038	0.00038	0.00038	0.00038
39	Brain to Plasma-D	RBRAN	0.00095	0.00095	0.00095	0.00095	0.00095	0.00095

[a] 0.0204 d^{-1} at birth.

TABLE 4-3. AALM-OF INPUT PARAMETERS CONTROLLING POST-ABSORPTION PB KINETICS

No.	Parameter	Unit	Value	Parameter Description
1	A1	–	4.0	Constant 1 for bone formation rate algorithm
2	A2	–	0.4	Constant 2 for bone formation rate algorithm
3	A3	–	4.0	Constant 3 for bone formation rate algorithm
4	A5	–	0.6	Constant 5 for bone formation rate algorithm
5	AGE0	year	0	Age at which simulation begins
6	BASE	–	0.1	Base bone formation rate in bone growth algorithm
7	BIND	mg/L	2.7	Maximum capacity of sites in red cells to bind Pb
8	C1	–	1.0	Constant 1 for urinary clearance of Pb as a fraction of GFR
9	C2	–	0.9	Constant 2 for urinary clearance of Pb as a fraction of GFR
10	C3	–	50	Constant 3 for urinary clearance of Pb as a fraction of GFR
11	CON	f	0.65	Fraction of bone blood flow to trabecular bone
12	D0	cm^3/day	0.0000005	Diffusion constant
13	EXPO	–	0.6	Exponent constant for bone volume participating in adult-type bone remodeling
14	G	NA	1.2	Linear parameter for unbound lead in red cells
15	KBIND	mg/L	0.0075	Half-saturation concentration of Pb for binding by sites in red cells
16	P0	cm^3/day	0.02	Permeability constant for diffusion from canaliculi to bone
17	PK	f	50	Kidney/plasma partition coefficient
18	PL	f	50	Liver/plasma partition coefficient
19	PP	f	2.0	Poorly perfused/plasma partition coefficient
20	PW	f	50	Well-perfused/plasma partition coefficient
21	QBONEC	f	0.05	Fraction cardiac output going to bone
22	QCC	L/day/kg	340	Cardiac output in the adult
23	QKC	f	0.17	Fraction cardiac output going to kidney
24	QLC	f	0.25	Fraction cardiac output going to liver
25	QWC	f	0.44	Fraction cardiac output going to other well-perfused tissues
26	R0	cm^3/day	0.0000005	Permeability constant for diffusion from bone to canaliculi
27	RAD1	cm	0.000027	Radius of shell 1 of bone in the canalicular diffusion region of deeper bone
28	RAD2	cm	0.000052	Radius of shell 2 of bone in the canalicular diffusion region of deeper bone

No.	Parameter	Unit	Value	Parameter Description
29	RAD3	cm	0.000079	Radius of shell 3 of bone in the canalicular diffusion region of deeper bone
30	RAD4	cm	0.000106	Radius of shell 4 of bone in the canalicular diffusion region of deeper bone
31	RAD5	cm	0.000133	Radius of shell 5 of bone in the canalicular diffusion region of deeper bone
32	RAD6	cm	0.000160	Radius of shell 6 of bone in the canalicular diffusion region of deeper bone
33	RAD7	cm	0.000187	Radius of shell 7 of bone in the canalicular diffusion region of deeper bone
34	RAD8	cm	0.000214	Radius of shell 8 of bone in the canalicular diffusion region of deeper bone
35	S	cm^2/cm	0.000126	Surface area of canaliculi

TABLE 4-4. AALM-LG STANDARDIZED SENSITIVITY COEFFICIENTS FOR BLOOD PB IN CHILDREN (5 YEARS) AND ADULTS (30 YEARS)

Variable	Parameter	Child	Adult	Parameter Description
ABLOOD	TEVF	9.16E+00	8.38E+00	Deposition fraction from diffusible plasma to extravascular fluid
ABLOOD	TORBC	5.30E+00	4.93E+00	Deposition fraction from diffusible plasma to RBCs, below non-linear threshold
ABLOOD	TOSOF0	1.50E+00	1.44E+00	Age-scaled deposition fraction from diffusible plasma to soft tissue compartment 0
ABLOOD	TBONEL	1.42E+00	1.30E+00	Terminal value of age-scaled deposition fraction from diffusible plasma to surface bone
ABLOOD	RRBC	1.00E+00	9.98E-01	Age-scaled transfer rate from RBC to diffusible plasma
ABLOOD	TOLVR1	4.90E-01	3.85E-01	Deposition fraction from diffusible plasma to liver compartment 2
ABLOOD	H1TOBL	3.25E-01	2.94E-01	Fraction of transfer out of liver compartment 1 to diffusible plasma
ABLOOD	TBONE	1.05E-01	7.16E-02	Age-scaled deposition fraction from diffusible plasma to surface bone
ABLOOD	TFRAC	8.33E-03	7.10E-02	Bone deposition-scaled fraction of diffusible plasma-to-bone deposition that goes to trabecular surface bone; 1-TFRAC is the fraction that goes to cortical surface bone
ABLOOD	H1TOH2	7.70E-02	6.58E-02	Fraction of transfer out of liver compartment 1 to liver compartment 2
ABLOOD	TOSOF1	1.16E-01	5.52E-02	Age-scaled deposition fraction from diffusible plasma to soft tissue compartment 1
ABLOOD	S2HAIR	7.63E-02	3.63E-02	Deposition fraction from soft tissue compartment 1 to other excreta
ABLOOD	H1TOSI	8.91E-02	2.49E-02	Fraction of transfer out of liver compartment 1 to the small intestine
ABLOOD	TOSOF2	9.31E-03	1.76E-02	Age-scaled deposition fraction from diffusible plasma to soft tissue compartment 2
ABLOOD	RCORT	9.00E-02	1.27E-02	Age-scaled transfer rate from non-exchangeable cortical bone to diffusible plasma
ABLOOD	RTS2B	8.11E-03	1.17E-02	Age-scaled transfer rate from surface trabecular bone to exchangeable trabecular bone
ABLOOD	RTS2DF	7.59E-03	1.17E-02	Age-scaled transfer rate from trabecular bone surface to diffusible plasma
ABLOOD	RTRAB	2.12E-02	1.06E-02	Age-scaled transfer rate from non-exchangeable trabecular bone to diffusible plasma
ABLOOD	RDIFF	6.04E-02	1.04E-02	Age-scaled transfer rate from the exchangeable bone, including transfer to surface and non-exchangeable bone

Variable	Parameter	Child	Adult	Parameter Description
ABLOOD	TOFECE	3.23E-02	9.00E-03	Deposition fraction from diffusible plasma directly to the small intestine (not including the transfer from biliary secretion, specified by RLVR1)
ABLOOD	TOPROT	1.06E-02	8.24E-03	Deposition fraction from diffusible plasma to protein-bound plasma
ABLOOD	TOKDN2	3.81E-03	3.28E-03	Deposition fraction from diffusible plasma to kidney compartment 2
ABLOOD	TOBRAN	5.10E-03	2.62E-03	Age-scaled deposition fraction from diffusible plasma to brain
ABLOOD	RSOF2	8.49E-03	2.40E-03	Transfer rate from soft tissue compartment 2 to diffusible plasma
ABLOOD	RPROT	3.38E-03	1.66E-03	Transfer rate from bound plasma to diffusible plasma
ABLOOD	RCS2DF	2.21E-02	1.57E-03	Age-scaled transfer rate from cortical bone surface to diffusible plasma
ABLOOD	RCS2B	2.42E-02	1.34E-03	Age-scaled transfer rate from cortical bone surface to exchangeable cortical bone
ABLOOD	FLONG	4.12E-02	1.25E-03	Age-scaled fraction of total transfer from the exchangeable bone directed to non-exchangeable bone
ABLOOD	RSOF1	5.63E-03	4.37E-04	Transfer rate from soft tissue compartment 1 to diffusible plasma
ABLOOD	RPLAS	6.95E-04	2.94E-04	Total transfer rate from diffusible plasma to all compartments
ABLOOD	RLVR2	3.70E-03	2.20E-04	Age-scaled transfer rate from the slow liver compartment 2 to diffusible plasma
ABLOOD	RBRAN	1.66E-03	1.76E-04	Age-scaled transfer rate from brain to diffusible plasma
ABLOOD	RLVR1	3.03E-03	1.00E-04	Transfer rate out of the liver compartment 1, including to small intestine and diffusible plasma
ABLOOD	RSOF0	3.74E-04	1.09E-05	Transfer rate from soft tissue compartment 0 to diffusible plasma
ABLOOD	RKDN2	1.93E-04	1.09E-05	Age-scaled transfer rate from kidney compartment 2 to diffusible plasma
ABLOOD	TOKDN1	1.18E-05	5.81E-06	Deposition fraction from diffusible plasma to kidney compartment 1
ABLOOD	TOURIN	8.88E-06	4.35E-06	Deposition fraction from diffusible plasma to urine
ABLOOD	RSTMC	1.42E-05	3.62E-06	Transfer rate from stomach to small intestine
ABLOOD	SIZEVF	6.52E-06	3.27E-06	Relative volume of the EVF compartment compared to plasma (EVF/Plasma)
ABLOOD	GSCAL	2.30E-05	2.63E-06	Age-scaling factor for GIT transfer
ABLOOD	RULI	4.98E-05	1.07E-06	Transfer rate from upper large intestine to lower large intestine

Variable	Parameter	Child	Adult	Parameter Description
ABLOOD	TOSWET	2.18E-06	1.06E-06	Deposition fraction from diffusible plasma to sweat
ABLOOD	RSIC	5.92E-05	7.18E-07	Transfer rate from small intestine to upper large intestine
ABLOOD	RLLI	5.28E-06	1.16E-07	Transfer rate from lower large intestine to feces
ABLOOD	RKDN1	5.83E-10	1.31E-08	Transfer rate from kidney compartment 1 to urinary pathway
ABLOOD	POWER	0.00E+00	0.00E+00	Exponent for RBC deposition
ABLOOD	RBCNL	0.00E+00	0.00E+00	Threshold concentration in RBC for non-linear deposition from diffusible plasma to RBC
ABLOOD	SATRAT	0.00E+00	0.00E+00	Maximum (saturating) concentration of lead in RBC
ABLOOD	RBLAD	0.00E+00	0.00E+00	Age-scaled transfer rate from urinary bladder to urine

TABLE 4-5. AALM-LG STANDARDIZED SENSITIVITY COEFFICIENTS FOR BONE PB IN CHILDREN (5 YEARS) AND ADULTS (30 YEARS)

Variable	Parameter	Child	Adult	Parameter Description
ABONE	TEVF	8.11E+00	8.12E+00	Deposition fraction from diffusible plasma to extravascular fluid
ABONE	TORBC	3.75E+00	3.71E+00	Deposition fraction from diffusible plasma to RBCs, below non-linear threshold
ABONE	TBONE	1.27E+00	1.42E+00	Age-scaled deposition fraction from diffusible plasma to surface bone
ABONE	TOSOF0	1.31E+00	1.32E+00	Age-scaled deposition fraction from diffusible plasma to soft tissue compartment 0
ABONE	TBONEL	1.07E+00	1.05E+00	Terminal value of age-scaled deposition fraction from diffusible plasma to surface bone
ABONE	FLONG	3.93E-01	6.80E-01	Age-scaled fraction of total transfer from the exchangeable bone directed to non-exchangeable bone
ABONE	RCS2DF	5.33E-01	6.02E-01	Age-scaled transfer rate from cortical bone surface to diffusible plasma
ABONE	TOLVR1	4.44E-01	3.70E-01	Deposition fraction from diffusible plasma to liver compartment 2
ABONE	H1TOBL	2.81E-01	2.78E-01	Fraction of transfer out of liver compartment 1 to diffusible plasma
ABONE	RTS2DF	1.36E-01	1.48E-01	Age-scaled transfer rate from trabecular bone surface to diffusible plasma
ABONE	TOSOF1	9.53E-02	7.79E-02	Age-scaled deposition fraction from diffusible plasma to soft tissue compartment 1
ABONE	H1TOH2	6.29E-02	6.13E-02	Fraction of transfer out of liver compartment 1 to liver compartment 2
ABONE	H1TOSI	9.98E-02	3.06E-02	Fraction of transfer out of liver compartment 1 to the small intestine
ABONE	TOSOF2	5.70E-03	1.94E-02	Age-scaled deposition fraction from diffusible plasma to soft tissue compartment 2
ABONE	TOFECE	3.60E-02	1.11E-02	Deposition fraction from diffusible plasma directly to the small intestine (not including the transfer from biliary secretion, specified by RLVR1)
ABONE	TOPROT	6.28E-03	6.20E-03	Deposition fraction from diffusible plasma to protein-bound plasma
ABONE	TOBRAN	3.68E-03	3.25E-03	Age-scaled deposition fraction from diffusible plasma to brain
ABONE	TOKDN2	3.13E-03	3.05E-03	Deposition fraction from diffusible plasma to kidney compartment 2
ABONE	RLVR2	8.15E-04	6.26E-04	Age-scaled transfer rate from the slow liver compartment 2 to diffusible plasma

Variable	Parameter	Child	Adult	Parameter Description
ABONE	RKDN2	3.09E-05	3.22E-05	Age-scaled transfer rate from kidney compartment 2 to diffusible plasma
ABONE	GSCAL	4.15E-05	1.35E-05	Age-scaling factor for GIT transfer
ABONE	RULI	8.28E-05	6.79E-06	Transfer rate from upper large intestine to lower large intestine
ABONE	RLLI	8.76E-06	7.29E-07	Transfer rate from lower large intestine to feces
ABONE	RKDN1	9.84E-10	8.50E-08	Transfer rate from kidney compartment 1 to urinary pathway
ABONE	POWER	0.00E+00	0.00E+00	Exponent for RBC deposition
ABONE	RBCNL	0.00E+00	0.00E+00	Threshold concentration in RBC for non-linear deposition from diffusible plasma to RBC
ABONE	SATRAT	0.00E+00	0.00E+00	Maximum (saturating) concentration of lead in RBC
ABONE	RBLAD	0.00E+00	0.00E+00	Age-scaled transfer rate from urinary bladder to urine
ABONE	TOSWET	1.38E-08	9.86E-09	Deposition fraction from diffusible plasma to sweat
ABONE	TOURIN	5.72E-08	4.07E-08	Deposition fraction from diffusible plasma to urine
ABONE	TOKDN1	7.63E-08	1.38E-07	Deposition fraction from diffusible plasma to kidney compartment 1
ABONE	RPROT	5.69E-06	3.42E-06	Transfer rate from bound plasma to diffusible plasma
ABONE	RSIC	1.12E-04	8.33E-06	Transfer rate from small intestine to upper large intestine
ABONE	SIZEVF	4.23E-06	2.34E-05	Relative volume of the EVF compartment compared to plasma (EVF/Plasma)
ABONE	RSTMC	1.52E-05	2.48E-05	Transfer rate from stomach to small intestine
ABONE	RPLAS	3.87E-05	3.19E-05	Total transfer rate from diffusible plasma to all compartments
ABONE	RSOF0	7.55E-05	4.18E-05	Transfer rate from soft tissue compartment 0 to diffusible plasma
ABONE	RRBC	1.06E-03	6.84E-05	Age-scaled transfer rate from RBC to diffusible plasma
ABONE	RLVR1	1.51E-04	4.01E-04	Transfer rate out of the liver compartment 1, including to small intestine and diffusible plasma
ABONE	RBRAN	1.82E-03	1.03E-03	Age-scaled transfer rate from brain to diffusible plasma
ABONE	RSOF2	6.31E-03	1.26E-03	Transfer rate from soft tissue compartment 2 to diffusible plasma
ABONE	RSOF1	1.16E-03	2.10E-03	Transfer rate from soft tissue compartment 1 to diffusible plasma
ABONE	S2HAIR	6.27E-02	5.13E-02	Deposition fraction from soft tissue compartment 1 to other excreta

Variable	Parameter	Child	Adult	Parameter Description
ABONE	RDIFF	2.93E-01	8.41E-02	Age-scaled transfer rate from the exchangeable bone, including transfer to surface and non-exchangeable bone
ABONE	RTS2B	1.38E-01	1.48E-01	Age-scaled transfer rate from surface trabecular bone to exchangeable trabecular bone
ABONE	RTRAB	1.17E-01	1.83E-01	Age-scaled transfer rate from non-exchangeable trabecular bone to diffusible plasma
ABONE	TFRAC	1.03E-02	3.00E-01	Bone deposition-scaled fraction of diffusible plasma-to-bone deposition that goes to trabecular surface bone; 1-TFRAC is the fraction that goes to cortical surface bone
ABONE	RCS2B	5.41E-01	6.03E-01	Age-scaled transfer rate from cortical bone surface to exchangeable cortical bone
ABONE	RCORT	4.61E-01	7.07E-01	Age-scaled transfer rate from non-exchangeable cortical bone to diffusible plasma

TABLE 4-6. AALM-LG STANDARDIZED SENSITIVITY COEFFICIENTS FOR LIVER PB IN CHILDREN (5 YEARS) AND ADULTS (30 YEARS)

Variable	Parameter	Child	Adult	Parameter Description
ALIVER	TEVF	8.91E+00	8.41E+00	Deposition fraction from diffusible plasma to extravascular fluid
ALIVER	TORBC	4.19E+00	3.94E+00	Deposition fraction from diffusible plasma to RBCs, below non-linear threshold
ALIVER	TOSOF0	1.46E+00	1.45E+00	Age-scaled deposition fraction from diffusible plasma to soft tissue compartment 0
ALIVER	TOLVR1	1.48E+00	1.39E+00	Deposition fraction from diffusible plasma to liver compartment 2
ALIVER	TBONEL	1.39E+00	1.31E+00	Terminal value of age-scaled deposition fraction from diffusible plasma to surface bone
ALIVER	H1TOH2	6.09E-01	8.54E-01	Fraction of transfer out of liver compartment 1 to liver compartment 2
ALIVER	RLVR2	5.99E-01	7.92E-01	Age-scaled transfer rate from the slow liver compartment 2 to diffusible plasma
ALIVER	H1TOBL	3.16E-01	2.95E-01	Fraction of transfer out of liver compartment 1 to diffusible plasma
ALIVER	RLVR1	4.83E-01	2.14E-01	Transfer rate out of the liver compartment 1, including to small intestine and diffusible plasma
ALIVER	TBONE	6.32E-02	7.96E-02	Age-scaled deposition fraction from diffusible plasma to surface bone
ALIVER	TFRAC	7.36E-03	7.60E-02	Bone deposition-scaled fraction of diffusible plasma-to-bone deposition that goes to trabecular surface bone; 1-TFRAC is the fraction that goes to cortical surface bone
ALIVER	TOSOF1	1.12E-01	5.62E-02	Age-scaled deposition fraction from diffusible plasma to soft tissue compartment 1
ALIVER	S2HAIR	7.35E-02	3.69E-02	Deposition fraction from soft tissue compartment 1 to other excreta
ALIVER	H1TOSI	9.28E-02	2.54E-02	Fraction of transfer out of liver compartment 1 to the small intestine
ALIVER	TOSOF2	8.37E-03	1.77E-02	Age-scaled deposition fraction from diffusible plasma to soft tissue compartment 2
ALIVER	RCORT	9.61E-02	1.41E-02	Age-scaled transfer rate from non-exchangeable cortical bone to diffusible plasma
ALIVER	RTS2B	3.07E-03	1.36E-02	Age-scaled transfer rate from surface trabecular bone to exchangeable trabecular bone
ALIVER	RTS2DF	2.66E-03	1.35E-02	Age-scaled transfer rate from trabecular bone surface to diffusible plasma
ALIVER	RDIFF	4.72E-02	1.26E-02	Age-scaled transfer rate from the exchangeable bone, including transfer to surface and non-exchangeable bone

Variable	Parameter	Child	Adult	Parameter Description
ALIVER	TOFECE	3.34E-02	9.08E-03	Deposition fraction from diffusible plasma directly to the small intestine (not including the transfer from biliary secretion, specified by RLVR1)
ALIVER	RTRAB	2.34E-02	8.01E-03	Age-scaled transfer rate from non-exchangeable trabecular bone to diffusible plasma
ALIVER	TOPROT	7.10E-03	6.65E-03	Deposition fraction from diffusible plasma to protein-bound plasma
ALIVER	TOKDN2	3.67E-03	3.29E-03	Deposition fraction from diffusible plasma to kidney compartment 2
ALIVER	TOBRAN	4.79E-03	2.64E-03	Age-scaled deposition fraction from diffusible plasma to brain
ALIVER	RSOF2	7.94E-03	2.61E-03	Transfer rate from soft tissue compartment 2 to diffusible plasma
ALIVER	RCS2DF	5.38E-03	1.75E-03	Age-scaled transfer rate from cortical bone surface to diffusible plasma
ALIVER	RCS2B	7.19E-03	1.48E-03	Age-scaled transfer rate from cortical bone surface to exchangeable cortical bone
ALIVER	FLONG	4.94E-02	7.59E-04	Age-scaled fraction of total transfer from the exchangeable bone directed to non-exchangeable bone
ALIVER	RSOF1	4.17E-03	5.79E-04	Transfer rate from soft tissue compartment 1 to diffusible plasma
ALIVER	RRBC	2.10E-03	2.48E-04	Age-scaled transfer rate from RBC to diffusible plasma
ALIVER	RBRAN	1.76E-03	1.89E-04	Age-scaled transfer rate from brain to diffusible plasma
ALIVER	RSOF0	3.13E-04	1.22E-05	Transfer rate from soft tissue compartment 0 to diffusible plasma
ALIVER	RPLAS	5.46E-05	5.13E-06	Total transfer rate from diffusible plasma to all compartments
ALIVER	GSCAL	2.56E-05	3.35E-06	Age-scaling factor for GIT transfer
ALIVER	RSTMC	2.51E-05	3.23E-06	Transfer rate from stomach to small intestine
ALIVER	SIZEVF	6.72E-06	2.84E-06	Relative volume of the EVF compartment compared to plasma (EVF/Plasma)
ALIVER	RKDN2	1.45E-04	2.69E-06	Age-scaled transfer rate from kidney compartment 2 to diffusible plasma
ALIVER	RULI	5.24E-05	1.17E-06	Transfer rate from upper large intestine to lower large intestine
ALIVER	RPROT	2.25E-05	9.68E-07	Transfer rate from bound plasma to diffusible plasma
ALIVER	RSIC	5.27E-05	2.33E-07	Transfer rate from small intestine to upper large intestine
ALIVER	RLLI	5.56E-06	1.27E-07	Transfer rate from lower large intestine to feces

Variable	Parameter	Child	Adult	Parameter Description
ALIVER	TOKDN1	3.12E-07	3.12E-08	Deposition fraction from diffusible plasma to kidney compartment 1
ALIVER	RKDN1	6.21E-10	1.44E-08	Transfer rate from kidney compartment 1 to urinary pathway
ALIVER	TOURIN	2.34E-07	1.28E-08	Deposition fraction from diffusible plasma to urine
ALIVER	TOSWET	5.69E-08	3.10E-09	Deposition fraction from diffusible plasma to sweat
ALIVER	POWER	0.00E+00	0.00E+00	Exponent for RBC deposition
ALIVER	RBCNL	0.00E+00	0.00E+00	Threshold concentration in RBC for non-linear deposition from diffusible plasma to RBC
ALIVER	SATRAT	0.00E+00	0.00E+00	Maximum (saturating) concentration of lead in RBC
ALIVER	RBLAD	0.00E+00	0.00E+00	Age-scaled transfer rate from urinary bladder to urine

TABLE 4-7. AALM-LG STANDARDIZED SENSITIVITY COEFFICIENTS FOR KIDNEY PB IN CHILDREN (5 YEARS) AND ADULTS (30 YEARS)

Variable	Parameter	Child	Adult	Parameter Description
AKIDNEY	TEVF	9.08E+00	8.40E+00	Deposition fraction from diffusible plasma to extravascular fluid
AKIDNEY	TORBC	4.27E+00	3.94E+00	Deposition fraction from diffusible plasma to RBCs, below non-linear threshold
AKIDNEY	TOSOF0	1.48E+00	1.44E+00	Age-scaled deposition fraction from diffusible plasma to soft tissue compartment 0
AKIDNEY	TBONEL	1.41E+00	1.31E+00	Terminal value of age-scaled deposition fraction from diffusible plasma to surface bone
AKIDNEY	RKDN1	8.20E-01	5.76E-01	Transfer rate from kidney compartment 1 to urinary pathway
AKIDNEY	TOKDN1	8.15E-01	5.76E-01	Deposition fraction from diffusible plasma to kidney compartment 1
AKIDNEY	TOKDN2	1.91E-01	4.30E-01	Deposition fraction from diffusible plasma to kidney compartment 2
AKIDNEY	RKDN2	2.08E-01	4.27E-01	Age-scaled transfer rate from kidney compartment 2 to diffusible plasma
AKIDNEY	TOLVR1	4.88E-01	3.87E-01	Deposition fraction from diffusible plasma to liver compartment 2
AKIDNEY	H1TOBL	3.22E-01	2.95E-01	Fraction of transfer out of liver compartment 1 to diffusible plasma
AKIDNEY	TBONE	9.11E-02	7.58E-02	Age-scaled deposition fraction from diffusible plasma to surface bone
AKIDNEY	TFRAC	8.00E-03	7.36E-02	Bone deposition-scaled fraction of diffusible plasma-to-bone deposition that goes to trabecular surface bone; 1-TFRAC is the fraction that goes to cortical surface bone
AKIDNEY	H1TOH2	7.60E-02	6.59E-02	Fraction of transfer out of liver compartment 1 to liver compartment 2
AKIDNEY	TOSOF1	1.15E-01	5.57E-02	Age-scaled deposition fraction from diffusible plasma to soft tissue compartment 1
AKIDNEY	S2HAIR	7.53E-02	3.66E-02	Deposition fraction from soft tissue compartment 1 to other excreta
AKIDNEY	H1TOSI	9.02E-02	2.51E-02	Fraction of transfer out of liver compartment 1 to the small intestine
AKIDNEY	TOSOF2	8.99E-03	1.76E-02	Age-scaled deposition fraction from diffusible plasma to soft tissue compartment 2
AKIDNEY	RCORT	9.20E-02	1.34E-02	Age-scaled transfer rate from non-exchangeable cortical bone to diffusible plasma
AKIDNEY	RTS2B	6.42E-03	1.27E-02	Age-scaled transfer rate from surface trabecular bone to exchangeable trabecular bone

Variable	Parameter	Child	Adult	Parameter Description
AKIDNEY	RTS2DF	5.94E-03	1.26E-02	Age-scaled transfer rate from trabecular bone surface to diffusible plasma
AKIDNEY	RDIFF	5.60E-02	1.16E-02	Age-scaled transfer rate from the exchangeable bone, including transfer to surface and non-exchangeable bone
AKIDNEY	RTRAB	2.21E-02	9.30E-03	Age-scaled transfer rate from non-exchangeable trabecular bone to diffusible plasma
AKIDNEY	TOFECE	3.27E-02	9.04E-03	Deposition fraction from diffusible plasma directly to the small intestine (not including the transfer from biliary secretion, specified by RLVR1)
AKIDNEY	TOPROT	7.16E-03	6.58E-03	Deposition fraction from diffusible plasma to protein-bound plasma
AKIDNEY	TOBRAN	4.99E-03	2.63E-03	Age-scaled deposition fraction from diffusible plasma to brain
AKIDNEY	RSOF2	8.31E-03	2.51E-03	Transfer rate from soft tissue compartment 2 to diffusible plasma
AKIDNEY	RCS2DF	1.65E-02	1.67E-03	Age-scaled transfer rate from cortical bone surface to diffusible plasma
AKIDNEY	RCS2B	1.85E-02	1.41E-03	Age-scaled transfer rate from cortical bone surface to exchangeable cortical bone
AKIDNEY	FLONG	4.39E-02	9.93E-04	Age-scaled fraction of total transfer from the exchangeable bone directed to non-exchangeable bone
AKIDNEY	RSOF1	5.14E-03	5.12E-04	Transfer rate from soft tissue compartment 1 to diffusible plasma
AKIDNEY	RRBC	2.76E-03	2.28E-04	Age-scaled transfer rate from RBC to diffusible plasma
AKIDNEY	RBRAN	1.69E-03	1.83E-04	Age-scaled transfer rate from brain to diffusible plasma
AKIDNEY	RLVR2	3.37E-03	1.32E-04	Age-scaled transfer rate from the slow liver compartment 2 to diffusible plasma
AKIDNEY	RLVR1	2.85E-03	1.07E-04	Transfer rate out of the liver compartment 1, including to small intestine and diffusible plasma
AKIDNEY	RSOF0	3.53E-04	1.16E-05	Transfer rate from soft tissue compartment 0 to diffusible plasma
AKIDNEY	RPLAS	4.93E-05	5.15E-06	Total transfer rate from diffusible plasma to all compartments
AKIDNEY	RSTMC	1.74E-05	3.41E-06	Transfer rate from stomach to small intestine
AKIDNEY	SIZEVF	2.54E-06	3.05E-06	Relative volume of the EVF compartment compared to plasma (EVF/Plasma)
AKIDNEY	GSCAL	2.37E-05	3.01E-06	Age-scaling factor for GIT transfer

Variable	Parameter	Child	Adult	Parameter Description
AKIDNEY	RULI	5.06E-05	1.12E-06	Transfer rate from upper large intestine to lower large intestine
AKIDNEY	RPROT	2.54E-05	9.09E-07	Transfer rate from bound plasma to diffusible plasma
AKIDNEY	RSIC	5.75E-05	2.19E-07	Transfer rate from small intestine to upper large intestine
AKIDNEY	RLLI	5.33E-06	1.21E-07	Transfer rate from lower large intestine to feces
AKIDNEY	TOURIN	2.64E-07	1.21E-08	Deposition fraction from diffusible plasma to urine
AKIDNEY	TOSWET	6.43E-08	2.93E-09	Deposition fraction from diffusible plasma to sweat
AKIDNEY	POWER	0.00E+00	0.00E+00	Exponent for RBC deposition
AKIDNEY	RBCNL	0.00E+00	0.00E+00	Threshold concentration in RBC for non-linear deposition from diffusible plasma to RBC
AKIDNEY	SATRAT	0.00E+00	0.00E+00	Maximum (saturating) concentration of lead in RBC
AKIDNEY	RBLAD	0.00E+00	0.00E+00	Age-scaled transfer rate from urinary bladder to urine

TABLE 4-8. AALM-LG STANDARDIZED SENSITIVITY COEFFICIENTS FOR OTHER SOFT TISSUE PB IN CHILDREN (5 YEARS) AND ADULTS (30 YEARS)

Variable	Parameter	Child	Adult	Parameter Description
ASOFT	TEVF	6.63E+00	8.12E+00	Deposition fraction from diffusible plasma to extravascular fluid
ASOFT	TORBC	3.14E+00	3.81E+00	Deposition fraction from diffusible plasma to RBCs, below non-linear threshold
ASOFT	TOSOF0	1.10E+00	1.39E+00	Age-scaled deposition fraction from diffusible plasma to soft tissue compartment 0
ASOFT	TBONEL	1.06E+00	1.27E+00	Terminal value of age-scaled deposition fraction from diffusible plasma to surface bone
ASOFT	RSOF2	2.36E-01	8.95E-01	Transfer rate from soft tissue compartment 2 to diffusible plasma
ASOFT	TOSOF2	4.68E-01	7.90E-01	Age-scaled deposition fraction from diffusible plasma to soft tissue compartment 2
ASOFT	TOLVR1	3.71E-01	3.80E-01	Deposition fraction from diffusible plasma to liver compartment 2
ASOFT	H1TOBL	2.35E-01	2.86E-01	Fraction of transfer out of liver compartment 1 to diffusible plasma
ASOFT	TOSOF1	4.74E-01	2.71E-01	Age-scaled deposition fraction from diffusible plasma to soft tissue compartment 1
ASOFT	RSOF1	4.36E-01	2.04E-01	Transfer rate from soft tissue compartment 1 to diffusible plasma
ASOFT	TFRAC	3.97E-03	6.66E-02	Bone deposition-scaled fraction of diffusible plasma-to-bone deposition that goes to trabecular surface bone; 1-TFRAC is the fraction that goes to cortical surface bone
ASOFT	H1TOH2	5.20E-02	6.32E-02	Fraction of transfer out of liver compartment 1 to liver compartment 2
ASOFT	S2HAIR	5.19E-02	4.28E-02	Deposition fraction from soft tissue compartment 1 to other excreta
ASOFT	TBONE	1.17E-01	3.82E-02	Age-scaled deposition fraction from diffusible plasma to surface bone
ASOFT	H1TOSI	8.38E-02	3.11E-02	Fraction of transfer out of liver compartment 1 to the small intestine
ASOFT	RCORT	9.33E-02	2.72E-02	Age-scaled transfer rate from non-exchangeable cortical bone to diffusible plasma
ASOFT	FLONG	6.62E-02	2.38E-02	Age-scaled fraction of total transfer from the exchangeable bone directed to non-exchangeable bone
ASOFT	RDIFF	1.38E-02	1.85E-02	Age-scaled transfer rate from the exchangeable bone, including transfer to surface and non-exchangeable bone

Variable	Parameter	Child	Adult	Parameter Description
ASOFT	RSOF0	9.54E-03	1.20E-02	Transfer rate from soft tissue compartment 0 to diffusible plasma
ASOFT	TOFECE	2.99E-02	1.12E-02	Deposition fraction from diffusible plasma directly to the small intestine (not including the transfer from biliary secretion, specified by RLVR1)
ASOFT	RCS2DF	5.93E-02	1.07E-02	Age-scaled transfer rate from cortical bone surface to diffusible plasma
ASOFT	RCS2B	5.94E-02	1.02E-02	Age-scaled transfer rate from cortical bone surface to exchangeable cortical bone
ASOFT	TOPROT	5.25E-03	6.37E-03	Deposition fraction from diffusible plasma to protein-bound plasma
ASOFT	RTS2B	1.48E-02	5.37E-03	Age-scaled transfer rate from surface trabecular bone to exchangeable trabecular bone
ASOFT	RTS2DF	1.48E-02	5.23E-03	Age-scaled transfer rate from trabecular bone surface to diffusible plasma
ASOFT	RTRAB	2.34E-02	3.25E-03	Age-scaled transfer rate from non-exchangeable trabecular bone to diffusible plasma
ASOFT	TOKDN2	2.59E-03	3.15E-03	Deposition fraction from diffusible plasma to kidney compartment 2
ASOFT	TOBRAN	3.04E-03	2.83E-03	Age-scaled deposition fraction from diffusible plasma to brain
ASOFT	RLVR2	1.04E-03	6.65E-04	Age-scaled transfer rate from the slow liver compartment 2 to diffusible plasma
ASOFT	RBRAN	1.49E-03	3.24E-04	Age-scaled transfer rate from brain to diffusible plasma
ASOFT	RLVR1	4.97E-04	8.64E-05	Transfer rate out of the liver compartment 1, including to small intestine and diffusible plasma
ASOFT	RRBC	1.51E-03	6.63E-05	Age-scaled transfer rate from RBC to diffusible plasma
ASOFT	RKDN2	4.71E-05	3.31E-05	Age-scaled transfer rate from kidney compartment 2 to diffusible plasma
ASOFT	RSIC	7.97E-05	1.29E-05	Transfer rate from small intestine to upper large intestine
ASOFT	GSCAL	5.87E-05	1.26E-05	Age-scaling factor for GIT transfer
ASOFT	RPLAS	4.96E-06	4.38E-06	Total transfer rate from diffusible plasma to all compartments
ASOFT	RULI	3.04E-05	4.28E-06	Transfer rate from upper large intestine to lower large intestine
ASOFT	RPROT	4.81E-07	1.18E-06	Transfer rate from bound plasma to diffusible plasma
ASOFT	RLLI	3.76E-06	5.16E-07	Transfer rate from lower large intestine to feces

Variable	Parameter	Child	Adult	Parameter Description
ASOFT	SIZEVF	5.87E-07	5.06E-07	Relative volume of the EVF compartment compared to plasma (EVF/Plasma)
ASOFT	RSTMC	5.46E-06	1.73E-07	Transfer rate from stomach to small intestine
ASOFT	TOKDN1	8.53E-09	4.76E-08	Deposition fraction from diffusible plasma to kidney compartment 1
ASOFT	RKDN1	3.29E-11	3.21E-08	Transfer rate from kidney compartment 1 to urinary pathway
ASOFT	TOURIN	6.40E-09	1.19E-08	Deposition fraction from diffusible plasma to urine
ASOFT	TOSWET	1.54E-09	2.88E-09	Deposition fraction from diffusible plasma to sweat
ASOFT	POWER	0.00E+00	0.00E+00	Exponent for RBC deposition
ASOFT	RBCNL	0.00E+00	0.00E+00	Threshold concentration in RBC for non-linear deposition from diffusible plasma to RBC
ASOFT	SATRAT	0.00E+00	0.00E+00	Maximum (saturating) concentration of lead in RBC
ASOFT	RBLAD	0.00E+00	0.00E+00	Age-scaled transfer rate from urinary bladder to urine

TABLE 4-9. AALM-OF STANDARDIZED SENSITIVITY COEFFICIENTS FOR BLOOD PB IN CHILDREN (5 YEARS) AND ADULTS (30 YEARS)

Variable	Parameter	Child	Adult	Parameter Description
ABLOOD	C1	2.41E+00	9.34E+00	Constant 1 for urinary clearance of Pb as a fraction of GFR
ABLOOD	C2	1.38E+00	7.54E+00	Constant 2 for urinary clearance of Pb as a fraction of GFR
ABLOOD	BIND	9.92E-01	9.92E-01	Maximum capacity of sites in red cells to bind Pb
ABLOOD	KBIND	9.88E-01	9.89E-01	Half-saturation concentration of Pb for binding by sites in red cells
ABLOOD	P0	5.73E-03	6.19E-02	Permeability constant for diffusion from canaliculi to bone
ABLOOD	R0	4.96E-03	5.58E-02	Permeability constant for diffusion from bone to canaliculi
ABLOOD	RAD8	4.27E-03	3.97E-02	Radius of shell 8 of bone in the canalicular diffusion region of deeper bone
ABLOOD	CON	7.51E-04	2.50E-02	Fraction of bone blood flow to trabecular bone
ABLOOD	D0	9.99E-04	1.07E-02	Diffusion constant
ABLOOD	BASE	1.72E-04	9.01E-03	Base bone formation rate in bone growth algorithm
ABLOOD	C3	4.46E-01	7.10E-03	Constant 3 for urinary clearance of Pb as a fraction of GFR
ABLOOD	S	8.26E-04	6.67E-03	Surface area of canaliculi
ABLOOD	RAD1	6.66E-04	5.09E-03	Radius of shell 1 of bone in the canalicular diffusion region of deeper bone
ABLOOD	G	1.13E-02	3.48E-03	Linear parameter for unbound lead in red cells
ABLOOD	RAD2	3.67E-04	2.85E-03	Radius of shell 2 of bone in the canalicular diffusion region of deeper bone
ABLOOD	RAD3	2.27E-04	2.16E-03	Radius of shell 3 of bone in the canalicular diffusion region of deeper bone
ABLOOD	PL	1.12E-02	2.08E-03	Liver/plasma partition coefficient
ABLOOD	RAD4	1.51E-04	1.88E-03	Radius of shell 4 of bone in the canalicular diffusion region of deeper bone
ABLOOD	RAD5	1.04E-04	1.64E-03	Radius of shell 5 of bone in the canalicular diffusion region of deeper bone
ABLOOD	RAD6	6.93E-05	1.29E-03	Radius of shell 6 of bone in the canalicular diffusion region of deeper bone
ABLOOD	EXPO	7.16E-03	1.12E-03	Exponent constant for bone volume participating in adult-type bone remodeling
ABLOOD	QKC	1.52E-03	1.11E-03	Fraction cardiac output going to kidney
ABLOOD	A1	9.16E-03	1.01E-03	Constant 1 for bone formation rate algorithm
ABLOOD	A3	4.20E-03	9.44E-04	Constant 3 for bone formation rate algorithm

Variable	Parameter	Child	Adult	Parameter Description
ABLOOD	QWC	1.33E-02	9.31E-04	Fraction cardiac output going to other well-perfused tissues
ABLOOD	QLC	1.32E-02	9.16E-04	Fraction cardiac output going to liver
ABLOOD	RAD7	3.62E-05	7.55E-04	Radius of shell 7 of bone in the canalicular diffusion region of deeper bone
ABLOOD	A5	0.00E+00	6.65E-04	Constant 5 for bone formation rate algorithm
ABLOOD	PW	2.64E-03	6.07E-04	Well-perfused/plasma partition coefficient
ABLOOD	A2	3.06E-03	1.98E-04	Constant 2 for bone formation rate algorithm
ABLOOD	QBONEC	7.94E-03	1.62E-04	Fraction cardiac output going to bone
ABLOOD	PP	8.01E-05	1.12E-04	Poorly perfused/plasma partition coefficient
ABLOOD	PK	3.60E-05	2.25E-05	Kidney/plasma partition coefficient
ABLOOD	QCC	0.00E+00	0.00E+00	Cardiac output in the adult

TABLE 4-10. AALM-OF STANDARDIZED SENSITIVITY COEFFICIENTS FOR BONE PB IN CHILDREN (5 YEARS) AND ADULTS (30 YEARS)

Variable	Parameter	Child	Adult	Parameter Description
ABONE	C1	1.99E+00	8.70E+00	Constant 1 for urinary clearance of Pb as a fraction of GFR
ABONE	C2	9.73E-01	7.12E+00	Constant 2 for urinary clearance of Pb as a fraction of GFR
ABONE	R0	2.79E-02	2.14E-01	Permeability constant for diffusion from bone to canaliculi
ABONE	RAD8	2.63E-02	1.64E-01	Radius of shell 8 of bone in the canalicular diffusion region of deeper bone
ABONE	P0	5.73E-03	6.19E-02	Permeability constant for diffusion from canaliculi to bone
ABONE	D0	5.61E-03	4.12E-02	Diffusion constant
ABONE	CON	8.59E-02	3.71E-02	Fraction of bone blood flow to trabecular bone
ABONE	EXPO	2.16E-01	3.07E-02	Exponent constant for bone volume participating in adult-type bone remodeling
ABONE	S	5.50E-03	2.97E-02	Surface area of canaliculi
ABONE	C3	3.78E-01	2.47E-02	Constant 3 for urinary clearance of Pb as a fraction of GFR
ABONE	RAD1	4.42E-03	2.35E-02	Radius of shell 1 of bone in the canalicular diffusion region of deeper bone
ABONE	RAD2	2.28E-03	1.29E-02	Radius of shell 2 of bone in the canalicular diffusion region of deeper bone
ABONE	BASE	4.36E-05	1.08E-02	Base bone formation rate in bone growth algorithm
ABONE	RAD3	1.35E-03	9.01E-03	Radius of shell 3 of bone in the canalicular diffusion region of deeper bone
ABONE	RAD4	8.09E-04	6.94E-03	Radius of shell 4 of bone in the canalicular diffusion region of deeper bone
ABONE	RAD5	4.66E-04	5.34E-03	Radius of shell 5 of bone in the canalicular diffusion region of deeper bone
ABONE	RAD6	2.46E-04	3.78E-03	Radius of shell 6 of bone in the canalicular diffusion region of deeper bone
ABONE	RAD7	1.06E-04	2.07E-03	Radius of shell 7 of bone in the canalicular diffusion region of deeper bone
ABONE	A3	6.95E-03	1.18E-03	Constant 3 for bone formation rate algorithm
ABONE	PL	3.82E-03	1.10E-03	Liver/plasma partition coefficient
ABONE	QKC	4.17E-03	9.41E-04	Fraction cardiac output going to kidney
ABONE	PW	6.23E-03	9.31E-04	Well-perfused/plasma partition coefficient
ABONE	BIND	1.37E-03	8.40E-04	Maximum capacity of sites in red cells to bind Pb
ABONE	KBIND	1.12E-03	8.30E-04	Half-saturation concentration of Pb for binding by sites in red cells

Variable	Parameter	Child	Adult	Parameter Description
ABONE	G	2.96E-03	5.62E-04	Linear parameter for unbound lead in red cells
ABONE	QBONEC	2.66E-03	5.61E-04	Fraction cardiac output going to bone
ABONE	A2	3.42E-03	4.88E-04	Constant 2 for bone formation rate algorithm
ABONE	A5	0.00E+00	2.72E-04	Constant 5 for bone formation rate algorithm
ABONE	QLC	9.11E-03	2.41E-04	Fraction cardiac output going to liver
ABONE	QWC	9.22E-03	2.24E-04	Fraction cardiac output going to other well-perfused tissues
ABONE	PP	1.43E-04	1.36E-04	Poorly perfused/plasma partition coefficient
ABONE	A1	1.50E-02	3.05E-05	Constant 1 for bone formation rate algorithm
ABONE	PK	1.73E-04	1.20E-05	Kidney/plasma partition coefficient
ABONE	QCC	0.00E+00	0.00E+00	Cardiac output in the adult

TABLE 4-11. AALM-OF STANDARDIZED SENSITIVITY COEFFICIENTS FOR LIVER PB IN CHILDREN (5 YEARS) AND ADULTS (30 YEARS)

Variable	Parameter	Child	Adult	Parameter Description
ALIVER	C1	2.39E+00	9.28E+00	Constant 1 for urinary clearance of Pb as a fraction of GFR
ALIVER	C2	1.38E+00	7.56E+00	Constant 2 for urinary clearance of Pb as a fraction of GFR
ALIVER	PL	1.01E+00	9.98E-01	Liver/plasma partition coefficient
ALIVER	P0	5.73E-03	6.19E-02	Permeability constant for diffusion from canaliculi to bone
ALIVER	R0	4.98E-03	5.60E-02	Permeability constant for diffusion from bone to canaliculi
ALIVER	RAD8	4.29E-03	3.98E-02	Radius of shell 8 of bone in the canalicular diffusion region of deeper bone
ALIVER	CON	7.53E-04	2.51E-02	Fraction of bone blood flow to trabecular bone
ALIVER	D0	1.00E-03	1.07E-02	Diffusion constant
ALIVER	BASE	1.73E-04	9.04E-03	Base bone formation rate in bone growth algorithm
ALIVER	C3	4.48E-01	7.12E-03	Constant 3 for urinary clearance of Pb as a fraction of GFR
ALIVER	S	8.29E-04	6.69E-03	Surface area of canaliculi
ALIVER	RAD1	6.69E-04	5.11E-03	Radius of shell 1 of bone in the canalicular diffusion region of deeper bone
ALIVER	RAD2	3.68E-04	2.85E-03	Radius of shell 2 of bone in the canalicular diffusion region of deeper bone
ALIVER	RAD3	2.28E-04	2.16E-03	Radius of shell 3 of bone in the canalicular diffusion region of deeper bone
ALIVER	RAD4	1.51E-04	1.89E-03	Radius of shell 4 of bone in the canalicular diffusion region of deeper bone
ALIVER	RAD5	1.05E-04	1.65E-03	Radius of shell 5 of bone in the canalicular diffusion region of deeper bone
ALIVER	RAD6	6.96E-05	1.29E-03	Radius of shell 6 of bone in the canalicular diffusion region of deeper bone
ALIVER	EXPO	7.19E-03	1.12E-03	Exponent constant for bone volume participating in adult-type bone remodeling
ALIVER	QKC	1.24E-03	1.12E-03	Fraction cardiac output going to kidney
ALIVER	A1	9.35E-03	1.01E-03	Constant 1 for bone formation rate algorithm
ALIVER	QLC	1.34E-02	9.67E-04	Fraction cardiac output going to liver
ALIVER	A3	4.21E-03	9.38E-04	Constant 3 for bone formation rate algorithm
ALIVER	QWC	1.33E-02	9.34E-04	Fraction cardiac output going to other well-perfused tissues
ALIVER	BIND	8.28E-04	7.63E-04	Maximum capacity of sites in red cells to bind Pb

Variable	Parameter	Child	Adult	Parameter Description
ALIVER	KBIND	8.44E-04	7.58E-04	Half-saturation concentration of Pb for binding by sites in red cells
ALIVER	RAD7	3.63E-05	7.57E-04	Radius of shell 7 of bone in the canalicular diffusion region of deeper bone
ALIVER	A5	0.00E+00	6.67E-04	Constant 5 for bone formation rate algorithm
ALIVER	PW	2.11E-03	6.09E-04	Well-perfused/plasma partition coefficient
ALIVER	A2	3.08E-03	1.98E-04	Constant 2 for bone formation rate algorithm
ALIVER	QBONEC	8.66E-03	1.62E-04	Fraction cardiac output going to bone
ALIVER	G	8.74E-03	1.60E-04	Linear parameter for unbound lead in red cells
ALIVER	PP	8.13E-05	1.14E-04	Poorly perfused/plasma partition coefficient
ALIVER	PK	3.61E-05	2.25E-05	Kidney/plasma partition coefficient
ALIVER	QCC	0.00E+00	0.00E+00	Cardiac output in the adult

TABLE 4-12. AALM-OF STANDARDIZED SENSITIVITY COEFFICIENTS FOR KIDNEY PB IN CHILDREN (5 YEARS) AND ADULTS (30 YEARS)

Variable	Parameter	Child	Adult	Parameter Description
AKIDNEY	C1	2.39E+00	9.28E+00	Constant 1 for urinary clearance of Pb as a fraction of GFR
AKIDNEY	C2	1.38E+00	7.56E+00	Constant 2 for urinary clearance of Pb as a fraction of GFR
AKIDNEY	PK	1.00E+00	9.99E-01	Kidney/plasma partition coefficient
AKIDNEY	P0	5.73E-03	6.19E-02	Permeability constant for diffusion from canaliculi to bone
AKIDNEY	R0	4.99E-03	5.60E-02	Permeability constant for diffusion from bone to canaliculi
AKIDNEY	RAD8	4.29E-03	3.98E-02	Radius of shell 8 of bone in the canalicular diffusion region of deeper bone
AKIDNEY	CON	7.53E-04	2.51E-02	Fraction of bone blood flow to trabecular bone
AKIDNEY	D0	1.00E-03	1.07E-02	Diffusion constant
AKIDNEY	BASE	1.73E-04	9.04E-03	Base bone formation rate in bone growth algorithm
AKIDNEY	C3	4.48E-01	7.12E-03	Constant 3 for urinary clearance of Pb as a fraction of GFR
AKIDNEY	S	8.29E-04	6.69E-03	Surface area of canaliculi
AKIDNEY	RAD1	6.69E-04	5.11E-03	Radius of shell 1 of bone in the canalicular diffusion region of deeper bone
AKIDNEY	RAD2	3.68E-04	2.85E-03	Radius of shell 2 of bone in the canalicular diffusion region of deeper bone
AKIDNEY	RAD3	2.28E-04	2.16E-03	Radius of shell 3 of bone in the canalicular diffusion region of deeper bone
AKIDNEY	PL	1.13E-02	2.10E-03	Liver/plasma partition coefficient
AKIDNEY	RAD4	1.51E-04	1.89E-03	Radius of shell 4 of bone in the canalicular diffusion region of deeper bone
AKIDNEY	RAD5	1.05E-04	1.65E-03	Radius of shell 5 of bone in the canalicular diffusion region of deeper bone
AKIDNEY	RAD6	6.96E-05	1.29E-03	Radius of shell 6 of bone in the canalicular diffusion region of deeper bone
AKIDNEY	EXPO	7.19E-03	1.12E-03	Exponent constant for bone volume participating in adult-type bone remodeling
AKIDNEY	QKC	1.47E-03	1.05E-03	Fraction cardiac output going to kidney
AKIDNEY	A1	9.32E-03	1.01E-03	Constant 1 for bone formation rate algorithm
AKIDNEY	A3	4.22E-03	9.37E-04	Constant 3 for bone formation rate algorithm
AKIDNEY	QWC	1.33E-02	9.34E-04	Fraction cardiac output going to other well-perfused tissues
AKIDNEY	QLC	1.32E-02	9.19E-04	Fraction cardiac output going to liver

Variable	Parameter	Child	Adult	Parameter Description
AKIDNEY	RAD7	3.63E-05	7.57E-04	Radius of shell 7 of bone in the canalicular diffusion region of deeper bone
AKIDNEY	A5	0.00E+00	6.67E-04	Constant 5 for bone formation rate algorithm
AKIDNEY	BIND	3.64E-04	6.52E-04	Maximum capacity of sites in red cells to bind Pb
AKIDNEY	KBIND	3.85E-04	6.47E-04	Half-saturation concentration of Pb for binding by sites in red cells
AKIDNEY	PW	2.05E-03	6.09E-04	Well-perfused/plasma partition coefficient
AKIDNEY	A2	3.08E-03	1.98E-04	Constant 2 for bone formation rate algorithm
AKIDNEY	QBONEC	8.68E-03	1.62E-04	Fraction cardiac output going to bone
AKIDNEY	G	8.77E-03	1.60E-04	Linear parameter for unbound lead in red cells
AKIDNEY	PP	8.05E-05	1.13E-04	Poorly perfused/plasma partition coefficient
AKIDNEY	QCC	0.00E+00	0.00E+00	Cardiac output in the adult

TABLE 4-13. AALM-OF STANDARDIZED SENSITIVITY COEFFICIENTS FOR POORLY PERFUSED TISSUES PB IN CHILDREN (5 YEARS) AND ADULTS (30 YEARS)

Variable	Parameter	Child	Adult	Parameter Description
APOOR	C1	2.39E+00	9.28E+00	Constant 1 for urinary clearance of Pb as a fraction of GFR
APOOR	C2	1.38E+00	7.56E+00	Constant 2 for urinary clearance of Pb as a fraction of GFR
APOOR	PP	1.00E+00	1.00E+00	Poorly perfused/plasma partition coefficient
APOOR	P0	5.73E-03	6.19E-02	Permeability constant for diffusion from canaliculi to bone
APOOR	R0	4.99E-03	5.60E-02	Permeability constant for diffusion from bone to canaliculi
APOOR	RAD8	4.29E-03	3.98E-02	Radius of shell 8 of bone in the canalicular diffusion region of deeper bone
APOOR	CON	7.54E-04	2.51E-02	Fraction of bone blood flow to trabecular bone
APOOR	D0	1.00E-03	1.07E-02	Diffusion constant
APOOR	BASE	1.73E-04	9.03E-03	Base bone formation rate in bone growth algorithm
APOOR	C3	4.48E-01	7.12E-03	Constant 3 for urinary clearance of Pb as a fraction of GFR
APOOR	S	8.29E-04	6.69E-03	Surface area of canaliculi
APOOR	RAD1	6.69E-04	5.11E-03	Radius of shell 1 of bone in the canalicular diffusion region of deeper bone
APOOR	RAD2	3.68E-04	2.85E-03	Radius of shell 2 of bone in the canalicular diffusion region of deeper bone
APOOR	RAD3	2.28E-04	2.16E-03	Radius of shell 3 of bone in the canalicular diffusion region of deeper bone
APOOR	PL	1.13E-02	2.08E-03	Liver/plasma partition coefficient
APOOR	RAD4	1.51E-04	1.89E-03	Radius of shell 4 of bone in the canalicular diffusion region of deeper bone
APOOR	RAD5	1.05E-04	1.65E-03	Radius of shell 5 of bone in the canalicular diffusion region of deeper bone
APOOR	RAD6	6.96E-05	1.29E-03	Radius of shell 6 of bone in the canalicular diffusion region of deeper bone
APOOR	EXPO	7.19E-03	1.12E-03	Exponent constant for bone volume participating in adult-type bone remodeling
APOOR	QKC	1.55E-03	1.12E-03	Fraction cardiac output going to kidney
APOOR	A1	9.13E-03	1.01E-03	Constant 1 for bone formation rate algorithm
APOOR	A3	4.22E-03	9.48E-04	Constant 3 for bone formation rate algorithm
APOOR	QWC	1.34E-02	9.34E-04	Fraction cardiac output going to other well-perfused tissues
APOOR	QLC	1.33E-02	9.19E-04	Fraction cardiac output going to liver

Variable	Parameter	Child	Adult	Parameter Description
APOOR	RAD7	3.63E-05	7.57E-04	Radius of shell 7 of bone in the canalicular diffusion region of deeper bone
APOOR	BIND	6.34E-04	7.16E-04	Maximum capacity of sites in red cells to bind Pb
APOOR	KBIND	6.52E-04	7.11E-04	Half-saturation concentration of Pb for binding by sites in red cells
APOOR	A5	0.00E+00	6.67E-04	Constant 5 for bone formation rate algorithm
APOOR	PW	2.74E-03	6.15E-04	Well-perfused/plasma partition coefficient
APOOR	A2	3.08E-03	1.98E-04	Constant 2 for bone formation rate algorithm
APOOR	QBONEC	7.84E-03	1.62E-04	Fraction cardiac output going to bone
APOOR	G	7.92E-03	1.60E-04	Linear parameter for unbound lead in red cells
APOOR	PK	3.62E-05	2.25E-05	Kidney/plasma partition coefficient
APOOR	QCC	0.00E+00	0.00E+00	Cardiac output in the adult

TABLE 4-14. AALM-OF STANDARDIZED SENSITIVITY COEFFICIENTS FOR WELL-PERFUSED TISSUES PB IN CHILDREN (5 YEARS) AND ADULTS (30 YEARS)

Variable	Parameter	Child	Adult	Parameter Description
AWELL	C1	2.39E+00	9.28E+00	Constant 1 for urinary clearance of Pb as a fraction of GFR
AWELL	C2	1.38E+00	7.56E+00	Constant 2 for urinary clearance of Pb as a fraction of GFR
AWELL	PW	1.00E+00	1.00E+00	Well-perfused/plasma partition coefficient
AWELL	P0	5.73E-03	6.19E-02	Permeability constant for diffusion from canaliculi to bone
AWELL	R0	4.99E-03	5.60E-02	Permeability constant for diffusion from bone to canaliculi
AWELL	RAD8	4.29E-03	3.98E-02	Radius of shell 8 of bone in the canalicular diffusion region of deeper bone
AWELL	CON	7.53E-04	2.51E-02	Fraction of bone blood flow to trabecular bone
AWELL	D0	1.00E-03	1.07E-02	Diffusion constant
AWELL	BASE	1.73E-04	9.05E-03	Base bone formation rate in bone growth algorithm
AWELL	C3	4.48E-01	7.12E-03	Constant 3 for urinary clearance of Pb as a fraction of GFR
AWELL	S	8.29E-04	6.69E-03	Surface area of canaliculi
AWELL	RAD1	6.69E-04	5.11E-03	Radius of shell 1 of bone in the canalicular diffusion region of deeper bone
AWELL	RAD2	3.68E-04	2.85E-03	Radius of shell 2 of bone in the canalicular diffusion region of deeper bone
AWELL	RAD3	2.28E-04	2.16E-03	Radius of shell 3 of bone in the canalicular diffusion region of deeper bone
AWELL	PL	1.11E-02	2.08E-03	Liver/plasma partition coefficient
AWELL	RAD4	1.51E-04	1.89E-03	Radius of shell 4 of bone in the canalicular diffusion region of deeper bone
AWELL	RAD5	1.05E-04	1.65E-03	Radius of shell 5 of bone in the canalicular diffusion region of deeper bone
AWELL	RAD6	6.96E-05	1.29E-03	Radius of shell 6 of bone in the canalicular diffusion region of deeper bone
AWELL	EXPO	7.19E-03	1.12E-03	Exponent constant for bone volume participating in adult-type bone remodeling
AWELL	QKC	1.09E-03	1.12E-03	Fraction cardiac output going to kidney
AWELL	A1	9.45E-03	1.01E-03	Constant 1 for bone formation rate algorithm
AWELL	QWC	1.32E-02	9.34E-04	Fraction cardiac output going to other well-perfused tissues
AWELL	A3	4.21E-03	9.30E-04	Constant 3 for bone formation rate algorithm
AWELL	QLC	1.31E-02	9.19E-04	Fraction cardiac output going to liver

Variable	Parameter	Child	Adult	Parameter Description
AWELL	RAD7	3.63E-05	7.57E-04	Radius of shell 7 of bone in the canalicular diffusion region of deeper bone
AWELL	BIND	6.34E-04	7.16E-04	Maximum capacity of sites in red cells to bind Pb
AWELL	KBIND	6.52E-04	7.11E-04	Half-saturation concentration of Pb for binding by sites in red cells
AWELL	A5	0.00E+00	6.67E-04	Constant 5 for bone formation rate algorithm
AWELL	A2	3.08E-03	1.98E-04	Constant 2 for bone formation rate algorithm
AWELL	QBONEC	9.15E-03	1.64E-04	Fraction cardiac output going to bone
AWELL	G	9.14E-03	1.60E-04	Linear parameter for unbound lead in red cells
AWELL	PP	8.05E-05	1.13E-04	Poorly perfused/plasma partition coefficient
AWELL	PK	3.61E-05	2.25E-05	Kidney/plasma partition coefficient
AWELL	QCC	0.00E+00	0.00E+00	Cardiac output in the adult

TABLE 4-15. DOMINANT PARAMETERS INFLUENCING MAJOR DIFFERENCES IN ESTIMATIONS FROM AALM-LG AND AALM-OF

Estimated Variable	Model Difference	Dominant Parameters	
		AALM-LG	**AALM-OF**
Child blood Pb	AALM-OF < AALM-LG	TEVF TORBC TOSOF0 RRBC TOLVR1 H1TOBL TBONE	C1 C2 BIND KBIND
Child bone Pb	AALM-OF < AALM-LG	TEVF TORBC TBONE TOSOF0 FLONG RCS2DF TOLVR1 H1TOBL RTS2DF	C1 C2 R0 RAD8
Liver Pb	AALM-OF < AALM-LG	TEVF TORBC TOSOF0 TOLVR1 H1TOH2 RLVR2 H1TOBL RLVR1	C1 C2 PL
Kidney Pb	AALM-OF < AALM-LG	TEVF TORBC TOSOF0 RKDN1 TOKDN1 TOKDN2 RKDN2	C1 C2 PK
Other soft tissues	AALM-OF < AALM-LG	TEVF TORBC TOSOF0 RSOF2 TOSOF2 TOLVR1 H1TOBL TOSOF1 RSOF1	C1 C2 PP PW

TABLE 4-16. STRATEGY USED FOR SEQUENTIAL OPTIMIZATION OF AALM BIOKINETICS MODEL

Step	Objective	Observation Data Sources
1	Unify parameter values for GI absorption and growth	(O'Flaherty, 1995, 1993)
2	Optimize plasma/RBC ratio	(Smith et al., 2002; Bergdahl et al., 1999; Bergdahl et al., 1998; Hernández-Avila et al., 1998; Bergdahl et al., 1997; Schütz et al., 1996)
3	Optimize plasma(blood)-to-urine clearance	(Rentschler et al., 2012; Dewoskin and Thompson, 2008; Manton and Cook, 1984; Manton and Malloy, 1983; Chamberlain et al., 1978)
4	Optimize soft tissue (kidney, liver, muscle)/bone ratios	(Gerhardsson et al., 1995; Barry, 1981; Barry, 1975; Gross et al., 1975)
5	Optimize plasma(blood)/bone ratios	(Hernández-Avila et al., 1998; Cake et al., 1996)
6	Optimize bone Pb elimination kinetics	(Nilsson et al., 1991)
7	Evaluate blood Pb elimination kinetics – adults	(Rabinowitz et al., 1976)
8	Evaluate blood Pb elimination kinetics – infants	(Sherlock and Quinn, 1986; Ryu et al., 1983)

TABLE 4-17. COMPARISON OF ESTIMATED AND OBSERVED PLASMA PB/BONE PB SLOPES

Model	Study	Bone	Estimated Slope	Observed Slope	SE	95%CL	Residual
AALM-LG	CA96	Cortical	0.037	0.052	0.013	0.027, 0.077	-1.16
AALM-LG	CA96	Trabecular	0.040	0.041	0.007	0.027, 0.054	-0.16
AALM-LG	HE98	Cortical	0.037	0.036	0.011	0.014, 0.058	0.12
AALM-LG	HE98	Trabecular	0.040	0.025	0.004	0.017, 0.033	3.67
AALM-OF	CA96	Cortical	0.042	0.052	0.013	0.027, 0.077	-0.81
AALM-OF	CA96	Trabecular	0.060	0.041	0.007	0.027, 0.054	2.70
AALM-OF	HE98	Cortical	0.042	0.036	0.011	0.014, 0.058	0.53
AALM-OF	HE98	Trabecular	0.060	0.025	0.004	0.017, 0.033	8.68

CA96, Cake et al. (1996); HE98, Hernández-Avila et al. (1998)

TABLE 4-18. CHANGES TO (O'FLAHERTY, 1995, 1993) AND (LEGGETT, 1993) MODELS INCORPORATED INTO AALM

Model Component	Parameter Change	AALM-LG	AALM-OF
Growth	Body and tissue growth as functions of age and body weight	X	
Respiratory tract	Simulation of deposition, mucociliary clearance and absorption of inhaled Pb based on ICRP HRTM	X	X
GI tract	Age-dependent absorption calculated with a continuous function rather than age array variable	X	
GI tract	Infant GI absorption fractions optimized	X	X
GI tract	Absorption fraction adjustable by user-specified media-specific relative bioavailability fractions	X	X
Tissue Pb	Age-dependent values for tissue-blood partition coefficients		X
Tissue Pb	Bone, kidney and liver concentrations calculated from Pb masses and tissue weights	X	
Neonate	Neonatal model which sets Pb masses in blood and tissues at birth as a function of maternal Pb concentration	X	X
RBC	Parameters for plasma-RBC binding and uptake optimized	X	X
GFR	Parameters for GFR adjusted to estimate adult GFR of 170 L/day/1.73m^2 (120 mL/min/1.73m^2) and 30% of adult in infants (<1 year)		X
Urine Pb	Parameters for Pb transfer to urine optimized	X	X

GFR, glomerular filtration rate; GI, gastrointestinal; ICRP, International Commission of Radiological Protection; RBC, red blood cell

TABLE 4-19. COMPARISON OF AALM-LG AND AALM-OF ESTIMATIONS OF BLOOD AND TISSUE PB CONCENTRATIONS

Dose (µg/day)	Age (year)	Sex	Tissue	Unit	AALM-LG	AALM-OF
5	2	M	Blood	µg/dL	1.86	2.39
5	2	M	Bone	µg/g	0.88	0.43
5	2	M	Kidney	µg/g	0.06	0.08
5	2	M	Liver	µg/g	0.14	0.09
5	40	M	Blood	µg/dL	0.28	0.50
5	40	M	Bone	µg/g	0.14	0.15
5	40	M	Kidney	µg/g	0.005	0.010
5	40	M	Liver	µg/g	0.008	0.012
5	2	F	Blood	µg/dL	1.95	2.39
5	2	F	Bone	µg/g	0.93	0.43
5	2	F	Kidney	µg/g	0.07	0.08
5	2	F	Liver	µg/g	0.15	0.09
5	40	F	Blood	µg/dL	0.36	0.50
5	40	F	Bone	µg/g	0.20	0.15
5	40	F	Kidney	µg/g	0.006	0.010
5	40	F	Liver	µg/g	0.010	0.012

F, female; M, male

TABLE 4-20. COMPARISON OF ADULT LEAD METHODOLOGY, AALM-LG AND AALM-OF ESTIMATIONS OF BLOOD PB CONCENTRATIONS IN ADULTS

Parameter	Description	Units	ALM	AALM-LG	AALM-OF
PbS	Soil lead concentration	µg/g or ppm	1000	1000	1000
BKSF	Biokinetic Slope Factor	µg/dL per µg/day	0.4	NA	NA
PbB_0	Baseline Blood Pb	µg/dL	1.5	1.5	1.5
IR_S	Soil Ingestion Rate	g/day	0.050	0.05	0.05
$AF_{S, D}$	Absorption Fraction	--	0.12	0.048	0.048
$EF_{S, D}$	Exposure Frequency	days/yr	219	219	219
$AT_{S, D}$	Averaging Time	days/yr	365	365	365
PbB_{adult}	Blood Pb Concentration	µg/dL	2.9	3.1	4.6

ALM, Adult Lead Methodology

TABLE 4-21. COMPARISON OF AALM-LG AND AALM-OF ESTIMATIONS OF BLOOD AND TISSUE PB CONCENTRATIONS AFTER CALIBRATING RBC PARAMETER VALUES TO THE IEUBK MODEL OUTPUT

Dose (µg/day)	Age (year)	Sex	Tissue	Unit	AALM-LG	AALM-OF
5	2	M	Blood	µg/dL	1.6	1.2
5	2	M	Bone	µg/g	1.33	0.43
5	2	M	Kidney	µg/g	0.10	0.08
5	2	M	Liver	µg/g	0.21	0.09
5	40	M	Blood	µg/dL	0.28	0.50
5	40	M	Bone	µg/g	0.15	0.15
5	40	M	Kidney	µg/g	0.005	0.010
5	40	M	Liver	µg/g	0.008	0.012
5	2	F	Blood	µg/dL	1.7	1.2
5	2	F	Bone	µg/g	1.42	0.46
5	2	F	Kidney	µg/g	0.10	0.08
5	2	F	Liver	µg/g	0.23	0.10
5	40	F	Blood	µg/dL	0.36	0.55
5	40	F	Bone	µg/g	0.20	0.14
5	40	F	Kidney	µg/g	0.006	0.012
5	40	F	Liver	µg/g	0.010	0.014

F, female; M, male

TABLE 4-22. CHANGES MADE TO THE (LEGGETT, 1993) MODEL TO CREATE AALM-LG.CSL

LEGGETT	AALM-LG	Output/Functionality Affected
Age-dependent blood volume	Age-dependent blood volume based on O'Flaherty (1995, 1993)	Age-dependent RBC and plasma volumes
Constant hematocrit	Age-dependent hematocrit based on O'Flaherty (1995, 1993)	Age-dependent RBC and plasma volumes
Adult bone mass	Age-dependent bone mass based on O'Flaherty (1995, 1993)	Age-dependent cortical and trabecular bone Pb concentration
Adult kidney mass	Age-dependent kidney mass based on O'Flaherty (1995, 1993)	Age-dependent kidney Pb concentration
NA	Age-dependent liver mass based on O'Flaherty (1995, 1993)	Age-dependent liver Pb concentration
Age-dependent absorption fraction (*F1*): • birth: 0.45 • 0.27 y: 0.45 • 1 y: 0.30 • 5 y: 0.30 • 10 y: 0.30 • 15 y: 0.30 • ≥25 y: 0.15	Age-dependent absorption fraction (*F1*): • birth: 0.39 • 0.27 y: 0.39 • 1 y: 0.38 • 5 y: 0.17 • ≥10 y: 0.12	Absorption fraction for ingested Pb
Absorption fraction for ingested Pb not adjusted for RBA	Absorption fraction adjusted for media-specific RBA	Absorption fraction of ingested Pb
RBC Pb saturation threshold: 60 µg/dL blood) Maximum: 350 µg/dL RBC	RBC Pb saturation threshold: 20 µg/dL blood) Maximum: 350 µg/dL RBC	Plasma-RBC Pb relationship
Transfer rate from (d^{-1}) RBC to diffusible plasma: • birth: 0.462 • 0.27 y: 0.462 • 1 y: 0.462 • 5 y: 0.277 • ≥10 y: 0.139	Transfer rate from (d^{-1}) from RBC to diffusible plasma: • birth: 0.462 • 0.27 y: 0.462 • 1 y: 0.785 • 5 y: 0.499 • 10 y: 0.195 • ≥ 15 y: 0.139	Plasma-RBC Pb relationship
Deposition fraction from diffusible plasma to RBC (0.24)	Deposition fraction from diffusible plasma to RBC (0.25)	Plasma-RBC relationship
Deposition fraction from diffusible plasma to urine (30)	Deposition fraction from diffusible plasma to urine (0)	Plasma to urine clearance

LEGGETT	AALM-LG	Output/Functionality Affected
Transfer rate (d^{-1}) from liver to diffusible plasma: • birth: 0.00693 • 0.27 y: 0.00693 • 1 y: 0.00693 • 5 y: 0.00693 • 10 y: 0.00190 • 15 y: 0.00190 • ≥25 y: 0.00190	Transfer rate (d^{-1}) from liver to diffusible plasma: • birth: 0.00693 • 0.27 y: 0.00693 • 1 y: 0.00693 • 5 y: 0.00139 • 10 y: 0.000570 • 15 y: 0.000570 • 25 y: 0.000570 • 30 y: 0.00142 • 40 y: 0.00304 • 60 y: 0.00342 • 90 y: 0.00380	Plasma to liver Pb kinetics
Deposition fraction from diffusible plasma to kidney (40)	Deposition fraction from diffusible plasma to kidney (50)	Urinary clearance of plasma Pb
Transfer rate (d^{-1}) from kidney to diffusible plasma (RKDN2): • birth: 0.00693 • 0.27 y: 0.00693 • 1 y: 0.00693 • 5 y: 0.00693 • 10 y: 0.00190 • 15 y: 0.00190 • ≥25 y: 0.00190	Transfer rate (d^{-1}) from kidney to diffusible plasma (RKDN2): • birth: 0.000693 • 0.27 y: 0.000693 • 1 y: 0.000693 • 5 y: 0.000693 • 10 y: 0.000190 • 15 y: 0.000190 • 25 y: 0.000190 • 30 y: 0.000950 • ≥40 y: 0.00190	Plasma to kidney Pb kinetics
Fraction of total transfer from exchangeable bone to nonexchangeable bone (0.2)	Fraction of total transfer from exchangeable bone to nonexchangeable bone (0.6)	Bone Pb retention
Transfer rate (d^{-1}) from non-exchangeable cortical bone to diffusible plasma: • birth: 0.00822 • 0.27 y: 0.00822 • 1 y: 0.00288 • 5 y: 0.00154 • 10 y: 0.000890 • 15 y: 0.000512 • ≥25 y: 0.0000822	Transfer rate (d^{-1}) from non-exchangeable cortical bone to diffusible plasma: • birth: 0.0204 • 0.27 y: 0.0164 • 1 y: 0.00576 • 5 y: 0.00308 • 10 y: 0.00178 • 15 y: 0.00102 • ≥25 y: 0.000164	Bone to plasma Pb kinetics

LEGGETT	AALM-LG	Output/Functionality Affected
Transfer rate (d^{-1}) from non-exchangeable trabecular bone to diffusible plasma: • birth: 0.00822 • 0.27 y: 0.00822 • 1 y: 0.00288 • 5 y: 0.00181 • 10 y: 0.00132 • 15 y: 0.000956 • ≥25 y: 0.000493	Transfer rate (d^{-1}) from non-exchangeable trabecular bone to diffusible plasma: • birth: 0.0102 • 0.27 y: 0.01644 • 1 y: 0.00576 • 5 y: 0.00362 • 10 y: 0.00264 • 15 y: 0.00192 • ≥25 y: 0.000986	Bone-to-plasma Pb transfer kinetics

FIGURE 4-1. DATA FLOW DIAGRAM FOR AALM.

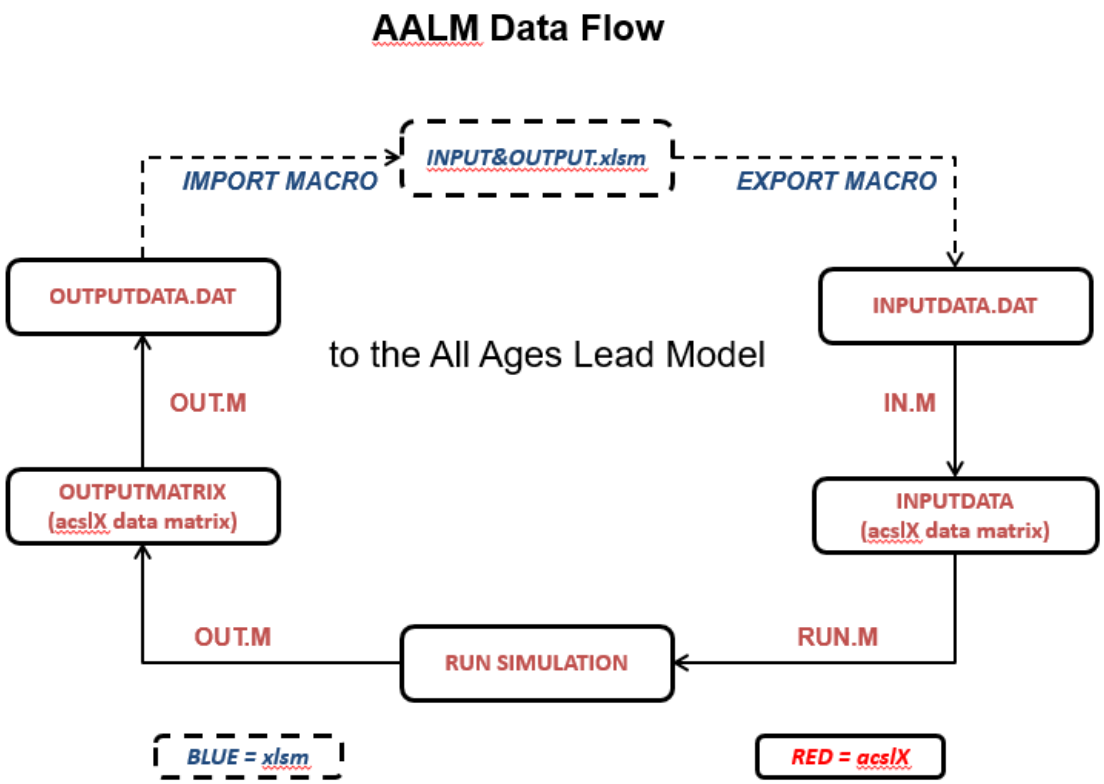

FIGURE 4-2. STRUCTURE OF AALM-LG MODEL.

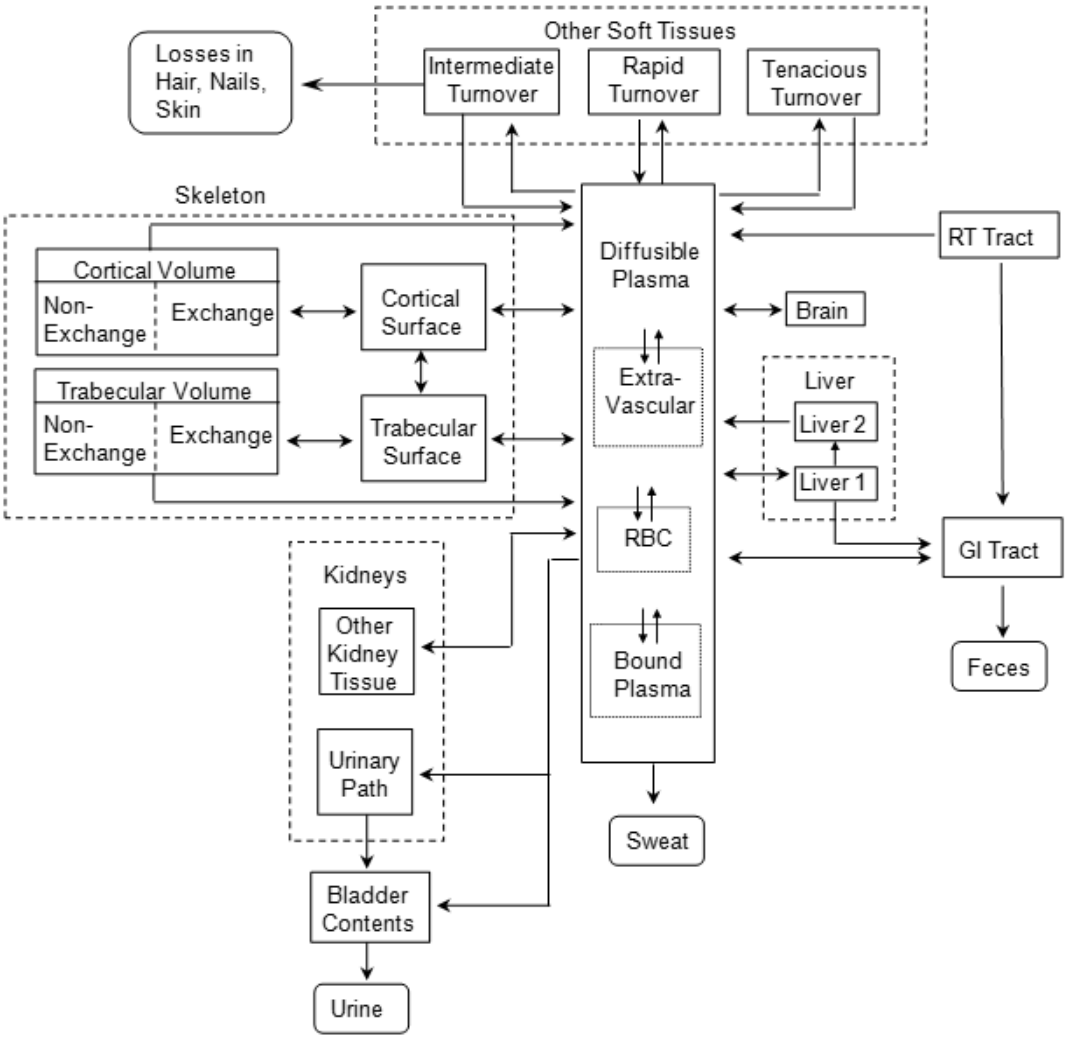

Figure is based on Leggett (1993).

FIGURE 4-3. STRUCTURE OF AALM-OF MODEL.

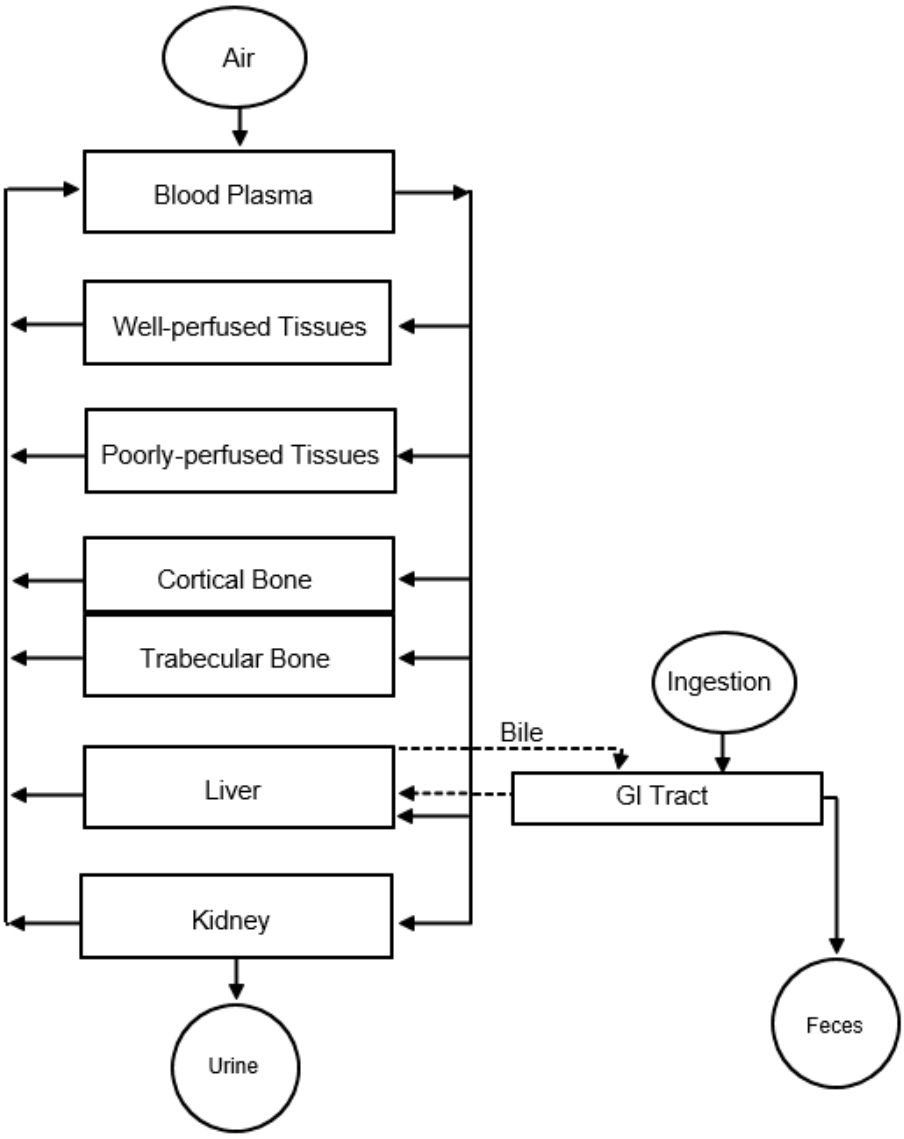

Figure is based on O'Flaherty (1993) .

FIGURE 4-4. STRUCTURE OF AALM-LG BONE MODEL.

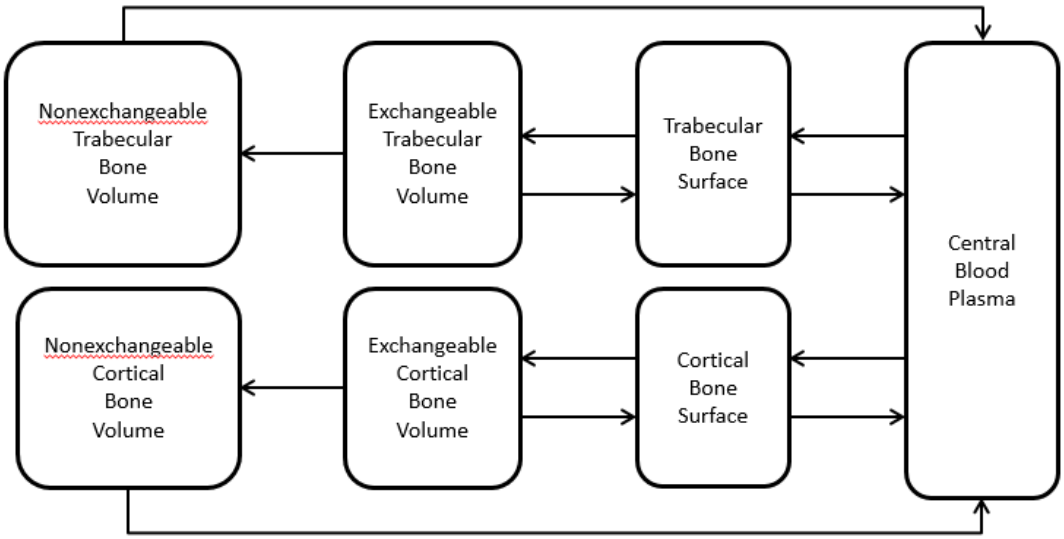

Figure is based on Leggett (1993).

FIGURE 4-5. STRUCTURE OF AALM-OF BONE MODEL.

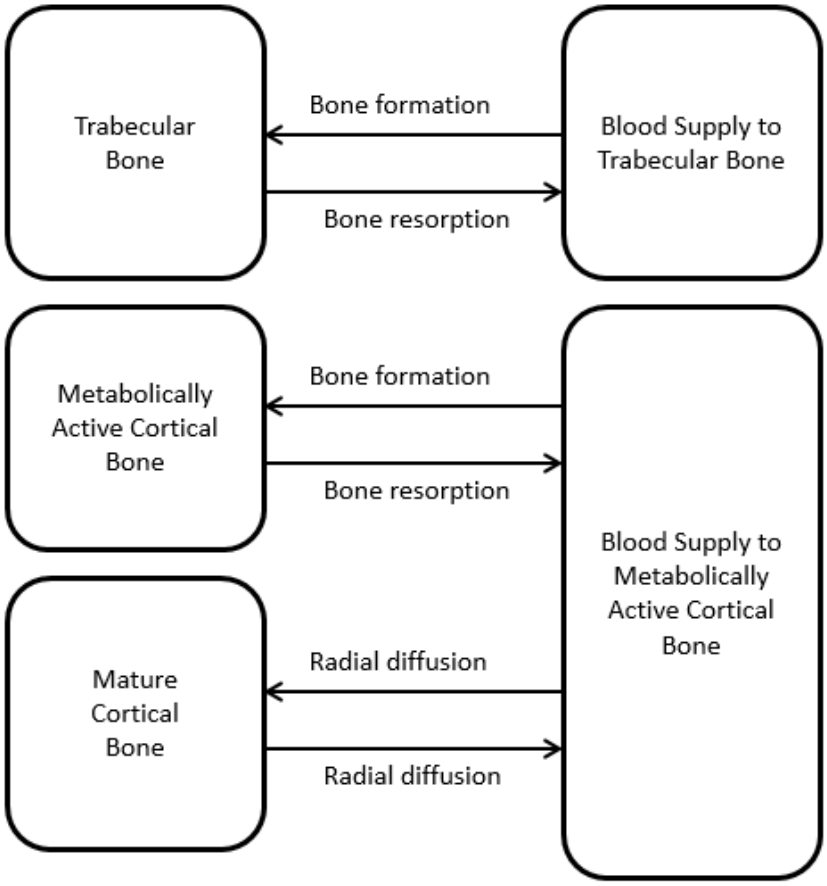

Figure is based on O'Flaherty (1993).

FIGURE 4-6. COMPARISON OF PB (µG) LEVELS ESTIMATED FROM AALM-OF AND AALM-LG FOR A CONSTANT INGESTION OF 5 µG PB/DAY FOR AGES 0 TO 30 YEARS.

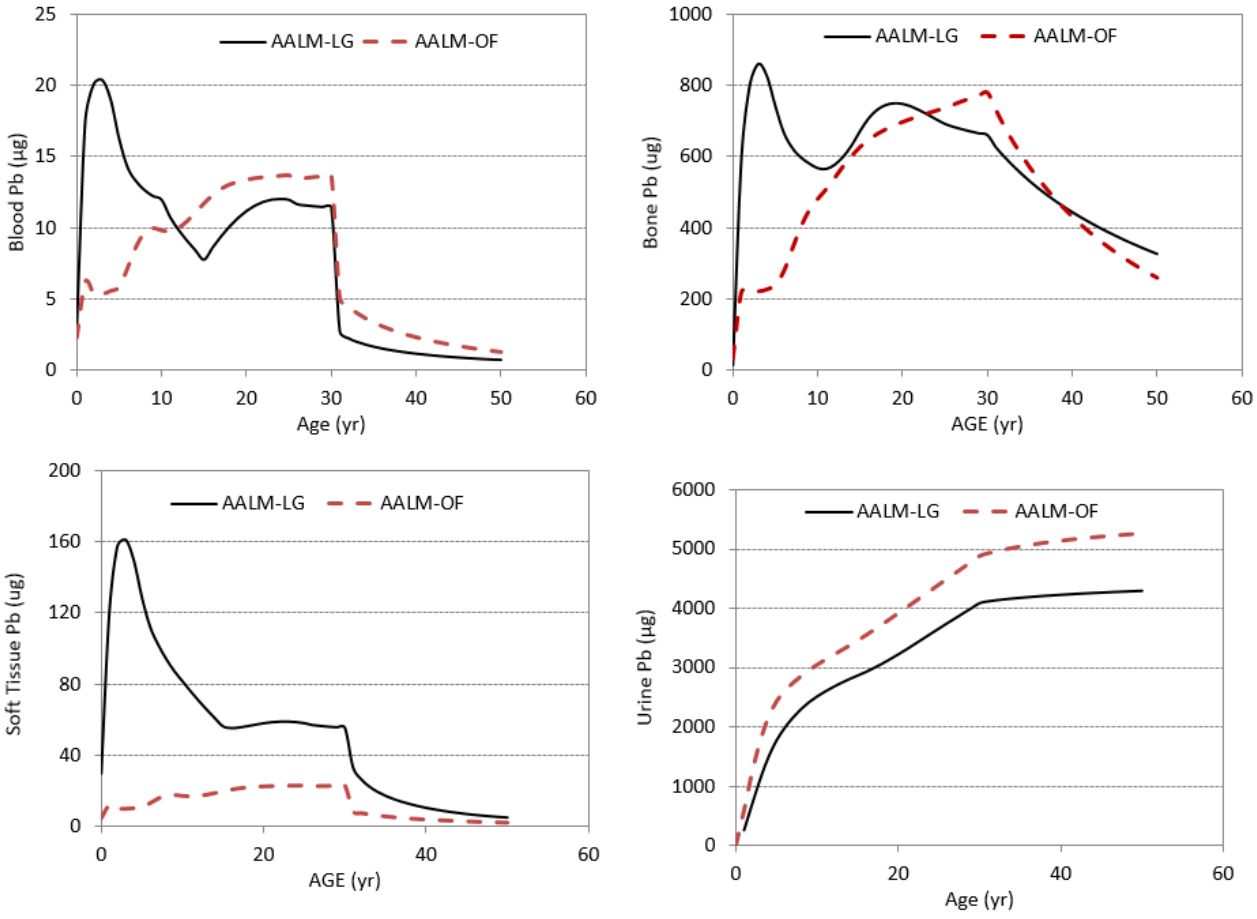

FIGURE 4-7. DIFFERENCES IN PB LEVELS ESTIMATED FROM AALM-LG AND AALM-OF.

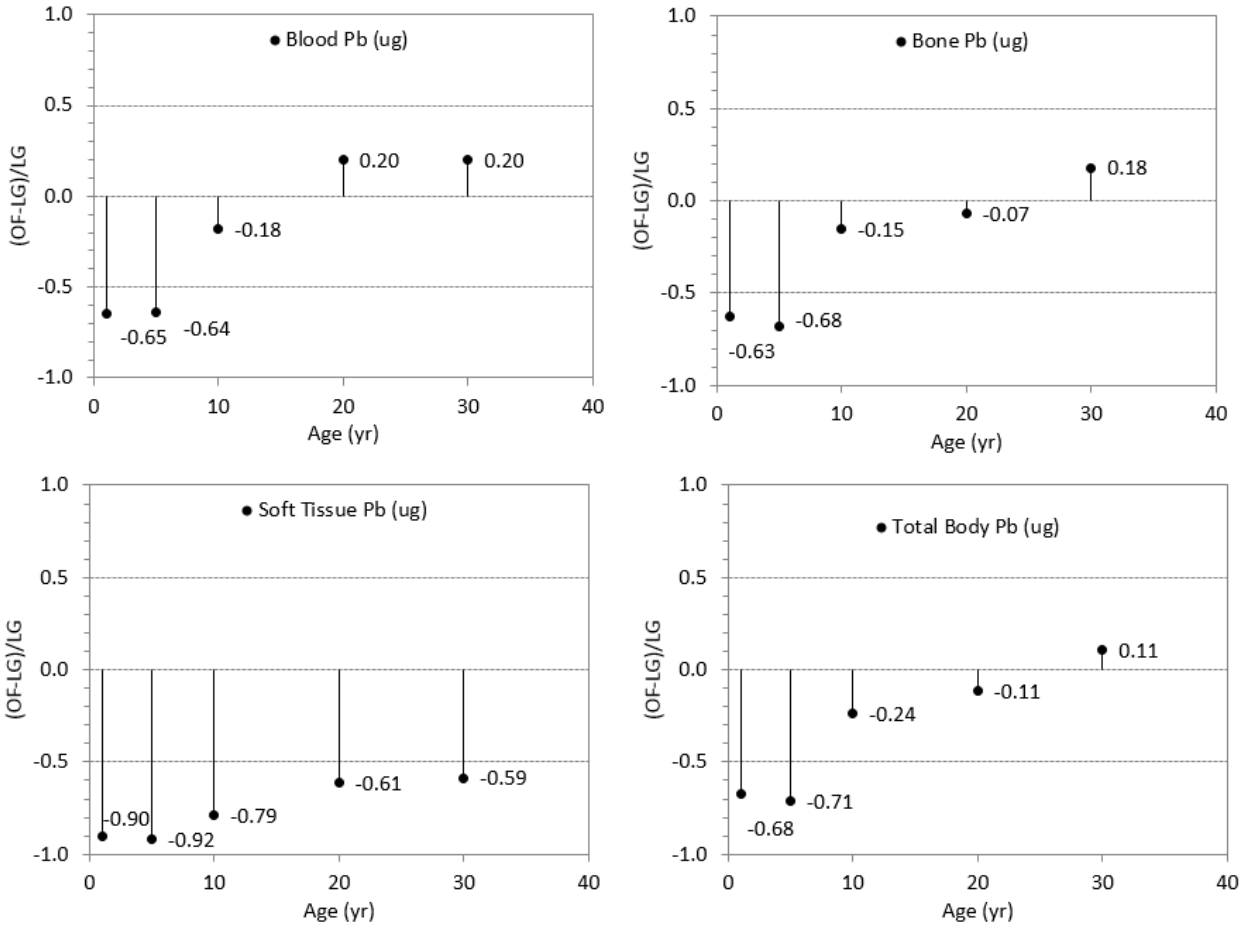

Differences are expressed relative to the estimation from AALM-LG.

FIGURE 4-8. COMPARISON OF CUMULATIVE URINARY AND FECAL PB EXCRETION (µG) LEVELS ESTIMATED FROM AALM-OF AND AALM-LG FOR A CONSTANT INGESTION OF 5 µG PB/DAY FOR AGES 0 TO 30 YEARS.

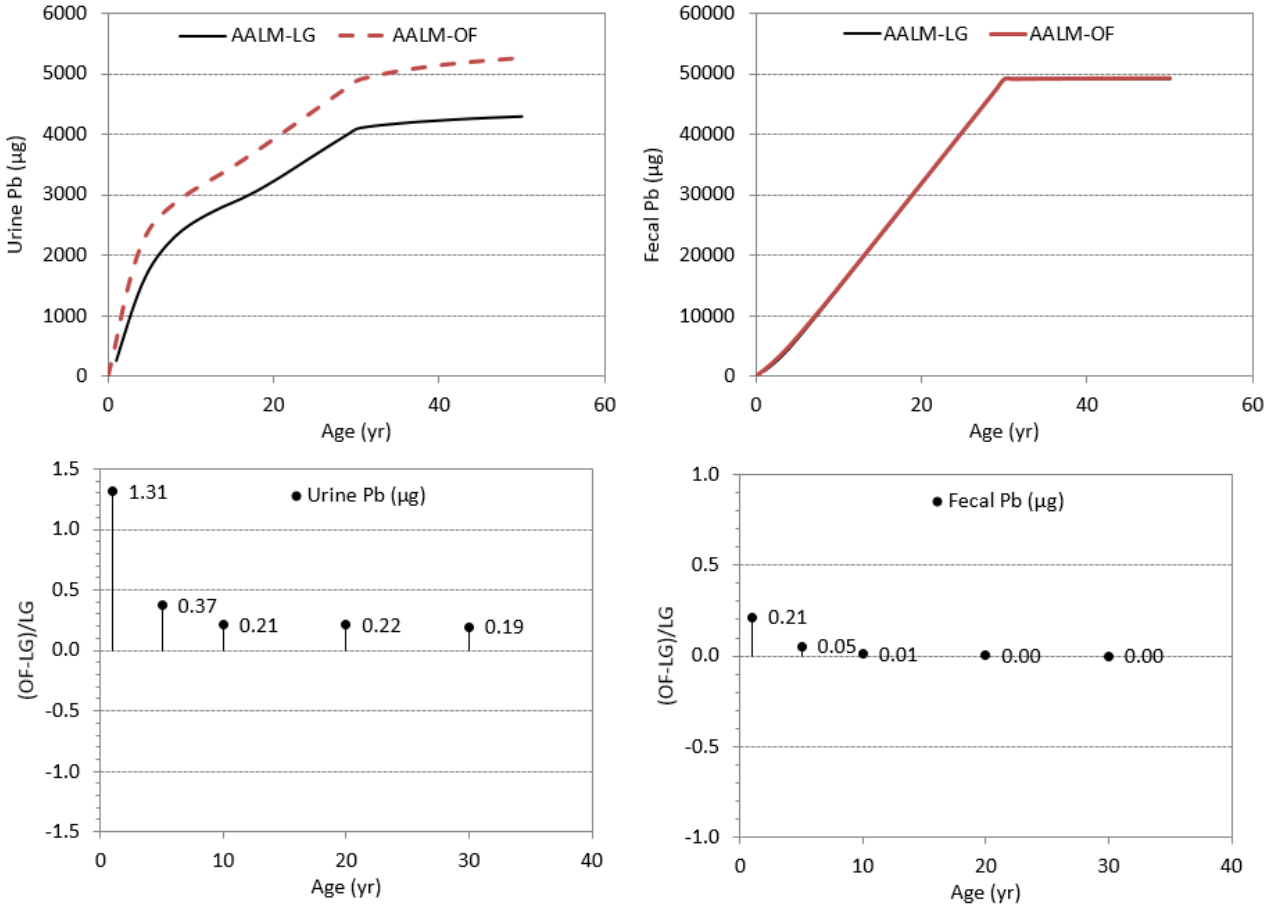

FIGURE 4-9. DECLINE IN PB LEVELS FOLLOWING CESSATION OF EXPOSURE ESTIMATED FROM AALM-LG AND AALM-OF FOR AGES 5 AND 30 YEARS.

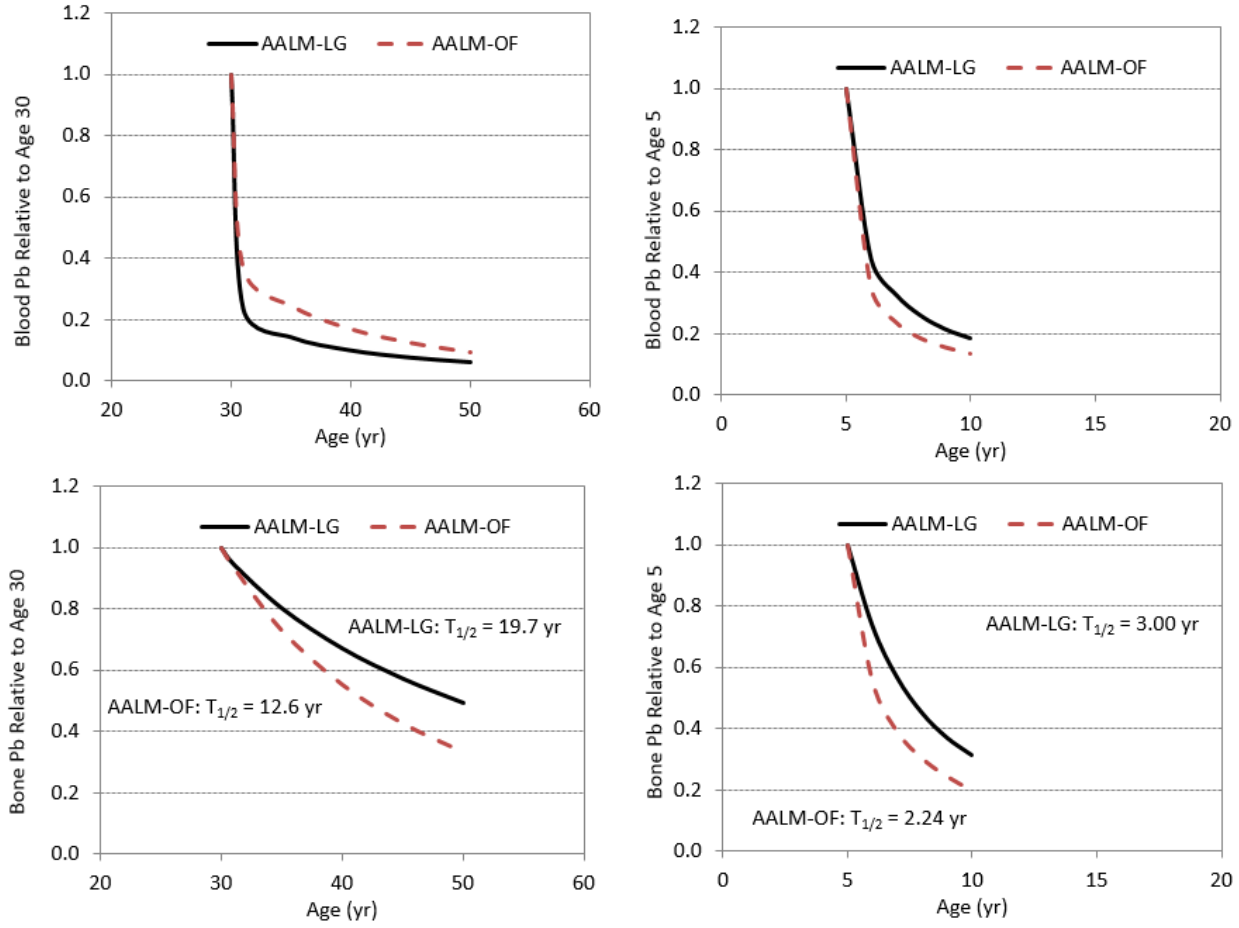

Half-times are based on applying a single exponential model to the estimated time series (i.e., $Pb_{t=i} = Pb_{t=0} \times e^{-kt}$). The decline in blood Pb has multiple rates. In adults, the half-time for the first 50 days following cessation of exposure is approximately 36 days in AALM-LG and 46 days in AALM-OF. The half-time for the period 5–20 years following cessation of exposure is 12.7 years in AALM-LG and 10.9 years in AALM-OF.

FIGURE 4-10. COMPARISON OF PB CONCENTRATIONS ESTIMATED FROM AALM-LG AND AALM-OF FOR A CONSTANT INGESTION OF 5 µG PB/DAY FOR AGES 0 TO 30 YEARS.

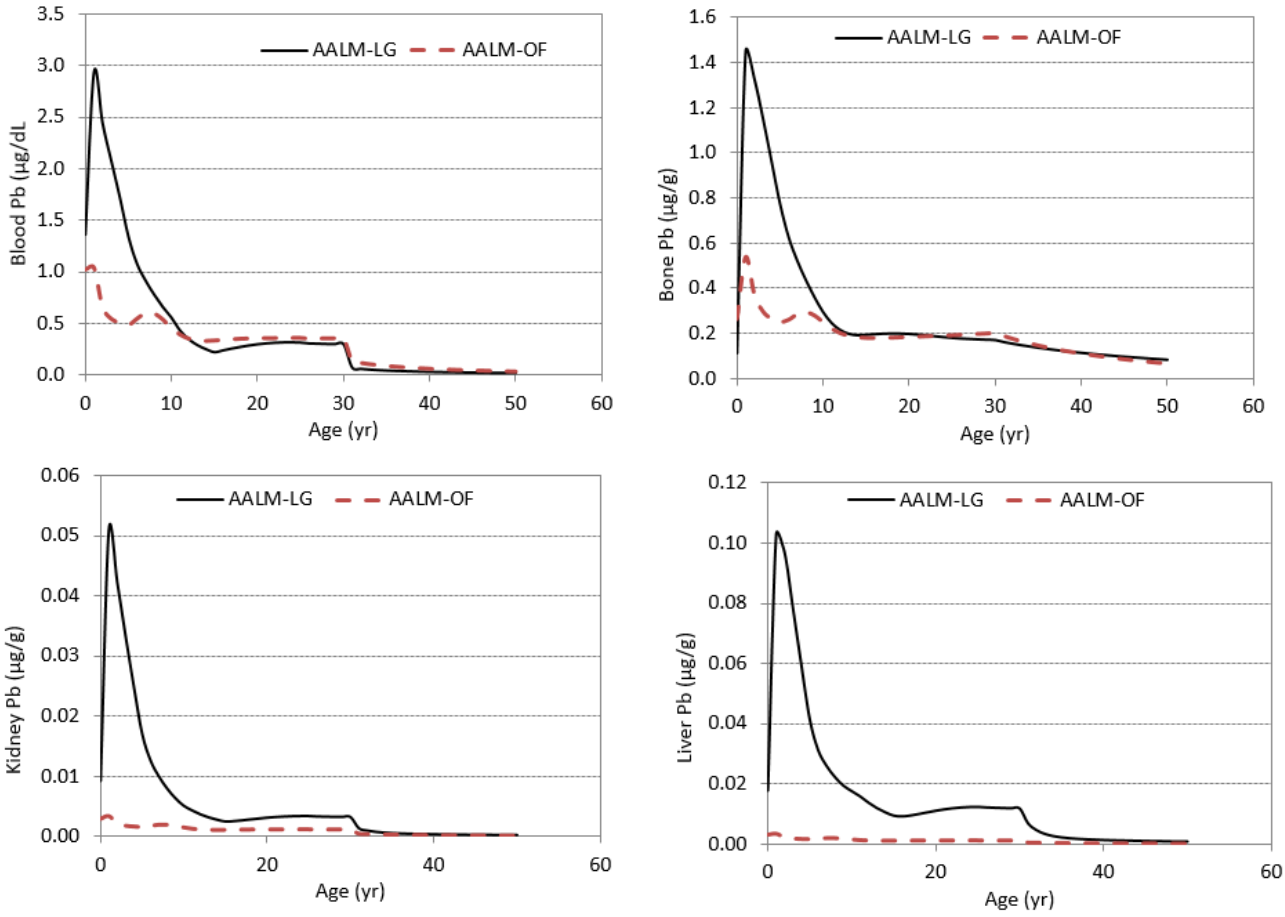

FIGURE 4-11. DOSE-RESPONSE RELATIONSHIP FOR PB LEVELS AT AGE 5 YEARS ESTIMATED FROM AALM-LG AND AALM-OF.

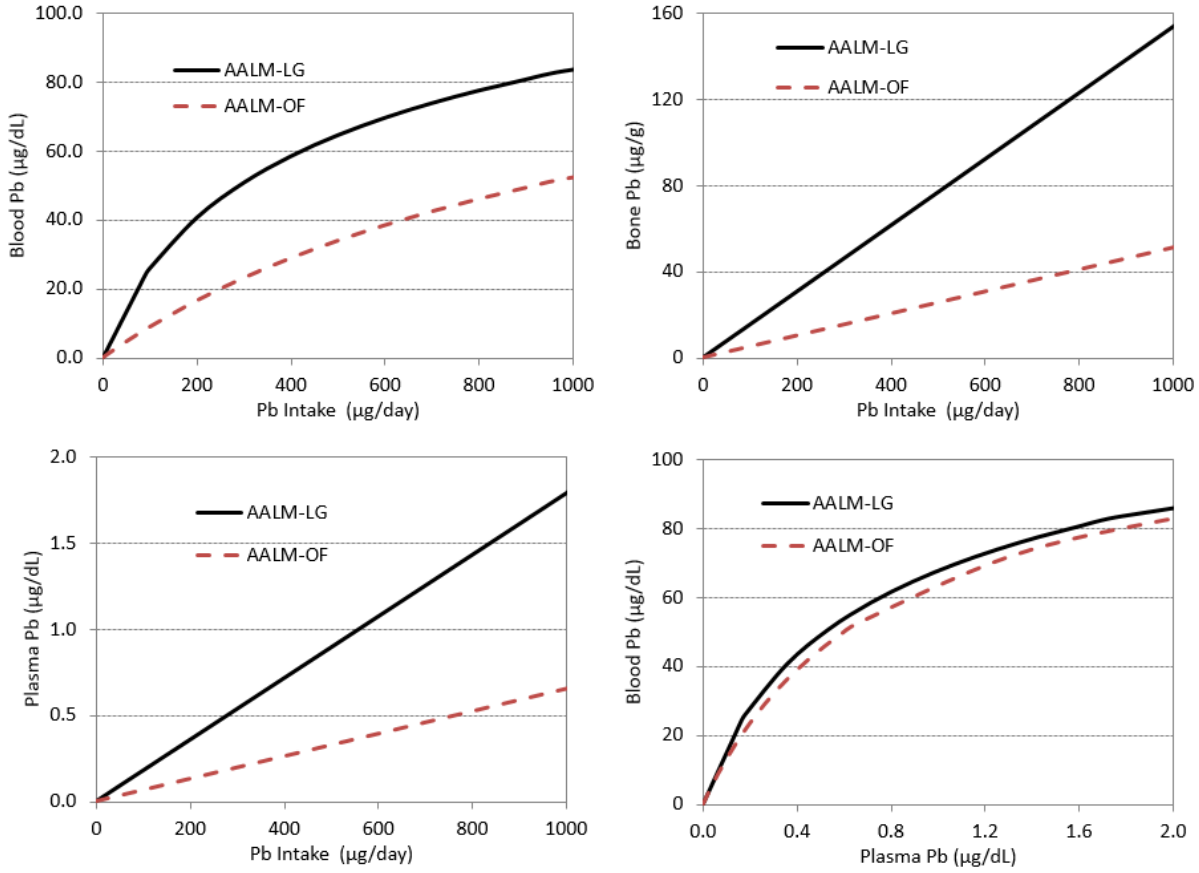

FIGURE 4-12. DOSE-RESPONSE RELATIONSHIP FOR PB LEVELS AT AGE 30 YEARS ESTIMATED FROM AALM-LG AND AALM-OF.

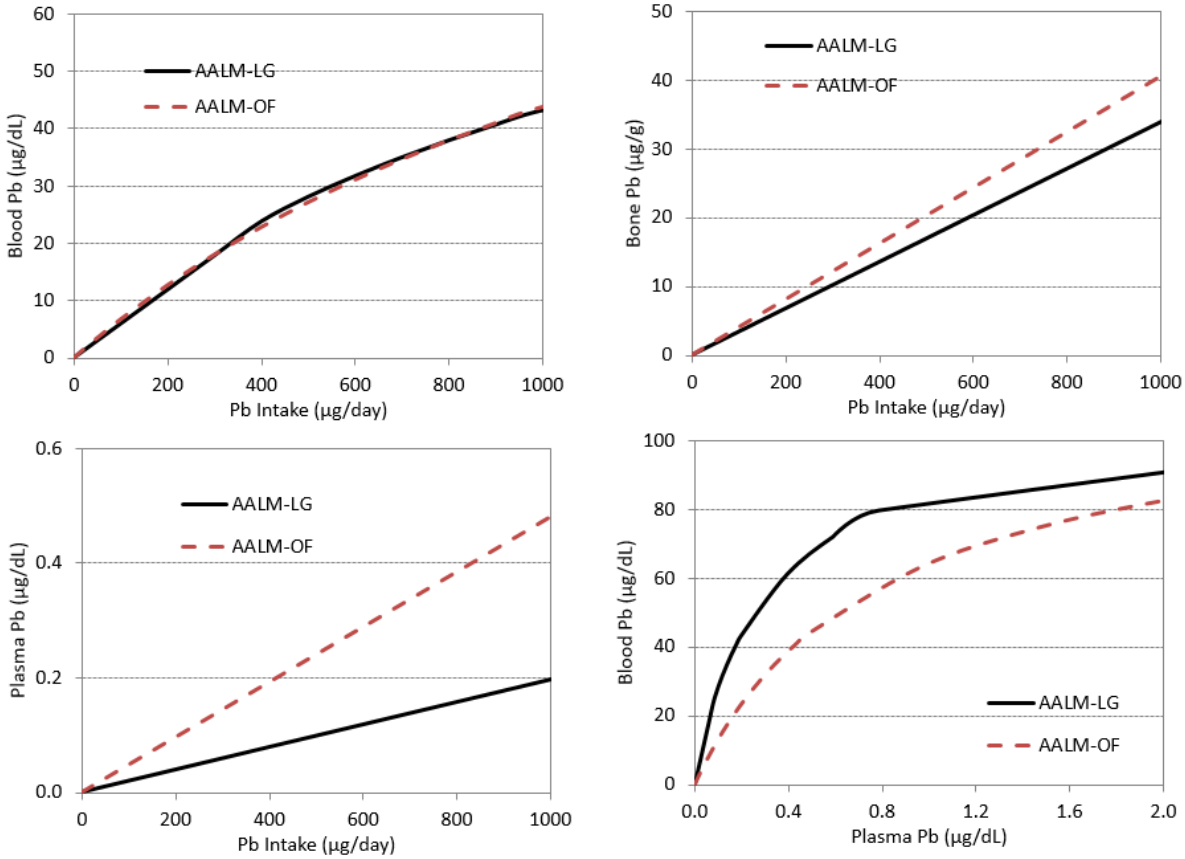

FIGURE 4-13. GASTROINTESTINAL ABSORPTION OF PB IN THE O'FLAHERTY MODEL (OF) AND LEGGETT MODEL (OF) AND AALM, OPTIMIZED TO (RYU ET AL., 1983).

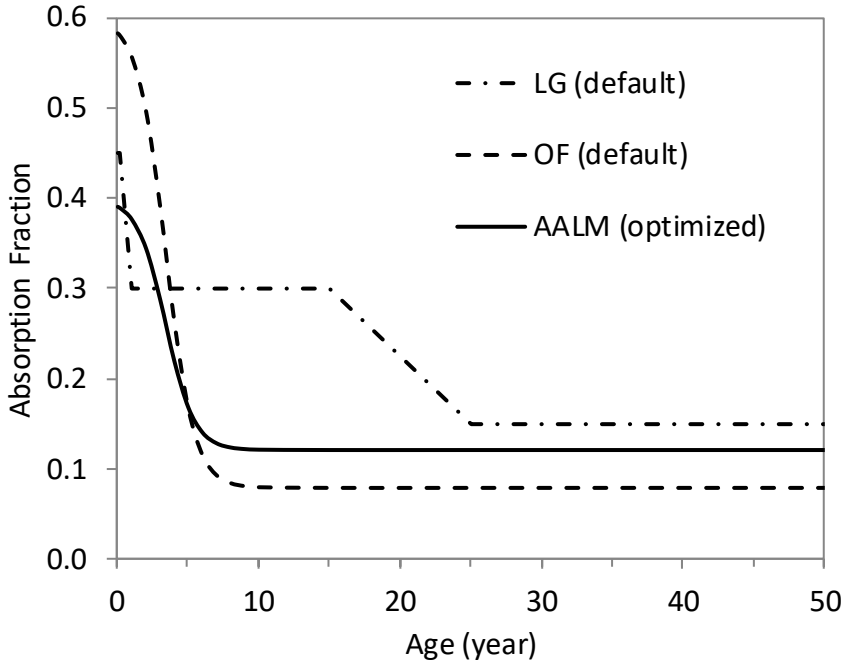

FIGURE 4-14. BODY AND TISSUE GROWTH IN AALM.

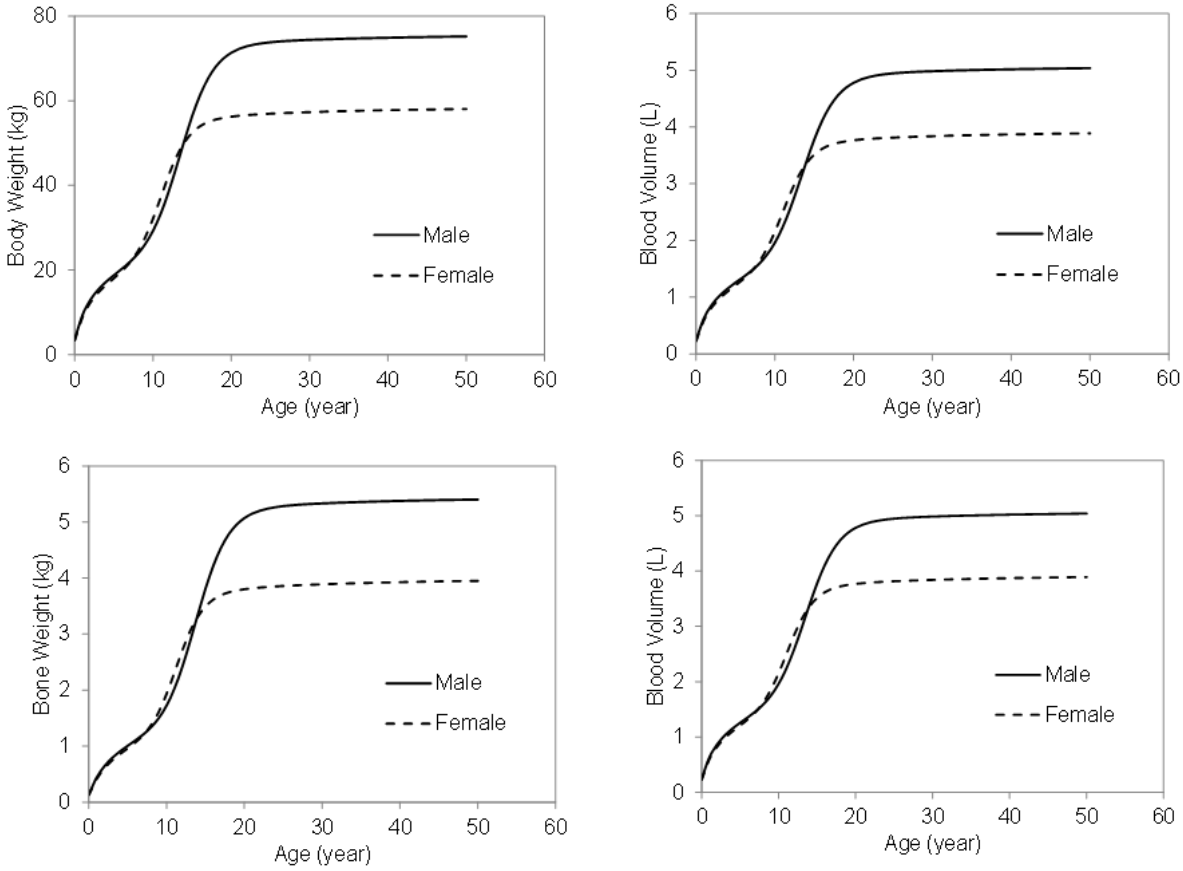

FIGURE 4-15. SIMULATION OF WHOLE BLOOD AND PLASMA PB IN ADULTS (SMITH ET AL., 2002; BERGDAHL ET AL., 1999; BERGDAHL ET AL., 1998; HERNÁNDEZ-AVILA ET AL., 1998; BERGDAHL ET AL., 1997; SCHÜTZ ET AL., 1996).

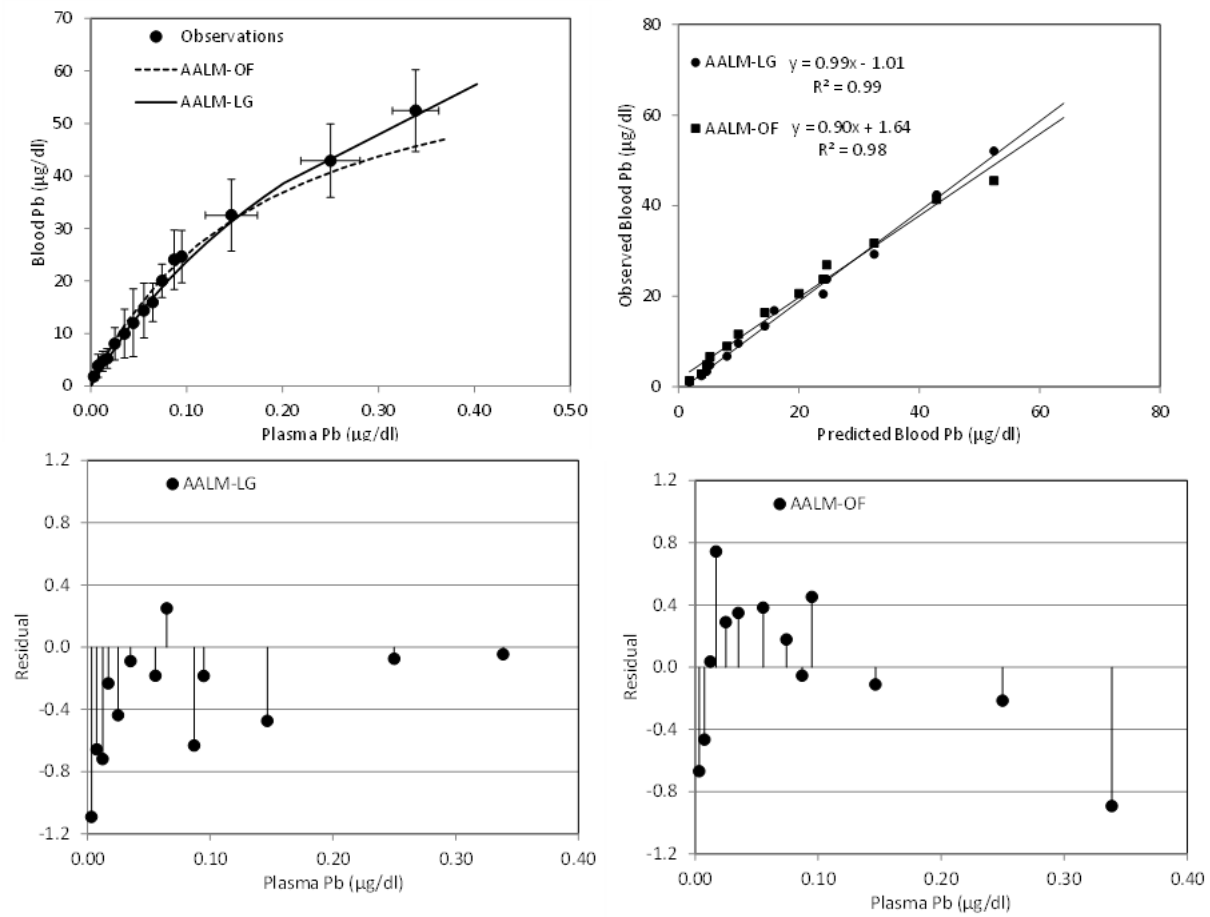

Combined data for individuals (N = 406) from all studies were quantized into ranges of plasma Pb; shown are mean and standard deviations for ranges. Upper right panel shows linear regression for predicted and observed blood Pb concentrations. Lower panels show residuals for estimations ([predicted-observed]/standard deviation).

FIGURE 4-16. SIMULATION OF PLASMA-TO-URINE CLEARANCE.

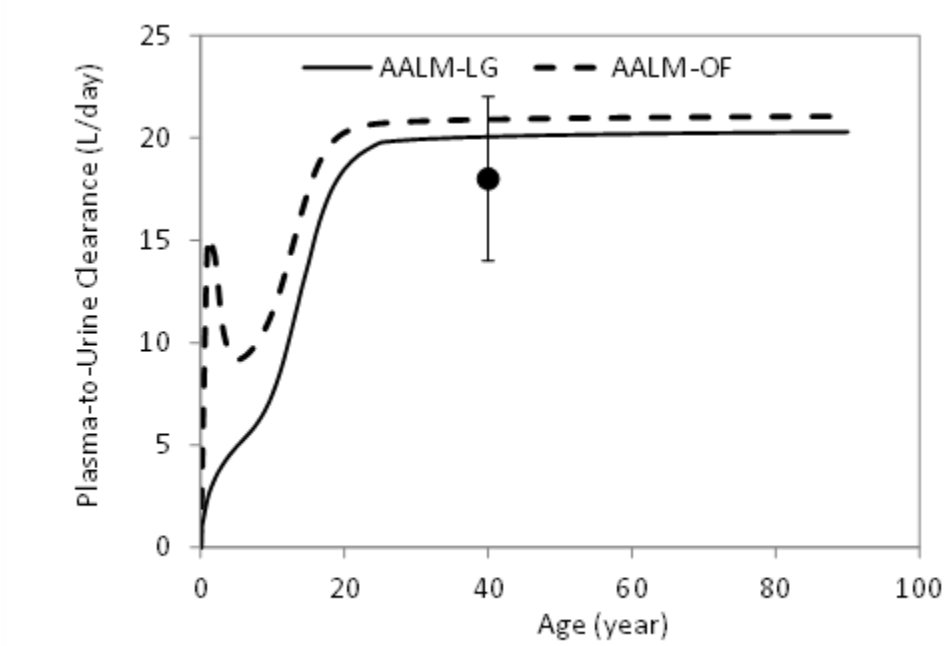

Data point is mean and standard deviation for four estimates based on 32 (normal) adults (Araki et al., 1986; Manton and Cook, 1984; Manton and Malloy, 1983; Chamberlain et al., 1978).

FIGURE 4-17. SIMULATION OF POST-MORTEM SOFT TISSUE/TIBIA PB RATIOS.

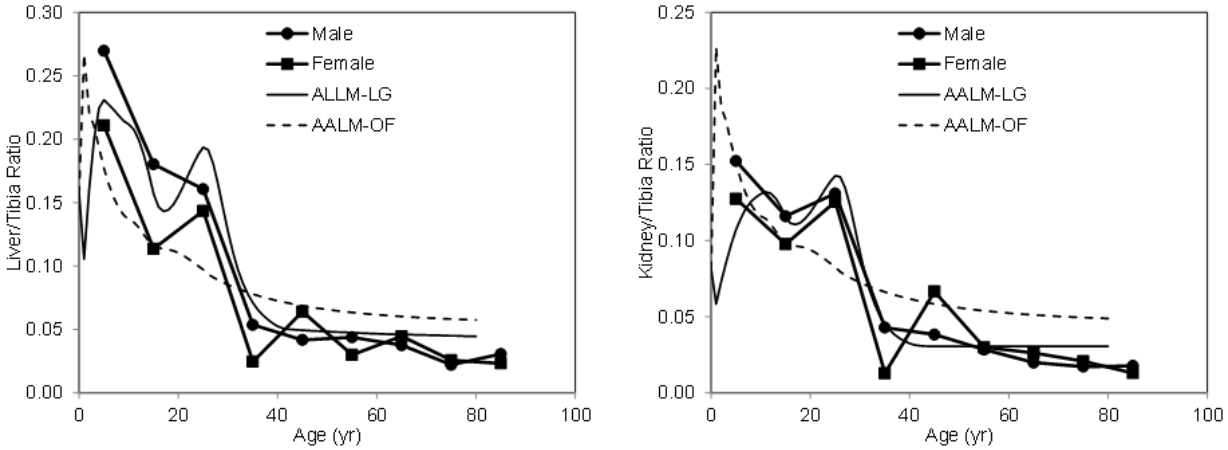

Shown are group means for kidney (n = 8) and for liver (n = 9), based on Barry (1975).

FIGURE 4-18. SIMULATION OF PLASMA PB/BONE PB RATIO IN ADULTS.

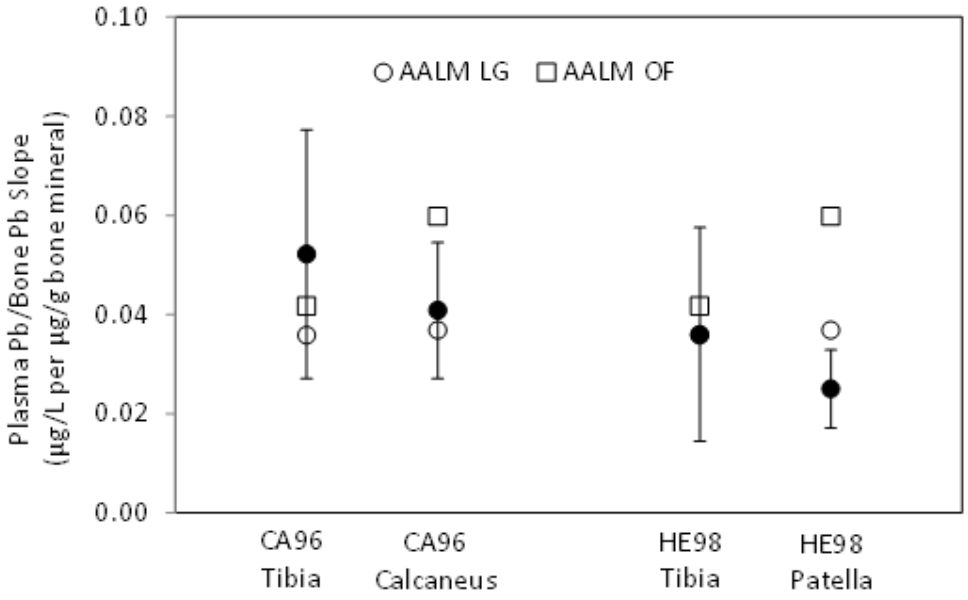

Observations are means and 95% CIs, based onCA96, Cake et al. (1996); and HE98, Hernández-Avila et al. (1998).

FIGURE 4-19. SIMULATION OF ELIMINATION KINETICS OF PB FROM BLOOD (LEFT PANEL) AND BONE (RIGHT PANEL).

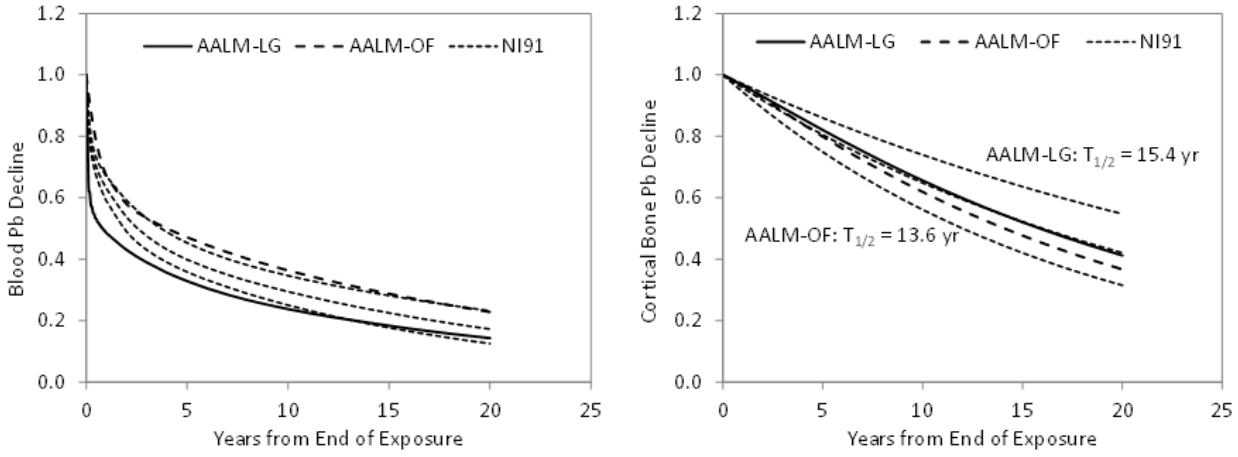

Dotted lines show the elimination from based on the median and upper and lower 95% confidence limits of the tri-exponential model retired Pb workers (n = 14, median age 60 years at time of retirement) reported in Nilsson et al. (1991).

FIGURE 4-20. COMPARISON OF OBSERVED AND ESTIMATED BLOOD PB CONCENTRATIONS IN INDIVIDUALS WHO RECEIVED INGESTION DOSES OF [202PB]-NITRATE (RABINOWITZ ET AL., 1976).

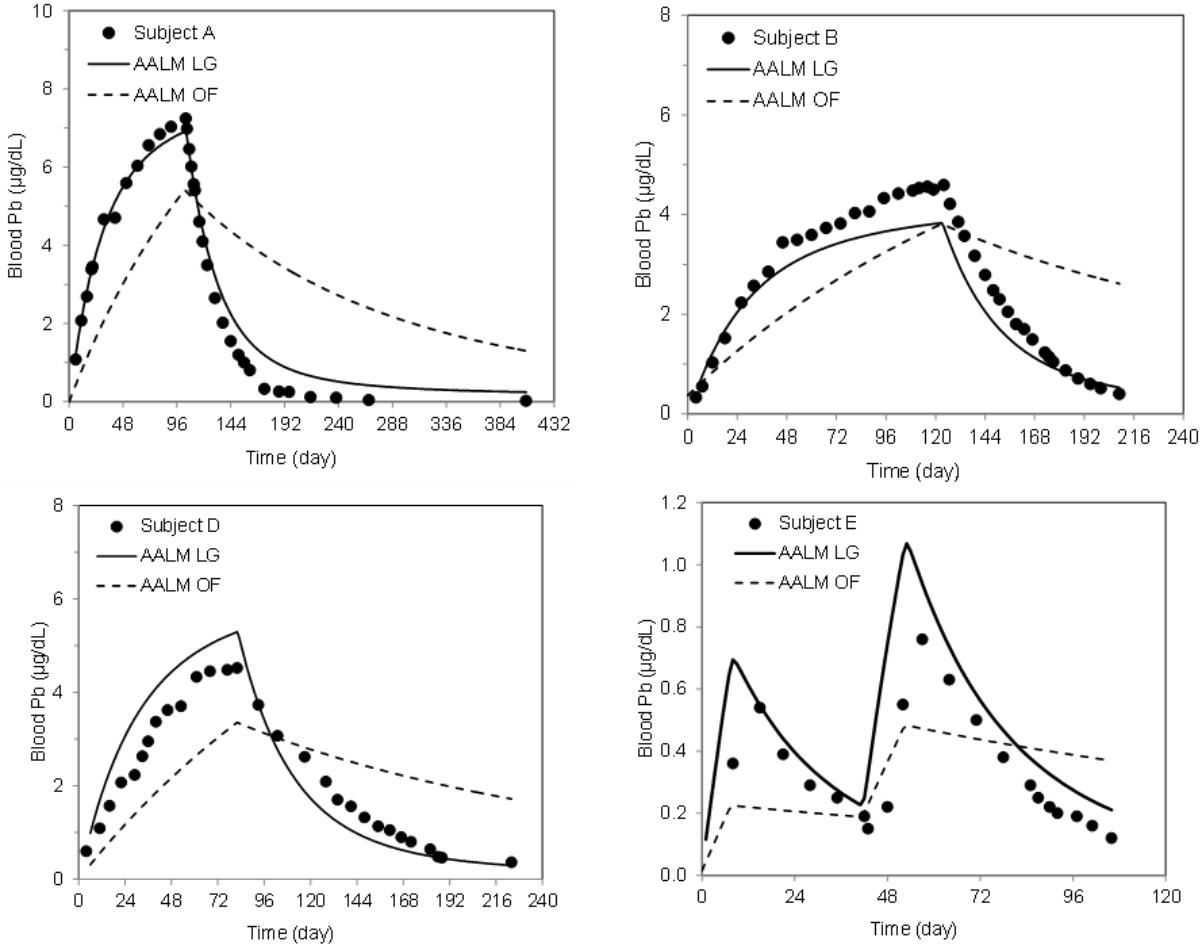

Subject A received 204 µg/day for 104 days, Subject B received 185 µg/day for 124 days, Subject D received 105 µg/day for 83 days, and Subject E received 99 µg/day for on days 1–8 and days 42–51. Estimated absorption fractions were 8.5% for Subject A, 6.5% for Subject B, 10.9% for Subject D and 9.1% for Subject E.

FIGURE 4-21. SIMULATION OF FORMULA-FED INFANTS FROM (RYU ET AL., 1983).

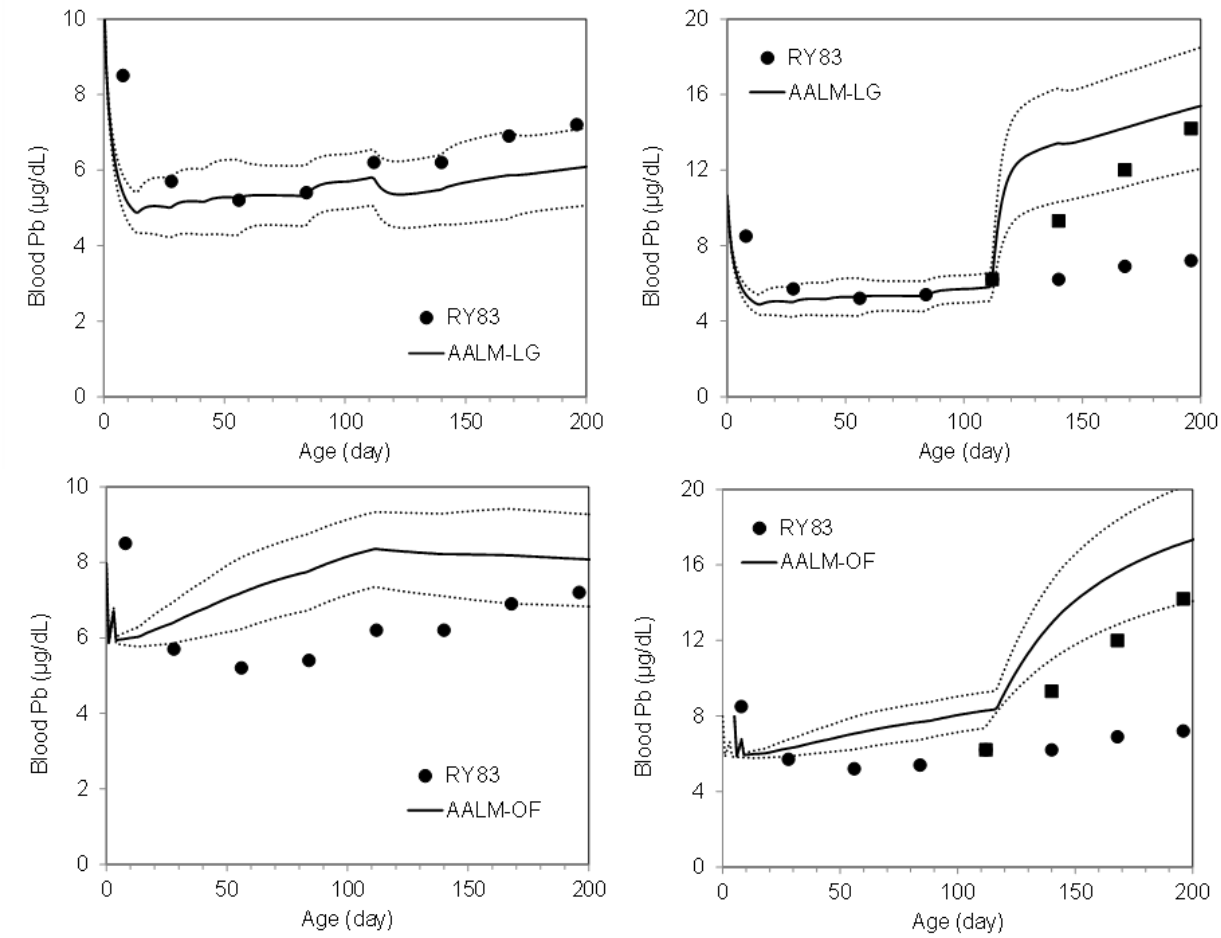

Data in left panels are from 25 infants fed formula from cartons (12–20 µg/day) from age 8–196 days. Data in right panels are show a subset (n = 7) that were switched to formula from cans at age 112 days (60–63 µg/day). Solid lines show simulations of the mean Pb intakes; dotted lines show simulations of ±1 SD of mean intakes.

FIGURE 4-22. SIMULATION OF FORMULA-FED INFANTS (N = 131, AGE 91 DAYS) FROM (SHERLOCK AND QUINN, 1986).

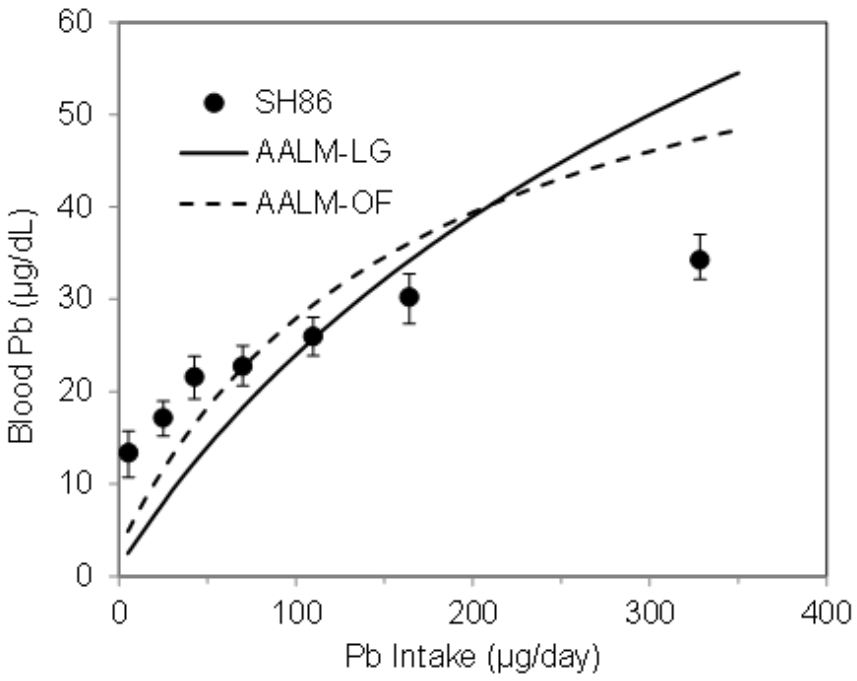

Blood Pb were measured and Pb intakes were estimated from duplicate diets assessed at age 91 days.

FIGURE 4-23. COMPARISON OF INITIAL AND OPTIMIZED AALM-LG AND AALM-OF MODELS FOR CONTINUOUS PB INTAKE OF 5 µG/DAY.

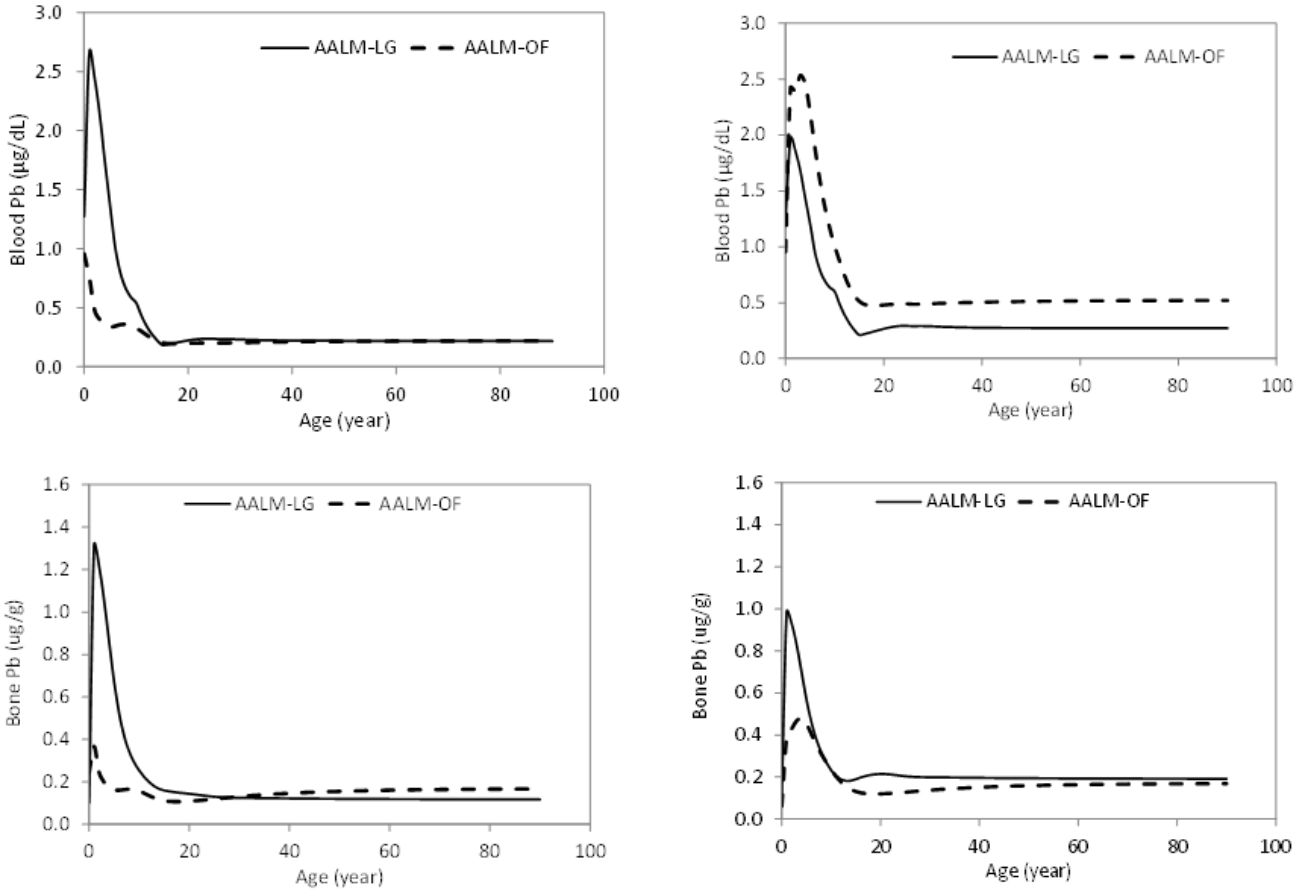

Right panels show optimized models.

FIGURE 4-24. COMPARISON OF INITIAL AND OPTIMIZED AALM-LG AND AALM-OF MODELS FOR CONTINUOUS PB INTAKE OF 5 µG/DAY.

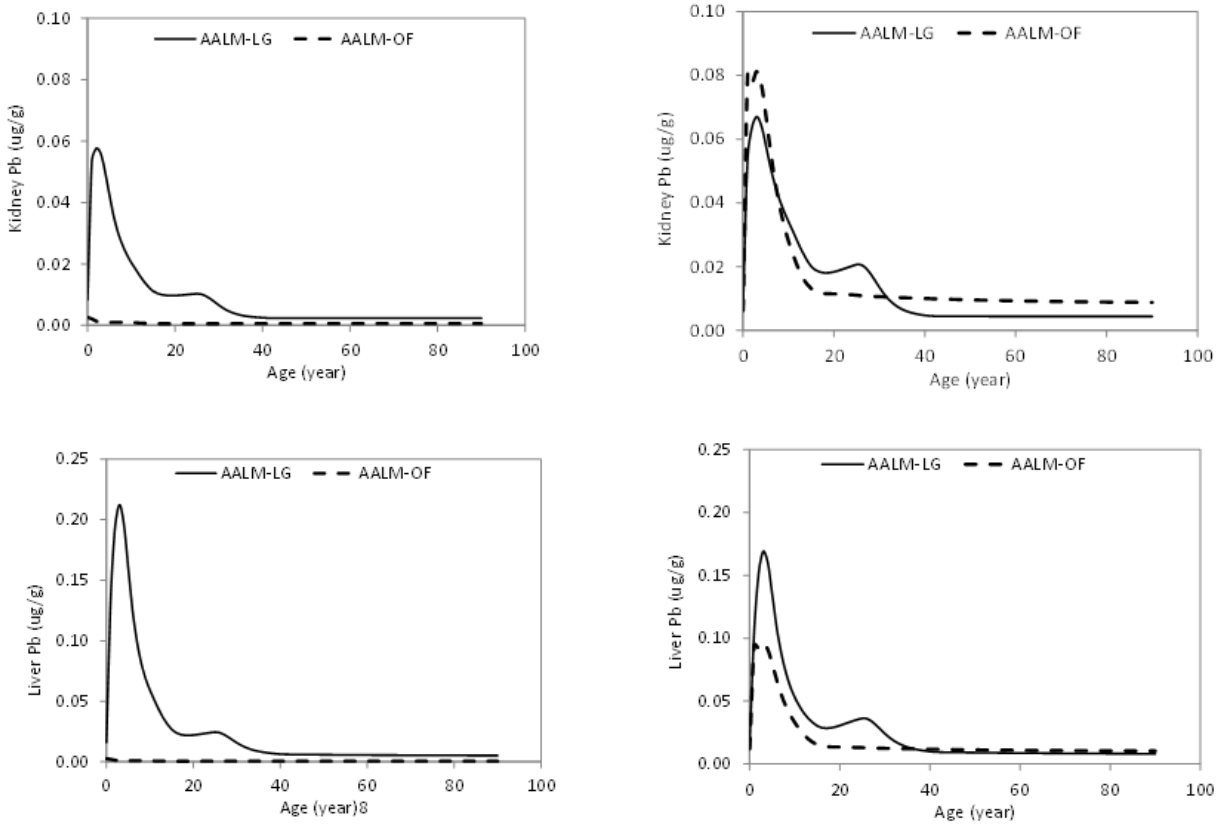

Right panels show optimized models.

FIGURE 4-25. COMPARISON OF BLOOD PB ESTIMATIONS OF AALM AND IEUBK MODEL.

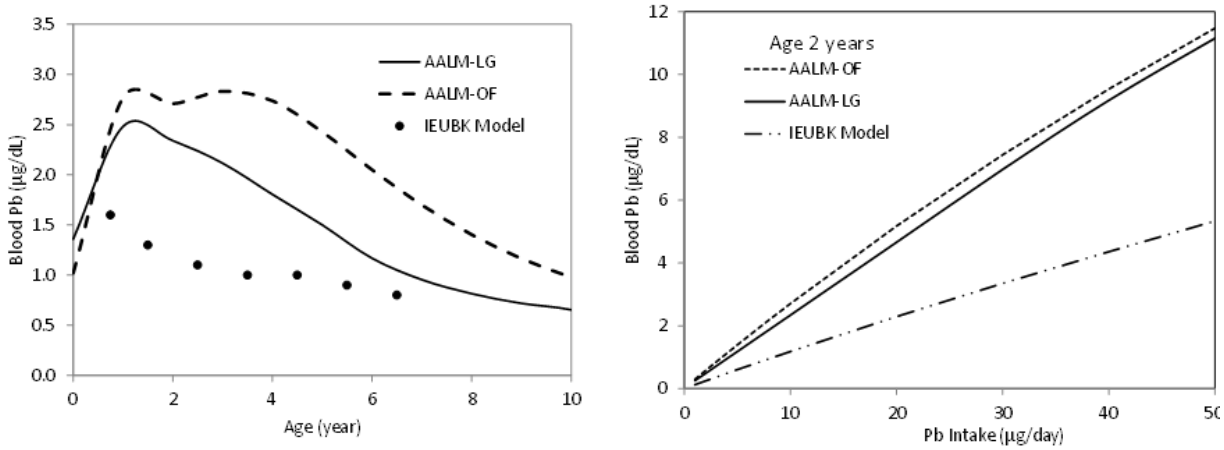

Left panel shows simulations of continuous intake of 10 µg Pb/day in dust. Right panel shows relationship between dust Pb intake and blood Pb concentration at 2 years of age. In both models, the RBA for Pb in dust was assumed to be 60%. This corresponds to an absolute bioavailability of approximately 20% at age 2 years in the AALM and 30% in the IEUBK model.

FIGURE 4-26. COMPARISON OF BLOOD PB ESTIMATIONS OF AALM AND IEUBK MODEL AFTER ADJUSTMENT OF RED BLOOD CELL PARAMETERS (RRBC IN AALM-LG, KBIND IN AALM-OF).

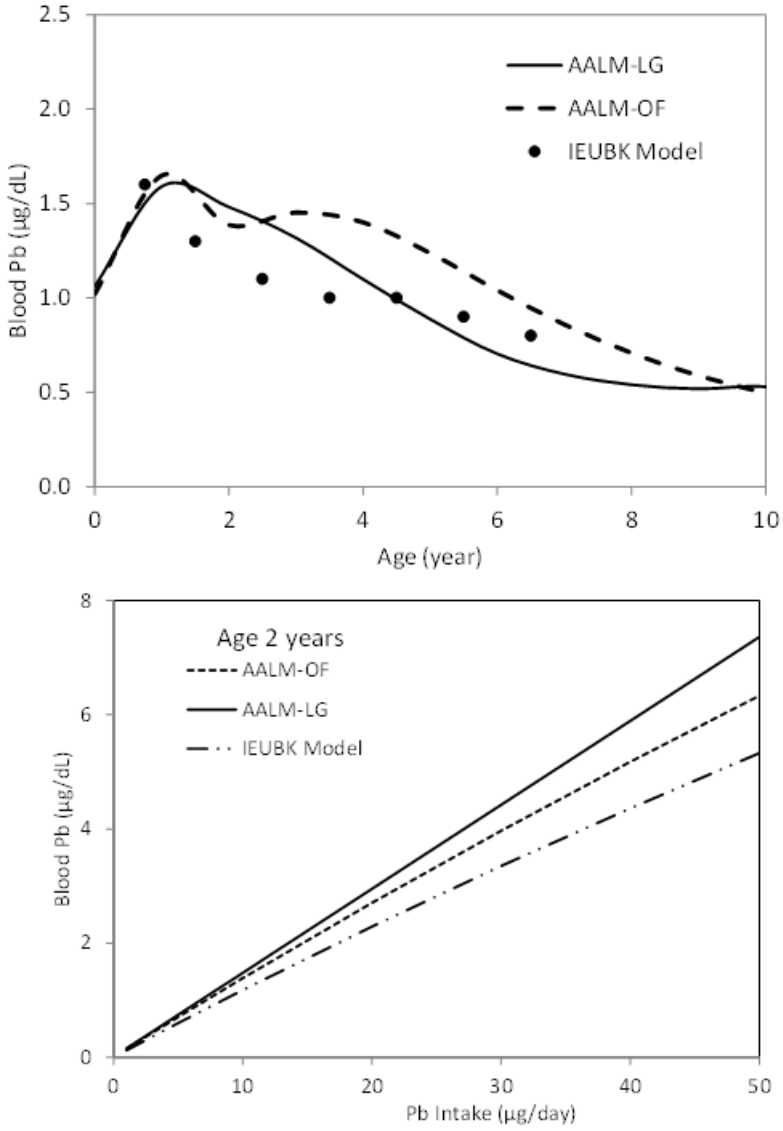

Upper panel shows simulations of continuous intake of 10 µg Pb/day in dust. Lower panel shows relationship between dust Pb intake and blood Pb concentration at 2 years of age. In both models, the RBA for Pb in dust was assumed to be 60%. This corresponds to an absolute bioavailability of approximately 20% at age 2 years in the AALM and 30% in the IEUBK model.

FIGURE 4-27. SIMULATION OF FORMULA-FED INFANTS FROM (RYU ET AL., 1983) AFTER ADJUSTMENT OF RED BLOOD CELL (RRBC IN AALM-LG, KBIND IN AALM-OF).

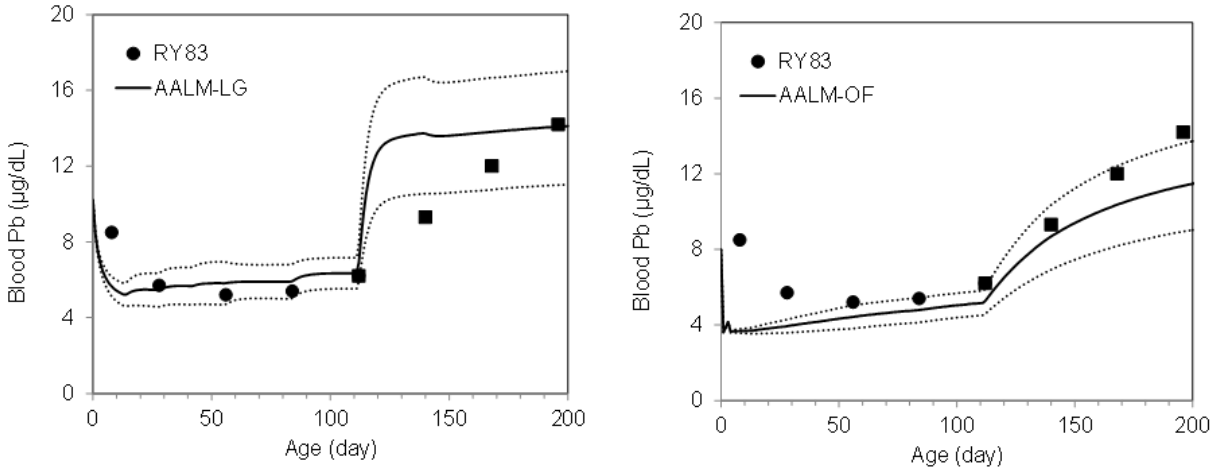

Data in left panels are from 25 infants fed formula from cartons (12–20 µg/day) from age 8–196 days (closed circles) and then a subset (n = 7) that were switched to formula from cans at age 112 days (60–63 µg/day, closed squares). Solid lines show simulations of the mean Pb intakes; dotted lines show simulations of ±1 SD of mean intakes.

FIGURE 4-28. SIMULATION OF FORMULA-FED INFANTS (N = 131, AGE 91 DAYS) FROM (SHERLOCK AND QUINN, 1986) AFTER ADJUSTMENT OF RED BLOOD CELL (RRBC IN AALM-LG, KBIND IN AALM-OF).

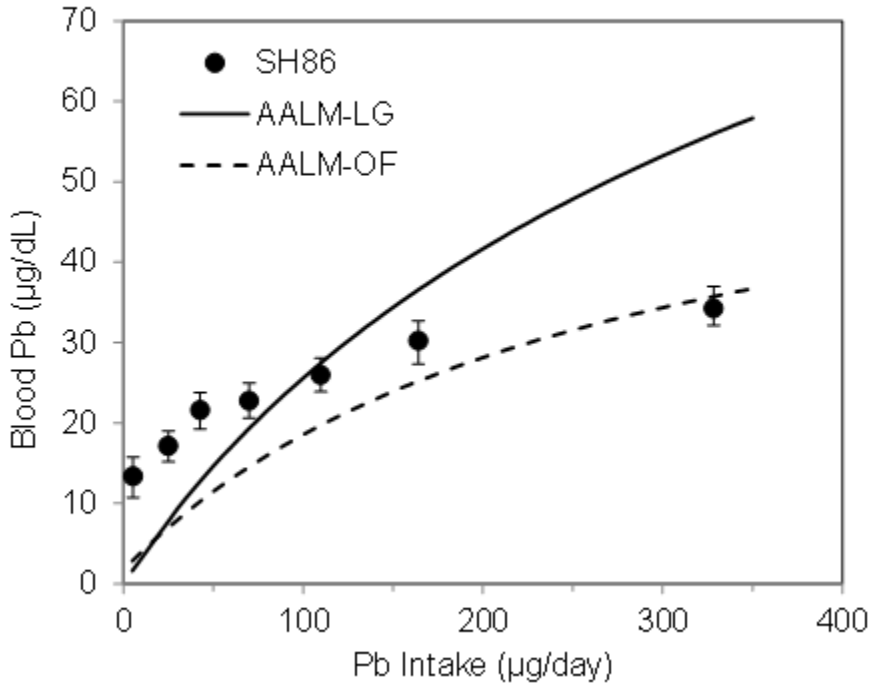

Blood Pb were measured and Pb intakes were estimated from duplicate diets assessed at age 91 days.

5. REFERENCES

Alexander, FW; Clayton, BE; Delves, HT. (1974). Mineral and trace-metal balances in children receiving normal and synthetic diets. Q J Med 43: 89-111. http://dx.doi.org/10.1093/oxfordjournals.qjmed.a067380.

Amaral, JH; Rezende, VB; Quintana, SM; Gerlach, RF; Barbosa, F, Jr.; Tanus-Santos, JE. (2010). The relationship between blood and serum lead levels in peripartum women and their respective umbilical cords. Basic Clin Pharmacol Toxicol 107: 971-975. http://dx.doi.org/10.1111/j.1742-7843.2010.00616.x.

Araki, S; Aono, H; Yokoyama, K; Murata, K. (1986). Filterable plasma concentration, glomerular filtration, tubular balance, and renal clearance of heavy metals and organic substances in metal workers. Arch Environ Occup Health 41: 216-221. http://dx.doi.org/10.1080/00039896.1986.9938336.

Baeyens, W; Vrijens, J; Gao, Y; Croes, K; Schoeters, G; Hond, ED; Sioen, I; Bruckers, L; Nawrot, T; Nelen, V; Van Den Mieroop, E; Morrens, B; Loots, I; Van Larebeke, N; Leermakers, M. (2014). Trace metals in blood and urine of newborn/mother pairs, adolescents and adults of the Flemish population (2007-2011). Int J Hyg Environ Health 217: 878-890. http://dx.doi.org/10.1016/j.ijheh.2014.06.007.

Bannon, DI; Drexler, JW; Fent, GM; Casteel, SW; Hunter, PJ; Brattin, WJ; Major, MA. (2009). Evaluation of small arms range soils for metal contamination and lead bioavailability. Environ Sci Technol 43: 9071-9076. http://dx.doi.org/10.1021/es901834h.

Baranowska-Bosiacka, I; Listos, J; Gutowska, I; Machoy-Mokrzyńska, A; Kolasa-Wołosiuk, A; Tarnowski, M; Puchałowicz, K; Prokopowicz, A; Talarek, S; Listos, P; Wąsik, A; Chlubek, D. (2016). Effects of perinatal exposure to lead (Pb) on purine receptor expression in the brain and gliosis in rats tolerant to morphine analgesia. Toxicology 339: 19-33. http://dx.doi.org/10.1016/j.tox.2015.10.003.

Barry, PS. (1975). A comparison of concentrations of lead in human tissues. Occup Environ Med 32: 119-139. http://dx.doi.org/10.1136/oem.32.2.119.

Barry, PSI. (1981). Concentrations of lead in the tissues of children. Br J Ind Med 38: 61-71.

Bergdahl, IA; Schütz, A; Gerhardsson, L; Jensen, A; Skerfving, S. (1997). Lead concentrations in human plasma, urine and whole blood. Scand J Work Environ Health 23: 359-363. http://dx.doi.org/10.5271/sjweh.232.

Bergdahl, IA; Sheveleva, M; Schütz, A; Artamonova, VG; Skerfving, S. (1998). Plasma and blood lead in humans: Capacity-limited binding to delta-aminolevulinic acid dehydratase and other lead-binding components. Toxicol Sci 46: 247-253. http://dx.doi.org/10.1093/toxsci/46.2.247.

Bergdahl, IA; Vahter, M; Counter, SA; Schütz, A; Buchanan, LH; Ortega, F; Laurell, G; Skerfving, S. (1999). Lead in plasma and whole blood from lead-exposed children. Environ Res 80: 25-33. http://dx.doi.org/10.1006/enrs.1998.3880.

Bevington, C; Gardner, HD; Cohen, J; Henning, C; Rasmussen, PE. (2021). Relationship between residential dust-lead loading and dust-lead concentration across multiple North American datasets. Build Environ 188: 107359. http://dx.doi.org/10.1016/j.buildenv.2020.107359.

Bolton, JB. (2004). Issuance of OMB's "Final Information Quality Bulletin for Peer Review" [Memorandum]. (M-05-03). Washington, DC: U.S. Office of Management and Budget, Executive Office of the President. https://www.whitehouse.gov/sites/whitehouse.gov/files/omb/memoranda/2005/m05-03.pdf.

Booker, DV; Chamberlain, AC; Newton, D; Stott, ANB. (1969). Uptake of radioactive lead following inhalation and injection. Br J Radiol 42: 457-466. http://dx.doi.org/10.1259/0007-1285-42-498-457.

Bornschein, RL; Succop, P; Dietrich, KN; Clark, CS; Que Hee, S; Hammond, PB. (1985). The influence of social and environmental factors on dust lead, hand lead, and blood lead levels in young children. Environ Res 38: 108-118. http://dx.doi.org/10.1016/0013-9351(85)90076-3.

Brochu, P; Ducré-Robitaille, JF; Brodeur, J. (2006). Physiological daily inhalation rates for free-living individuals aged 1 month to 96 years, using data from doubly labeled water measurements: A proposal for air quality criteria, standard calculations and health risk assessment. Hum Ecol Risk Assess 12: 675-701. http://dx.doi.org/10.1080/10807030600801550.

Brown, JS; Diamond, GL. (2023). Derivation of first-order dissolution rates to estimate particle clearance and burden in the human respiratory tract. Part Fibre Toxicol 20: 17. http://dx.doi.org/10.1186/s12989-023-00523-z.

Cake, KM; Bowins, RJ; Vaillancourt, C; Gordon, CL; McNutt, RH; Laporte, R; Webber, CE; Chettle, DR. (1996). Partition of circulating lead between serum and red cells is different for internal and external sources of lead. Am J Ind Med 29: 440-445. http://dx.doi.org/10.1002/(SICI)1097-0274(199605)29:5<440::AID-AJIM2>3.0.CO;2-Q.

CalEpa. (2013). Estimating workplace air and worker blood lead concentration using an updated physiologically-based pharmacokinetics (PBPK) model. Sacramento, CA. https://oehha.ca.gov/air/document/estimating-workplace-air-and-worker-blood-lead-concentration-using-updated-pbpk-model.

Campbell, BC; Meredith, PA; Moore, MR; Watson, WS. (1984). Kinetics of lead following intravenous administration in man. Toxicol Lett 21: 231-235.

Carbone, R; Laforgia, N; Crollo, E; Mautone, A; Iolascon, A. (1998). Maternal and neonatal lead exposure in southern Italy. Neonatology 73: 362-366. http://dx.doi.org/10.1159/000013998.

Casteel, SW; Weis, CP; Henningsen, GM; Brattin, WJ. (2006). Estimation of relative bioavailability of lead in soil and soil-like materials using young swine. Environ Health Perspect 114: 1162-1171. http://dx.doi.org/10.1289/ehp.8852.

CDC. (2013). Fourth national report on human exposure to environmental chemicals, updated tables, September 2013. (CS244702-A). Atlanta, GA. http://www.cdc.gov/exposurereport/pdf/FourthReport_UpdatedTables_Sep2013.pdf.

Chamberlain, AC. (1985). Prediction of response of blood lead to airborne and dietary lead from volunteer experiments with lead isotopes. 224: 149-182. http://dx.doi.org/10.1098/rspb.1985.0027.

Chamberlain, AC; Heard, MJ; Little, P; Newton, D; Wells, AC; Wiffin, RD. (1978). Investigations into lead from motor vehicles. (AERE-R9198). Berkshire, England: Transportation and Road Research Laboratory.

Chen, Z; Myers, R; Wei, T; Bind, E; Kassim, P; Wang, G; Ji, Y; Hong, X; Caruso, D; Bartell, T; Gong, Y; Strickland, P; Navas-Acien, A; Guallar, E; Wang, X. (2014). Placental transfer and concentrations of cadmium, mercury, lead, and selenium in mothers, newborns, and young children. J Expo Sci Environ Epidemiol 24: 537-544. http://dx.doi.org/10.1038/jes.2014.26.

Cho, SH; Richmond-Bryant, J; Thornburg, J; Portzer, J; Vanderpool, R; Cavender, K; Rice, J. (2011). A literature review of concentrations and size distributions of ambient airborne Pb-containing particulate matter. Atmos Environ 45: 5005-5015. http://dx.doi.org/10.1016/j.atmosenv.2011.05.009.

Clayton, CA; Pellizzari, ED; Whitmore, RW; Perritt, RL; Quackenboss, JJ. (1999). National Human Exposure Assessment Survey (NHEXAS): Distributions and associations of lead, arsenic, and volatile organic compounds in EPA Region 5. J Expo Anal Environ Epidemiol 9: 381-392. http://dx.doi.org/10.1038/sj.jea.7500055.

Clickner, RP; Marker, D; Viet, SM; Rogers, J; Broene, P. (2002). National Survey of Lead and Allergens in Housing. Volume I: Analysis of lead hazards. Final report. Revision 7.1. Washington, DC: U.S. Department of Housing and Urban Development.

Cohen, N; Eisenbud, M; Wrenn, ME. (1970). Radioactivity studies. Volume I. The retention and distribution of 210Pb in the adult baboon. Annual progress report, September 1, 1969-August 31, 1970. (NYO-3086-10(Vol.1); DOE Contract AT(30-1)-3086). New York, NY: New York University, Institute of Environmental Medicine. https://www.osti.gov/biblio/4018237-

radioactivity-studies-volume-retention-distribution-sup-pb-adult-baboon-annual-progress-report-september-august.
Cooper, WC; Tabershaw, IR; Nelson, KW. (1973). Laboratory studies of workers in lead smelting and refining.
Corazziari, E; Cucchiara, S; Staiano, A; Romaniello, G; Tamburrini, O; Torsoli, A; Auricchio, S. (1985). Gastrointestinal transit time, frequency of defecation, and anorectal manometry in healthy and constipated children. J Pediatr 106: 379-382.
deSilva, PE. (1981). Determination of lead in plasma and studies on its relationship to lead in erythrocytes. Br J Ind Med 38: 209-217. http://dx.doi.org/10.1136/oem.38.3.209.
Dewoskin, RS; Thompson, CM. (2008). Renal clearance parameters for PBPK model analysis of early lifestage differences in the disposition of environmental toxicants [Review]. Regul Toxicol Pharmacol 51: 66-86. http://dx.doi.org/10.1016/j.yrtph.2008.02.005.
Diamond, GL. (1992). Review of default value for lead plasma-to-urine transfer coefficient (TPLUR) in the U.S. EPA uptake/biokinetic model. (SRC TR-92-135). Syracuse, NY: Syracuse Research Corporation.
Dixon, SL; Gaitens, JM; Jacobs, DE; Strauss, W; Nagaraja, J; Pivetz, T; Wilson, JW; Ashley, PJ. (2009). Exposure of US children to residential dust lead, 1999-2004: II. The contribution of lead-contaminated dust to children's blood lead levels. Environ Health Perspect 117: 468-474. http://dx.doi.org/10.1289/ehp.11918.
Ettinger, AS; Roy, A; Amarasiriwardena, CJ; Smith, D; Lupoli, N; Mercado-García, A; Lamadrid-Figueroa, H; Tellez-Rojo, MM; Hu, H; Hernández-Avila, M. (2014). Maternal blood, plasma, and breast milk lead: Lactational transfer and contribution to infant exposure. Environ Health Perspect 122: 87-92. http://dx.doi.org/10.1289/ehp.1307187.
Ettinger, AS; Tellez-Rojo, MM; Amarasiriwardena, C; Bellinger, D; Peterson, K; Schwartz, J; Hu, H; Hernandez-Avila, M. (2004). Effect of breast milk lead on infant blood lead levels at 1 month of age. Environ Health Perspect 112: 1381-1385. http://dx.doi.org/10.1289/ehp.6616.
FDA. (2006). Total diet study [Website]. https://www.fda.gov/Food/FoodScienceResearch/TotalDietStudy/default.htm.
FDA. (2007). Total diet study statistics on element results, Revision 4.1, Market baskets 1991–3 through 2004–5.
Gear, CW. (1971). The automatic integration of ordinary differential equations [Magazine]. Association for Computing Machinery Communications, 14, 176-179.
Gerhardsson, L; Englyst, V; Lundström, NG; Nordberg, G; Sandberg, S; Steinvall, F. (1995). Lead in tissues of deceased lead smelter worker. J Trace Elem Med Biol 9: 136-143. http://dx.doi.org/10.1016/S0946-672X(11)80037-4.
Goyer, RA. (1990). Transplacental transport of lead [Review]. Environ Health Perspect 89: 101-105. http://dx.doi.org/10.2307/3430905.
Grandjean, P. (1978). Regional distribution of lead in human brains. Toxicol Lett 2: 65-69. http://dx.doi.org/10.1016/0378-4274(78)90065-6.
Graziano, JH; Popovac, D; Factor-Litvak, P; Shrout, P; Kline, J; Murphy, MJ; Zhao, YH; Mehmeti, A; Ahmedi, X; Rajovic, B; Zvicer, Z; Nenezic, DU; Lolacono, NJ; Stein, Z. (1990). Determinants of elevated blood lead during pregnancy in a population surrounding a lead smelter in Kosovo, Yugoslavia. Environ Health Perspect 89: 95-100. http://dx.doi.org/10.1289/ehp.908995.
Gregus, Z; Klaassen, CD. (1986). Disposition of metals in rats: a comparative study of fecal, urinary, and biliary excretion and tissue distribution of eighteen metals. Toxicol Appl Pharmacol 85: 24-38. http://dx.doi.org/10.1016/0041-008X(86)90384-4.
Gross, SB; Pfitzer, EA; Yeager, DW; Kehoe, RA. (1975). Lead in human tissues. Toxicol Appl Pharmacol 32: 638-651. http://dx.doi.org/10.1016/0041-008X(75)90127-1.
Gulson, B; Jameson, CW; Mahaffey, KR; Mizon, KJ; Patison, N; Law, AJ; Korsch, MJ; Salter, MA. (1998). Relationships of lead in breast milk to lead in blood, urine, and diet of the infant and mother. Environ Health Perspect 106: 667-674. http://dx.doi.org/10.1289/ehp.98106667.

Gulson, B; Mizon, K; Korsch, M; Taylor, A. (2016). Revisiting mobilisation of skeletal lead during pregnancy based on monthly sampling and cord/maternal blood lead relationships confirm placental transfer of lead. Arch Toxicol 90: 805-816. http://dx.doi.org/10.1007/s00204-015-1515-8.

Harrison, GE; Carr, TEF; Sutton, A. (1967). Distribution of radioactive calcium, strontium, barium and radium following intravenous injection into a healthy man. Int J Radiat Biol 13: 235-247. http://dx.doi.org/10.1080/09553006814550161.

Hart, HE; Spencer, H. (1976). Vascular and extravascular calcium interchange in man determined with radioactive calcium. Radiat Res 67: 149-161. http://dx.doi.org/10.2307/3574505.

Hattis, D. (1981). Dynamics of medical removal protection for lead--A reappraisal. (CPA-81-25). Cambridge, MA: Massachusetts Institute of Technology, Center for Policy Alternatives.

Heard, MJ; Chamberlain, AC. (1982). Effect of minerals and food on uptake of lead from the gastrointestinal tract in humans. Hum Toxicol 1: 411-415. http://dx.doi.org/10.1177/096032718200100407.

Heard, MJ; Chamberlain, AC. (1984). Uptake of Pb by human skeleton and comparative metabolism of Pb and alkaline earth elements. Health Phys 47: 857-865.

Hernández-Avila, M; Smith, D; Meneses, F; Sanin, LH; Hu, H. (1998). The influence of bone and blood lead on plasma lead levels in environmentally exposed adults. Environ Health Perspect 106: 473-477. http://dx.doi.org/10.1289/ehp.106-1533211.

Hogan, K; Marcus, A; Smith, R; White, P. (1998). Integrated exposure uptake biokinetic model for lead in children: Empirical comparisons with epidemiologic data. Environ Health Perspect 106 (Suppl. 6): 1557-1567. http://dx.doi.org/10.1289/ehp.98106s61557.

Hu, H; Shih, R; Rothenberg, S; Schwartz, BS. (2007). The epidemiology of lead toxicity in adults: Measuring dose and consideration of other methodologic issues [Review]. Environ Health Perspect 115: 455-462. http://dx.doi.org/10.1289/ehp.9783.

HUD. (2011). American Healthy Homes Survey: Lead and arsenic findings. Washington, DC: U.S. Department of Housing and Urban Development, Office of Healthy Homes and Lead Hazard Control. http://portal.hud.gov/hudportal/documents/huddoc?id=AHHS_REPORT.pdf.

Hursh, JB; Mercer, TT. (1970). Measurement of 212Pb loss rate from human lungs. J Appl Physiol (1985) 28: 268-274. http://dx.doi.org/10.1152/jappl.1970.28.3.268.

Hursh, JB; Schraub, A; Sattler, EL; Hofmann, HP. (1969). Fate of 212Pb inhaled by human subjects. Health Phys 16: 257-267. http://dx.doi.org/10.1097/00004032-196903000-00001.

Hursh, JB; Suomela, J. (1968). Absorption of 212Pb from the gastrointestinal tract of man. Acta Radiol Ther Phys Biol 7: 108-120. http://dx.doi.org/10.3109/02841866809133184.

ICRP. (1975). Report of the task group on reference man. In ICRP Publication 23. Oxford, UK: Pergamon Press. http://dx.doi.org/10.1016/S0074-2740(75)80015-8.

ICRP. (1979). Limits for intakes of radionuclides by workers. (ICRP 30 (Part 1)). https://www.icrp.org/publication.asp?id=ICRP%20Publication%2030%20(Part%201).

ICRP. (1990). Age-dependent doses to members of the public from intake of radionuclides: Part 1. In Annals of the ICRP, vol 20(2). (ICRP Publication 56). Oxford, UK: Pergamon.

ICRP. (1993). Appendix A: Age-specific biokinetic models for the alkaline earth elements and lead. Ann ICRP 23(3-4): 95-120. http://dx.doi.org/10.1016/0146-6453(93)90031-3.

ICRP. (1994). Human respiratory tract model for radiological protection. Ann ICRP 24.

ICRP. (2002). Basic anatomical and physiological data for use in radiological protection: Reference values. In Annals of the ICRP, vol 32, no 3-4. (ICRP Publication 89). New York, NY: Pergamon Press. http://dx.doi.org/10.1016/S0146-6453(03)00002-2.

ICRP. (1996). Basic anatomical & physiological data for use in radiological protection: The skeleton. In H Smith (Ed.), Annals of the ICRP Publication 70. Tarrytown, NY: Elsevier Science Inc.

IOM (Institute of Medicine). (2005). Dietary reference intakes for energy, carbohydrate, fiber, fat, fatty acids, cholesterol, protein, and amino acids. Washington, DC: The National Academies Press. http://dx.doi.org/10.17226/10490.

Iyengar, V; Woittiez, J. (1988). Trace elements in human clinical specimens: Evaluation of literature data to identify reference values [Review]. Clin Chem 34: 474-481. http://dx.doi.org/10.1093/clinchem/34.3.474.
James, HM; Hilburn, ME; Blair, JA. (1985). Effects of meals and meal times on uptake of lead from the gastrointestinal tract of humans. Hum Exp Toxicol 4: 401-407. http://dx.doi.org/10.1177/096032718500400406.
Juhasz, AL; Weber, J; Smith, E. (2011). Impact of soil particle size and bioaccessibility on children and adult lead exposure in peri-urban contaminated soil. J Hazard Mater 186: 1870-1879. http://dx.doi.org/10.1016/j.jhazmat.2010.12.095.
Kahn, HD; Stralka, K. (2009). Estimated daily average per capita water ingestion by child and adult age categories based on USDA's 1994-1996 and 1998 continuing survey of food intakes by individuals. J Expo Sci Environ Epidemiol 19: 396-404. http://dx.doi.org/10.1038/jes.2008.29.
Kayaalti, Z; Kaya-Akyüzlü, D; Söylemez, E; Söylemezoğlu, T. (2015). Maternal hemochromatosis gene H63D single-nucleotide polymorphism and lead levels of placental tissue, maternal and umbilical cord blood. Environ Res 140: 456-461. http://dx.doi.org/10.1016/j.envres.2015.05.004.
Kazi, TG; Shah, F; Shaikh, HR; Afridi, HI; Shah, A; Naeemullah, A; Arain, SS. (2014). Exposure of lead to mothers and their new born infants, residents of industrial and domestic areas of Pakistan. Environ Sci Pollut Res Int 21: 3021-3030. http://dx.doi.org/10.1007/s11356-013-2223-7.
Kim, YM; Chung, JY; An, HS; Park, SY; Kim, BG; Bae, JW; Han, M; Cho, YJ; Hong, YS. (2015). Biomonitoring of Lead, Cadmium, Total Mercury, and Methylmercury Levels in Maternal Blood and in Umbilical Cord Blood at Birth in South Korea. Int J Environ Res Public Health 12: 13482-13493. http://dx.doi.org/10.3390/ijerph121013482.
Kordas, K; Ettinger, AS; Lamadrid-Figueroa, H; Tellez-Rojo, MM; Hérnandez-Avila, M; Hu, H; Wright, RO. (2009). Methylenetetrahydrofolate reductase (MTHFR) C677T, A1298C and G1793A genotypes, and the relationship between maternal folate intake, tibia lead and infant size at birth. Br J Nutr 102: 907-914. http://dx.doi.org/10.1017/s0007114509318280.
Lanphear, BP; Matte, TD; Rogers, J; Clickner, RP; Dietz, B; Bornschein, RL; Succop, P; Mahaffey, KR; Dixon, S; Galke, W; Rabinowitz, M; Farfel, M; Rohde, C; Schwartz, J; Ashley, P; Jacobs, DE. (1998). The contribution of lead-contaminated house dust and residential soil to children's blood lead levels: A pooled analysis of 12 epidemiologic studies. Environ Res 79: 51-68. http://dx.doi.org/10.1006/enrs.1998.3859.
Lanphear, BP; Roghmann, KJ. (1997). Pathways of lead exposure in urban children. Environ Res 74: 67-73. http://dx.doi.org/10.1006/enrs.1997.3726.
Layton, DW. (1993). Metabolically consistent breathing rates for use in dose assessments. Health Phys 64: 23-36.
Leggett, RW. (1985). A model of the retention, translocation and excretion of systemic public health. Health Phys 49: 1115-1137.
Leggett, RW. (1992a). A generic age-specific biokinetic model for calcium-like elements. Radiat Prot Dosimetry 41: 183-198.
Leggett, RW. (1992b). A retention-excretion model for americium in humans. Health Phys 62: 288-310.
Leggett, RW. (1993). An age-specific kinetic model of lead metabolism in humans [Review]. Environ Health Perspect 101: 598-616. http://dx.doi.org/10.1289/ehp.93101598.
Leggett, RW; Eckerman, KF; Williams, LR. (1982). Strontium-90 in bone: a case study in age-dependent dosimetric modeling. Health Phys 43: 307-322.
Leggett, RW; Eckerman, KF; Williams, LR. (1993). An elementary method for implementing complex biokinetic models. Health Phys 64: 260-271. http://dx.doi.org/10.1097/00004032-199303000-00004.
Lloyd, RD; Mays, CW; Atherton, DR; Bruenger, FW. (1970). Distribution and retention of Pb-210 in the beagle (pp. 105-177). (COO-241). Salt Lake City, UT: University of Utah College of Medicine.
Lloyd, RD; Mays, CW; Atherton, DR; Bruenger, FW. (1975). 210Pb studies in beagles. Health Phys 28: 575-583. http://dx.doi.org/10.1097/00004032-197505000-00011.

Lorenzana, RM; Troast, R; Klotzbach, JM; Follansbee, MH; Diamond, GL. (2005). Issues related to time averaging of exposure in modeling risks associated with intermittent exposures to lead. Risk Anal 25: 169-178. http://dx.doi.org/10.1111/j.0272-4332.2005.00576.x.

Lu, Y; Yin, W; Huang, L; Zhang, G; Zhao, Y. (2011). Assessment of bioaccessibility and exposure risk of arsenic and lead in urban soils of Guangzhou City, China. Environ Geochem Health 33: 93-102. http://dx.doi.org/10.1007/s10653-010-9324-8.

Maddaloni, M; Ballew, M; Diamond, G; Follansbee, M; Gefell, D; Goodrum, P; Johnson, M; Koporec, K; Khoury, G; Luey, J; Odin, M; Troast, R; Van Leeuwen, P; Zaragoza, L. (2005). Assessing lead risks at non-residential hazardous waste sites. Hum Ecol Risk Assess 11: 967-1003. http://dx.doi.org/10.1080/10807030500257838.

Malcoe, LH; Lynch, RA; Kegler, MC; Skaggs, VJ. (2002). Lead sources, behaviors, and socioeconomic factors in relation to blood lead of Native American and white children: A community-based assessment of a former mining area. Environ Health Perspect 110: 221-231. http://dx.doi.org/10.1289/ehp.02110s2221.

Manton, WI; Cook, JD. (1984). High accuracy (stable isotope dilution) measurements of lead in serum and cerebrospinal fluid. Br J Ind Med 41: 313-319. http://dx.doi.org/10.1136/oem.41.3.313.

Manton, WI; Malloy, CR. (1983). Distribution of lead in body fluids after ingestion of soft solder. Br J Ind Med 40: 51-57. http://dx.doi.org/10.1136/oem.40.1.51.

Manton, WI; Rothenberg, SJ; Manalo, M. (2001). The lead content of blood serum. Environ Res 86: 263-273. http://dx.doi.org/10.1006/enrs.2001.4271.

Marschner, B; Welge, P; Hack, A; Wittsiepe, J; Wilhelm, M. (2006). Comparison of soil Pb in vitro bioaccessibility and in vivo bioavailability with Pb pools from a sequential soil extraction. Environ Sci Technol 40: 2812-2818. http://dx.doi.org/10.1021/es051617p.

Miller, FJ; Asgharian, B; Schroeter, JD; Price, O. (2016). Improvements and additions to the Multiple Path Particle Dosimetry model. J Aerosol Sci 99: 14-26. http://dx.doi.org/10.1016/j.jaerosci.2016.01.018.

Minoia, C; Sabbioni, E; Apostoli, P; Pietra, R; Pozzoli, L; Gallorini, M; Nicolaou, G; Alessio, L; Capodaglio, E. (1990). Trace element reference values in tissues from inhabitants of the European Community I A study of 46 elements in urine, blood and serum of Italian subjects. Sci Total Environ 95: 89-105.

Nie, HL; Chettle, DR; Webber, CE; Brito, JAA; O'Meara, JM; McNeill, FE. (2005). The study of age influence on human bone lead metabolism by using a simplified model and X-ray fluorescence data. J Environ Monit 7: 1069-1073. http://dx.doi.org/10.1039/b507749d.

Nilsson, U; Attewell, R; Christoffersson, JO; Schütz, A; Ahlgren, L; Skerfving, S; Mattsson, S. (1991). Kinetics of lead in bone and blood after end of occupational exposure. Basic Clin Pharmacol Toxicol 68: 477-484. http://dx.doi.org/10.1111/j.1600-0773.1991.tb01273.x.

Niyogi, SK. (1974). Tissue distribution of lead in cases of poisoning in children. Forensic Sci 3: 199-202.

O'Flaherty, EJ. (1991a). Physiologically based models for bone-seeking elements. I. Rat skeletal and bone growth [Review]. Toxicol Appl Pharmacol 111: 299-312. http://dx.doi.org/10.1016/0041-008X(91)90032-A.

O'Flaherty, EJ. (1991b). Physiologically based models for bone-seeking elements. II. Kinetics of lead disposition in rats. Toxicol Appl Pharmacol 111: 313-331. http://dx.doi.org/10.1016/0041-008X(91)90033-B.

O'Flaherty, EJ. (1991c). Physiologically based models for bone-seeking elements. III. Human skeletal and bone growth. Toxicol Appl Pharmacol 111: 332-341. http://dx.doi.org/10.1016/0041-008X(91)90034-C.

O'Flaherty, EJ. (1993). Physiologically based models for bone-seeking elements. IV. Kinetics of lead disposition in humans. Toxicol Appl Pharmacol 118: 16-29. http://dx.doi.org/10.1006/taap.1993.1004.

O'Flaherty, EJ. (1995). Physiologically based models for bone-seeking elements. V. Lead absorption and disposition in childhood [Review]. Toxicol Appl Pharmacol 131: 297-308. http://dx.doi.org/10.1006/taap.1995.1072.
O'Flaherty, EJ. (1998). A physiologically based kinetic model for lead in children and adults [Review]. Environ Health Perspect 106(Suppl. 6): 1495-1503. http://dx.doi.org/10.1289/ehp.98106s61495.
O'Flaherty, EJ. (2000). Modeling normal aging bone loss, with consideration of bone loss in osteoporosis. Toxicol Sci 55: 171-188. http://dx.doi.org/10.1093/toxsci/55.1.171.
O'Flaherty, EJ; Inskip, MJ; Franklin, CA; Durbin, PW; Manton, WI; Baccanale, CL. (1998). Evaluation and modification of a physiologically based model of lead kinetics using data from a sequential isotope study in cynomolgus monkeys. Toxicol Appl Pharmacol 149: 1-16. http://dx.doi.org/10.1006/taap.1997.8328.
O'Rourke, MK; Van De Water, PK; Jin, S; Rogan, SP; Weiss, AD; Gordon, SM; Moschandreas, DM; Lebowitz, MD. (1999). Evaluations of primary metals from NHEXAS Arizona: distributions and preliminary exposures. National Human Exposure Assessment Survey. J Expo Anal Environ Epidemiol 9: 435-445.
Orten, JM; Neuhaus, OW. (1982). Human biochemistry (10th ed.). London, UK: Mosby.
Ozkaynak, H; Xue, J; Zartarian, VG; Glen, G; Smith, L. (2011). Modeled estimates of soil and dust ingestion rates for children. Risk Anal 31: 592-608. http://dx.doi.org/10.1111/j.1539-6924.2010.01524.x.
Patel, AB; Prabhu, AS. (2009). Determinants of lead level in umbilical cord blood. Indian Pediatr 46: 791-793.
Peters, A; Henderson, BL; Lui, D. (2000). Indexed glomerular filtration rate as a function of age and body size. Clin Sci (Lond) 98: 439-444. http://dx.doi.org/10.1042/cs0980439.
Peters, AM. (2004). The kinetic basis of glomerular filtration rate measurement and new concepts of indexation to body size [Review]. Eur J Nucl Med Mol Imaging 31: 137-149. http://dx.doi.org/10.1007/s00259-003-1341-8.
Potter, GD; McIntyre, DR; Vattuone, GM. (1971). The fate and implications of 203 Pb ingestion in a dairy cow and a calf. Health Phys 20: 650-653.
Pounds, JG; Leggett, RW. (1998). The ICRP age-specific biokinetic model for lead: Validations, empirical comparisons, and explorations [Review]. Environ Health Perspect 106(Suppl. 6): 1505-1511. http://dx.doi.org/10.1289/ehp.98106s61505.
Rabinowitz, MB; Kopple, JD; Wetherill, GW. (1980). Effect of food intake and fasting on gastrointestinal lead absorption in humans. Am J Clin Nutr 33: 1784-1788. http://dx.doi.org/10.1093/ajcn/33.8.1784.
Rabinowitz, MB; Wetherill, GW; Kopple, JD. (1976). Kinetic analysis of lead metabolism in healthy humans. J Clin Invest 58: 260-270. http://dx.doi.org/10.1172/JCI108467.
Reddy, YS; Y, A; Ramalaksmi, BA; Kumar, BD. (2014). Lead and trace element levels in placenta, maternal and cord blood: a cross-sectional pilot study. J Obstet Gynaecol Res 40: 2184-2190. http://dx.doi.org/10.1111/jog.12469.
Reimann, C; Smith, DB; Woodruff, LG; Flem, B. (2011). Pb-concentrations and Pb-isotope ratios in soils collected along an east-west transect across the United States. Appl Geochem 26: 1623-1631. http://dx.doi.org/10.1016/j.apgeochem.2011.04.018.
Rentschler, G; Broberg, K; Lundh, T; Skerfving, S. (2012). Long-term lead elimination from plasma and whole blood after poisoning. Int Arch Occup Environ Health 85: 311-316. http://dx.doi.org/10.1007/s00420-011-0673-0.
Robertson, GL; Lebowitz, MD; O'Rourke, MK; Gordon, S; Moschandreas, D. (1999). The National Human Exposure Assessment Survey (NHEXAS) study in Arizona--introduction and preliminary results. J Expo Anal Environ Epidemiol 9: 427-434.
Roussel, H; Waterlot, C; Pelfrene, A; Pruvot, C; Mazzuca, M; Douay, F. (2010). Cd, Pb and Zn oral bioaccessibility of urban soils contaminated in the past by atmospheric emissions from two lead

and zinc smelters. Arch Environ Contam Toxicol 58: 945-954. http://dx.doi.org/10.1007/s00244-009-9425-5.
Ryu, JE; Ziegler, EE; Nelson, SE; Fomon, SJ. (1983). Dietary intake of lead and blood lead concentration in early infancy. Am J Dis Child 137: 886-891. http://dx.doi.org/10.1001/archpedi.1983.02140350060015.
Schütz, A; Bergdahl, IA; Ekholm, A; Skerfving, S. (1996). Measurement by ICP-MS of lead in plasma and whole blood of lead workers and controls. Occup Environ Med 53: 736-740. http://dx.doi.org/10.1136/oem.53.11.736.
Schütz, A; Skerfving, S. (1976). Effect of a short, heavy exposure to lead dust upon blood lead level, erythrocyte delta-aminolevulinic acid dehydratase activity and urinary excretion of lead delta-aminolevulinic acid coproporphyrin. Results of a 6-month follow-up of two male subjects. Scand J Work Environ Health 2: 176-184.
Sherlock, JC; Quinn, MJ. (1986). Relationship between blood and lead concentrations and dietary lead intake in infants: The Glasgow Duplicate Diet Study 1979-1980. Food Addit Contam 3: 167-176. http://dx.doi.org/10.1080/02652038609373579.
Skerfving, S; Ahlgren, L; Christoffersson, JO; Haeger-Aronson, B; Mattsson, S; Schutz, A; Lindberg, G. (1985). Metabolism of inorganic lead in man. Adv Food Nutr Res 1: 601-607.
Smith, D; Hernandez-Avila, M; Téllez-Rojo, MM; Mercado, A; Hu, H. (2002). The relationship between lead in plasma and whole blood in women. Environ Health Perspect 110: 263-268. http://dx.doi.org/10.1289/ehp.02110263.
Smith, DB; Cannon, WF; Woodruff, LG; Solano, F; Kilburn, JE; Fey, DL. (2013). Geochemical and mineralogical data for soils of the conterminous United States. (Data Series 801). Reston, VA: U.S. Department of the Interior, U.S. Geological Survey. http://pubs.usgs.gov/ds/801/.
Smith, DM; Mielke, HW; Heneghan, JB. (2009). Subchronic lead feeding study in male rats and micropigs. Environ Toxicol 24: 453-461. http://dx.doi.org/10.1002/tox.20448.
Smith, E; Weber, J; Naidu, R; McLaren, RG; Juhasz, AL. (2011). Assessment of lead bioaccessibility in peri-urban contaminated soil. J Hazard Mater 186: 300-305. http://dx.doi.org/10.1016/j.jhazmat.2010.10.111.
Somervaille, LJ; Chettle, DR; Scott, MC; Tennant, DR; McKiernan, MJ; Skilbeck, A; Trethowan, WN. (1988). In vivo tibia lead measurements as an index of cumulative exposure in occupationally exposed subjects. Occup Environ Med 45: 174-181.
SRC. (2008). Theoretical framework for the All Ages Lead Model. (SRC TR-08-142).
SRC. (2009a). Evidence supporting further refinement of the EPA All Ages Lead Model. (SRC TR-09-178).
SRC. (2009b). Review of lead exposure biokinetics models. (SRC TR-09-139).
SRC. (2021). REDACTED appendices: Upper Columbia River final site-wide human health risk assessment. Washington, DC: U.S. Environmental Protection Agency. https://semspub.epa.gov/work/10/100311307.pdf.
Stifelman, M. (2007). Using doubly-labeled water measurements of human energy expenditure to estimate inhalation rates. Sci Total Environ 373: 585-590. http://dx.doi.org/10.1016/j.scitotenv.2006.11.041.
Stover, BJ. (1959). Pb212 (ThB) tracer studies in adult beagle dogs. Proc Soc Exp Biol Med 100: 269-272. http://dx.doi.org/10.3181/00379727-100-24596.
TerraGraphics. (2004). Final human health remedial evaluation report for the Bunker Hill Superfund Site box. Moscow, ID.
Thomas, K; Pellizzari, E; Berry, M. (1999). Population-based dietary intakes and tap water concentrations for selected elements in the EPA region V National Human Exposure Assessment Survey (NHEXAS). J Expo Anal Environ Epidemiol 9: 402-413. http://dx.doi.org/10.1038/sj.jea.7500051.

U.S. EPA (U.S. Environmental Protection Agency). (1989). Review of the national ambient air quality standard for lead: Exposure analysis methodology and validation [EPA Report]. (EPA/450/2-89-011).
U.S. EPA (U.S. Environmental Protection Agency). (1994a). Guidance manual for the integrated exposure uptake biokinetic model for lead in children [EPA Report]. (EPA/540/R-93/081). Washington, DC. http://nepis.epa.gov/Exe/ZyPURL.cgi?Dockey=2000WN4R.txt.
U.S. EPA (U.S. Environmental Protection Agency). (1994b). Revised interim soil lead guidance for CERCLA sites and RCRA corrective action facilities [EPA Report]. (OSWER Directive #9355.4-12; EPA/540/F-94/043). Washington, DC: U.S. Environmental Protection Agency, Office of Solid Waste and Emergency Response. https://nepis.epa.gov/Exe/ZyPURL.cgi?Dockey=P100A72S.txt.
U.S. EPA (U.S. Environmental Protection Agency). (1994c). Technical support document: Parameters and equations used in integrated exposure uptake biokinetic model for lead in children (v 0.99d) [EPA Report]. (EPA/540/R-94/040). Washington, DC. https://ntrl.ntis.gov/NTRL/dashboard/searchResults/titleDetail/PB94963505.xhtml.
U.S. EPA (U.S. Environmental Protection Agency). (1998). Federal guidance report no. 13: Part I - Interim version: Health risks from low level environmental exposures to radionuclides: Radionuclide-specific lifetime radiogenic cancer risk coefficients for the U.S. population, based on age-dependent intake, dosimetry, and risk models [EPA Report]. (EPA 402-R-97-014).
U.S. EPA (U.S. Environmental Protection Agency). (2003a). Evaluation of the ICRP lead biokinetics model: Empirical comparisons with observations of plasma-blood lead concentration relationships in humans [draft final]. (SRC No. FA332). Washington, DC.
U.S. EPA (U.S. Environmental Protection Agency). (2003b). Recommendations of the Technical Review Workgroup for Lead for an approach to assessing risks associated with adult exposures to lead in soil [EPA Report]. (EPA-540-R-03-001). Washington, DC. https://semspub.epa.gov/work/HQ/174559.pdf.
U.S. EPA (U.S. Environmental Protection Agency). (2006). Air quality criteria for lead (Final report, 2006): Volume I of II [EPA Report]. (EPA/600/R-05/144aF). Washington, DC. http://cfpub.epa.gov/ncea/CFM/recordisplay.cfm?deid=158823.
U.S. EPA (U.S. Environmental Protection Agency). (2007a). EPA science advisory board (SAB) ad hoc all-ages lead model review panel's peer review of the "all-ages lead model (AALM) version 1.05 (External review draft) ". (EPA-SAB-07-002). https://cfpub.epa.gov/si/si_public_record_report.cfm?dirEntryId=139314&Lab=NCEA.
U.S. EPA (U.S. Environmental Protection Agency). (2007b). National primary drinking water regulations for lead and copper: Short-term regulatory revisions and clarifications. Fed Reg 72: 57782-57820.
U.S. EPA (U.S. Environmental Protection Agency). (2011). Exposure factors handbook: 2011 edition [EPA Report]. (EPA/600/R-090/052F). Washington, DC: U.S. Environmental Protection Agency, Office of Research and Development, National Center for Environmental Assessment. https://nepis.epa.gov/Exe/ZyPURL.cgi?Dockey=P100F2OS.txt.
U.S. EPA (U.S. Environmental Protection Agency). (2013). Integrated science assessment for lead [EPA Report]. (EPA/600/R-10/075F). Washington, DC. https://nepis.epa.gov/Exe/ZyPURL.cgi?Dockey=P100K82L.txt.
U.S. EPA (U.S. Environmental Protection Agency). (2014a). Appendices to the approach for estimating exposures and incremental health effects from lead due to renovation, repair, and painting activities in public and commercial buildings. Washington, DC. https://www.epa.gov/lead/approach-estimating-exposures-and-incremental-health-effects-lead-due-renovation-repair-and.
U.S. EPA (U.S. Environmental Protection Agency). (2014b). Approach for estimating exposures and incremental health effects from lead due to renovation, repair, and painting activities in public and commercial building. Washington, DC. https://www.epa.gov/lead/approach-estimating-exposures-and-incremental-health-effects-lead-due-renovation-repair-and.

U.S. EPA (U.S. Environmental Protection Agency). (2014c). Framework for identifying and evaluating lead-based paint hazards from renovation, repair, and painting activities in public and commercial buildings. Washington, DC. https://www.epa.gov/sites/production/files/2014-05/documents/lead_pncb_framework_document.pdf.
U.S. EPA (U.S. Environmental Protection Agency). (2017a). Transmittal of update to the adult lead methodology's default baseline blood lead concentration and geometric standard deviation. OLEM directive 9285: 6–56.
U.S. EPA (U.S. Environmental Protection Agency). (2017b). Update for Chapter 5 of the Exposure Factors Handbook: Soil and dust ingestion [EPA Report]. (EPA/600R-17/384F). Washington, DC: National Center for Environmental Assessment, Office of Research and Development. https://nepis.epa.gov/Exe/ZyPURL.cgi?Dockey=P100TTX4.txt.
U.S. EPA (U.S. Environmental Protection Agency). (2019a). Integrated Science Assessment (ISA) for particulate matter (final report, Dec 2019). (EPA/600/R-19/188). Washington, DC. https://cfpub.epa.gov/ncea/isa/recordisplay.cfm?deid=347534.
U.S. EPA (U.S. Environmental Protection Agency). (2019b). Technical support document for residential dust-lead hazard standards rulemaking. Title Page. (EPA TSD LDHS).
Versar. (2015). Post-meeting peer review summary report: External peer review of EPA's approach for estimating exposures and incremental health effects from lead due to renovation, repair, and painting activities in public and commercial buildings. https://www.regulations.gov/document?D=EPA-HQ-OPPT-2010-0173-0259.
Victery, W; Vander, AJ; Mouw, DR. (1979). Renal handling of lead in dogs: stop-flow analysis. Am J Physiol 237: F408-F414. http://dx.doi.org/10.1152/ajprenal.1979.237.5.F408.
von Lindern, I; Spalinger, S; Stifelman, ML; Stanek, LW; Bartrem, C. (2016). Estimating children's soil/dust ingestion rates through retrospective analyses of blood lead biomonitoring from the Bunker Hill Superfund Site in Idaho. Environ Health Perspect 124: 1462-1470. http://dx.doi.org/10.1289/ehp.1510144.
Watson, WS; Morrison, J; Bethel, MIF; Baldwin, NM; Lyon, DTB; Dobson, H; Moore, MR; Hume, R. (1986). Food iron and lead absorption in humans. Am J Clin Nutr 44: 248-256. http://dx.doi.org/10.1093/ajcn/44.2.248.
Wells, AC; Venn, JB; Heard, MJ. (1977). Deposition in the lung and uptake to blood of motor exhaust labelled with 203Pb. In WH Walton; B McGovern (Eds.), (pp. 175-189). Oxford, UK: Pergamon.
White, PD; Van Leeuwan, P; Davis, BD; Maddaloni, M; Hogan, KA; Marcus, AH; Elias, RW. (1998). The conceptual structure of the integrated exposure uptake biokinetic model for lead in children [Review]. Environ Health Perspect 106(Suppl. 6): 1513-1530. http://dx.doi.org/10.1289/ehp.98106s61513.
Wilson, R; Jones-Otazo, H; Petrovic, S; Mitchell, I; Bonvalot, Y; Williams, D; Richardson, GM. (2013). Revisiting dust and soil ingestion rates based on hand-to-mouth transfer. Hum Ecol Risk Assess 19: 158-188. http://dx.doi.org/10.1080/10807039.2012.685807.
Yu, CH; Yiin, LM; Lioy, PJ. (2006). The bioaccessibility of lead (Pb) from vacuumed house dust on carpets in urban residences. Risk Anal 26: 125-134. http://dx.doi.org/10.1111/j.1539-6924.2006.00710.x.
Zaragoza, L; Hogan, K. (1998). The integrated exposure uptake biokinetic model for lead in children: Independent validation and verification [Review]. Environ Health Perspect 6: 1551-1556. http://dx.doi.org/10.1289/ehp.98106s61551.
Zartarian, V; Xue, J; Tornero-Velez, R; Brown, J. (2017). Children's lead exposure: A multimedia modeling analysis to guide public health decision-making. Environ Health Perspect 125: 097009. http://dx.doi.org/10.1289/EHP1605.
Ziegler, EE; Edwards, BB; Jensen, RL; Mahaffey, KR; Fomon, SJ. (1978). Absorption and retention of lead by infants. Pediatr Res 12: 29-34. http://dx.doi.org/10.1203/00006450-197801000-00008.

APPENDIX A – EQUATIONS IN AALM FORTRAN CODE

TABLE A-1. EQUATIONS WITHIN TEXT OF CHAPTER 2

No.		Equation
		2.2 Exposure Model
2.2	1	$IN_j = Pb_j \cdot f_j \cdot IR_{medium} \cdot M_{j1} \cdot M_{j2} \ldots / N$ j = source index for air, dust, soil, water
2.2	2	$IN_j = Pb_j \cdot M_{j1} \cdot M_{j2} \ldots / N$ j = source index for food, other
		2.3 Biokinetics
2.3	1	$\frac{dY_j}{dt} = -R_j \cdot Y_j(t) + P_j$
2.3	2	$Y(t+\Delta t) = \left(Y(t) - \frac{P}{R}\right) e^{-R\,\Delta t} + \frac{P}{R}$
2.3	3	$YINT(t+\Delta t) = \left(Y(t) - \frac{P}{R}\right) \cdot \frac{1 - e^{-R\,\Delta t}}{R} + \frac{P\,\Delta t}{R}$
2.3	4	$FL(t+\Delta t) = Y(t) + P\,\Delta t - Y(t+\Delta t)$
2.3	5	$P(t+\Delta t) = FL(t+\Delta t)/\Delta t$
2.3	6	$P_{j\,k}(t) = IN_j(t) \cdot Dep_k$ j = air source index
2.3	7	$R_{PLAS \to j} = T_{PLAS \to j} \cdot RPLAS$
2.3	8	$AGESCL = \frac{1 - TEVF - TBONE}{1 - TEVF - TBONEL}$
2.3	9	$T_{PLAS \to j} = AGESCL \cdot TO_{PLAS \to j}$
2.3	10	$CF = \frac{1 - TOORBC}{1 - TRBC}$
2.3	11	$WBODY = WBIRTH + \frac{WCHILD \cdot AGEYEAR}{HALF + AGEYEAR} + \frac{WADULT}{1 + KAPPA \cdot e^{-LAMBDA \cdot WADULT \cdot AGEYEAR}}$
2.3	12	$AMTBLD = VBLC \cdot WBODY \cdot 10$
2.3	13	$BLDHCT(AGEYEAR) = HCTB + (HCTA - HCTB)\,Exp(-13.9\,AGEYEAR)$
2.3	14	$KIDWT = 1050 \cdot VKC \cdot (WBIRTH + WADULT + WCHILD) \cdot \left(\frac{WBODY}{WBIRTH + WADULT + WCHILD}\right)^{0.84}$

2.3	15	$LIVWT = 1050 \cdot VLC \cdot (WBIRTH + WADULT + WCHILD) \cdot \left(\frac{WBODY}{WBIRTH + WADULT + WCHILD}\right)^{0.85}$
2.3	16	$WBONE = 1000 \cdot 0.0290 \cdot WBODY^{1.21}$
2.3	17	$VBONE = 1000 \cdot 0.0168 \cdot WBODY^{1.188}$
2.3	18	$CVBONE = 0.8 \cdot VBONE$
2.3	19	$\mathrm{AF1(AGE}_{YEAR}) = AF_{C1} - \frac{AF_{C2}}{1+30 \cdot \mathrm{Exp}(-AGE_{YEAR})}$
2.3	20	$AF1_j(\mathrm{t}) = \mathrm{F1(t)} \cdot \mathrm{RBA}_j$
2.3	21	$FL_{PLAS \to C} = T_C(\mathrm{t}) \cdot \mathrm{CF(t)} \cdot outplas$
2.3	22	$HEMAT = HCTA + (HCTB - HCTA) \cdot Exp(-13.9 \cdot AGE_{YEAR})$
2.3	23	$RBCONC = YRBC/(HEMAT \cdot BLDVOL)$
2.3	24	$\mathrm{TOORBC} = \mathrm{TRBC} * (1 - \left(\frac{\mathrm{RBCONC-RBCNL}}{\mathrm{SATRAT-RBCNL}}\right)^{\mathrm{power}})$
2.3	25	$CF = \frac{1-TOORBC}{1-TRBC}$, if RBCONC>RBCNL, else CF=1
2.3	26	$FL_{LVR1 \to SIC} = H1TOSI \cdot FL_{LVR1}$
2.3	27	$Y_i = \frac{YF_i \cdot PbB_M \cdot PbB_{F/M} \cdot 3}{YF_{RBC}}$

TABLE A-2. EQUATIONS FROM TABLES 2-1 AND 2-2

No.		**Equation**
A		**Pb Intake from source j (µg/timestep)**
A	1	$IN_{\mathrm{j}} = Pb_j \cdot f_j \cdot IR_{medium} \cdot \mathrm{M}_{j1} \cdot \mathrm{M}_{j2} \ldots / \mathrm{N}$ j = source index for air, dust, soil, water
A	2	$IN_{\mathrm{j}} = Pb_j \cdot \mathrm{M}_{j1} \cdot \mathrm{M}_{j2} \ldots / \mathrm{N}$ j = source index for food, other
		Notes: 1) All variables except N (timesteps per day) are time dependent. 2) Input variable defined at user-specified ages (up to 100 ages). 3) Timesteps are filled in by the front end, either stepwise or interpolation. 4) 6 media, maximum of 3 sources per medium, for 18 sources maximum. 5) Masks M_{j1}, M_{j2}, etc. are optional, each periodically blocks intake for one source. 6) Each of the 6 media can support up to 9 masks.
		Pb deposited in lung compartment k (µg/timestep)
B	1	$P_{j\,k}(\mathrm{t}) = IN_{\mathrm{j}}(\mathrm{t}) \cdot \mathrm{Dep}_k$ j = air source index
		Notes: 1) Only 3 lung compartments (ET, TB, ALV) have deposition. 2) With maximum of 3 air sources, up to 9 lung intake timeseries.

C		**Pb Intake from Ingestion**
C	1	Ingest(t) = $\sum_j IN_j(t)$ j = all non-inhalation sources
		Notes: 1) Up to 15 ingestion sources. 2) While some inhaled Pb is transferred to the gut, this does not count as ingestion.
D		**Growth Equations**
D	1	$\mathrm{AGE}_{YEAR} = \mathrm{AGE}/365$
D	2	$WBODY = \mathrm{WBIRTH} + \frac{WCHILD \cdot \mathrm{AGE}_{YEAR}}{(HALF + \mathrm{AGE}_{YEAR})} + \frac{WADULT}{(1 + KAPPA \cdot \mathrm{Exp}(-13.9 \cdot \mathrm{AGE}_{YEAR}))}$
D	3	$BLDVOL = \mathrm{WBODY} \cdot \mathrm{VBLC} \cdot 10$
D	4	$WGTSUM = \mathrm{WBIRTH} + \mathrm{WCHILD} + \mathrm{WADULT}$
D	5	$KIDWT = 1050 \cdot \mathrm{VKC} \cdot \mathrm{WGTSUM} \cdot \left(\frac{WBODY}{WGTSUM}\right)^{0.84}$
D	6	$LIVWT = 1050 \cdot \mathrm{VLC} \cdot \mathrm{WGTSUM} \cdot \left(\frac{WBODY}{WGTSUM}\right)^{0.85}$
D	7	$BONEWT = 1000 \cdot 0.0290 \cdot (\mathrm{WBODY})^{1.21}$
D	8	$BONEVOL = 1000 \cdot 0.0168 \cdot (\mathrm{WBODY})^{1.188}$
D	9	$CORTWT = 0.8 \cdot \mathrm{BONEWT}$
D	10	$TRABWT = 0.28 \cdot \mathrm{BONEWT}$
A		**General Timestep Equations for all Compartments**
A	1	$\mathrm{Y}(t + \Delta t) = \left(\mathrm{Y(t)} - \frac{P}{R}\right) e^{-\mathrm{R}\,\Delta t} + \frac{\mathrm{P}}{R}$
A	2	$\mathrm{FL}(t + \Delta t) = \mathrm{Y(t)} + P\,\Delta t - Y(t + \Delta t)$
A	3	$\mathrm{P}(t + \Delta t) = \mathrm{FL}(t + \Delta t)/\Delta t$
A	Notes	1) The Pb mass (µg) within each compartment is Y. 2) The inflow rate (assumed uniform over a timestep) of Pb (µg/day) is P. 3) The Pb outflow rate constant is R (1/day). 4) The outflow Pb mass (µg) on each timestep is FL. 5) Outflow on one timestep becomes an inflow on the next timestep. 6) Every simulation timestep Δt is the same size.
B		**Pb Masses at Birth**
B	1	$YRBC = BLDMOT \cdot BRATIO \cdot 3$
B	2	$YBRAN = BRANIN * YRBC \,/\, RBCIN$
B	3	$YKDN2 = RENIN * YRBC \,/\, RBCIN$
B	4	$YLVR2 = HEPIN * YRBC \,/\, RBCIN$
B	5	$YSOF2 = SOFIN * YRBC \,/\, RBCIN$
B	6	$YCVOL = 0.8 * BONIN * YRBC \,/\, RBCIN$
B	7	$YTVOL = 0.2 * BONIN * YRBC \,/\, RBCIN$
C		**Age-scaling of Diffusible Plasma-to-tissue Deposition Fractions**
C	1	$AGESCL = \frac{1 - TEVF - TBONE}{1 - TEVF - TBONE(AGEmax)}$

C	2	$TBRAN = AGESCL \cdot TOBRAN$
C	3	$TFECE = AGESCL \cdot TOFECE$
C	4	$TKDN1 = AGESCL \cdot TOKDN1$
C	5	$TKDN2 = AGESCL \cdot TOKDN2$
C	6	$TLVR1 = AGESCL \cdot TOLVR1$
C	7	$TPROT = AGESCL \cdot TOPROT$
C	8	$TRBC = AGESCL \cdot TORBC$
C	9	$TSOF0 = AGESCL \cdot TOSOF0$
C	10	$TSOF1 = AGESCL \cdot TOSOF1$
C	12	$TSOF2 = AGESCL \cdot TOSOF2$
C	13	$TSWET = AGESCL \cdot TOSWET$
C	14	$TURIN = AGESCL \cdot TOURIN$
C	15	$HEMAT = HCTA + (HCTB - HCTA) \cdot Exp(-13.9 \cdot AGE_{YEAR})$
C	16	$RBCONC = YRBC/(HEMAT \cdot BLDVOL)$
C	17	$\text{TOORBC} = \text{TRBC} * (1 - \left(\frac{\text{RBCONC-RBCNL}}{\text{SATRAT-RBCNL}}\right)^{\text{power}})$, if RBCONC>RBCNL
C	18	$CF = \frac{1-TOORBC}{1-TRBC}$, if RBCONC>RBCNL, else CF=1
D		**Respiratory Tract (RT)**
D	1	ET, k=1: $P_j = P_{j\,1} + FL_{j,TB\rightarrow \text{ET}} \,/\, \Delta t$
D	2	ET, k=1: $R_j = R_{j,ET\rightarrow PLAS} + R_{j,ET\rightarrow STOM}$
D	3	TB, k=2: $P_j = P_{j\,2} + FL_{j,ALV\rightarrow \text{TB}} \,/\, \Delta t$
D	4	TB, k=2: $R_j = R_{j,TB\rightarrow PLAS} + R_{j,TB\rightarrow \text{ET}}$
D	5	ALV, k=3: $P_j = P_{j\,3}$
D	6	ALV, k=3: $R_j = R_{j,ALV\rightarrow PLAS} + R_{j,ALV\rightarrow TB} + R_{j,ALV\rightarrow INT}$
D	7	INT, k=4: $P_j = FL_{j,ALV\rightarrow INT} \,/\, \Delta t$
D	8	INT, k=4: $R_j = R_{j,INT\rightarrow PLAS}$
D	9	$FL_{k\rightarrow PLAS} = \sum_j FL_{j,k\rightarrow PLAS}$
D	10	$UP_{LUNG} = \sum_j FL_{k\rightarrow PLAS}$
D	Notes	1) Each lung equation above is evaluated separately for each air source *j*.
E		**Gastrointestinal Tract (GI) – Stomach (STOM)**
E	1	$P_j = IN_j$ for j not an air source (4−18) $P_j = FL_{j,ET\rightarrow STOM} \,/\, \Delta t$ for j an air source (1−3)
E	2	$R_j = R_{STOM}$

E	Notes	1) The outflow rate constant is the same for all source types. 2) Outflow goes to small intestine and is tracked by source.
E		**Gastrointestinal Tract (GI) – Small Intestine (SI)**
E	3	$P_j = FL_{j,STOM \rightarrow SI} \ / \Delta t$ for j = 1 to 18 $P_0 = (FL_{LVR1 \rightarrow SI} + FL_{PLAS \rightarrow SI}) / \Delta t$ for j=0
E	4	$R_j = R_{SI}$
E	Notes	3) 18 external sources plus source 0 for Pb coming from liver or plasma 4) Loss rate is the same for all sources. 5) Loss fraction going to PLAS is $(\mathrm{F1(t)} \cdot \mathrm{RBA}_j)$, the remainder goes to ULI. 6) The loss fractions vary by source. For source 0, RBA=1.
E		**Gastrointestinal Tract (GI) – Upper Large Intestine (ULI)**
E	5	$P_j = FL_{j,SI \rightarrow \mathrm{ULI}} \ / \Delta t$ for j = 0 to 18
E	6	$R_j = R_{ULI}$
E		**Gastrointestinal Tract (GI) – Lower Large Intestine (LLI)**
E	7	$P_j = FL_{j,ULI \rightarrow \mathrm{LLI}} \ / \Delta t$ for j = 0 to 18
E	8	$R_j = R_{LLI}$
E	Notes	7) Each GI compartment has a Y_j for Pb from each source j (from 1 to 18). 8) Each GI compartment except STOM also has a j=0 term, 9) Each compartment also has a combined Y for the sum over all j.
E		**Uptake into PLAS from Gastrointestinal Tract (GI)**
E	9	$UP_j = FL_{j,SI} \cdot \mathrm{F1} \cdot \mathrm{RBA}_j$
E	10	$FL_{j,SI \rightarrow \mathrm{ULI}} = FL_{j,SI} \cdot (1 - \mathrm{F1} \cdot \mathrm{RBA}_j)$
E	11	$UP_{GI} = \sum_{j=0}^{18} UP_j$
E	12	$UP_{ING} = \sum_{j=4}^{18} UP_j$
E	Notes	10) The total GI tract uptake is the sum of UP_j from j=0 to 18 11) The ingestion uptake is the sum not including j=0 or air sources (j=1-3) 12) These uptakes are per timestep (μg Pb/timestep). 13) Uptakes reported on the daily output file are sums over the timesteps each day.
F		**Blood – Plasma (Diffusible) (PLAS)**
F	1	$P = UP_{GI} + UP_{LUNG} + \sum_k FL_{k \rightarrow PLAS} / \Delta t$
F	2	$TSUM = \sum_C T_C$
F	3	$R = RPLAS \cdot TSUM$
F	4	$FL_{PLAS \rightarrow C} = FL_{PLAS} \cdot T_C \cdot \mathrm{CF} \ / \ TSUM$
F	Notes	1) The T_C are the "T" variables in equations C2 – C14.

		2) TSUM is evaluated in the front end, without accounting for RBC saturation. 3) CF is defined in equation C18. 4) When TRBC is reduced by saturation effects, then CF>1. 5) The CF adjustment in F4 is not applied to RBC but applied to all the others. Equation F4 uses TOORBC (C17), whereas F2 uses TRBC (C8). 6) The compartments *k* supplying Pb to PLAS are listed in C2 – C14. 7) FL_{PLAS} is the total Pb mass lost from the plasma on this timestep, computed from A1 and A2 using P and R from F1 and F3. 8) The compartments *C* receiving Pb from PLAS: RBC, PROT, SI, EVF, SOF0, SOF1, SOF2, BRAN, CSUR, TSUR, LVR1, KDN1, KDN2, BLAD, SWET. 9) While still present in the code, the bladder BLAD receives nothing directly from PLAS, the Pb in urine now all comes from KDN1.
F		**Blood – Plasma – Protein Bound (PROT)**
F	5	$P = FL_{\text{PLAS}\rightarrow\text{PROT}} \ / \Delta t$
F	6	$R = RPROT$
F		**Blood – Red Blood Cell (RBC)**
F	7	$P = FL_{\text{PLAS}\rightarrow\text{RBC}} \ / \Delta t$
F	8	$R = RRBC$
G		**Blood and Other Concentrations (output variables)**
G	9	$C_{BLOOD} = (Y_{PLAS} + Y_{PROT} + Y_{RBC})/BLDVOL$
G	10	$C_{PLAS} = (Y_{PLAS} + Y_{PROT})/BLDVOL$
G	11	$C_{KIDNEY} = (Y_{KDN1} + Y_{KDN2})/KIDWT$
G	12	$C_{LIVER} = (Y_{LVR1} + Y_{LIVR2})/LIVWT$
G	13	$C_{CORT} = (Y_{CSUR} + Y_{CDIF} + Y_{CVOL})/CORTWT$
G	14	$C_{TRAB} = (Y_{TSUR} + Y_{TDIF} + Y_{TVOL})/CORTWT$
G	15	$C_{BONE} = (Y_{CSUR} + Y_{CDIF} + Y_{CVOL} + Y_{TSUR} + Y_{TDIF} + Y_{TVOL})/BONEWT$
G	Notes	1) The denominators are timeseries that depend on body weight WBODY and were evaluated on all timesteps in the Fortran front end. 2) The concentrations do not affect the biokinetics, so equation G9-G15 are evaluated once each, after the loop over timesteps has been completed, using the timeseries variables Y_x for the compartmental Pb masses.
H		**Extravascular Fluid (EVF)**
H	1	$P = FL_{\text{PLAS}\rightarrow\text{EVF}} \ / \Delta t$
H	2	$R = REVF$
I		**Soft Tissue: Fast transfer (SOF0)**
I	1	$P = FL_{\text{PLAS}\rightarrow\text{SOF0}} \ / \Delta t$
I	2	$R = RSOF0$
I		**Soft Tissue: Intermediate transfer (SOF1)**
I	3	$P = FL_{\text{PLAS}\rightarrow\text{SOF1}} \ / \Delta t$

I	4	$R = RSOF1$
I	Notes	1) The outflow from SOF1 is split, with a fraction S2HAIR going to HAIR and the remainder going back to PLAS.
I		**Soft Tissue: Slow transfer (SOF2)**
I	5	$P = FL_{\text{PLAS}\rightarrow\text{SOF2}} \ / \Delta t$
I	6	$R = RSOF2$
J		**Brain (BRAN)**
J	1	$P = FL_{\text{PLAS}\rightarrow\text{BRAN}} \ / \Delta t$
J	2	$R = RBRAN$
K		**Bone – Cortical Bone Surface (CSUR)**
K	1	$P = (FL_{\text{PLAS}\rightarrow\text{CSUR}} + FL_{\text{CDIF}\rightarrow\text{CSUR}}) \ / \Delta t$
K	2	$R = RCS2B + RCS2DF$
K		**Bone – Exchangeable Cortical Bone (CDIF)**
K	3	$P = FL_{\text{CSUR}\rightarrow\text{CDIF}} \ / \Delta t$
K	4	$R = RDIFF$
K	Notes	1) The outflow from CDIF is split with a fraction FLONG going to CVOL and the remainder going to CSUR.
K		**Bone – Non-Exchangeable Cortical Bone Volume (CVOL)**
K	5	$P = FL_{\text{CDIF}\rightarrow\text{CVOL}} \ / \Delta t$
K	6	$R = RCORT$
K		**Bone – Trabecular Bone Surface (TSUR)**
K	7	$P = (FL_{\text{PLAS}\rightarrow\text{TSUR}} + FL_{\text{TDIF}\rightarrow\text{TSUR}}) \ / \Delta t$
K	8	$R = RTS2B + RTS2DF$
K		**Bone – Exchangeable Trabecular Bone (TDIF)**
K	9	$P = FL_{\text{TSUR}\rightarrow\text{TDIF}} \ / \Delta t$
K	10	$R = RDIFF$
K	Notes	2) The rate constant is the same variable for both TDIF and CDIF. 3) The outflow is split with a fraction FLONG going to TVOL, with the remainder going to TSUR.
K		**Bone – Non-Exchangeable Trabecular Bone (TVOL)**
K	11	$P = FL_{\text{TDIF}\rightarrow\text{TVOL}} \ / \Delta t$
K	12	$R = RTRAB$
L		**Kidney – Compartment 1 (fast, urinary path) (KDN1)**
L	1	$P = FL_{\text{PLAS}\rightarrow\text{KDN1}} \ / \Delta t$
L	2	$R = RKDN1$
L		**Kidney – Compartment 2 (slow path) (KDN2)**
L	3	$P = FL_{\text{PLAS}\rightarrow\text{KDN2}} \ / \Delta t$

L	4	$R = RKDN2$
L		**Bladder (BLAD)**
L	5	$P = (FL_{\text{KDN1}\rightarrow\text{BLAD}} + FL_{\text{PLAS}\rightarrow\text{BLAD}}) \,/\, \Delta t$
L	6	$R = RBLAD$
L	Notes	1) The outflow from KDN1 goes to BLAD. 2) The outflow from KDN2 goes to PLAS. 3) The outflow from BLAD exits the body as urine.
M		**Liver – Fast Compartment 1 (LVR1)**
M	1	$P = FL_{\text{PLAS}\rightarrow\text{LVR1}} \,/\, \Delta t$
M	2	$R = RLVR1$
M		**Liver – Slow Compartment 2**
M	3	$P = FL_{\text{LVR1}\rightarrow\text{LVR2}} \,/\, \Delta t$
M	4	$R = RLVR2$
M	Notes	1) The outflow from LVR1 is split into 3 parts: a fraction H1toH2 to LVR2, Fraction H1toSI to small intestine, and fraction H1toBl to PLAS. 2) The interface should check that the above fractions sum to one. 3) The outflow from LVR2 goes entirely to PLAS.
N		**Exit pathways – (URIN, FECE, SWET, HAIR)**
N	1	$Y_{URIN}(t + \Delta t) = Y_{URIN}(t) + FL_{\text{BLAD}\rightarrow\text{URIN}}(t)$
N	2	$Y_{FECE}(t + \Delta t) = Y_{FECE}(t) + FL_{\text{LLI}\rightarrow\text{FECE}}(t)$
N	3	$Y_{SWET}(t + \Delta t) = Y_{SWET}(t) + FL_{\text{PLAS}\rightarrow\text{SWET}}(t)$
N	4	$Y_{HAIR}(t + \Delta t) = Y_{HAIR}(t) + FL_{\text{SOF1}\rightarrow\text{HAIR}}(t)$
N	Notes	1) Each exit pathway accumulates losses over the simulation. 2) Hair is a generic name that includes hair, fingernails, toenails, as well as skin dander that is sloughed off. 3) The purpose of tracking accumulated losses is to check mass balance (see below).
O		**Mass balance calculations – Air sources (j=1 to 3)**
O	1	$SOURCE_j(T) = \sum_{t=0}^{T} IN_j(t)$
O	2	$NONDEP_j(T) = (1 - DEP_j) \cdot \sum_{t=0}^{T} IN_j(\text{t})$
O	3	$INTAKE_j(T) = SOURCE_j(T) - NONDEP_j(T)$
O	4	$GITRACT_j(T) = Y_{j,STOM} + Y_{j,SI} + Y_{j,ULI} + Y_{j,LLI} + FL_{j,STOM\rightarrow SI} + FL_{j,SI\rightarrow PLAS} + FL_{j,SI\rightarrow ULI} + FL_{j,ULI\rightarrow\text{LLI}} + FL_{j,LLI\rightarrow\text{FECE}}$
O	5	$LUNGS_j(T) = Y_{j,ET} + Y_{j,TB} + Y_{j,ALV} + Y_{j,INT} + FL_{j,TB\rightarrow ET} + FL_{j,ALV\rightarrow\text{TB}} + FL_{j,ALV\rightarrow INT} + FL_{j,ET\rightarrow\text{STOM}} + FL_{j,ET\rightarrow\text{PLAS}} + FL_{j,TB\rightarrow\text{PLAS}} + FL_{j,ALV\rightarrow\text{PLAS}} + FL_{j,INT\rightarrow\text{PLAS}}$

O	6	$ABSORB_j(T) = \sum_{t=0}^{T-\Delta t} \left(FL_{j,ET\rightarrow \text{PLAS}} + FL_{j,TB\rightarrow \text{PLAS}} + FL_{j,ALV\rightarrow \text{PLAS}} + FL_{j,INT\rightarrow \text{PLAS}}\right)$
O	7	$ELIM_j(T) = \sum_{t=0}^{T-\Delta t} FL_{j,LLI\rightarrow \text{FECE}}$
O	8	$SUM_j(T) = LUNGS_j(T) + GITRACT_j(T) + ABSORB_j(T) + ELIM_j(T)$
O	Notes	1) $INTAKE_j(T)$ is the time integrated Pb intake from air source j 2) $SUM_j(T)$ is the Pb mass still in the body, absorbed into PLAS, or eliminated. 3) For mass balance, $INTAKE_j(T)$ should equal $SUM_j(T)$ at all times T.
O		**Mass balance calculations – non-Air sources (j=4 to 18)**
O	9	$INTAKE_j(T) = \sum_{t=0}^{T} IN_j(t)$
O	10	$GITRACT_j(T) = Y_{j,STOM} + Y_{j,SI} + Y_{j,ULI} + Y_{j,LLI} + FL_{j,STOM\rightarrow SI} + FL_{j,SI\rightarrow PLAS} + FL_{j,SI\rightarrow ULI} + FL_{j,ULI\rightarrow \text{LLI}} + FL_{j,LLI\rightarrow \text{FECE}}$
O	11	$ABSORB_j(T) = \sum_{t=0}^{T-\Delta t} FL_{j,SI\rightarrow \text{PLAS}}$
O	12	$ELIM_j(T) = \sum_{t=0}^{T-\Delta t} FL_{j,LLI\rightarrow \text{FECE}}$
O	13	$SUM_j(T) = GITRACT_j(T) + ABSORB_j(T) + ELIM_j(T)$
O	Notes	4) $INTAKE_j(T)$ is the time integrated Pb intake from non-air source j 5) $SUM_j(T)$ is the Pb mass still in the GI tract, absorbed into PLAS, or eliminated. 6) For mass balance, $INTAKE_j(T)$ should equal $SUM_j(T)$ at all times T.
O		**Mass balance calculations for all Pb**
O	14	$START = YRBC(0) + YBRAN(0) + YSOF0(0) + YKDN2(0) + YLVR2(0) + YCVOL(0) + YTVOL(0)$
O	15	$INTAKE(T) = \sum_{j=1}^{18} INTAKE_j(T)$
O	16	$COMPART(T) = \sum_{k=1}^{31} Y_k(T)$
O	17	$FLOWS(T) = \sum_{m=1}^{55} FL_m(T)$
O	18	$ELIM(T) = YURIN(T) + YFECE(T) + YSWET(T) + YHAIR(T)$
O	Notes	7) START is the Pb present at birth 8) There are (up to) 18 sources, 31 compartments and 55 intercompartmental flows. 9) The total Pb "available" at time T is START + INTAKE(T). 10) The total Pb in the body is COMPART(T) + FLOWS(T) 11) The total Pb eliminated from the body up to time T is ELIM(T) 12) If START + INTAKE(T) = COMPART(T) + FLOWS(T) + ELIM(T) then Pb mass has been conserved. This should be true at all times T, but an explicit comparison is made only at the end of the simulation. If it holds then, it must hold at earlier times, as it is very improbable that a discrepancy would occur

		and then later be cancelled by an equal and opposite discrepancy.

APPENDIX B – ALL AGES LEAD MODEL FORTRAN CODE PARAMETERS

TABLE B-1. ALL AGES LEAD MODEL PARAMETER DESCRIPTIONS

Variable	Form	Type	Description
ADJUST	Vector	Real	Source specific multipliers with one value per source
ADJUSTABLE	Vector	Integer	Identifies which sources are adjustable
AGE_TS	Vector	Real	The age at each timestep
AGESCL	Vector	Real	Age scaling factor for PLAS loss deposition fractions
ALLOCERR	Scalar	Integer	Error status when allocating memory for arrays
ALLSOURCE	Vector	Special	Holds 5 source parameters for each of 19 sources
BLL	Scalar	Special	Holds 5 blood lead parameters
BUFF4	Vector	Real	Buffer for writing real (4 bytes) front end vectors to file 12
BUFF8	Vector	Real	Buffer for writing real (8 bytes) front end vectors to file 12
CF	Scalar	Real	Adjustment factor for TO variables (i.e., deposition fractions from plasma)
CONC	Array	Real	Linearly interpolated vector of concentrations: dim 1 = source, dim 2 = timestep
COUT	Array	Real	Concentrations for output: dim 1 = compartment, dim 2 = timestep
DATETIME	Vector	String	Buffers for holding string results of date and time query
DAYNUM	Vector	Integer	Days since start of simulation
DELT	Scalar	Real	Timestep duration in days (cannot exceed one)
DEP	Vector	Real	Pb mass deposited in lungs for one source in all compartments
DTVALUES	Vector	Integer	Buffers for holding integer results of date and time query
EAT	Scalar	Real	Total Pb mass ingested on this timestep
EXCRETE	Array	Real	Daily excreted mass: dim 1 = pathway, dim 2 = day #
FL	Array	Real	Intercompartmental Flow masses: dim 1 = flow #, dim 2 = timestep
FMT1	Scalar	String	Buffer for holding format specifier for writing output
FMT2	Scalar	String	Buffer for holding format specifier for writing output
FULL_TS	Vector	Real	Values on all timesteps over full lifetime (used for multiple modeling variables)

Variable	Form	Type	Description
GIABS	Scalar	Real	Source-specific gut absorption fraction
GR	Scalar	Special	Holds 9 growth parameters
I	Scalar	Integer	Looping index variable
INDX_AGE	Vector	Integer	List of days of age covered by the simulation
INDX_FULL	Vector	Integer	Shifted timestep indices starting each day from birth to age 100
INDX_TS	Vector	Integer	List of timestep numbers covered by the simulation
INDX_WRITE	Vector	Integer	Which timesteps are written to file 12 in front end calculations
INHAL	Scalar	Real	Pb mass deposited in lungs for one source on this timestep
INMASS	Scalar	Real	Sum of compartmental inflows when more than one is present
INTAKE_FRAC	Array	Real	Intake fractions for one medium: dim 1 = source, dim 2 = timestep
INTAKE_TOT	Array	Real	Total intake for one medium on each timestep
INTAKES	Array	Real	Daily exposure Intakes: dim 1 = variable #, dim 2 = day #
IOERR	Scalar	Integer	Error status indicator for reading or writing files
ITER	Scalar	Special	Holds 11 iteration input parameters
ITERATION	Scalar	Integer	Looping index for iterations in allowable concentration option
J	Scalar	Integer	Looping index variable
K	Scalar	Integer	Looping index variable
LASTADJUST	Vector	Real	source specific multipliers with one value per source
LASTSCALAR	Scalar	Real	Previous multiplier for the allowable concentrations
LINE	Scalar	Integer	Line number counter
LUNG	Vector	Special	Holds 11 lungs variables specific to each source
LUNGPLAS	Scalar	Real	Pb mass flowing from lungs to plasma on this timestep
MASK10	Vector	Real	Vector for masking timesteps (1=source on, 0=source masked)
MB	Array	Real	Holds 7 mass balance summary variables: dim 1 = variable #, dim 2 = timestep
MED3	Vector	String	First 3 letters of each of the 6 media
MEDIA	Vector	String	Names of the 6 source media
NBYMEDIA	Vector	Integer	Number of sources within each media type
NDAYS	Scalar	Integer	Number of days in the simulation
NDEP	Array	Real	Lung non-deposition masses: dim 1 = source, dim 2 = timestep
NEXSCALAR	Scalar	Real	Next multiplier for the allowable concentrations
NLEV	Scalar	Integer	Vector length for reading inputs

Variable	Form	Type	Description
NLUNG	Scalar	Integer	Number of lung compartments
NPERDAY	Scalar	Integer	Number of timesteps per day
NSOURCE	Scalar	Integer	Maximum source number
NTS	Scalar	Integer	Number of timesteps in the simulation
OUTFILE	Scalar	String	Buffer for holding names of output files (reused for each file)
OUTMASS	Scalar	Real	Compartmental outflow mass
OUTMASS	Scalar	Real	Sum of compartmental outflows when more than one is present
OUTPLAS	Scalar	Real	Sum of outflows from PLAS compartment
OUTRATE	Scalar	Real	Compartmental outflow rate
P	Scalar	Real	Compartmental inflow rate
PARFILE	Scalar	String	Buffer for holding name of input file
PC	Vector	Real	Physiological constants (variables within the array listed below)
POS1	Scalar	Integer	Parsing location in string
POS2	Scalar	Integer	Parsing location in string
PVARRAY	Array	Real	Physiological Variable array: dim 1 = variable #, dim 2 = timestep
PVIN	Array	Real	Input value for age-dependent physiological variables: dim 1 = variable #, dim 2 = age
PVROW	Vector	Real	No longer required
RUNNAME	Scalar	String	Name of this run from input file
SCALAR	Scalar	Real	Current value of multiplier for the allowable concentrations
SIM	Scalar	Special	Hold 7 simulation parameters
SOURCE	Array	Real	Source strengths: dim 1 = source number, dim 2 = timestep
SRCT	Array	Real	GI tract Pb by source: dim 1 = source #, dim 2 = timestep
SRCTM1	Array	Real	GI tract Pb by source: dim 1 = source #, dim 2 = timestep
SUPPRESS	Scalar	Real	Suppression factor for TORBC
T	Scalar	Integer	Number of current timestep
TIMESERIES	Vector	Real	Result of stepwise or interpolation filling for all timesteps over lifetime
TS_AGE	Array	Special	Time-varying quantities from front end: dim 1 = variable #, dim 2 = timestep
TS_AGE	Vector	Integer	Timestep number starting each day of age
UPTAKES	Array	Real	Daily plasma uptakes: dim 1 = medium and statistic, dim 2 =day #
VAR	Scalar	String	Buffer for reading variable name from input file
VARTYPE	Scalar	String	Category of each input line

Variable	Form	Type	Description
VI	Vector	Integer	Buffer for reading integer data from input file
VR	Vector	Real	Buffer for reading real data from input file
Y	Array	Real	Compartmental Pb masses: dim 1 = compartment #, dim 2 = timestep
YLUNGT	Array	Real	Lung Pb by source: dim 1 = compartment or flow #, dim 2 = source #
YLUNGTM1	Array	Real	Lung Pb by source: dim 1 = compartment or flow #, dim 2 = source #

Array Index	Variable	Unit	Explanation
PC Array			
1	ASHWT	g	Skeletal Ash weight (not currently used)
2	BLDMOT	µg/dL	Maternal blood Pb concentration
3	BONIN	unitless	Fraction of blood Pb in bone at birth
4	BRANIN	unitless	Fraction of blood Pb in brain at birth
5	BRATIO	unitless	Child (at birth):maternal blood Pb concentration ratio
6	CRTWT	g	cortical bone weight
7	H1TOBL	unitless	Fraction of Pb transfer out of liver compartment 1 that goes to diffusible plasma
8	H1TOH2	unitless	Fraction of Pb transfer out of liver compartment 1 that goes to liver compartment 2
9	H1TOSI	unitless	Fraction of Pb transfer out of liver compartment 1 that goes to the small intestine
10	HEPIN	unitless	Fraction of blood Pb in liver at birth
11	IFETAL	unitless	Switch for fetal simulation on (1) or off (0)
12	KWT	g	Adult kidney weight
13	PLSVOL	dL	Plasma volume
14	POWER	unitless	Exponent for non-linear deposition of Pb from diffusible plasma to RBC

Array Index	Variable	Unit	Explanation
15	RBCIN	unitless	Amount of Pb in RBC as a fraction of body Pb, at birth
16	RBCNL	µg/dL	Threshold Pb concentration in RBC for non-linear deposition of Pb from diffusible plasma to RBC
17	RBCVOL	dL	RBC volume
18	RENIN	unitless	Fraction of blood Pb in kidney at birth
19	RKDN1	day^{-1}	Rate coefficient for transfer from kidney compartment 1 to urinary pathway
20	RLLI	day^{-1}	Rate coefficient for Pb transfer from lower large intestine to feces
21	RLVR1	day^{-1}	Rate coefficient for Pb transfer from liver compartment 1 to small intestine or diffusible plasma
22	RPLS	day^{-1}	Rate coefficient for Pb transfer from diffusible plasma scaled to bone surface deposition (see RPLAS)
23	RPROT	day^{-1}	Rate coefficient for Pb transfer from bound plasma to diffusible plasma
24	RSIC	day^{-1}	Rate coefficient for Pb transfer from small intestine to upper large intestine
25	RSOF0	day^{-1}	Rate coefficient for Pb transfer from soft tissue compartment 0 to diffusible plasma
26	RSOF1	day^{-1}	Rate coefficient for Pb transfer from soft tissue compartment 1 to diffusible plasma
27	RSOF2	day^{-1}	Rate coefficient for Pb transfer from soft tissue compartment 2 to diffusible plasma
28	RSTMC	day^{-1}	Rate coefficient for Pb transfer from stomach to small intestine
29	RULI	day^{-1}	Rate coefficient for Pb transfer from upper large intestine to lower large intestine

Array Index	Variable	Unit	Explanation
30	S2HAIR	unitless	Deposition fraction for Pb from soft tissue compartment 1 to other excreta
31	SATRAT	µg/dL	Maximum (saturating) concentration of Pb in RBC
32	SIZEVF	unitless	Relative volume of the EVF compartment compared to plasma (EVF/Plasma)
33	SOFIN	unitless	Amount of Pb in other soft tissue as a fraction of total body Pb, at birth
34	TBONEL	unitless	Value of TBONE at end of life
35	TEVF	unitless	Deposition fraction for Pb from diffusible plasma to extravascular fluid
36	TFECE	unitless	Deposition fraction for Pb from diffusible plasma directly to the small intestine at time(t) scaled bone surface deposition (not including the transfer from biliary secretion, specified by RLVR1) (see TOFECE)
37	TKDN1	unitless	Deposition fraction for Pb from diffusible plasma to kidney compartment 1 scaled to bone surface deposition (see TOKDN1)
38	TKDN2	unitless	Deposition fraction for Pb from diffusible plasma to liver compartment 2 scaled to bone surface deposition (see TOKDN2)
39	TLVR1	unitless	Deposition fraction for Pb from diffusible plasma to liver compartment 1 scaled to bone surface deposition (see TOLVR1)
40	TOPROT	unitless	Deposition fraction for Pb from diffusible plasma to protein-bound plasma not scaled to bone surface deposition (see TPROT)
41	TORBC	unitless	Deposition fraction from diffusible plasma to RBC not scaled to bone surface (see TRBC)
42	TOSWET	unitless	Deposition fraction for Pb from diffusible plasma to sweat not scaled to bone surface deposition (see TSWET)

Array Index	Variable	Unit	Explanation
43	TOURIN	unitless	Deposition fraction for Pb from diffusible plasma to urine not scaled to bone surface deposition (see TURIN)
44	TRBWT	g	Trabecular bone weight
45	VBLC	L/kg	Blood volume fraction of body weight
46	VKC	L/kg	Kidney volume fraction of body weight
47	VLC	L/kg	Liver volume fraction of body weight
48	VLUC	L/kg	Lung volume fraction of body weight
49	HCTA	unitless	Adult hematocrit
50	HCTB	unitless	Birth hematocrit
			PV Array
1	AMTBLD	dL	Amount of blood at time(t)
2	F1	unitless	Fractional absorption of Pb from small intestine at time(t) (see AF1)
3	FLONG	unitless	Fraction of total Pb transfer from the exchangeable bone to non-exchangeable bone
4	GSCAL	unitless	Age scaling factor for gastrointestinal transfers at time(t) (see AGSCL)
5	RBLAD	day^{-1}	Rate coefficient for Pb transfer from urinary bladder to urine at time(t) (see ARBLAD)
6	RBRAN	day^{-1}	Rate coefficient for Pb transfer from brain to diffusible plasma at time(t) (see ABRAN)
7	RCORT	day^{-1}	Rate coefficient for Pb transfer from non-exchangeable cortical bone to diffusible plasma at time(t) (see ACORT)
8	RCS2B	day^{-1}	Rate coefficient for Pb transfer from cortical bone surface to diffusible plasma at time(t) (see ARCS2B)
9	RCS2DF	day^{-1}	Rate coefficient for Pb transfer from cortical bone surface to exchangeable cortical bone at time(t) (see ARCSDF)
10	RDIFF	day^{-1}	Rate coefficient for Pb transfer from exchangeable bone (cortical or trabecular) to surface and non-exchangeable bone – age array (see FLONG for fraction to non-exchangeable)

Array Index	Variable	Unit	Explanation
11	RKDN2	day^{-1}	Rate coefficient for transfer from kidney compartment 2 to diffusible plasma at time(t) (see ARKDN2)
12	RLVR2	day^{-1}	Rate coefficient for Pb transfer from the slow liver compartment 2 to diffusible plasma at time(t) (see ARLVR2)
13	RRBC	day^{-1}	Rate coefficient for Pb transfer from RBC to diffusible plasma at time(t) (see ARRBC)
14	RTRAB	day^{-1}	Rate coefficient for Pb transfer from non-exchangeable trabecular bone to diffusible plasma at time(t) (see ARTRAB)
15	RTS2B	day^{-1}	Rate coefficient for Pb transfer from trabecular bone surface to diffusible plasma at time(t) (see ARTS2B)
16	RTS2DF	day^{-1}	Rate coefficient for Pb transfer from surface trabecular bone to exchangeable trabecular bone at time(t) (see ARTSDF)
17	TBONE	unitless	Deposition fraction for Pb from diffusible plasma to surface bone at time(t) (see ATBONE)
18	TFRAC	unitless	Fraction of diffusible plasma-to-bone deposition that goes to trabecular surface bone at time(t); 1-TFRAC is the fraction that goes to cortical surface bone
19	TOBRAN	unitless	Deposition fraction for Pb from diffusible plasma to brain at time(t) (not scaled for bone surface deposition – see TBRAN)
20	TOSOF0	unitless	Deposition fraction for Pb from diffusible plasma to soft tissue compartment 0 at time (t), not scaled to bone surface deposition (see TSOF0)
21	TOSOF1	unitless	Deposition fraction for Pb from diffusible plasma to soft tissue compartment 1 at time (t), not scaled to bone surface deposition (see TSOF1)
22	TOSOF2	unitless	Deposition fraction from diffusible plasma to soft tissue compartment 2 at time (t), not scaled to bone surface deposition (see TSOF2)
Y Array			
1	STOM	µg	Stomach
2	SI	µg	Small Intestine
3	ULI	µg	Upper Large Intestine
4	LLI	µg	Lower Large Intestine
5	CSUR	µg	Cortical Bone Surface
6	CDIF	µg	Cortical Diffusive Bone
7	CVOL	µg	Cortical Non-diffusive Bone
8	TSUR	µg	Trabecular Bone Surface

Array Index	Variable	Unit	Explanation
9	TDIF	µg	Trabecular Diffusive Bone
10	TVOL	µg	Trabecular Non-diffusive Bone
11	PLAS	µg	Diffusible Blood Plasma
12	PROT	µg	Protein-Bound Blood Plasma
13	RBC	µg	Red Blood Cells
14	LVR1	µg	Liver Compartment 1 (receives from plasma)
15	LVR2	µg	Liver Compartment 2 (slow release)
16	KDN1	µg	Kidney Urinary Compartment
17	KDN2	µg	Kidney non-Urinary Compartment
18	BLAD	µg	Bladder
19	BRAN	µg	Brain
20	EVF	µg	Extra-vascular fluid
21	SOF0	µg	Soft Tissues 0 (Fast transfer)
22	SOF1	µg	Soft Tissues 1 (Intermediate transfer)
23	SOF2	µg	Soft Tissues 2 (Slow transfer)
24	URIN	µg	Urine
25	FECE	µg	Feces
26	SWET	µg	Sweat
27	HAIR	µg	Hair and Nails
28	LET	µg	Lung - Extrathoracic
29	LTB	µg	Lung – Tracheobronchial
30	LALV	µg	Lung-Alveolar
31	LINT	µg	Lung-Interstitial
FL Array			
1	LUNG_PLAS	µg	Total flow from lungs to plasma
2	LUNG_STOM	µg	Total flow from lungs to stomach
3	STOM_SI	µg	Flow from stomach to small intestine
4	SI_PLAS	µg	Flow from small intestine to plasma
5	SI_ULI	µg	Flow from small intestine to upper large intestine
6	ULI_LLI	µg	Flow from upper large intestine to lower large intestine
7	LLI_FECE	µg	Flow from lower large intestine to feces
8	CSUR_PLAS	µg	Flow from cortical bone surface to plasma
9	CSUR_CDIF	µg	Flow from cortical surface to cortical diffusive
10	CDIF_CSUR	µg	Flow from cortical diffusive to cortical surface
11	CDIF_CVOL	µg	Flow from cortical diffusive to cortical non-diffusive
12	CVOL_PLAS	µg	Flow from cortical non-diffusive to plasma
13	TSUR_PLAS	µg	Flow from trabecular bone surface to plasma
14	TSUR_TDIF	µg	Flow from trabecular surface to trabecular diffusive

Array Index	Variable	Unit	Explanation
15	TDIF_TSUR	µg	Flow from trabecular diffusive to trabecular surface
16	TDIF_TVOL	µg	Flow from cortical diffusive to cortical non-diffusive
17	TVOL_PLAS	µg	Flow from trabecular non-diffusive to plasma
18	LVR1_LVR2	µg	Flow from Liver 1 to Liver 2
19	LVR1_PLAS	µg	Flow from Liver 1 to plasma
20	LVR1_SI	µg	Flow from Liver 1 to small intestine
21	LVR2_PLAS	µg	Flow from Liver 2 to plasma
22	KDN1_BLAD	µg	Flow from kidney 1 to bladder
23	KDN2_PLAS	µg	Flow from kidney 1 to plasma
24	BLAD_URIN	µg	Flow from bladder to urine
25	BRAN_PLAS	µg	Flow from brain to plasma
26	EVF_PLAS	µg	Flow from extra-vascular fluid to plasma
27	SOF0_PLAS	µg	Flow from soft tissue 0 to plasma
28	SOF1_PLAS	µg	Flow from soft tissue 1 to plasma
29	SOF1_HAIR	µg	Flow from soft tissue 1 to hair
30	SOF2_PLAS	µg	Flow from soft tissue 2 to plasma
31	PROT_PLAS	µg	Flow from protein-bound plasma to (diffusible) plasma
32	RBC_PLAS	µg	Flow from red blood cells to plasma
33	PLAS_SI	µg	Flow from plasma to small intestine
34	PLAS_PROT	µg	Flow from plasma to protein-bound plasma
35	PLAS_RBC	µg	Flow from plasma to red blood cells
36	PLAS_EVF	µg	Flow from plasma to extra-vascular fluid
37	PLAS_SOF0	µg	Flow from plasma to soft tissue 0
38	PLAS_SOF1	µg	Flow from plasma to soft tissue 1
39	PLAS_SOF2	µg	Flow from plasma to soft tissue 2
40	PLAS_BRAN	µg	Flow from plasma to brain
41	PLAS_CSUR	µg	Flow from plasma to cortical bone surface
42	PLAS_TSUR	µg	Flow from plasma to trabecular bone surface
43	PLAS_LVR1	µg	Flow from plasma to liver 1
44	PLAS_KDN1	µg	Flow from plasma to kidney 1
45	PLAS_KDN2	µg	Flow from plasma to kidney 2
46	PLAS_BLAD	µg	Flow from plasma to bladder
47	PLAS_SWET	µg	Flow from plasma to sweat
48	LET_PLAS	µg	Flow from Lung-extrathoracic to plasma
49	LET_STOM	µg	Flow from lung-extrathoracic to stomach
50	LTB_PLAS	µg	Flow from lung-tracheobronchial to plasma
51	LTB_LET	µg	Flow from lung-tracheobronchial to lung-extrathoracic
52	LALV_PLAS	µg	Flow from lung-alveolar to plasma

Array Index	Variable	Unit	Explanation
53	LALV_LTB	µg	Flow from lung-alveolar to lung-tracheobronchial
54	LALV_LINT	µg	Flow from lung-alveolar to lung-interstitial
55	LINT_PLAS	µg	Flow from lung-interstitial to plasma
TS Array			
1	BLOOD_VOL	dL	Blood volume (dL)
2	BODY_WT	kg	Body weight (kg)
3	BONE_VOL	mL	Bone volume (mL)
4	BONE_WT	g	Bone weight (g)
5	CORT_WT	g	Cortical bone weight (g)
6	F1_ABS	unitless	GI tract absorption fraction (-)
7	HEMATOCRIT	unitless	Blood hematocrit fraction (-)
8	KID_WT	g	Kidney weight (g)
9	LIV_WT	g	Liver weight (g)
10	PLAS_VOL	dL	Plasma volume (dL)
11	RBC_CONC	µg/dL	Red blood cell Pb concentration (ug/dL)
12	RBC_VOL	dL	Red blood cell volume (dL)
13	R_BLAD	1/day	Loss rate constant for bladder
14	R_BRAN	1/day	Loss rate constant for brain
15	R_CDIFCSUR	1/day	Rate constant for transfer from CDIF to CSUR
16	R_CDIFCVOL	1/day	Rate constant for transfer from CDIF to CVOL
17	R_CORT	1/day	Loss rate constant for cortical volume
18	R_CSURPLAS	1/day	Rate constant for transfer from CSUR to plasma
19	R_CSURCDIF	1/day	Rate constant for transfer from CSUR to CDIF
20	R_EVF	1/day	Loss rate constant for extra-vascular fluid
21	R_KDN2	1/day	Loss rate constant for kidney 2 (to plasma)
22	R_LVR2	1/day	Loss rate constant for liver 2 (to plasma)
23	R_PLAS	1/day	Loss rate constant for diffusible plasma (PLAS)
24	R_RBC	1/day	Loss rate constant for bladder
25	R_TDIFTSUR	1/day	Loss rate constant for bladder
26	R_TDIFTVOL	1/day	Loss rate constant for bladder
27	R_TRAB	1/day	Loss rate constant for bladder
28	R_TSURPLAS	1/day	Loss rate constant for bladder
29	R_TSURTDIF	1/day	Loss rate constant for bladder
30	SKEL_WT	g	Skeletal weight (g) (not used)
31	TRAB_WT	g	Trabecular bone weight (kg)
32	T_BONE	unitless	Deposition fraction for plasma loss to bone
33	T_BRAN	unitless	Deposition fraction for plasma loss to brain
34	T_EVF	unitless	Deposition fraction for plasma loss to EVF
35	T_FRAC	unitless	Fraction of T_Bone going to Trabecular bone
36	T_KDN1	unitless	Deposition fraction for plasma loss to kidney 1

Array Index	Variable	Unit	Explanation
37	T_KDN2	unitless	Deposition fraction for plasma loss to kidney 2
38	T_LVR1	unitless	Deposition fraction for plasma loss to liver 1
39	T_PROT	unitless	Deposition fraction for plasma loss to protein-bound
40	T_RBC	unitless	Deposition fraction for plasma loss to red blood cells
41	T_SI	unitless	Deposition fraction for plasma loss to small intestine
42	T_SOF0	unitless	Deposition fraction for plasma loss to soft tissue 0
43	T_SOF1	unitless	Deposition fraction for plasma loss to soft tissue 1
44	T_SOF2	unitless	Deposition fraction for plasma loss to soft tissue 2
45	T_SUM	unitless	Sum of Deposition fractions for plasma loss
46	T_SWET	unitless	Deposition fraction for plasma loss to sweat
47	T_URIN	unitless	Deposition fraction for plasma loss to urine
Ylung Array			
1	LET	µg	Pb mass in lung-extrathoracic
2	LTB	µg	Pb mass in lung-tracheobronchial
3	LALV	µg	Pb mass in lung-alveolar
4	LINT	µg	Pb mass in lung-interstitial
5	F3LTBLET	µg	Pb lung flow from tracheobronchial to extrathoracic
6	F3LALVLTB	µg	Pb lung flow from alveolar to tracheobronchial
7	F3LALVLINT	µg	Pb lung flow from alveolar to interstitial
8	F3LETSTOM	µg	Pb lung flow from extrathoracic to stomach
9	F3LETPLAS	µg	Pb lung flow from extrathoracic to plasma
10	F3LTBPLAS	µg	Pb lung flow from tracheobronchial to plasma
11	F3LALVPLAS	µg	Pb lung flow from alveolar to plasma
12	F3LINTPLAS	µg	Pb lung flow from interstitial to plasma
Src Array			
1	INGEST18	µg	Ingested mass (this timetstep) from each source
2	F18LUNGPLAS	µg	Flow from lungs to plasma from each source
3	F18LUNGSTOM	µg	Flow from lungs to stomach from each source
4	Y18STOM	µg	Pb mass in stomach from each source
5	F18STOMSI	µg	Flow from stomach to small intestine from each source
6	Y18SI	µg	Pb mass in small intestine from each source
7	F18SIPLAS	µg	Flow from small intestine to plasma from each source
8	F18SIULI	µg	Flow from small intestine to ULI from each source
9	Y18ULI	µg	Pb mass in upper large intestine from each source
10	F18ULILLI	µg	Flow from ULI to LLI from each source
11	Y18LLI	µg	Pb mass in lower large intestine from each source

Array Index	Variable	Unit	Explanation
12	F18LLIFE	µg	Flow from LLI to feces from each source
13	Y18PLAS	µg	Pb mass absorbed into plasma from each source
14	Y18FE	µg	Time-integrated Pb mass in feces from each source
15	DIFF18	µg	Mass balance difference by source (for debugging)
			MB Array
1	YIN	µg	Time-integrated Pb mass entering body
2	YEAT	µg	Pb mass ingested on this timestep
3	YINHAL	µg	Pb mass inhaled on this timestep
4	YCOMP	µg	Sum of Pb mass in body compartments
5	YFLOW	µg	Sum of Pb mass in intercompartment flows
6	YBODY	µg	Total Pb mass in body
7	YOUT	µg	Time-integrated Pb mass leaving body

APPENDIX C – ALL AGES LEAD MODEL (VERSION 3.0) EXPOSURE PARAMETER VALUES

Exposure variables include variables that represent the concentration of Pb in air, indoor dust, soil, food and water, and activity factors that represent the intensity of exposure to contaminated environmental media (e.g., water consumption rates). All exposure variables that are accessible to the user are discussed in this appendix. Default values are intended to be central tendency estimates that are representative of the U.S. population. Sources for the default values are provided along with a brief summary of the sources. Some exposure variables were not assigned default values. Some of these variables were considered to be inherently site-specific and assigning default values to them would therefore be arbitrary. For others, reliable sources of data upon which to base a default value were not identified.

In general, the activity factors were taken from the Exposure Factors Handbook [EFH; (U.S. EPA, 2011)]. The EFH recommendations for default values for activity factors are based on thorough reviews of the exposure science literature and independent analyses of exposure data from surveys performed by others. The use of the EFH-recommended default values in the AALM, when appropriate, also promotes consistency in risk assessments performed by or for the Agency. In some cases, default values were based on recent studies that were not included in the EFH when the studies were deemed to be sufficiently reliable. Default values for activity factors recommended for use in the AALM are intended to correspond to U.S. population averages. These defaults may not apply to other populations. For example, intakes of soil dust, food and water may be affected by levels and types of activities. For these reasons, empirical estimates of activity factors are preferred to the default values if such data for the population of interest are available.

A strong preference was placed on basing default values for environmental concentration variables and activity factors on data from statistical surveys that were designed to provide data representative of the entire U.S. Equally important was ensuring that analyses of data from these surveys were done properly to produce unbiased estimates (i.e., properly used the sampling weights in calculating estimates and considered the complex sampling design when calculating standard errors).

AIR LEAD CONCENTRATION

The AALM allows the user to define multiple exposures to Pb in air. These can include up to three discrete (i.e., age-specific) exposure concentrations, a constant baseline concentration and up to two pulse trains in which air Pb concentration can vary at inputted durations and periods. Multiple exposures could be used to represent exposures to air Pb in various settings such as outdoor and indoor air; air at the home, school, workplace, or recreational sites; or continuous exposure or intermittent exposures.

Concentrations of Pb in air can be expected to vary considerably by location, depending on proximity to local sources (U.S. EPA, 2013). Based on analysis of data from U.S. national monitoring networks collected during the period 2008-2010, air Pb concentrations were as follows (U.S. EPA, 2013):

	Source Oriented	Non-source Oriented
Mean	0.21	0.012
Median	0.079	0.010
95th percentile	0.88	0.037

Units: µg/m^3

3-month rolling average, 2008-2010.

Source-oriented monitors are within one mile of ≥0.5 ton/year emission non-airport source or near airports in which use of leaded aviation fuels are estimated to result in >1 tone/year emissions.

A detailed description the national monitoring networks and related data can be found in U.S. EPA (2013).

Recommendations. Based on these data, 0.01 µg/m^3 is recommended as a default value for ambient air Pb concentration to represent average U.S. exposure concentrations distant from substantial emissions sources. For simulations of populations living near emissions sources, the source-oriented average could be used as a default for average air concentrations, however, it should be recognized that air Pb concentrations near emission sources could vary considerably depending on the strength of the source and other geographic and weather factors that would affect dispersion and deposition of emissions.

Although, the default values are based on measurements made of outdoor air, indoor and outdoor air Pb concentrations are expected to be similar if indoor environments that do not have substantial indoor sources of Pb (Clayton et al., 1999; Robertson et al., 1999).

INDOOR DUST LEAD CONCENTRATION

The AALM allows the user to define multiple exposures to Pb in indoor dusts. These can include up to three discrete (i.e., age-specific) exposure concentrations, a constant baseline concentration and up to three pulse trains in which dust Pb concentration can vary at inputted durations and periods. These could be used to represent exposures to Pb in various sources of dust such dusts at various locations (e.g., at the home, school, workplace, or recreational sites); or continuous exposure or intermittent exposures.

The National Human Exposure Assessment Surveys (NHEXAS) provides data on indoor dust Pb concentrations in statistical samples from various locations. Based on data for approximately 250 residences in EPA Region 5 (Great Lakes region), the mean Pb concentrations were as follows (Clayton et al., 1999):

Surface	Window Sill
463	954
(188, 738)	(481, 3164)

Units: µg/g (95% CL)

Based on NHEXAS data for approximately 119 residences in Arizona, the median Pb concentration (XRF) was 21 µg/g [90th percentile: 122; (Robertson et al., 1999)].

Concentrations of Pb in dusts can be expected to vary considerably by location, depending on proximity to local sources, presence in lead-based paint, and dust cleaning practices (U.S. EPA, 2013). The National Survey of Lead and Allergens (NSLAH) conducted by the Department of Housing and Urban

Development; (Clickner et al., 2002) provides data in Table 5.7 of their report on Pb in residential indoor dusts for a statistical sample of U.S. residences. Based on a sample of approximately 2000 homes, the mean Pb loading (µg/ft^2) were as follows:

Floors (n = 3,894	Window Sills (n = 2,302)	Window Troughs (n = 1,607)
13.6±484	195±1683	1991±12,086

Units: µg/ft^2

Data on dust Pb loading on indoor surfaces (µg Pb/ft^2) provide additional sources estimated of indoor dust Pb concentration (U.S. EPA, 2019b). An analysis of data on Pb loading collected as part of the American Healthy Housing Survey [AHHS; (HUD, 2011)] provided the following central estimates for residential Pb loading and concentration (U.S. EPA, 2019b):

Loading (µg/ft^2)		Concentration (µg/g)	
Median	**Mean**	**Median**	**Mean**
0.8	1.2	107.8	175.0

Recommendations. Based on the above data, 175 µg/g is recommended as a default value for the parameter indoor dust Pb concentration to represent average U.S. exposure concentrations distant from substantial current or historical emission sources (e.g., background) that could impact the indoor environment (e.g., track in from contaminated soil). A value of equal to 70% of the soil Pb concentration (see section on *Soil Lead Concentration*) is recommended for indoor dust Pb concentration for simulating residences where soil derived dust is the major source of indoor dust Pb (e.g., no other significant indoor sources such as paint or hobbies). This assumption is consistent with the IEUBK model. Indoor dust Pb concentrations in residences impacted by Pb-based paint can be expected to vary considerably within and between residences and local exposure conditions should be considered to establish a representative estimate.

In addition to this recommended value, a dust loading to concentration calculator is included in the AALM User Interface within the dust media. This calculation uses the following equation from Bevington et al. (2021):

$$Pb\ dust\ concentration = e^{5.291+0.413(ln(Pb\ dust\ loading)-1.272)}$$

SOIL LEAD CONCENTRATION

The AALM allows the user to define multiple exposures to Pb in soil. These can include up to three discrete (i.e., age-specific) exposure concentrations, a constant baseline concentration and up to three pulse trains in which dust Pb concentration can vary at inputted durations and periods. These could be

used to represent exposures to Pb in various sources of surface soil such soils at various locations (e.g., at the home, school, workplace, or recreational sites), or continuous exposure or intermittent exposures.

Concentrations of Pb in soils can be expected to vary considerably by location, depending on proximity to local sources (U.S. EPA, 2013). A study conducted by the U.S. Geological Survey measured soil Pb concentrations along a 4000 km east-west transect of the U.S. (Smith et al., 2013; Reimann et al., 2011). Sampling locations were selected to avoid local sources, including roads, buildings, power plants and smelters. The mean concentrations for samples collected a depth of 0–5 cm depth (sieved at 2 mm) are as follows:

Full Transect (µg/g; n = 4841)		Sitewide average (µg/g; n = 48)	
Mean	**5th-95th percentiles**	**Mean**	**5th-95th percentiles**
25	8 - 44	107.8	14 - 48

Data for individual U.S. states and physiographic provinces are provided in Smith et al. (2013).

NSLAH conducted by the Department of Housing and Urban Development; Clickner et al. (2002) provide data in Table 6.3 of their report on Pb in residential soil for a statistical sample of U.S. residences. Based on a sample of approximately 700 residential yards, the mean Pb concentrations (µg/g) were as follows:

Main Entryway	Dripline 1	Dripline 2	Midyard 1	Midyard 2
235±1094	243±818	404±1613	87±195	123±360

µg/g, mean ± SD

Based on data from the AHHS (HUD, 2011; Clickner et al., 2002), the following central estimates for soil Pb concentration were estimated (U.S. EPA, 2019b):

Housing Stock	GM	GSD	Median	Mean
Pre-1940	113.4	3.58	113.4	246.8
1940-1977	28.6	2.9	28.6	50.0
Pre-1978	26.3	3.8	26.3	64.1

GM, geometric mean, µg/g; GSD, geometric standard deviation

Recommendations. Based on the above data, 25 µg/g is recommended as a default value for yard soil Pb concentration to represent average U.S. exposure concentrations distant from substantial current or historical emission sources (e.g., background). Means for individual U.S. states ranged 6 to 80 µg/g. These estimates are based on measurements made in soils sieved to <2 mm and which may have underestimated Pb concentration in the fine fraction (e.g., <250 µm or <150 µm) that is typically used to represent the exposure term for the adherence to hand-to-mouth pathway used in risk assessment. The

value 50 µg/g is recommended as a value for yard soils associated with post 1940 housing stock and 250 µg/g for older housing stock.

WATER LEAD CONCENTRATION

The AALM allows the user to define multiple exposures to Pb in drinking water. These can include up to three discrete (i.e., age-specific) exposure concentrations, a constant baseline concentration and up to two pulse trains in which water Pb concentration can vary at inputted durations and periods. These could be used to represent exposures to Pb in various exposure settings such: home, school, workplace, or recreational sites; or continuous exposure or intermittent exposures.

Concentrations of Pb in drinking water can be expected to vary considerably by location, depending on water source, Pb in service lines and extent of plumbing corrosion (U.S. EPA, 2007a). In residences served by lines containing Pb, first-draw water that has been stagnant in plumbing will tend to have a higher Pb concentration than after the system has been flushed. The NHEXAS provides data on drinking water Pb concentrations in statistical samples from various locations. Based on data for approximately 250 residences in EPA Region 5 (Great Lakes region), the mean Pb concentrations were as follows (Clayton et al., 1999):

First draw	Flushed
3.92	0.84
(3.06, 4.79)	(0.6, 1.07)

Units: µg/L (95% CL)

Based on NHEXAS data for approximately 82 residences in Arizona, median, 75th and 90th percentile of Pb concentrations in flushed unfiltered tap water were 0.4, 0.9, and 1.3 µg/L, respectively (O'Rourke et al., 1999).

The EPA TRW analysed data tap water concentrations reported for the Six-Year Review-ICR dataset. This survey conducted during the period 1998-2005 measured first-draw tap water concentration in residences supplied by approximately 883 public water suppliers in the U.S. Based on this analysis, the mean tap water concentrations were as follows:

Sample Mean	Population Weighted Mean
4.89	0.89
(4.38, 5.39)	(0.78, 1.01)

Units: µg/L (95% CL)
Population weighted mean is weighted for number of people served by each supplier.

Based on data in Supplemental Information from Zartarian et al. (2017), the average, 95th percentile and 99th percentile values from this dataset are 0.89, 2.25 and 13.27 µg/L, respectively. The following central estimates for water Pb concentration were estimated (U.S. EPA, 2019b):

GM	GSD	Median	Mean
0.69	2.1	0.69	0.89

GM, geometric mean, µg/g; GSD, geometric standard deviation

Recommendations. Based on the above data, 0.9 µg/L is recommended as a default value for the parameter household drinking water Pb concentration to represent average U.S. exposure concentrations to tap water from public water supplies. This default value may not apply to local conditions that contribute to leaching of Pb into tap water (e.g., Pb service lines, Pb solder, corrosion).

FOOD LEAD INTAKE

The AALM allows the user to define multiple exposures to Pb in food. These can include up to three discrete (i.e., age-specific) food Pb intakes (µg/day), a constant baseline intake and up to two pulse trains in which food Pb intake can vary at inputted durations and periods. These could be used to represent exposures to Pb in various diets or sources of food (e.g., market basket, home grown produce, local fish or game); or continuous exposure or intermittent exposures.

The rate of Pb intake from food can be expected to vary considerably depending on the diet and age. The NHEXAS provides data on food Pb intakes in statistical samples from various locations (Clayton et al., 1999; Thomas et al., 1999). Based on a sample for 159 residences (children and adults), the mean food Pb intakes was 7.96 µg/day [95% CL: 4.2, 11.6; (Clayton et al., 1999)].

The EPA TRW estimated food Pb intakes in children based on data from the U.S. Food and Drug Administration Total Diet Studies performed between 1995–2005 (FDA, 2007, 2006) and food consumption data from the National Food Consumption Survey (NCFS) that was performed as part of the Third National Health and Nutrition Examination Survey (NHANES 2003–2006). Age category mean Pb intakes were as follows:

Age Category (months)	Dietary Pb Intake (µg/day)
0 to <12	2.26
12 to <24	1.96
24 to <36	2.13
36 to <48	2.04
40 to <60	1.95
60 to <72	2.05
72 to <84	2.22

Recommendations. Based on the above data, 10 µg/day is recommended as a default value for dietary Pb intake from food in adults. This corresponds to an intake of approximately 0.14 µg/kg bw/day which yields lead intake estimates of 7.9 µg/day in adult females (56.2 kg body weight) and 10.0 µg/day in adult males (71.4 kg body weight), if AALM.FOR growth is assumed. The adult female and male values were scaled to age using the following equation:

$$CR_{age_i} = CR_{adult} \cdot \frac{EER_{age_i}}{EER_{adult}}$$

where CR is the food Pb consumption rate (µg/day) for any given age (age_i) or adults (≥20 years), and EER is the Estimated Energy Requirement [see Appendix 14 of SRC (2021)]. Values for EER for specific ages were estimated from regression equations reported in IOM (2005) that related EER to body size (body mass and length) and activity level. IOM (2005) derived regression models for four activity levels: sedentary, low active, active, very active. The AALM defaults assume EERs for the low active category, which was described in IOM (2005) as equivalent *walking at a pace of 2.5 miles/hour for 2 hours*, and considered to represent average activity of the general population. The resulting default values for age-category food Pb intakes are as follows:

Age (year)	Female EER (kcal/day)	Male BW (kcal/day)	Female Pb Intake (µg/day)	Male Pb Intake (µg/day)
1	596	652	2.3	2.3
2	864	928	3.3	3.3
3	1057	1106	4.0	3.9
4	1512	1580	5.7	5.6
5	1597	1673	6.0	6.0
6	1685	1758	6.4	6.3
7	1764	1858	6.7	6.6
8	1859	1949	7.0	6.9
9	1941	2063	7.3	7.3
10	2026	2170	7.7	7.7
15	2429	3044	9.2	10.8
≥20	2090	2811	7.9	10.0

For intake 0.14 µg/kg bw/day.
EER, Estimated Energy Requirement for low-active activity level SRC (2021).

The above age array of food Pb intakes are recommended default values for dietary Pb intake by age category for the average U.S. diet. Several factors should be considered in applying the above defaults to simulations of populations of interest. The EER scaling approach to deriving age-specific food Pb intakes assumes that food consumption is directly proportional to EER and Pb content of consumed foods is independent of age. The latter assumption may not hold for all ages. For example, infants, children, adolescents, and adults may not consume the same foods. This will be particularly important for infant exposures, which may derive calories substantially from sources unique to that age, such as breast milk or formula diets. For this reason, empirical estimates of age-specific food Pb intakes are preferred to the default values if such data for the population of interest are available. Exposures to food Pb sources specific to an age range such as breast milk can be inputted into the AALM as a specific food Pb source.

Fetal Pb intake from breast milk can be estimated based on maternal blood Pb level and daily milk consumption. Studies of mothers in Mexico City, Mexico having mean maternal blood Pb levels of 7.7 to 9.4 µg/dL had mean breast milk Pb concentrations of 0.8 to 1.5 µg/L yielding ratios of 0.10 to 0.16 µg/L

milk per µg/dL maternal blood Pb (Ettinger et al., 2014; Ettinger et al., 2004). In a study of women migrating to Australia, women with a mean blood Pb level of 2.9 µg/dL had a mean breast milk Pb concentration of 0.73 µg/L yielding a ratio of 0.25 µg/L milk per µg/dL maternal blood Pb (Gulson et al., 1998). Gulson et al. (1998) cautioned that studies reporting >1.5 µg/L milk Pb per µg/dL maternal blood Pb are likely due to contamination of samples (e.g., contamination due to Pb on hands of women as they collect their milk). Daily milk intake for infants <12 months of age is 0.66 L/day (central tendency) with an upper percentile (mean + 2SD; i.e., the 98th percentile) intake rate of milk of 1.0 L/day [see Table 15-1 of U.S. EPA (2011)]. A central tendency estimate of infant exposure to Pb in maternal breast milk is 0.66 L/day at a 0.2 µg/L milk Pb per µg/dL maternal blood Pb. This yields a central tendency daily exposure rate estimate which would be entered as a food source having a rate of 0.132 µg Pb per µg/dL maternal blood Pb. For example, food intake from breast milk is 0.66 µg/day (i.e., 0.132×5) for a child whose mother has a blood Pb concentration of 5 µg/dL. A conservative (upper percentile) estimate of infant exposure to Pb in maternal breast milk is 1.0 L/day milk consumption at a 1.0 µg/L milk Pb per µg/dL maternal blood Pb. This yields a protective upper percentile daily exposure rate estimate which would be entered as a food source having a rate of 1.0 µg Pb per µg/dL maternal blood Pb (e.g., food intake from breast milk is 5 µg/day [i.e., 1.0×5] for a child whose mother has a blood Pb concentration of 5 µg/dL).

DUST AND SOIL INGESTION RATES

The EPA Exposure Factors Handbook (U.S. EPA, 2017b) provides the following recommendations for dust and soil ingestion rates to be used in U.S. EPA risk assessments.

Age Category	Dust (g/day)	Soil (g/day)	Dust + Soil (g/day)
<6 months	0.020	0.020	0.040
6 months to 1 year	0.040	0.030	0.070
1 to <2 years	0.050	0.040	0.090
2 to <6 years	0.030	0.030	0.060
1 to 6 years	0.040	0.040	0.080
6 to <12 years	0.030	0.030	0.060
>12 years	0.020	0.010	0.030

The EPA TRW estimated combined soil and dust ingestion rates in children based on the best fit model from von Lindern et al. (2016) and supported by modelled estimates from Ozkaynak et al. (2011) and Wilson et al. (2013).

Age category mean ingestion rates were as follows:

Age Category (months)	Soil + Dust (g/day)
0 to 12	0.086
13 to 24	0.094
25 to 36	0.067
37 to 48	0.063
49 to 60	0.067
61 to 72	0.052
73 to 84	0.055

Recommendations. Based on the Exposure Factors Handbook (U.S. EPA, 2017b), the following values are recommended as default values for average U.S. ingestion rates of soil and dust in children and adults. The default values for adults may not represent activities that result in intensive dermal contact with surface dusts, such as construction or excavation.

Age (days)	Dust Ingestion *IR_dust* (g/day)	Soil Ingestion *IR_soil* (g/day)	Combined Dust and Soil *IR_sd* (g/day)	Soil Fraction *f_IR_soil*
0	0.022	0.018	0.040	0.45
90	0.039	0.032	0.070	0.45
365	0.050	0.041	0.090	0.45
1825	0.044	0.036	0.080	0.45
3650	0.033	0.027	0.060	0.45
5475	0.017	0.014	0.030	0.45
9125	0.017	0.014	0.030	0.45
≥18250	0.017	0.014	0.030	0.45

The AALM default values cover a much wider age range than the default values for the IEUBK model but result in similar average combined intake of soil and dust over age range 0 to 7 years (AALM = 0.079 g/day; IEUBK model = 0.069 mg/day).

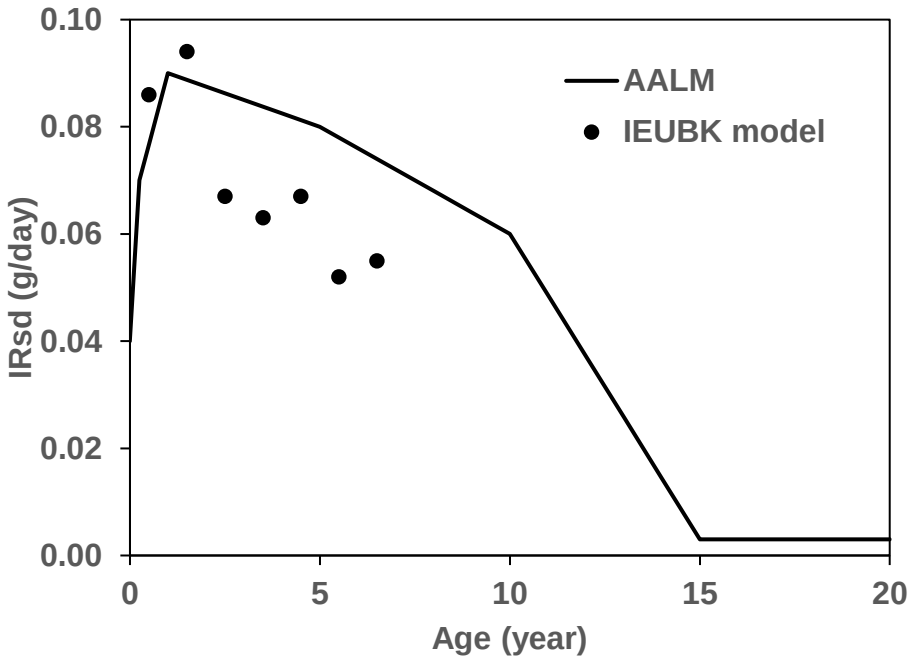

WATER INTAKE RATE

Water ingestion rate can be expected to vary with age, activity level and environmental factors (e.g., temperature, humidity). U.S. EPA (2011) has recommended the following age-specific water ingestion rates for use in EPA risk assessments of the general population:

Age	Mean Intake (mL/day)	95th Percentile (mL/day)
Birth to <1 mo	184	839
1 to <3 mo	227	896
3 to < 6 mo	362	1056
6 to <12 mo	360	1055
1 to <2 yr	271	837
2 to <3yr	317	877
3 to <6 yr	327	959
6 to <11 yr	414	1316
11 to <16 yr	520	1821
16 to <21 yr	573	1783
18 to <21 yr	681	2368
≥21 yr	1043	2958
≥65 yr	1046	2733
All ages	869	2717

The EPA TRW estimated drinking water intakes rates in children based on and analysis of data from the 1994–1996 and 1998 Continuing Survey of Food Intakes by Individuals (USDA, 2000) as reported by Kahn and Stralka (2009). Age category mean water ingestion rates were as follows:

Age Category (months)	Water Intake (L/day)
0 to <12	0.40
12 to <24	0.43
24 to <36	0.51
36 to <48	0.54
40 to <60	0.57
60 to <72	0.60
72 to <84	0.63

Recommendations. Based on the above data, the following water consumption values are recommended as default values to represent average U.S. drinking water ingestion rates in children and adults:

Age (days)	Water Intake (L/day)
0	0.20
90	0.30
365	0.35
1825	0.35
3650	0.45
5475	0.55
9125	0.70
≥18250	1.04

VENTILATION RATE

The AALM assigns values from the user interface for regional deposition of inhaled Pb (see parameters DEPFracLET, DEPFracLTB, DEPFracLalv; Appendix D) and clearance in the RT (see parameters RlalvLint, RlalvLplas, RLalvLTB, RLETLplas, RLETLstom, RlintLplas, RLTBLET, RLTBLplas; Appendix D). Values for the regional deposition and clearance into plasma are based on experimental studies conducted adults who inhaled submicron particles from automobile exhausts (see Section 2.3.3.1).

Regional deposition and clearance in the RT depend on numerous factors, including age and particle size, as well as various factors that affect ventilation rates (m^3/day) which vary with age, disease and physical activity [see Chapter 4 of U.S. EPA (2019a) for more detail]. It is anticipated that deposition fractions calculated using the Multi-Path Particle Dosimetry model (MPPD; Version 3.04, ©2016 or a subsequent

version) might be used in a future release.[9] It is also anticipated that particle dissolution rates derived from Brown and Diamond (2023) might be used to estimate compartmental outflows to plasma in a future release.

The ICRP (1994) has recommended the following age-specific activity-based breathing patterns for use in radiation dosimetry assessments of the general population:

Age	Sex	Respiratory Parameter	Sitting	Light Exercise	Heavy Exercise
Adult (30 years)	Male [a]	V_T (mL)	750	1250	1923
		f (min^{-1})	12	20	26
		Intake (m^3/hr)	0.54	1.50	3.00
	Female [b]	V_T (L)	464	992	1364
		f (min^{-1})	14	21	33
		Intake (m^3/hr)	0.39	1.25	2.70
Adolescent (15 years) [b]	Male	V_T (L)	533	1000	1352
		f (min^{-1})	15	23	36
		Intake (m^3/hr)	0.48	1.38	2.92
	Female	V_T (L)	417	903	1127
		f (min^{-1})	16	24	38
		Intake (m^3/hr)	0.40	1.30	2.57
Child (10 yrs) [b]	Male	V_T (L)	333	583	841
		f (min^{-1})	19	32	44
		Intake (m^3/hr)	0.38	1.12	2.22
	Female	V_T (L)	333	583	667
		f (min^{-1})	19	32	46
		Intake (m^3/hr)	0.38	1.12	1.84

V_T, tidal volume; f, breathing frequency; Data from Table B.15 of ICRP (1994).
[a] Based on ¶B66 of ICRP (1994) – Sitting is awake and sedentary activity with ventilation rate of ~12% of an untrained adult male's maximum workload. Light exercise is one third of an untrained adult male's maximum workload and includes activities such as working in laboratories or workshops, active housecleaning, painting, woodworking, etc. Heavy exercise is two thirds of an untrained adult male's maximum workload for periods not to exceed two hours and includes activities such as firefighting, intensive construction or farm work, digging, and splitting logs.
[b] From ¶B66 of ICRP (1994) – Values for females, adolescents, and children were scaled from on adult male values.

[9] The MPPD model can be used to calculate particle deposition and clearance in multiple species. A description of the model, recent model improvements, and advancements incorporated into the MPPD model are provided by Miller et al. (2016). For additional information about the MPPD model (Version 3.04) or to obtain a copy, the reader is referred to: http://www.ara.com/products/mppd.htm.

The intake rates above can be multiped by the number of hours that an individual is engaged in a specific activity to estimate a daily intake. It is anticipated that the above tidal volumes and breathing frequencies can be used for MPPD-based estimates of deposition fractions in a future version of the AALM.

U.S. EPA (2011) has recommended the following age-specific activity weighted ventilation rates for use in EPA risk assessments of the general population:

Age Category	Mean Ventilation (m^3/day)	95th Percentile (m^3/day)
Birth to <1 mo	3.6	7.1
1 to <3 mo	3.5	5.8
3 to < 6 mo	4.1	6.1
6 to <12 mo	5.4	8.0
Birth to <1 yr	5.4	9.2
1 to <2 yr	8.0	12.8
2 to <3yr	8.9	13.7
3 to <6 yr	10.1	13.8
6 to <11 yr	12.0	16.6
11 to <16 yr	15.2	21.9
16 to <21 yr	16.3	24.6
21 to <31 yr	15.7	21.3
31 to <41 yr	16.0	21.4
41 to 51 yr	16.0	21.2
51 to 61 yr	15.7	21.3
61 to 71 yr	14.2	18.1
71 to <81 yr	12.9	16.6
≥ 81 yr	12.2	15.7

The EPA TRW estimated ventilation rates in children based on and analysis of data on total energy expenditure (estimated from doubly labeled water studies) and relationships between energy expenditure and ventilation rate (Stifelman, 2007; Brochu et al., 2006; Layton, 1993). Age category mean ventilation rates were as follows:

Age Category (months)	Ventilation Rate (m^3/day)
0 to <12	3.22
12 to <24	4.97
24 to <36	6.09
36 to <48	6.95
40 to <60	7.68
60 to <72	8.32
72 to <84	8.89

Recommendations. Based on the above data, it is recommended for children and adults exposed to Pb in ambient air that the U.S. EPA (2011) mean ventilation rates are used as default values. For children or adults exposed to Pb-associated aerosols for brief periods such as associated with hobbies or occupation exposures, it is recommended that the intake rates from ICRP (1994) in m^3/hr be multiplied by the number of hours of exposure per day to yield an intake m^3/day based on the age, sex, and activity of the exposed individual.

LEAD RBA IN DUST

A discussion of available data on RBA of Pb in indoor dust can be found in U.S. EPA (2013). RBA of Pb in house dusts has not been rigorously evaluated quantitatively in humans or in experimental animal models, unlike soil (see section on *RBA soil*). As with soil, RBA of dust Pb can be expected to vary depending on the Pb mineralogy, physical characteristics of the Pb in the dust (e.g., encapsulated or exposed) and size of the Pb-bearing particles. The RBA for paint Pb mixed with soil (relative to lead acetate) was reported to be approximately 0.72 (95% CI: 0.44, 0.98) in juvenile swine, suggesting that paint Pb dust reaching the gastrointestinal tract maybe highly bioavailable (Casteel et al., 2006). Several studies have measured in vitro bioaccessibility (IVBA) of Pb in residential indoor dust; however, with few exceptions, these have not used IVBA methods for from which RBA can be reliably estimated (Juhasz et al., 2011; Lu et al., 2011; Smith et al., 2011; Roussel et al., 2010; Yu et al., 2006). A study conducted at two sites in EPA Region 7 compared Pb RBA estimated from IVBA using a estimation method that had been validated for soil as described in U.S. EPA (2013). At the Herculaneum site, mean RBA was 0.47 (SD 0.07, 10 samples) for indoor dust and 0.69 (SD 0.03, 12 samples) for soil. At the Omaha site, mean Pb RBA was 0.73 (SD 0.10, 90 samples) for indoor dust and 0.70 (SD 0.10, 45 samples) for soil.

LEAD RBA IN SOIL

A discussion of available data on RBA of Pb in soil can be found in U.S. EPA (2013). RBA of soil Pb can be expected to vary depending on the Pb mineralogy, physical characteristics of the Pb in the soil (e.g., encapsulated or exposed) and size of the Pb-bearing particles. The EPA TRW has recommended a value of 60% for RBA for ingested soil Pb based on analysis of data on soil Pb RBA estimated in bioassays of juvenile swine (Bannon et al., 2009; Smith et al., 2009; Casteel et al., 2006; Marschner et al., 2006); and other unpublished data collected as part of site risk assessments. The soil RBA measured in the swine assay is equivalent to the ratio of the absorbed fraction of an ingested dose of soil Pb to that of water-soluble Pb acetate. Analysis of 31 soils (excluding galena-enriched soil, soils from firing ranges, and soils sieved at >250 µm) resulted in a median RBA estimate of 60% with the 5th–95th percentile range from 11–97%; the mean RBA is 54% ±32 SD. RBA estimates for soils collected from eight firing ranges were approximately 100% [mean =108% ± 18; (Bannon et al., 2009)]. The relatively high RBA for the firing range soils may reflect the high abundance of relatively un-encapsulated lead carbonate (30-90% abundance) and lead oxide (1–60%) in these soils. Similarly, a soil sample (low Pb concentration) mixed with a National Institute of Standards and Technology paint standard (55% lead carbonate, 44% lead oxide) also had a relatively high bioavailability [72%; (Casteel et al., 2006)]. Samples of smelter slag, or soils contaminated with slag, had relatively low RBA (14–40%, n = 3) as did a sample from a mine tailings pile (RBA = 6%), and a sample of finely ground galena mixed with soil [1%; (Casteel et al.,

2006)]. A single estimate for RBA of interior dust was 51% for a sample collected at the Herculaneum site.

LEAD RBA IN FOOD

RBA of water-soluble Pb dissolved in food is assumed to be 1. RBA of Pb in foods has not been studied and it is possible that certain exposure settings could result in ingestion of Pb that has and TBA <1 in association with food. For example, adherence of surface dust, soil or sediments to consumed foods.

LEAD RBA IN WATER

RBA of Pb dissolved in water is assumed to be 1. This is based on evidence that dissolution of Pb from the soil/mineralogical matrix in the stomach appears to be the major process that renders soil Pb bioaccessible for absorption in the GI tract (U.S. EPA, 2013, 2007b). However, his may not apply to Pb-bearing particles suspended in surface water and this may be relevant to certain exposure settings (e.g., incidental ingestion of suspended sediments during activities such as swimming or play near shorelines).

Recommendations. Based on the above data, the following values are recommended as default RBA values:

Medium	RBA
Dust_paint[a]	1
Dust_soil[b]	0.6
Soil	0.6
Food	1
Water	1

[a]Indoor dust derived from Pb-based paint
[b]Indoor dust derived from soil

APPENDIX D – ALL AGES LEAD MODEL BIOKINETICS PARAMETER VALUES

AALM biokinetics parameters and values are listed in Table D-1. The bases for values assigned to each parameter are summarized below. Parameters are presented in alphabetical order, according to the parameter name. Default values assigned to these parameters are intended to represent average values expected in a population of healthy individuals.

AGE_RANGE: Age years for parameters that are assigned values at specific ages. Values assigned to *AGE_RANGE* are 0-90 years.

BLDMOT: Maternal blood Pb concentration. The value 0.6 µg/dL is based on an analysis of blood Pb concentration data for U.S. females aged 17–45 years reported in the NHANES 2009–2014 and assessed by U.S. EPA (2017a).

BRATIO: Child (at birth):maternal blood Pb concentration ratio. The value assigned to BRATIO is from Leggett (1993). The value of 0.85 is based on studies that have compared maternal and fetal cord blood Pb concentrations which have observed cord-maternal ratios ranging from 0.7 to 1 (Baranowska-Bosiacka et al., 2016; Gulson et al., 2016; Kayaalti et al., 2015; Kim et al., 2015; Baeyens et al., 2014; Chen et al., 2014; Kazi et al., 2014; Reddy et al., 2014; Amaral et al., 2010; Kordas et al., 2009; Patel and Prabhu, 2009; Carbone et al., 1998; Goyer, 1990; Graziano et al., 1990).

DepFracLalv: Inhaled particle deposition fraction in the alveolar region of the respiratory tract. Default is 0.040 to have a total deposition fraction of 0.40 in a three-compartment lung clearance model to match the four-compartment lung clearance model of Leggett (1993) as described in Section 2.3.3.1.

DepFracLET: Inhaled particle deposition fraction in the extrathoracic region of the respiratory tract. Default is 0.200 to have a total deposition fraction of 0.40 in a three-compartment lung clearance model to match the four-compartment lung clearance model of Leggett (1993) as described in Section 2.3.3.1.

DepFracLTB: Inhaled particle deposition fraction in the extrathoracic region of the respiratory tract. Default is 0.159 to have a total deposition fraction of 0.40 in a three-compartment lung clearance model to match the four-compartment lung clearance model of Leggett (1993) as described in Section 2.3.3.1.

F1: Parameters used calculating age-specific absorption fraction of Pb from small intestine (see variable *F1* in Biokinetics GI Tract, Appendix A). The absorption fraction is calculated based on an expression from O'Flaherty (1995, 1993) and from Leggett (1993).

FLONG: Fraction of total Pb transfer from the exchangeable bone volume to non-exchangeable bone volume. The fraction of total Pb transfer from the exchangeable bone volume to bone surface (cortical or trabecular) is 1.0-FLONG. The value of 20% from Leggett (1993) was revised to 0.6, based on calibration of simulations (see Chapter 4) of bone Pb elimination kinetics in retired Pb workers (Nilsson et al., 1991).

GSCAL: Age-scaling factor for gastrointestinal transfer rates. Age-dependent values assigned to *GSCAL* are the same as those in Leggett (1993). The value of 1is assigned to adults and higher values for infants and children. This results in a slower removal kinetics in children compared to adults (Corazziari et al., 1985).

H1TOBL: Fraction of Pb transfer from liver compartment 1 to diffusible plasma. The value assigned to *H1TOBL* is from Leggett (1993). Transfer out of liver compartment 1 includes 45% to diffusible plasma

(*H1TOBL*), 45% to small intestine (*H1TOSI*) and 10% to liver compartment 2 (*H1TOH2*). These assumptions based on estimates of hepatic uptake and retention in humans and animals, and biliary secretion in humans (Heard and Chamberlain, 1984; Lloyd et al., 1975; Cohen et al., 1970).

H1TOH2: Fraction of Pb transfer from liver compartment 1 to liver compartment 2. The value assigned to *H1TOH2* is from Leggett (1993). Transfer out of liver compartment 1 includes 45% to diffusible plasma (*H1TOBL*), 45% to small intestine (*H1TOSI*) and 10% to liver compartment 2 (*H1TOH2*). These assumptions based on estimates of hepatic uptake and retention in humans and animals, and biliary secretion in humans (Heard and Chamberlain, 1984; Lloyd et al., 1975; Cohen et al., 1970).

H1TOSI: Fraction of Pb transfer from liver compartment 1 to the small intestine. The value assigned to *H1TOSI* is from Leggett (1993). Transfer out of liver compartment 1 includes 45% to diffusible plasma (*H1TOBL*), 45% to small intestine (*H1TOSI*) and 10% to liver compartment 2 (*H1TOH2*). These assumptions based on estimates of hepatic uptake and retention in humans and animals, and biliary secretion in humans (Heard and Chamberlain, 1984; Lloyd et al., 1975; Cohen et al., 1970).

HALF: Age at which body weight is half of *WCHILD*. This parameter is used in body weight and tissue volume growth equations (see variables *WBODY*, *VK*, *VL*, Appendix A). The value assigned to *WCHILD* is from O'Flaherty (1995, 1993).

HCTA: Adult hematocrit. Sex-specific values assigned to *HCTA* are from O'Flaherty (1995, 1993).

HCTB: Birth hematocrit. Values assigned to *HCTB* are from O'Flaherty (1995, 1993).

IFETAL: Switch for fetal simulation on (1) or off (0). The default value is 1 which turns on calculations of Pb body burden at birth based on maternal blood Pb (*BLDMOT*, see variables for Pb Masses at Birth, Appendix A).

IRBC: Switch for linear (0) or non-linear (1) RBC uptake. The default value is 1 which implements a threshold-specified RBC uptake of Pb from plasma.

KAPPA: Logistic parameter for calculation of body weight (see variable *WBODY* in Appendix A). The parameters *KAPPA* and *LAMBDA* determine the pre-adult rate of increase of body weight. The default value for *KAPPA* is 600 (O'Flaherty, 1995, 1993).

LAMBDA: Logistic parameter in calculation of body weight (see variable *WBODY* in Appendix A). The parameters *KAPPA* and *LAMBDA* determine the pre-adult rate of increase of body weight during. The default value for *LAMBDA* is 0.017 for females and 0.0095 for males (O'Flaherty, 1995, 1993).

POWER: Exponent factor for non-linear expression for RBC deposition. The value assigned to *POWER* is from Leggett (1993). The value of 1.5 was empirically derived based on data on Pb in human urine, plasma, and blood (Minoia et al., 1990; Iyengar and Woittiez, 1988; Somervaille et al., 1988; Skerfving et al., 1985; Manton and Cook, 1984; deSilva, 1981; Chamberlain et al., 1978; Schütz and Skerfving, 1976; Cooper et al., 1973).

RBCNL: Threshold Pb concentration in RBCs at which non-linear deposition of Pb from diffusible plasma to RBC occurs. Leggett (1993) assigned a value of 60 µg dL^{-1} based on an observed RBC Pb concentration threshold above which non-linear kinetics of Pb in the body were observed (Chamberlain, 1985). The value was revised to 20 µg/dL based on calibration to data on plasma-whole blood Pb concentrations measured in adults (Smith et al., 2002; Manton et al., 2001; Bergdahl et al., 1999; Bergdahl et al., 1998; Hernández-Avila et al., 1998; Bergdahl et al., 1997; Schütz et al., 1996).

RBLAD: Rate coefficient for Pb transfer from urinary bladder to urine. The value assigned to *ARBLAD* is from Leggett (1993). The value of 5 d^{-1} for adults is based on a removal $t_{1/2}$ of 0.1 days for Pb being voided from the bladder (ICRP, 1975), which approximates a transfer rate of 0.693/0.1 d = 7 d^{-1}. The rate coefficients for children are 7, 8, 11, 15, 12, and 12 d^{-1} for 15, 10, 5, and 1 year old, 3 months old, and birth, respectively.

RBRAN: Rate coefficient for Pb transfer from brain to diffusible plasma. The value assigned to *ARBRAN* is from Leggett (1993). The value of 0.00095 d^{-1} derives from a removal $t_{1/2}$ of 2 years (0.693/2 yrs = 9.5×10^{-4} d^{-1}). The values for *ABRAN* and *TOBRAN* (deposition of 0.015% of Pb from diffusible plasma), are based on comparison of predicted and observed brain Pb in dogs and baboons (Lloyd et al., 1975; Cohen et al., 1970) and human autopsy observations (Grandjean, 1978; Niyogi, 1974).

RCORT: Rate coefficient for Pb transfer from non-exchangeable cortical bone to diffusible plasma. Leggett (1993) assigned a value of 0.000082 d^{-1} for *ACORT* in adults based on the assumption that removal of Pb from the non-exchangeable bone volume is occurs at same rate as bone resorption. Childhood and adult rates were adopted from ICRP (1990) for bone-seeking radionuclides, based on histomorphometric measurements taken of human ribs, iliac crest, and various long bones. By adulthood, trabecular bone resorption is about 6-fold higher than in cortical bone. As discussed in Chapter 4, values for children and adults were increased by a factor of 2, based on calibration of simulations of bone Pb elimination kinetics in retired Pb workers (Nilsson et al., 1991).

RCS2B: Rate coefficient for Pb transfer from cortical bone surface to diffusible plasma. The value assigned to *RCS2B* is from Leggett (1993). The value of 0.5 d^{-1} for adults was based on model fit of skeletal Pb data for humans (Heard and Chamberlain, 1984), baboons (Cohen et al., 1970), and dogs (Lloyd et al., 1975), assuming a transfer rate of 1 d^{-1} from bone surface and 0.5 d^{-1} each to plasma or exchangeable bone volume. For children, the rate coefficient 0.65 d^{-1} was assigned to *ARCS2B* based on the assumption that, in children, a larger fraction of Pb leaving bone surfaces goes to plasma. By analogy to strontium, approximately 1.25-fold more Pb transfers from bone surface to plasma in children, compared to adults (1.25×0.5 d^{-1} = 0.65 d^{-1}).

RCS2DF: Rate coefficient for Pb transfer from cortical bone surface to exchangeable cortical bone volume. The value assigned to *RCS2DF* is from Leggett (1993). The value of 0.5 d^{-1} in adults was based on model fits to skeletal Pb data for humans (Heard and Chamberlain, 1984), baboons (Cohen et al., 1970), and dogs (Lloyd et al., 1975) assuming transfer rate of 1 d^{-1} from bone surface and 0.5 d^{-1} each to plasma or exchangeable bone volume. For children to age 15, the rate coefficient is 0.35 d^{-1}. By analogy to strontium, approximately 1.25-fold more Pb transfers from bone surface to plasma in children, compared to adults (1.25×0.5 d^{-1} = 0.65 d^{-1}). The remaining Pb transfers to exchangeable bone volume at a rate of 0.35 d^{-1}.

RDECAY: Rate coefficient for radioactive decay of unstable Pb isotope. This parameter is set to 0 by default in the AALM.FOR which simulates biokinetics of stable isotopes of Pb.

RDIFF: Rate coefficient for Pb transfer from exchangeable bone (cortical or trabecular) volume to surface or non-exchangeable bone volume (see FLONG for fraction to non-exchangeable). The value assigned to *RDIFF* is from Leggett (1993). The value of 0.0231 d^{-1} was based on observed rates of removal of Pb from bone of dogs, baboons, and chronically exposed humans appears, which were similar to removal of radium, which has a removal $t_{1/2}$ of 30 days (Leggett, 1992a), resulting in a rate coefficient of 0.693/30 days = 0.00231 d^{-1}.

RKDN1: Rate coefficient for transfer from kidney compartment 1 to urinary pathway. The value assigned to *RKDN1* is from Leggett (1993). The value of 0.139 d^{-1} was chosen based on a removal $t_{1/2}$ of 5 days (transfer rate of 0.693/5 days = 0.139 d^{-1}) and a deposition fraction of 2%, which predicts kidney levels in rats and baboons (Cohen et al., 1970) and is also consistent with human excretion data (Campbell et al., 1984; Chamberlain et al., 1978; Hursh and Mercer, 1970; Booker et al., 1969; Hursh and Suomela, 1968).

RKDN2: Rate coefficient for transfer from kidney compartment 2 to diffusible plasma. Leggett (1993) assigned a value of 0.0019 d^{-1} for adults. After parameter values for *TOKDN1* and *RKDN1* were set, 0.02% deposition from diffusible plasma and a removal $t_{1/2}$ of 1 year (rate coefficient: 0.693/1 yrs = 0.0019 d^{-1}) replicated and overestimated slow renal Pb loss in humans (Heard and Chamberlain, 1984) and animals (Lloyd et al., 1975; Cohen et al., 1970), respectively. Rate coefficients for children ages 10-15 years were assigned the adult value, while 0.00693 d^{-1} was used to represent birth to 5 years of age, assuming a removal $t_{1/2}$ of 100 days. This assumption was needed to keep estimated Pb levels from overly accumulating in long-term kidney compartments. These values were revised downward in the AALM.FOR based on calibration of simulations (see Chapter 4) of post-mortem soft tissue-bone Pb concentrations in children and adults reported by Barry (1975). The adjustments were a factor of ×0.1 for ages ≤25 years, increasing to 0.5 at age 30 ears and 1 by age 40 years.

RLalvLint: Clearance rate (d^{-1}) from in the alveolar (Alv) compartment of the respiratory tract to the interstitial (Int) compartment. Default is 0.0 d^{-1} as a placeholder for a rate to be recommended in a future release of the model.

RLalvLplas: Clearance rate (d^{-1}) from in the alveolar (Alv) compartment of the respiratory tract to the plasma. Default is 0.347 d^{-1} (halftime of 47.9 h) based on the lung clearance model of Leggett (1993) as described in Section 2.3.3.1.

RLalvLTB: Clearance rate (d^{-1}) from in the alveolar (Alv) compartment of the respiratory tract to the tracheobronchial (TB) compartment. Default is 0.0 d^{-1} as a placeholder for a rate to be recommended in a future release of the model.

RLETLplas: Clearance rate (d^{-1}) from in the extrathoracic (ET) compartment of the respiratory tract to the plasma. Default is 7.68 d^{-1} (halftime of 2.17 h) based on the lung clearance model of Leggett (1993) as described in Section 2.3.3.1.

RLETLstom: Clearance rate (d^{-1}) from in the extrathoracic (ET) compartment of the respiratory tract to the stomach. Default is 0.0 d^{-1} as a placeholder for a rate to be recommended in a future release of the model.

RLintLplas: Clearance rate (d^{-1}) from in the interstitial (Int) compartment of the respiratory tract to the plasma. Default is 0.0 d^{-1} as a placeholder for a rate to be recommended in a future release of the model.

RLTBLET: Clearance rate (d^{-1}) from in the tracheobronchial (TB) compartment of the respiratory tract to the extrathoracic (ET) compartment. Default is 0.0 d^{-1} as a placeholder for a rate to be recommended in a future release of the model.

RLTBLplas: Clearance rate (d^{-1}) from in the extrathoracic (ET) compartment of the respiratory tract to the plasma. Default is 1.94 d^{-1} (halftime of 8.58 h) based on the lung clearance model of Leggett (1993) as described in Section 2.3.3.1.

RLLI: Rate coefficient for Pb transfer from lower large intestine to feces. The value assigned to *RLLI* is from Leggett (1993). The value of 1 d^{-1} is from the ICRP (1979) gastrointestinal tract model.

RLVR1: Rate coefficient for Pb transfer from liver compartment 1 to small intestine or diffusible plasma. The value assigned to *RLVR1* (0.693 d^{-1}) is from Leggett (1993). The removal $t_{1/2}$ for liver compartment 1 is assumed to be 10 days, resulting in a rate coefficient of 0.693/10 days = 0.693 d^{-1}. A relatively short $t_{1/2}$ is needed to reproduce hepatic uptake and loss in humans (Chamberlain et al., 1978), baboons (Cohen et al., 1970), and dogs (Lloyd et al., 1975) for the first weeks following intravenous Pb injection.

RLVR2: Rate coefficient for Pb transfer from the slow liver compartment 2 to diffusible plasma. Leggett (1993) assigned a value of 0.0019 d^{-1} for adults and children ≥10 years of age to reproduce observations of 2% fraction of body Pb in liver of chronically exposed humans. For children ages 10–15 years, the rate coefficient was the same as adults, while 0.00693 d^{-1} was used for birth to 5 years of age, assuming a removal $t_{1/2}$ of 100 days. This assumption was made to keep estimated Pb levels from overly accumulating in long-term compartments. Values for children and adults were revised downward in the AALM.FOR based on calibration of simulations (see Chapter 4) of post-mortem soft tissue-bone Pb concentration ratios in children and adults reported by Barry (1975). The adjustments were a factor of 0.1 for ages ≤1 year, increasing progressively to 0.3 at age 10 years, 0.75 at age 30 years, 1.6 at age 40 years, and 1.8 at 60 years.

RPLAS: Rate coefficient for Pb transfer from diffusible plasma to all compartments, scaled to bone surface deposition. The value assigned to *RPLAS* is from Leggett (1993). The value of 2000 d^{-1} reflects the removal of radio-Pb from plasma at about 1 minute (Campbell et al., 1984; Wells et al., 1977; Booker et al., 1969). Adjusting for rapid uptake in to RBCs and EVF, the rate becomes 1.3–1.4 min^{-1}, rounded to 2000 d^{-1}.

RPROT: Rate coefficient for Pb transfer from bound plasma to diffusible plasma. The value assigned to *RPROT* is from Leggett (1993). The value of 0.139 d^{-1} (0.693/5 days = 0.139 d^{-1}) is based on a removal $t_{1/2}$ of approximately 5 days, the same as observed for plasma proteins (Orten and Neuhaus, 1982).

RRBC: Rate coefficient for Pb transfer from RBC to diffusible plasma. Leggett (1993) assigned a value of 0.0019 for adults and children ≥10 years of age, based on a removal $t_{1/2}$ from RBCs to plasma of 5 days [0.693/5 days = 0.0019 d^{-1}; (Chamberlain et al., 1978)]. For children from birth to 5 years of age, 0.00693 d^{-1} was assigned to provide reasonable agreement with the reference distributions of RBC levels derived by Leggett (1993). Values for ages 1−10 years were revised upward in the AALM.FOR to achieve alignment of Pb uptake-blood Pb concentration relationships in children estimated by the AALM and IEUBK model (Chapter 4). The adjustments were a factor of ×1.7 at age 1 year, ×1.4 at age 5 years and ×1.4 at age 10 years.

RSIC: Rate coefficient for Pb transfer from small intestine to upper large intestine. The value assigned to *RSIC* is from Leggett (1993). The value of 6 d^{-1} is from the first-order transfer rate in the ICRP (1979) gastrointestinal tract model.

RSOF0: Rate coefficient for Pb transfer from soft tissues with fast Pb clearance to diffusible plasma. The value assigned to *RSOF0* is from Leggett (1993). The value of 2.079 d^{-1}, based on a removal $t_{1/2}$ of 8 hours (0.693/8 hours = 2.079 d^{-1}) and a deposition fraction of 8.875% from diffusible plasma, reproduces Pb reappearance in blood from EVF after the first day following Pb injections in animals (Gregus and

Klaassen, 1986; Victery et al., 1979; Lloyd et al., 1975; Potter et al., 1971; Cohen et al., 1970; Lloyd et al., 1970).

RSOF1: Rate coefficient for Pb transfer from soft tissues with medium Pb clearance to diffusible plasma. The value assigned to *RSOF1* is from Leggett (1993). The value of 0.00693 d^{-1}, based on an removal $t_{1/2}$ of 100 days (0.693/100 days = 0.00693 d^{-1}) and a deposition fraction of 0.5% from diffusible plasma, reproduces Pb reappearance in blood from EVF after the first day following Pb injections in animals (Gregus and Klaassen, 1986; Victery et al., 1979; Lloyd et al., 1975; Potter et al., 1971; Cohen et al., 1970; Lloyd et al., 1970).

RSOF2: Rate coefficient for Pb transfer from soft tissues with slow Pb clearance to diffusible plasma. The value assigned to *RSOF2* (0.00038 d^{-1}) is from Leggett (1993). Assuming no more than 0.1% of diffusible plasma Pb is deposited into soft tissue having tenacious Pb retention, and the retention time is at least 5 years, consistent with autopsy data for chronically exposed humans (Grandjean, 1978; Niyogi, 1974).

RSTMC: Rate coefficient for Pb transfer from stomach to small intestine. The value assigned to *RSTMC* is from Leggett (1993). The value of 24 d^{-1} is from the ICRP (1979) gastrointestinal tract model.

RTRAB: Rate coefficient for Pb transfer from non-exchangeable trabecular bone volume to diffusible plasma. Leggett assigned a value of 0.000493 d^{-1} to adults (assuming that removal of Pb from the non-exchangeable bone volume occurs at same rate as bone resorption). Childhood and adult rates were adopted from ICRP (1990) for bone-seeking radionuclides, based on histomorphometric measurements taken of human ribs, iliac crest, and various long bones. By adulthood, trabecular bone resorption is about 6-fold higher than in cortical bone. Values for children and adults were increased by a factor of ×3, based on calibration of simulations (see Chapter 4) of bone Pb elimination kinetics in retired Pb workers (Nilsson et al., 1991).

RTS2B: Rate coefficient for Pb transfer from trabecular bone surface to diffusible plasma. Values for *RTS2B* are from Leggett (1993). For adults, the value 0.5 d^{-1} was based on model fit to skeletal Pb data for humans (Heard and Chamberlain, 1984), baboons (Cohen et al., 1970), and dogs (Lloyd et al., 1975). Assuming a total transfer rate of 1 d^{-1} from bone surface, a rate of 0.5 d^{-1} each transfers Pb to plasma or exchangeable bone volume. The rate coefficient for children (≤15 years) is 0.65 d^{-1}, based on the assumption that, in children, a larger fraction of Pb leaves bone surfaces and goes to plasma. By analogy to strontium, approximately 1.25-fold more Pb transfers from bone surface to plasma in children, compared to adults (1.25×0.5 d^{-1} = 0.65 d^{-1}).

RTS2DF: Rate coefficient for Pb transfer from surface trabecular bone to exchangeable trabecular bone volume. Values for *RTS2DF* are from Leggett (1993). For adults, the value 0.5 d^{-1} was based on model fit to skeletal Pb data for humans (Heard and Chamberlain, 1984), baboons (Cohen et al., 1970), and dogs (Lloyd et al., 1975). Assuming a total transfer rate of 1d^{-1} from bone surface, a rate of 0.5 d^{-1} each transfers Pb to plasma or exchangeable bone volume. the rate coefficient for children ≤15 years is 0.35 d^{-1}. By analogy to strontium, approximately 1.25-fold more Pb transfers from bone surface to plasma in children, compared to adults (1.25×0.5 d^{-1} = 0.65 d^{-1}). The remaining Pb transfers to exchangeable bone volume at a rate of 0.35 d^{-1}.

RULI: Rate coefficient for Pb transfer from upper large intestine to lower large intestine. The value assigned to *RULI* is from Leggett (1993). The value of 1.85 d^{-1} is from the ICRP (1979) gastrointestinal tract model.

S2HAIR: Fraction of Pb transfer from intermediate soft tissue (*SOF2*) to hair, nails, and desquamated skin. The value assigned to *S2HAIR* is from Leggett (1993). The value of40% is based on observations of 3% of the Pb body burden in soft tissues and the remainder in pelt of animals at 28 days after injection (Lloyd et al., 1975, 1970). The remaining fraction leaving *SOF2* (1-*S2HAIR* = 60%) returns to diffusible plasma.

SATRAT: Maximum (saturating) concentration of Pb in RBCs. The value assigned to *SATRAT* is from Leggett (1993). The concentration of 350 µg dL^{-1} was assigned based on the observed upward inflection of ratios of urinary:blood Pb and plasma:blood Pb at RBC concentrations above this level (Minoia et al., 1990; Iyengar and Woittiez, 1988; Somervaille et al., 1988; Skerfving et al., 1985; Manton and Cook, 1984; deSilva, 1981; Chamberlain et al., 1978; Schütz and Skerfving, 1976; Cooper et al., 1973).

SIZEVF: Relative volume of the EVF compartment compared to plasma (EVF/Plasma). The value assigned to *SIZEVF* is from Leggett (1993). The value of 3-fold was chosen because plasma Pb is about three times that of EVF at equilibrium.

STEPS_PER_DAY: Value numerical integration time steps computed daily. The default value, 100 steps per day, is intended to provide adequate specificity of calculation. More or fewer timesteps can be used successfully. Currently each simulation must start at birth. The last year of the simulation may change.

TBONE: Deposition fraction for Pb from diffusible plasma to surface bone. The value of 8% for adults reproduces observations of Pb deposition to total bone of humans (Heard and Chamberlain, 1984), baboons (Cohen et al., 1970), and dogs (Lloyd et al., 1975). For children, the following deposition fractions were used: 23.7% at 15 years, 17.9% at 10 years, 12.8% at 5 years, 14.4% at year, and 24% at birth and 3 months. These values arise from the assumption that Pb deposits to bone surfaces proportional to the rate of calcium addition, as described by Leggett (1992a).

TBRAN: Deposition fraction for Pb from diffusible plasma to brain. Values for *TBRAN* are from Leggett (1993). For children ≥5 years old and adults, the value of 0.015%, combined with a removal $t_{1/2}$ of 2 years (0.693/2 yrs = 9.49×10^{-4} d^{-1}) were assigned based on model fit to observations of brain Pb levels in dogs (Lloyd et al., 1975) and baboons (Cohen et al., 1970) and human autopsy observations (Grandjean, 1978; Niyogi, 1974). For children from birth to 1 year, the a 3-fold higher value of 0.045% was assigned to account for the relatively larger brain mass:body weight ratio in this age range.

TOEVF: Deposition fraction for Pb from diffusible plasma to extravascular fluid. The value assigned to *TOEVF* is from Leggett (1993). The value of 50% was based on observations of rapid return of Pb to blood from extravascular spaces (Heard and Chamberlain, 1984; Booker et al., 1969; Hursh and Suomela, 1968; Stover, 1959).

TOFECE: Deposition fraction for Pb from diffusible plasma directly to the small intestine (not including the transfer from biliary secretion, specified by *RLVR1*). The value assigned to *TOFECE* is from Leggett (1993). The value of 0.6%, as well as Pb entering from biliary excretion (*H1TOSI*) was based on observations of fecal excretion and the feces-to-urine Pb ratios in adults (Heard and Chamberlain, 1984; Chamberlain et al., 1978; Wells et al., 1977).

TFRAC: Fraction of diffusible plasma-to-bone deposition that goes to trabecular surface bone. Values for *TFRAC* are from Leggett (1993). For adults, the value of 55.6% was assigned based on an approximate 4-fold larger trabecular bone mass than cortical bone in humans (ICRP, 1975), and that calcium deposits in trabecular bone are 5- to 6-fold greater than in cortical bone in humans (Leggett, 1992a; Leggett et al., 1982). The fraction transferring from diffusible plasma to cortical bone is 1-*TFRAC*, or 0.444. For children, the following values were assigned: 27.95% for 15 years, 25% for 10 years, 22.2% for 5 years, or 20% for birth to 3 months.

TOKDN1: Deposition fraction for Pb from diffusible plasma to kidney compartment 1. Leggett (1993) assigned a value of 2% and a removal $t_{1/2}$ of 5 days (*RKDN1*) based on observed kidney levels in rats and baboons (Cohen et al., 1970) that were also consistent with human excretion data (Campbell et al., 1984; Chamberlain et al., 1978; Hursh and Mercer, 1970; Booker et al., 1969; Hursh and Suomela, 1968). Values for children and adults were revised upward in the AALM.FOR by a factor of ×1.25 based on calibration of simulations of plasma-to-urine clearance estimated for adults from data reported in (Araki et al., 1986; Manton and Cook, 1984; Manton and Malloy, 1983; Chamberlain et al., 1978).

TOKDN2: Deposition fraction for Pb from diffusible plasma to kidney compartment. The value of 0.02% was chosen. Leggett (1993) assigned a value of 0.02% and a removal $t_{1/2}$ of 1 year (*RKDN2*), after values for *TOKDN1* and *RKND1* were set, based on observations of a slow component for loss of Pb from kidney in humans (Heard and Chamberlain, 1984) and animals (Lloyd et al., 1975; Cohen et al., 1970), respectively. Values for children and adults were revised upward in the AALM.FOR by a factor of ×2 based on calibration of simulations (see Chapter 4) of post-mortem soft tissue-bone Pb concentrations in children and adults reported by Barry (1975).

TOLVR1: Deposition fraction for Pb from diffusible plasma to liver compartment 2. The value assigned to *TOLVR1* is from Leggett (1993). The value of 4% was assigned based on observed uptake and retention of Pb in liver in humans and animals, and biliary secretion in humans (Heard and Chamberlain, 1984; Lloyd et al., 1975; Cohen et al., 1970).

TOPROT: Deposition fraction for Pb from diffusible plasma to protein-bound plasma. The value assigned to *TOPROT* is from Leggett (1993). The value of 0.04% was selected to achieve (1) early bifurcation of tracer Pb between plasma and RBCs, (2) observed urinary clearance of plasma Pb, (3) plasma containing 0.2% of blood Pb at equilibrium, and (4) 15% ultrafilterable plasma Pb at equilibrium.

TORBC: Deposition fraction from diffusible plasma to RBCs. The value assigned to *TORBC* is from Leggett (1993). The value of 24% was based on the observation that approximately one quarter of Pb depositing to RBCs provides good fits to data of Hursh et al. (1969).

TOSOF0: Deposition fraction for Pb from diffusible plasma to the fast soft tissue compartment 0. Values for *TOSOF0* are from Leggett (1993). For adults, the value of 8.88%, and a removal $t_{1/2}$ of 8 hours (RSOF0) was assumed in order to replicate Pb reappearance in blood from extravascular fluid after the first day following Pb injections in animals (Gregus and Klaassen, 1986; Victery et al., 1979; Lloyd et al., 1975; Potter et al., 1971; Cohen et al., 1970; Lloyd et al., 1970). For children, values of 8.38 and 8.35% were assigned to ages 5 to 15 years and birth to 1 year, respectively.

TOSOF1: Deposition fraction for Pb from diffusible plasma to the intermediate soft tissue compartment 1. Values for *TOSOF1* are from Leggett (1993). For adults, the value of 0.5% produced an intermediate-rate loss of Pb from soft tissues and that aligned with blood Pb and excretion kinetics (hair, nails, and

skin) in humans (Rabinowitz et al., 1976). A value of 1% was assigned children up to 15 years of age (Leggett, 1993).

TOSOF2: Deposition fraction for Pb from diffusible plasma to the slow soft tissue compartment 2. Values for *TOSOF2* are from Leggett (1993). The value of 0.1% for adults and children, along with a retention time of at ≥5 years was based on comparisons of predicted and observed post-mortem soft tissue Pb levels in chronically exposed humans (Grandjean, 1978; Niyogi, 1974).

TOSWET: Deposition fraction for Pb from diffusible plasma to sweat. The value assigned to *TOSWET* is from Leggett (1993). The value of 0.35% was assigned based on observations of Pb excretion in sweat and which was approximately 10% of urinary excretion for chronic exposure (Rabinowitz et al., 1976).

TOURIN: Deposition fraction for Pb from diffusible plasma to urine. Leggett (1993) assigned a value of 1.5% for *TOURIN*, in addition to 2% being removed from urinary path to bladder (*TOKDN1*), based on observations of human urinary clearance (Minoia et al., 1990; Iyengar and Woittiez, 1988; Somervaille et al., 1988; Skerfving et al., 1985; Chamberlain et al., 1978; Schütz and Skerfving, 1976; Cooper et al., 1973). This parameter was set to zero in the AALM.FOR after calibration of parameter *TOKDN1* to data on plasma-to-urine clearance adults (Araki et al., 1986; Manton and Cook, 1984; Manton and Malloy, 1983; Chamberlain et al., 1978).

VBLC: Blood volume fraction of body weight. The value assigned to *VBLC* is from O'Flaherty (1995, 1993).

VKC: Blood volume fraction of body weight. The value assigned to *VKC* is from O'Flaherty (1995, 1993).

VLC: Liver volume fraction of body weight. The value assigned to *VLC* is from O'Flaherty (1995, 1993).

VLUC: Lung volume fraction of body weight. The value assigned to *VLC* is from O'Flaherty (1995, 1993).

WADULT: Adult maximum weight (lean body mass) used in calculation of body weight growth (see variable *WBODY* in Appendix A). The value assigned to *WADULT* is from O'Flaherty (1995, 1993).

WBIRTH: Weight at birth used in calculation of body weight growth (see variable *WBODY* in Appendix A). The value assigned to *WBIRTH* is from O'Flaherty (1995, 1993).

WCHILD: Maximum body weight achieved during early hyperbolic growth phase, used in calculation of body weight growth (see variable *WBODY* in Appendix A). The value assigned to *WCHILD* is from O'Flaherty (1995, 1993).

TABLE D-1. AALM BIOKINETICS PARAMETERS AND VALUES

Parameter	Unit	Form	Type	Description	Value	Source
Phys, AGE	years	A	F	Age years for parameters that are assigned values at specific ages	0 0.274 1.0 5.0 10.0 15.0 25.0 30.0 40.0 60.0 90.0	(Leggett, 1993) Also see Chapters 2 and 4
AGE_RANGE	years	C	F	Age at end of simulation	0-90	NA
BLDMOT	µg/dL	C	F	Maternal blood Pb concentration	0.62	NHANES 2009–2014; (U.S. EPA, 2017a)
BONIN	unitless	C	N/A	Fraction of body lead, at birth, in bone	0.32	(Leggett, 1993)
BRANIN	unitless	C	N/A	Fraction of body lead, at birth, in brain	0.45	(Leggett, 1993)
BRATIO	unitless	C	F	Child (at birth):maternal blood Pb concentration ratio	0.85	Multiple references, see summary for BRATIO in this Appendix
DEPFracLalv	unit-less	C	F	Inhaled particle deposition fraction in alveolar region	0.040	Section 2.3.3.1
DEPFracLET	unit-less	C	F	Inhaled particle deposition fraction in extrathoracic region	0.2	Section 2.3.3.1

Parameter	Unit	Form	Type	Description	Value	Source
DEPFracLTB	unit-less	C	F	Inhaled particle deposition fraction in tracheobronchial region	0.159	Section 2.3.3.1
F1	Unitless	C	N/A	GI-tract absorption fraction which are applied to Pb ingested from all sources. (based on Leggett 1993)	$0.4-0.28/(1+30*e^{(-AGE)})$	(O'Flaherty, 1995, 1993)
FLONG	unitless	A	F	Fraction of total Pb transfer from the exchangeable bone volume to non-exchangeable bone volume; the fraction of total Pb transfer from the exchangeable bone volume to bone surface (cortical or trabecular) is 1.0-FLONG	0.6	(Leggett, 1993, 1992a; Nilsson et al., 1991; Leggett et al., 1982) Also see Chapters 2 and 4
GSCAL	unitless	A	F	Age scaling factor for gastrointestinal transfer rates	Age: Value ≥25 yr: 1 15 yr: 1.33 10 yr: 1.67 5 yr: 1.67 1 yr: 1.67 0.274 yr: 1.67 Birth: 1.67	(Leggett, 1993)

Parameter	Unit	Form	Type	Description	Value	Source
H1TOBL	unitless	C	F	Fraction of Pb transfer out of liver compartment 1 that goes to diffusible plasma	0.45	(Leggett, 1993)
H1TOH2	unitless	C	F	Fraction of Pb transfer out of liver compartment 1 that goes to liver compartment 2	0.1	(Leggett, 1993)
H1TOSI	unitless	C	F	Fraction of Pb transfer out of liver compartment 1 that goes to the small intestine	0.45	(Leggett, 1993)
HALF	year	C	F	Age at which body weight is half of *WCHILD*	3	(O'Flaherty, 1995, 1993)
HCTA	unitless	C	F	Adult hematocrit	0.41 (female) 0.46 (male)	(O'Flaherty, 1995, 1993)
HCTB	unitless	C	F	Birth hematocrit	0.52	(O'Flaherty, 1995, 1993)
HEPIN	unitless	C	N/A	Fraction of body lead, at birth, in liver	0.055	(Leggett, 1993)
IFETAL	unitless	C	I	Switch for fetal simulation on (1) or off (0)	1	NA
IRBC	unitless	C	I	Switch for linear (0) or non-linear (1) RBC uptake	Non-linear RBC	NA

Parameter	Unit	Form	Type	Description	Value	Source
INTERP	unitless	N/A	N/A	Switch indicating if concentration of lead should be linearly interpolated between user defined values or stepwise in calculation	Stepwise	NA
ITERATE	unitless	N/A	N/A	Switch indicating if the simulation should use forward calculation or solve for an allowable concentration	Forward	NA
KAPPA	unitless	C	F	Logistic parameter for calculation of body weight (see variable WBODY)	600	(O'Flaherty, 1995, 1993)
LAMBDA	unitless	C	F	Logistic parameter for calculation of body weight (see variable WBODY)	0.017 (female) 0.0095 (male)	(O'Flaherty, 1995, 1993)
OUTWRITE	unitless	N/A	N/A	Frequency of output written containing lead loading and distribution calculations	100	Sim Control Variable
POWER	unitless	C	F	Exponent factor for non-linear expression for RBC deposition.	1.5	(Leggett, 1993)

Parameter	Unit	Form	Type	Description	Value		Source
RBRAN	d^{-1}	A	F	Rate coefficient for Pb transfer from brain to diffusible plasma	9.5E-04		(Leggett, 1993)
RBCIN	unitless	C	N/A	Fraction of body lead, at birth, in red blood cells	0.07		(Leggett, 1993)
RBCNL	µg/dL	C	F	Threshold Pb concentration in RBC for non-linear deposition of Pb from diffusible plasma to RBC	20		(Leggett, 1993) Also see Chapters 2 and 4
RBLAD	Unitless	C	N/A	Age-scaled transfer rate from urinary bladder to urine	varied		(Leggett, 1993)
RCORT	d^{-1}	A	F	Rate coefficient for Pb transfer from non-exchangeable cortical bone to diffusible plasma	Age	Value	(Leggett, 1993; Nilsson et al., 1991) Also see Chapters 2 and 4
					≥25 yr	1.644E-04	
					15 yr	1.024E-03	
					10 yr	1.780E-03	
					5 yr	3.080E-03	
					1 yr	5.760E-03	
					0.274 yr	1.644E-02	
					Birth	2.040E-02	
RCS2B	d^{-1}	A	F	Rate coefficient for Pb transfer from cortical bone surface to diffusible plasma.	Age	Value	(Leggett, 1993)
					≥25 yr	0.50	
					15 yr	0.35	
					10 yr	0.35	
					5 yr	0.35	
					1 yr	0.35	
					0.274 yr	0.35	
					Birth	0.35	

Parameter	Unit	Form	Type	Description	Value		Source
RCS2DF	d^{-1}	A	F	Rate coefficient for Pb transfer from cortical bone surface to exchangeable cortical bone volume	Age	Value	(Leggett, 1993)
					≥25 yr	0.50	
					15 yr	0.65	
					10 yr	0.65	
					5 yr	0.65	
					1 yr	0.65	
					0.274 yr	0.65	
					Birth	0.65	
RDIFF	d^{-1}	C	F	Rate coefficient for Pb transfer from exchangeable bone (cortical or trabecular) volume to surface or non-exchangeable bone volume (see FLONG for fraction to non-exchangeable)	0.023105		(Leggett, 1993)
RENIN	Unitless	C	N/A	Fraction of body lead, at birth, in kidney	0.01		(Leggett, 1993)
RKDN1	d^{-1}	C	F	Rate coefficient for transfer from kidney compartment 1 to urinary pathway	0.139		(Leggett, 1993)
RKDN2	d^{-1}	A	F	Rate coefficient for transfer from kidney compartment 2 to diffusible plasma	Age	Value	(Leggett, 1993; Barry, 1975) Also see Chapter 4
					≥40 yr	1.90E-03	
					30 yr	9.50E-04	
					25 yr	1.90E-04	
					15 yr	1.90E-04	
					10 yr	1.90E-04	
					5 yr	6.93E-04	
					1 yr	6.93E-04	

Parameter	Unit	Form	Type	Description	Value		Source
					0.274 yr	6.93E-04	
					Birth	6.93E-04	
RLalvLint	d^{-1}	C	F	Clearance rate from Alv compartment of the respiratory tract to Int compartment	0.0		Section 2.3.3.1
RLalvplas	d^{-1}	C	F	Clearance rate from Alv region to plasma	0.347		Section 2.3.3.1
RLalvLTB	d^{-1}	C	F	Clearance rate from Alv compartment of the respiratory tract to TB compartment	0.0		Section 2.3.3.1
RLETplas	d^{-1}	C	F	Clearance rate from ET region to plasma	7.68		Section 2.3.3.1
RLETstom	d^{-1}	C	F	Clearance rate from ET region to stomach	0.0		Section 2.3.3.1
RLintplas	d^{-1}	C	F	Clearance rate from Int compartment to plasma	0.0		Section 2.3.3.1
RLTBLET	d^{-1}	C	F	Clearance rate from TB compartment of the respiratory tract to ET compartment	0.0		Section 2.3.3.1
RLTBplas	d^{-1}	C	F	Clearance rate from TB region to plasma	1.94		Section 2.3.3.1
RLLI	d^{-1}	C	F	Rate coefficient for Pb transfer from lower large intestine to feces	1		(Leggett, 1993)

Parameter	Unit	Form	Type	Description	Value		Source
RLVR1	d^{-1}	C	F	Rate coefficient for Pb transfer from liver compartment 1 to small intestine or diffusible plasma	0.0693		(Leggett, 1993)
RLVR2	d^{-1}	A	F	Rate coefficient for Pb transfer from the slow liver compartment 2 to diffusible plasma	Age	Value	
					90 yr	3.800E-03	
					60 yr	3.420E-03	
					40 yr	3.040E-03	
					30 yr	1.425E-03	
					25 yr	5.700E-04	
					15 yr	5.700E-04	
					10 yr	5.700E-04	
					5 yr	1.386E-03	
					1 yr	6.930E-04	
					0.274 yr	6.930E-04	
					Birth	6.930E-04	
RPLAS	d^{-1}	C	F	Rate coefficient for Pb transfer from diffusible plasma to all compartments, scaled to bone surface deposition	2000		(Leggett, 1993)
RPROT	d^{-1}	C	F	Rate coefficient for Pb transfer from bound plasma to diffusible plasma	0.139		(Leggett, 1993)
RRBC	d^{-1}	A	F	Rate coefficient for Pb transfer from RBC to diffusible plasma	Age	Value	(Leggett, 1993) Also see Chapter 4
					≥15 yr	1.390E-01	
					10 yr	1.946E-01	
					5 yr	4.986E-01	
					1 yr	7.854E-01	

Parameter	Unit	Form	Type	Description	Value		Source
					0.274 yr	4.620E-01	
					Birth	4.620E-01	
RSIC	d^{-1}	C	F	Rate coefficient for Pb transfer from small intestine to upper large intestine	6		(Leggett, 1993)
RSOF0	d^{-1}	C	F	Rate coefficient for Pb transfer from soft tissues with fast Pb clearance to diffusible plasma	2.079		(Leggett, 1993)
RSOF1	d^{-1}	C	F	Rate coefficient for Pb transfer from soft tissues with medium Pb clearance to diffusible plasma	0.00693		(Leggett, 1993)
RSOF2	d^{-1}	C	F	Rate coefficient for Pb transfer from soft tissues with slow Pb clearance to diffusible plasma	0.00038		(Leggett, 1993)
RSTMC	d^{-1}	C	F	Rate coefficient for Pb transfer from stomach to small intestine	24		(Leggett, 1993)
RTRAB	d^{-1}	A	F	Rate coefficient for Pb transfer from non-exchangeable trabecular bone volume to diffusible plasma	Age	Value	(Leggett, 1993; Nilsson et al., 1991) Also see Chapter 4
					≥25 yr	9.860E-04	
					15 yr	1.912E-03	
					10 yr	2.640E-03	
					5 yr	3.620E-03	
					1 yr	5.760E-03	
					0.274 yr	1.644E-02	

Parameter	Unit	Form	Type	Description	Value		Source
					Birth	2.040E-02	
RTS2B	d^{-1}	A	F	Rate coefficient for Pb transfer from trabecular bone surface to diffusible plasma	Age	Value	(Leggett, 1993)
					≥25 yr	0.50	
					15 yr	0.35	
					10 yr	0.35	
					5 yr	0.35	
					1 yr	0.35	
					0.274 yr	0.35	
					Birth	0.35	
RTS2DF	d^{-1}	A	F	Rate coefficient for Pb transfer from surface trabecular bone to exchangeable trabecular bone volume	Age	Value	(Leggett, 1993)
					≥25 yr	0.50	
					15 yr	0.65	
					10 yr	0.65	
					5 yr	0.65	
					1 yr	0.65	
					0.274 yr	0.65	
					Birth	0.65	
RULI	d^{-1}	C	F	Rate coefficient for Pb transfer from upper large intestine to lower large intestine	1.85		(Leggett, 1993)
S2HAIR	unitless	C	F	Fraction of Pb transfer from intermediate soft tissue to hair, nails, and desquamated skin	0.4		(Leggett, 1993)
SATRAT	$\mu g\ dL^{-1}$	C	F	Maximum (saturating) concentration of Pb in RBC	350		(Leggett, 1993)

Parameter	Unit	Form	Type	Description	Value		Source
SEX	Unitless	N/A	N/A	Sex of the simulated individual	Female		NA
SIZEVF	unitless	C	F	Relative volume of the EVF compartment compared to plasma (EVF/Plasma)	3		(Leggett, 1993)
SOFIN	Unitless	C	N/A	Fraction of body lead, at birth, in soft tissue	0.5		(Leggett, 1993)
STEPS_PER_DAY	day	C	F	Numerical integration time steps per day	100		NA
TBONE	unitless	A	F	Deposition fraction for Pb from diffusible plasma to surface bone	Age	Value	(Leggett, 1993)
					≥25 yr	8.00E-02	
					15 yr	2.37E-01	
					10 yr	1.79E-01	
					5 yr	1.28E-01	
					1 yr	1.44E-01	
					0.274 yr	2.40E-01	
					Birth	2.40E-01	
TBONEL	Unitless	C	N/A	End value of TBONE-age array	0.08		(Leggett, 1993)
TEVF	unitless	C	F	Deposition fraction for Pb from diffusible plasma to extravascular fluid	0.5		(Leggett, 1993)
TFRAC	unitless	A	F	Fraction of diffusible plasma-to-bone deposition that goes to trabecular surface bone	Age	Value	(Leggett, 1993)
					≥25 yr	0.556	
					15 yr	0.279	
					10 yr	0.250	
					5 yr	0.222	
					1 yr	0.200	

Parameter	Unit	Form	Type	Description	Value		Source
					0.274 yr	0.200	
TOBRAN	unitless	A	F	Deposition fraction for Pb from diffusible plasma to brain	Birth	0.200	(Leggett, 1993)
					≥5 yr	1.5E-04	
					1 yr	4.5E-04	
					0.274 yr	4.5E-04	
					Birth	4.5E-04	
TOFECE	unitless	C	F	Deposition fraction for Pb from diffusible plasma directly to the small intestine (not including the transfer from biliary secretion, specified by *RLVR1*) not scaled to bone surface deposition	0.006		(Leggett, 1993)
TOKDN1	unitless	C	F	Deposition fraction for Pb from diffusible plasma to kidney compartment 1, not scaled to bone surface deposition	0.025		(Leggett, 1993)
TOKDN2	unitless	C	F	Deposition fraction for Pb from diffusible plasma to kidney compartment 2, not scaled to bone surface deposition	0.0004		(Leggett, 1993)

Parameter	Unit	Form	Type	Description	Value		Source
TOLVR1	unitless	C	F	Deposition fraction for Pb from diffusible plasma to liver compartment 2, not scaled to bone surface deposition	0.04		(Leggett, 1993)
TOPROT	unitless	C	F	Deposition fraction for Pb from diffusible plasma to protein-bound plasma, not scaled to bone surface deposition	0.0004		(Leggett, 1993)
TORBC	unitless	C	F	Deposition fraction from diffusible plasma to RBC, not scaled to bone surface deposition	0.25		(Leggett, 1993)
TOSOF0	unitless	A	F	Deposition fraction for Pb from diffusible plasma to the fast soft tissue compartment 0	Age	Value	(Leggett, 1993)
					≥25 yr	8.875E-02	
					15 yr	8.375E-02	
					10 yr	8.375E-02	
					5 yr	8.375E-02	
					1 yr	8.345E-02	
					0.274 yr	8.345E-02	
					Birth	8.345E-02	
TOSOF1	unitless	A	F	Deposition fraction for Pb from diffusible plasma to the intermediate soft tissue compartment 1	Age	Value	(Leggett, 1993)
					≥25 yr	0.005	
					15 yr	0.010	
					10 yr	0.010	
					5 yr	0.010	
					1 yr	0.010	

Parameter	Unit	Form	Type	Description	Value		Source
					0.274 yr	0.010	
					Birth	0.010	
TOSOF2	unitless	A	F	Deposition fraction for Pb from diffusible plasma to the slow soft tissue compartment 2	0.001		(Leggett, 1993)
TOSWET	–	C	F	Deposition fraction for Pb from diffusible plasma to sweat not scaled to bone surface deposition, not scaled to bone surface deposition	0.0035		(Leggett, 1993)
TOURIN	–	C	F	Deposition fraction for Pb from diffusible plasma to urine, not scaled to bone surface deposition	0.0		(Leggett, 1993) Also see Chapter 4
VBLC	unitless	C	F	Blood volume fraction of body weight.	0.067		(O'Flaherty, 1995, 1993)
VKC	unitless	C	F	Kidney volume fraction of body weight.	0.0085		(O'Flaherty, 1995, 1993)
VLC	unitless	C	F	Liver volume fraction of body weight.	0.025		(O'Flaherty, 1995, 1993)
VLUC	unitless	C	F	Lung volume fraction of body weight.	0.015		(O'Flaherty, 1995, 1993)

Parameter	Unit	Form	Type	Description	Value	Source
WADULT	kg	C	F	Adult maximum weight used in calculation of body weight growth (see variable WBODY)	34 (female) 50 (male)	(O'Flaherty, 1995, 1993)
WBIRTH	kg	C	F	Weight at birth used in calculation of body weight growth (see variable WBODY)	3.3 (female) 3.5 (male)	(O'Flaherty, 1995, 1993)
WCHILD	kg	C	F	Maximum body weight achieved during early hyperbolic growth phase, used in calculation of body weight growth (see variable *WBODY)*	22 (female) 23 (male)	(O'Flaherty, 1995, 1993)

A, array; C, constant; F, floating point, I, integer, NA, not applicable.

EPA
United States
Environmental Protection
Agency

PRESORTED STANDARD
POSTAGE & FEES PAID
EPA
PERMIT NO. G-35

Office of Research and Development (8101R)
Washington, DC 20460

Official Business
Penalty for Private Use
$300